Université d'Ottawa · University of Ottawa

Measurements of Small-Scale Statistics and Probability Density Functions in Passively Heated Shear Flow

by

Mohsen Ferchichi

A thesis
presented to the University of Ottawa
in partial fulfilment of the
requirement for the degree of

DOCTOR OF PHILOSOPHY
in
MECHANICAL ENGINEERING

**Ottawa-Carleton Institute for
Mechanical and Aerospace Engineering**

Ottawa, Ontario, May 1999

0-612-48098-4

Abstract

This study is an experimental investigation consisting of two parts. In the first part, the fine structure of uniformly sheared turbulence was investigated within the framework of Kolmogorov's (1941) similarity hypotheses. The second part, consisted of the study of the scalar mixing in uniformly sheared turbulence with an imposed mean scalar gradient, with the emphasis on measurements relevant to the probability density function formulation and on scalar derivative statistics.

The velocity fine structure was invoked from statistics of the streamwise and transverse derivatives of the streamwise velocity as well as velocity differences and structure functions, measured with hot wire anemometry for turbulence Reynolds numbers, Re_λ, in the range between 140 and 660. The streamwise derivative skewness and flatness agreed with previously reported results in that they increased with increasing Re_λ, with the flatness increasing at a higher rate. The skewness of the transverse derivative decreased with increasing Re_λ and the flatness of this derivative increased with Re_λ but a lower rate than the streamwise derivative flatness. The high order (up to sixth) transverse structure functions of the streamwise velocity showed the same trends as the corresponding streamwise structure functions.

In the second part of this experimental study, an array of heated ribbons was introduced into the flow to produce a constant mean temperature gradient, such that the temperature acted as a passive scalar. The Re_λ in this study varied from 184 to 253. Cold wire thermometry and hot wire anemometry were used for simultaneous measurements of temperature and velocity. The scalar pdf was found to be nearly Gaussian. Various tests of joint statistics of the scalar and its rate of destruction revealed that the scalar dissipation rate was essentially independent of the scalar value. The measured joint statistics of the scalar and the velocity suggested that they were nearly jointly normal and that the normalized conditioned expectations varied linearly with the scalar with slopes corresponding to the scalar-velocity correlation coefficients. Finally, the measured streamwise and transverse scalar derivatives and differences revealed that the scalar fine structure was intermittent not only in the dissipative range, but in the inertial range as well.

Acknowledgments

I wish to express my sincere gratitude to Professor Stavros Tavoularis for his guidance, motivation and encouragements when needed. On countless occasions, he explained to me many theoretical and experimental aspects about turbulence and taught me the art of conducting rigorous experimental procedures and, for that, I am really thankful.

During my graduate studies, I had the honour of meeting many friends and colleagues with whom I shared an enjoyable working atmosphere. I wish to thank all of them, especially Sadok Guellouz and Sebastien Marineau-Mes. I extend my thanks to the staff of the Department of Mechanical Engineering Workshop for their technical assistance.

The financial support provided by the Natural Sciences and Engineering Research Council of Canada (NSERC) and the Scientific Mission of Tunisia is greatly appreciated.

Je tiens à remercier ma famille, mes trés chers parents, Habiba et Salah et tous mes frères qui, malgré la distance, n'ont cessé de m'encourager et de me supporter moralement.

Table of Contents

List of Tables

List of Figures

Nomenclature

A	calibration constant in King's law
B	calibration constant in King's law
C	Kolmogorov's spectral constant
d_w	wire diameter
E_1	one-dimensional wave number spectrum, also anemometer voltage
$E_{1\theta}$	one-dimensional wave number spectrum of the scalar
F	flatness or the normalized fourth moment
f	frequency
f_c	filter's frequency cut-off
f_K	Kolmogorov frequency
f_{K_θ}	Kolmogorov frequency for the scalar
h	wind tunnel height
k	turbulent kinetic energy
k_s	shear constant
L	integral length scale
l	characteristic length
l_w	wire length
P	instantaneous pressure
p	pressure fluctuations, also probability density function

$\wp$	probability distribution function
Pr	Prandtl number
Pe_{ϵ_r}	Peclet number based on averaged dissipation
R	autocorrelation
Ra	Rayleigh number
R_a	wire resistance at the free stream temperature
Re	Reynolds number
Re_L	Reynolds number based on the streamwise integral length scale
Re_{ϵ_r}	Reynolds number based on averaged dissipation
Re_λ	Turbulence Reynolds number
R_w	wire operating electric resistance
r	separation distance between two points in space
S	skewness or the normalized third order moment
T_a	free stream temperature
$\overline{T}$	mean temperature rise
$\overline{T}_c$	mean centerline temperature rise
T_w	wire temperature
t	time
$\overline{U}_i$	mean velocity
$\overline{U}_c$	mean centerline velocity
U_j	jet velocity
u	characteristic velocity
u_i	velocity fluctuations $i = 1, 2, 3$

V stochastic variable corresponding to normalized velocity difference

V_θ stochastic variable corresponding to normalized temperature difference

x_i coordinate axes, $i = 1, 2, 3$

Greek symbols

α Correction to the spectra in the inertial range, also fitted constant in pdf

α_t temperature coefficient of resistivity

β fitted constant in pdf

γ thermal diffusivity

δ Dirac's function

ϵ energy dissipation rate

ϵ_θ scalar dissipation rate

ϵ_r energy dissipation rate averaged over a sphere of radius r

ϵ_{θ_r} scalar dissipation rate averaged over a sphere of radius r

ζ_n intermittency exponent

η Kolmogorov microscale

η_θ Corrsin-Obukhov microscale

η_B Batchelor microscale

κ_1 one-dimensional wave number

λ_{11} Streamwise Taylor microscale

$\lambda_{1\theta}$ Streamwise Corrsin microscale

μ_n n^{th} moment

ν kinematic viscosity

ρ fluid density, also dimensionless correlation coefficient

τ time

ψ scalar space

ω cyclic frequency

φ jet angle with respect to probe body

Subscripts

a free stream quantity

c centerline quantity or cut-off

i referring to coordinate system, $i = 1, 2, 3$

K based on the Kolmogorov scale

n order of structure function

p order of structure function

L based on integral length scale

Other notation

$\overline{(\ )}$ Time average

()' root mean squared value

$< >$ space average

$<q_1 \mid q_2>$ conditioned expectation of a quantity q_1 conditional upon a quantity q_2

Chapter 1

Introduction

Turbulent flows occur in a wide range of engineering applications. Turbulent motions are random in time and space and analytical models describing turbulent flows contain nonlinear effects which make exact solutions impossible. Turbulence is regarded as one of the major unsolved problems in Mechanics. In 1932, a physicist addressed a meeting of the British Association of the Advancement of Science and said: "I am an old man now and when I die and go to heaven there are two matters on which I hope for enlightenment. One is the quantum electrodynamics and the other is the turbulent motion of fluids; about the former I am really rather optimistic" (Briggs, 1992).

Examples of turbulent flows are wakes behind boats and cars, ocean currents, and boundary layers on the wings of airplanes. In certain applications, considerable advantage may be gained when turbulence is encountered, such as in combustion chambers, turbulent mixers and heat exchangers, because mixing of fluids is enhanced by turbulence. But, in other cases, turbulence is detrimental as, for example, it increases the drag force on airplanes and other vehicles. These examples and many more, make engineers and scientists engage in research to find ways of controlling turbulent flows.

An increased difficulty that is encountered in analyzing turbulence is that it involves a wide range of motions of different scales. These can be distinguished into: large scale motions, which are comparable in extent to the width of the flow, contain most of the flow energy and are responsible for the mixing and the transport of momentum, heat and chemical species; small scale motions, which dissipate the turbulent kinetic energy into heat; and intermediate scale motions which are mostly responsible for transferring energy from larger to smaller scales. The traditional means of analyzing turbulent flow problems is by averaging all fluctuating quantities using the Reynolds decomposition, namely decomposing the instantaneous quantities into mean and fluctuating components. The resulting equations form an open system, namely one that contains more unknowns than equations. An approach that bypasses this impass is to solve approximate equations using turbulence models. For example, a popular model is the k-ϵ model, in which an approximate relationship between the turbulent kinetic energy k and its dissipation rate ϵ is assumed. Unfortunately, these models are found not to be well suited for complicated flows, moreover, they cannot express all physical mechanisms present in turbulence. Additional insight may come from relating the dynamics of the small scales (fine structure) to those of the large scales, as the former would likely be in universal equilibrium regardless how the latter may be evolving. Such a universality has been the focus of many theoretical and experimental studies.

The study of the fine structure of turbulent flows is regarded as a cornerstone in elucidating aspects of combustion and chemical reactions, which occur at the molecular level. In these cases, the turbulent motions are responsible for the creation of fluctuations in the scalar (chemical species or reactant) field which, ultimately, are destroyed by molecular interactions, expressed as the scalar fluctuation destruction rate, commonly referred to as the scalar dissipation rate ϵ_θ. Proper accounting for fine-structure quantities, such as the turbulent kinetic energy dissipation rate ϵ and the scalar dissipation rate ϵ_θ, is also important for turbulence models. Furthermore, modeling of the fine structure is necessary for a powerful numerical technique developed in recent years, known as Large Eddy Simulation (LES), in which large scales, steady or unsteady, are resolved by the numerical scheme, but the fine structure is modeled. LES is becoming increasingly popular because it is within the capabilities of available computers, while being relatively free of errors introduced by averaging fluctuating quantities.

Kolmogorov (1941) was the first to provide scaling laws related to the statistics of fine structure in turbulent flows. Corrsin (1951) and Obukhov (1949) independently extended Kolmogorov's (1941) ideas to include the description of a passive scalar mixed by turbulence and showed that, for Prandtl or Schmidt numbers of the order of one, the scalar fine structure would display scaling laws similar to that of the velocity. The papers by Kolmogorov(1941), Obukhov (1949) and Corrsin (1951) (KOC) have played a major role in the advancement of the understanding of turbulent flows. In particular, the study of the "internal intermittency" of the fine structure of turbulent flows, namely the concept that the fine structure is not uniform but rather localized in space, has led to many intermittency models. These models have been based on numerous experimental and numerical investigations on the statistics of velocity and temperature differences, and dissipation rates in different turbulent flow configurations.

Another aspect of studying the fine structure is its relationship to the large features of a turbulent field, which is expressed by the expectation of the scalar dissipation rate conditional upon the scalar. This approach stems from the derivation of conservation equations for the evolution of the scalar probability density function (pdf) in a turbulent flow (Dopazo and O'Brien, 1974; Pope, 1976; Dopazo, 1976). The formulation of turbulent mixing and/or reaction in terms of probabilities seems to have some distinct advantages over the conventional formulation by terms of statistical moments, which, as mentioned above, requires the use of turbulence models. The pdf approach is capable of treating turbulent reactive flows with arbitrarily complicated reactions without approximation and the closure problem is essentially no more difficult than that for a scalar mixing without reaction, whereas the success of the moments formulation is limited to special cases in which the reaction rates are linear or they are either very fast or very slow compared to the turbulent time scales (Pope, 1985). However, the closure of the scalar dissipation terms is thought to be the stumbling obstacle to the progress in the pdf formulation of turbulent mixing problems. Earlier closures to the transport equation of a scalar pdf, making use of KOC hypotheses (namely that the scalar fine structure is locally isotropic), led to the requirement that the conditional expectation of the scalar dissipation should be independent of the scalar and, in the case of homogeneous turbulence, that the scalar pdf should have a Gaussian distribution. Recent experimental and numerical studies have shown that the distribution of the scalar pdf and the conditional expectation of the scalar dissipation depends strongly on the intermittency and on the initial conditions of the scalar field and that the scalar fine structure evolves differently from the velocity fine structure. In particular, the scalar field was found to be more intermittent than the velocity field, even for Prandtl (or Schmidt) number of the order of one.

As will be shown in the literature review (Chapter 2), most of the experimental studies related to fine structure and intermittency have focused on the statistics of the streamwise velocity derivatives and differences and the effect of Reynolds number on such statistics. These derivatives and differences have been obtained from their time counterparts using Taylor's "frozen flow" approximation. However, only a few references have reported measurements of the statistics of the transverse velocity derivatives and velocity differences and only at a few values of the Reynolds number. The importance of measuring the transverse velocity derivatives and differences is that they are determined without the implication of Taylor's approximation, which cannot be applied accurately in high turbulent intensity flows and in at least part of the inertial spectral range. Furthermore, although a great deal of measurements have been collected in grid-generated, "isotropic" turbulence, this flow is not suitable for measuring the statistics of the transverse velocity derivatives and differences, because many of these properties would vanish under symmetry. A more suitable simplified environment is a uniformly sheared, nearly homogeneous turbulent flow (USF). USF shares many features with non-homogeneous shear flows, namely that their kinetic energy grows due to the production by the mean shear, their Reynolds stresses are anisotropic and they contain coherent motions. On the other hand, USF is unbounded and is free of complex effects such as bursts of fluid near boundaries or turbulent-non turbulent interfaces. Thus, USF permits a simplified analytical description, while at the same time its features are relevant to more complex non-homogeneous turbulent shear flows.

The present work will focus on experimentally studying the streamwise as well as the transverse velocity derivatives and differences in a uniformly sheared, nearly homogeneous turbulent flow. The effect of the variation of Reynolds number on the statistics of such quantities will be assessed. The measured longitudinal and transverse structure functions will be used in the context of the similarity hypotheses (Kolmogorov, 1941) to evaluate existing intermittency models.

Measurements of the streamwise and the transverse scalar derivatives and scalar differences have been extensive. Most of these studies have been conducted in non-homogeneous turbulence and in grid-generated turbulence with a mean scalar gradient. In the latter, the turbulent kinetic energy decays in time whereas the scalar variance increases, which makes the scalar and the velocity fields to evolve differently, and thus complicates a comparison between the states of local isotropy of the two fields. When a mean scalar gradient is imposed on a USF, the balance equation of the turbulent kinetic energy and that of the scalar variance are similar in form and both quantities grow, presumably at the same rate. Such a flow would be more appropriate for comparing the scalar and velocity fine structure statistics without the complicating effect of large scale inhomogeneity found in non-homogeneous shear flows. This was achieved by Tavoularis and Corrsin (1981 b), although at a single Reynolds number and without providing specific inertial scalar structure function measurements. In the present study, scalar derivative and scalar difference statistics will be measured for varying Reynolds number in the same basic configuration, namely a USF with an imposed constant mean scalar gradient.

The literature available on the pdf formulation of scalar mixing has focused on studying the conditional expectation of the scalar dissipation, conditional upon the scalar, which is a term in the transport equation of the scalar pdf. Although numerical simulations and modeling of such a quantity have been extensive, only few experimental results are available. These have been conducted in non-homogeneous shear flows and in grid-generated turbulence. In the present study, the joint statistics between the scalar and the scalar dissipation rate will be evaluated in USF to assess possible dependence of the scalar dissipation rate on the scalar as they evolve under the effect of the mean shear. Furthermore, the literature has also contemplated a relationship between the scalar pdf shape and the resulting conditional scalar dissipation rate. The effect of the advecting velocity field on the scalar mixing has not received as much attention. The scalar pdf shape may reveal the effect of the mean shear on the scalar mixing. Finally, as will be shown in Chapter 4, the evolution equation of the scalar pdf in shear flows with a non-zero mean scalar gradient contains the conditional expectation of the velocity fluctuations conditional upon the scalar. Measurements of this term have been reported in passing in only two experimental studies. The present research will include measurements of such terms and an analysis of their effect on the evolution of the scalar pdf.

The objectives of the present study, briefly outlined above, will be discussed in more detail in Chapter 2, following the literature survey.

It is hoped that the present work will provide a ground for further enhancing the understanding of the fine structure of turbulent flows and that the velocity structure functions obtained in this study will serve as a database for intermenttency models testing. Moreover, statistics obtained for the scalar derivatives and scalar structure functions will allow for better comparison between the fine structures of the scalar and the velocity fields. It is hoped that the results of the conditional scalar dissipation rate in this flow will contribute to the development of better models for the transport equation of the scalar pdf and that the measurements of the conditional expectation of the velocity fluctuations will encourage modelers to include the effect of the velocity field on the mixing in the pdf formulation.

Chapter 2

Literature Review

2.1 The Fine Structure of Turbulence

It was in the early twenties that the concept of a cascade of the breakdown of the turbulent fluctuations into smaller and smaller eddies was introduced. This process suggests that, in turbulent flows, the turbulent kinetic energy of the flow is transferred from the large-scale motions to smaller and smaller motions until it finally dissipates under the effect of viscosity in the eddies of the smallest size. Given this qualitative scheme, Kolmogorov (1941) derived the well known theory of locally isotropic turbulence, namely that, at sufficiently large Reynolds numbers, $Re = ul/\nu$ (u is a characteristic scale of the turbulent velocity fluctuations, l is a characteristic length of the flow and ν is the kinematic viscosity), the fine structure of the flow would be independent of orientation and, therefore, the fine structure would be isotropic. This implies that the joint probability of the differences of velocities at separate points in space would be independent of reflections and rotations of the coordinate system. Physically, local isotropy or universal equilibrium implies that the small scale motions have time scales short enough to rapidly adjust to changing states of the large scale motions, which possess much longer time scales. Then, the fine structure appears to be in equilibrium with the mean flow, even if the latter may be evolving.

An extensive review of Kolmogorov's local isotropy theory has been made by Frisch (1995). Only a brief summary of Kolmogorov's (1941) two similarity hypotheses will be given here. The first hypothesis postulates that, at sufficiently high Reynolds numbers, the motion of the fine structure is independent of the large scales of the flow and that local characteristic length, time and velocity are universal and uniquely determined by the average dissipation rate ϵ, averaged over a volume with a characteristic length L, representing the size of the energy-containing eddies, and the kinematic viscosity ν. An immediate result of the first similarity hypothesis is that normalized moments of velocity derivatives should be constant irrespective of the overall flow geometry and Reynolds number. More specifically, all odd moments of transverse velocity derivatives, such as $\partial u_1/\partial x_2$ must vanish, while even order moments of all derivatives and odd moments of derivatives with reflectional invariance, such as $\partial u_1/\partial x_1$ must be universal. Kolmogorov's second similarity hypothesis states that, for a high enough Reynolds number turbulence, there is a range of scales, smaller then the energy-containing-eddy scale, L, and larger then the Kolmogorov microscale, $\eta = (\nu^3/<\epsilon>)^{1/4}$, called the inertial subrange, in which all statistical laws are governed by the single parameter ϵ and are independent of ν. An implication of the second hypothesis is that the probability density functions of the normalized velocity increments, $\overline{\Delta u}/(r<\epsilon>)^{1/3}$, where $\Delta u = u(x_i+r)-u(x_i)$ and r is a separation distance in the inertial sub-range, would be independent of the flow geometry, r and Reynolds number. Moreover, the second order moment of the longitudinal velocity increment should be related to r and ϵ as $\overline{\Delta u^2} \sim (r<\epsilon>)^{2/3}$.. A more familiar spectral expression of the previous relation is $E_1(\kappa_1) = C_{1\kappa}\langle\epsilon\rangle^{2/3}\kappa_1^{-5/3}$, where $E_l(\kappa_1)$ is the one-dimensional spectrum of the turbulent kinetic energy, κ_1 is the wave-number and C is called the Kolmogorov constant. A more general expression, applying to a structure function of order p, is given by $\overline{\Delta u^p} \sim (r\langle\epsilon\rangle)^{p/3}$. When $p = 3$, an exact relation known as the 4/5 law was given by Kolmogorov (1941) as $\overline{\Delta u^3} = -4/5\ (r\langle\epsilon\rangle)$. Then the skewness of the longitudinal velocity difference should be scale-invariant for scales corresponding to the inertial subrange.

Corrsin (1951) and Obukhov (1949) extended Kolmogorov's theory to describe the local structure of the passive scalar (namely a scalar that has no effect on the velocity field, such as temperature fluctuations in a slightly heated flow) field advected by a high Reynolds number turbulent flow. They hypothesized that, for Prandtl number, $Pr = \nu/\gamma \approx 1$, local isotropy would also manifest itself in the temperature field and that the local parameters would be uniquely determined by ϵ, ν, ϵ_θ and γ, where ϵ_θ and γ are the temperature dissipation rate and the thermal diffusivity respectively. Furthermore, they showed that, within a range of temperature eddies of sizes much smaller than the integral scale but larger than the smallest temperature scale, $\eta_\theta = \eta Pr^{-3/4}$, called the inertial-convective subrange, the statistics would only be determined by ϵ and ϵ_θ and the temperature spectrum would be expressed as $E_\theta(\kappa_1) = C_\theta \langle\epsilon\rangle^{-1/3}\langle\epsilon_\theta\rangle\,\kappa_1^{-5/3}$, where C_θ is called the Corrsin-Obukhov constant. The Kolmogorov scaling for any scalar structure function of order $m + n$ is given by $\overline{\Delta u(r)^m \Delta\theta(r)^n} = C_{mn}(r^{1/3}\epsilon^{1/3})^m(r^{1/3}\epsilon^{-1/6}\epsilon_\theta^{1/2})^n$. An expression for such a structure function in the inertial-convective range when $m = 1$ and $n = 2$ was derived independently of the local isotropy theory by Yaglom (1949) as $\overline{\Delta u(r)\Delta\theta(r)^2} = -4/3\langle\epsilon_\theta\rangle\, r$. Further expressions for structure functions mentioned above were provided by Antonia et al. (1997). Batchelor (1959) elaborated on the Corrsin-Obukhov extension of local isotropy theory to include the effect of Prandtl number ($\nu > \gamma$ and $\nu < \gamma$) on the temperature wave number spectra.

Soon after the introduction of the similarity hypotheses, Landau (1963) argued that the scaling laws may not be universal because the average of the dissipation rate over a volume characteristic of the energy-containing eddies may not be the same for different flows, because these eddies would evolve differently in different flows and Reynolds numbers. The randomness of the dissipation rate has been referred to as internal intermittency.

Early experimental studies on similarity hypotheses have been reported in great detail by Monin and Yaglom (1975). The general assessment of these studies seemed to corroborate Kolmogorov's scaling laws. In particular, the spectra measured in different flow configurations agreed well with the universal scaling. On the other hand, others, by measuring the pdf of velocity derivatives (Batchelor and Townsend, 1949) or the intermittency factor (Kuo and Corrsin, 1971) have shown that the velocity fine structure was indeed intermittent. Some physical models have been proposed (Corrsin, 1962; Tennekes, 1968) to explain the spatial randomness of the dissipative scales.

In order to ensure the consistency of the random spatial variation (intermittency) of the local energy dissipation with the concept of the energy cascade, Obukhov (1962) and Kolmogorov (1962) refined the earlier scaling theories. First, they assumed a log-normal distribution function for the dissipation rate averaged over a sphere of diameter r, ϵ_r. Second, they postulated that the probability distribution of the normalized velocity difference $V = \Delta u/(\epsilon_r\, r)^{1/3}$, would be a universal function of the local Reynolds number $Re_{\epsilon_r} = \epsilon_r^{1/3} r^{4/3}/\nu$. The second similarity hypothesis of Kolmogorov (1941) was refined by Kolmogorov (1962) by assuming that the p^{th} moment of the velocity difference, conditional upon ϵ_r, would be related to r and ϵ_r as, $\Delta u_r^{\,p}|_{\epsilon_r} \sim (r\epsilon_r)^{p/3}$ when $Re_{\epsilon_r} \gg 1$. Kolmogorov

(1962), by using the log-normal model, showed that in the inertial range the longitudinal structure function of order p is given by $\overline{\Delta u_r^p} \sim <\epsilon>^{p/3} r^{\xi_p}$, where the parameter $\xi_p = p/3-(1/18)\mathrm{v}p(p-3)$ is called the scaling exponent. This anomalous scaling is the heart of the study of intermittency in the inertial subrange of high Reynolds numbers incompressible turbulent flow. Furthermore, Wyngaard and Tennekes (1970) showed that, if the log-normal model of ϵ_r applies for very small r, the skewness and flatness of velocity derivatives would be related as $S \sim F^{3/8}$.

The refined similarity hypotheses for a passive scalar, described by Van Atta (1971) and extended or written in other forms by Stolovitzky et al. (1995), can be summarized as follows: the probability distribution of the normalized scalar difference $V_\theta = \Delta\theta(r\epsilon_r)^{1/6}/(r\epsilon_{\theta r})^{1/2}$ is a universal function of the local Reynolds number $Re_{\epsilon_r} = \epsilon_r^{1/3} r^{4/3}/\mathrm{v}$ and the local Peclet number $Pe_{\epsilon_r} = PrRe_{\epsilon_r}$. The second similarity hypothesis states that the pdf of V_θ conditional upon ϵ_r and ϵ_{θ_r} becomes independent of Pe_{ϵ_r} and Re_{ϵ_r} when $Re_{\epsilon_r} \gg 1$, $Pe_{\epsilon_r} \gg 1$ and is, thus, universal.

Research related to the intermittency corrections to the scaling theory of Kolmogorov (1941) includes two aspects: first, experimental and numerical studies of the statistics of the small scales, namely the skewness and flatness of velocity and passive scalar derivatives and their dependence on the turbulent Reynolds number Re_λ, where λ is the Taylor microscale, which may be a bridge in assessing inertial-range intermittency; second, measurements of the structure functions and the pdf of velocity and passive scalar differences, in the hope of determining appropriate corrections and testing of different models of velocity structure functions in the inertial subrange.

Over the past three decades, a large number of experimental and numerical results on the skewness and flatness of the longitudinal velocity derivatives have become available. These include the experimental studies by Gibson et al. (1970), Wyngaard and Tennekes (1970) and Antonia et al. (1981) in atmospheric turbulence, by Antonia et al. (1982) in turbulent plane and circular jets, by Mydlarski and Warhaft (1996) in high Re_λ grid-generated turbulence and the numerical simulations of isotropic turbulence by Kerr (1985) and Jimenez et al. (1993). Most of the measurements of skewness and flatness of velocity derivatives obtained in the above studies have been plotted by Sreenivasan and Antonia (1997) vs. Re_λ. These show a power law growth with Re_λ with the slope for the flatness being steeper than that of the skewness. Frisch (1995) concluded that the data of Benzi et al. (1995) can be described by $S_{\partial u_1/\partial x_1} \sim Re_\lambda^{0.07}$ and $F_{\partial u_1/\partial x_1} \sim Re_\lambda^{0.18}$ and that the data of Anselmet et al. (1984) in a turbulent jet and a turbulent duct flow by $F_{\partial u_1/\partial x_1} \sim Re_\lambda^{0.15}$. Tabeling et al. (1996) measured the skewness and flatness of the longitudinal velocity derivative in helium at 5 K flowing between counter rotating disks, for Re_λ varying from 180 to 5000. Contrary to what has been reported earlier, their results suggested that $S_{\partial u_1/\partial x_1}$ and $F_{\partial u_1/\partial x_1}$ followed an increasing trend up to $Re_\lambda \sim 800$, but decreased as Re_λ increased to about 5000.

In the earlier studies, measurements of higher-order structure functions, necessary for estimating corrections to the inertial range scaling laws, were very limited because these require long and accurate samples of velocities in order to capture the large and rare events which contribute to the higher order structure functions. Among the first experimental studies that reported such measurements is that of Anselmet et al. (1984). These authors measured the longitudinal structure functions up to the 18th order in a turbulent jet and a turbulent duct flow. The main conclusion of their work is that the anomalous exponents of the structure functions had a non-linear variation as the structure function order increased. Structure function exponents have also been obtained by Benzi et al. (1995), who applied the ESS (Extended Self Similarity) method in which the inertial range is determined from plots of $ln(\Delta u^n)$ versus $ln(\Delta u^3)$ instead of $ln(r)$ on the data of Gagne and Hopfinger (1987) and found that the scaling exponents followed the trend described by Anselmet et al. (1984). Other isolated measurements can be found in the book of Frisch (1995).

The log-normal model (Kolmogorov, 1962) has been dismissed based on experimental evidence because it was found to fit the data of Anselmet et al.(1984) only for $n<8$, and for mathematical reasons, as described by Frisch (1995). Other models have been suggested, including the β-model of Frisch et al. (1978), the multi-fractal model (Parisi and Frisch, 1985), the p-model of Meneveau and Sreenivasan (1987), the shell model of She (1991) and the log-Poisson model introduced by She and Lévêque (1994). The mathematical formulations of these models have been given in great detail by Frisch (1995).

Refined similarity hypotheses (RSH) have been tested only recently. The numerical simulation of a 3-D isotropic turbulence of Hosokawa and Yamamoto (1992) was among the first studies on RSH. Their simulation suggested that there was no correlation between the velocity increments $\Delta u_{l,r}$ and the locally averaged dissipation rate ϵ_r, which they claimed as evidence against RSH. Chen et al. (1993) found, in numerical simulations of forced and of decaying turbulence, that $\Delta u_{l,r}$ and ϵ_r were strongly correlated. Chen et al. (1993) also mentioned in their paper that the results of Hosokawa and Yamamoto (1992) were erroneous. Strong correlations between $\Delta u_{l,r}$ and ϵ_r were also found experimentally in a cylindrical wake (Thoroddsen and Van Atta, 1992), in the atmospheric surface layer (Kailasnath et al., 1992) and in a jet and the atmospheric surface layer (Zhu et al., 1995). All the above experimental studies used the surrogate dissipation, namely they evaluated ϵ from the longitudinal streamwise velocity derivative, which can easily be obtained from a single hot-wire. Thoroddsen (1995) obtained estimates of the joint pdf of Δu_{1r} and $\epsilon=15\nu\overline{(\partial u_1/\partial x_1)^2}$ and Δu_{1r} and $\epsilon^*=7.5\nu\overline{(\partial u_2/\partial x_1)^2}$, where u_1 and u_2 are the streamwise and the transverse velocities, in grid-generated turbulence at Re_λ = 208. He found that, while a strong correlation was obtained when using ϵ, the correlation was lost when, instead, ϵ^* was used. Furthermore, the same author suggested that the earlier support for RSH should be revised and that the strong correlation between Δu_{1r} and ϵ was only an artifact of the kinematical content of Δu_{1r} and ϵ. Mydlarski and Warhaft (1996) measured these correlations in high Reynolds number grid-generated turbulence and reported that the correlation between Δu_{1r} and ϵ^* became more pronounced for Re_λ larger than 200, which supports the RSH. The authors suggested that, in grid-generated turbulence, Re_λ should be larger that 200 to separate the dynamical from the kinematical content of the correlation between Δu_{1r} and ϵ^* and Δu_{2r} and ϵ. The support for the RSH has also been reached by Wang et al. (1996) in their simulation of free-decaying, forced and stationary turbulence and Praskovsky et al. (1997) in their experimental work in a mixing layer and in a turbulent channel flow.

Extensive numerical and experimental studies have concentrated on the structure of passive scalars advected by turbulence, with the reasoning that, if local isotropy holds for the scalar field, then, it would also hold for the velocity field. Earlier experiments focused on the estimation of the scalar spectra and the estimation of the Corrsin-Obukhov constant in different turbulent flow configurations (Monin and Yaglom, 1975). More recently, the focus has shifted towards the estimation of the moments of the scalar gradients, in particular of the scalar derivative skewness and flatness. Non-zero skewness of the streamwise scalar gradient, of the order of 1 and almost independent of Reynolds number, has been reported by many researchers, including Gibson et al. (1970) and Sreenivasan et al. (1977) in the atmospheric boundary layer, Sreenivasan et al. (1979) in a turbulent heated jet, Sreenivasan and Tavoularis (1980) in grid-generated turbulence and uniformly sheared turbulence with and without a mean temperature gradient, and by Tavoularis and Corrsin (1981 b) in a uniformly sheared turbulence with a mean temperature gradient. With the exception of the results of Sreenivasan and Tavoularis (1980), the flatness of the streamwise temperature derivative reported in the above studies was larger than the flatness of the streamwise velocity gradient and had a stronger dependence on Reynolds number. Gibson et al. (1977) reported that, in shear flows, the temperature signals possess large scale ramp structures, which they attributed to the coherent nature of these flows, while Sreenivasan et al. (1979) showed that the skewness of streamwise temperature derivatives is a result of these ramp structures. Furthermore, Sreenivasan and Tavoularis (1980) and Tavoularis and Sreenivasan (1981) showed that the skewness is strongly dependent on the large structures of the temperature and the velocity fields and they also confirmed that the sign of the skewness of the streamwise temperature gradient is determined by the sign of both the mean shear and the mean temperature gradient. The above investigations suggest that the scalar structure would be more intermittent than that of the velocity and that local isotropy may be less applicable to a scalar field advected by turbulence.

The scalar transverse derivative skewness and flatness have also been measured in inhomogeneous sheared turbulence (Sreenivasan et al., 1977), in homogeneous shear flow (Tavoularis and Corrsin, 1981b), in stably stratified turbulence (Thoroddsen and Van Atta,1992) and in grid-turbulence with a mean temperature gradient (Tong and Warhaft, 1994; Mydlarski and Warhaft, 1998). The skewness in these flows was also found to depart from the locally isotropic value. Phenomenological models have been put forward by Tavoularis and Corrsin (1981 b), Budwig et al. (1985) and Thoroddsen and Van Atta (1992) to explain possible reasons for non-zero values of the scalar derivative skewness. A more systematic study of this phenomenon has been conducted by Holzer and Siggia (1994) in a numerical simulation of non-convective two-dimensional isotropic flow with a constant mean temperature gradient. This simulation showed that the parallel and perpendicular scalar gradients displayed exponential tails and that the pdf of the perpendicular scalar gradient peaked at zero and thus had very low skewness values, whereas that of the parallel gradient peaked at a value corresponding to the mean temperature gradient $\partial\overline{T}/\partial x_2$ with a skewness of the order of one independently of Reynolds number. Holzer and Siggia (1994) suggested that this skewness gets its contribution form the fact that the scalar gradient from large regions in the flow became concentrated in sharp fronts, a pattern they referred to as "ramp-cliff" structure. This structure has been confirmed by Pumir (1994) in his numerical simulation of scalar mixing in three-dimensional turbulence and by Tong and Warhaft (1994) in their measurements of scalar derivatives in grid-generated turbulence. The latter authors found the parallel-probe derivative skewness to be of the order of 1.8, independently of Reynolds number. This result was partly supported by Mydlarski and Warhaft (1998) in their high Reynolds number grid turbulence with an imposed constant mean scalar gradient, in which the transverse scalar derivative skewness was about 1.4.

In recent years, there has been a renewed interest in examining the intermittent nature of a scalar field by considering the pdf of the scalar derivatives. Among the recent experimental investigations, one could mention those by Castaing et al. (1989), on thermal convection at high Raleigh numbers, Thoroddsen and Van Atta (1992), in stably stratified turbulence, Tong and Warhaft (1994) and Mydlarski and Warhaft (1998) in grid-generated turbulence. Furthermore, large eddy simulations of stably stratified turbulence have been reported by Metais and Lesieur (1992), Pumir (1994 a, b) and Holzer and Siggia (1994). All these studies have concluded that the pdf of the scalar derivatives adopt exponential distributions which are more flared than those of the velocity derivatives, which indicates that the fine structure of the scalar is more intermittent than that of the velocity. Available results on the flatness of the streamwise scalar gradient from different experimental and numerical studies, summarized by Sreenivasan and Antonia (1997), show that, for the scalar field, the fine structure becomes increasingly intermittent as Reynolds number increases.

Another issue related to the intermittency of the scalar fine structure is whether the three components of the scalar dissipation rate are equal, as local isotropy dictates. There have been several experimental studies that attempted the evaluation of the components of the scalar dissipation rate. Sreenivasan et al. (1977) reported that, in a heated turbulent boundary layer, the ratios $R_1=\overline{(\partial\theta/\partial x_2)^2}/\overline{(\partial\theta/\partial x_1)^2}$ and $R_2=\overline{(\partial\theta/\partial x_3)^2}/\overline{(\partial\theta/\partial x_1)^2}$ were larger than 1. Tavoularis and Corrsin (1981 b) found that R_1 and R_2 were roughly equal to 1.8. Antonia and Browne (1986) measured the components of temperature dissipation rate in a turbulent wake and reported that R_1 and R_2 differed from 1 and varied across the wake and that, on the centerline, the measured dissipation was 50% higher than the local isotropy estimates. Thoroddsen and Van Atta (1996) reported values of R_1 and R_2 that departed from 1 in turbulence with a density gradient. Mydlarski and Warhaft (1998) found R_1 to be roughly equal to about 1.4, independently of Reynolds number.

Van Atta (1991) and Thoroddsen and Van Atta (1992) relied on isotropic spectral relations instead of using the equality of the moments of the derivatives to verify the validity of local isotropy theory. Measurements by Thoroddsen and Van Atta (1992) in stably stratified grid-turbulence flow showed that the measured and predicted spectra of the temperature fluctuation derivatives agreed well except at low wave numbers. They suggested that the discrepancy at low wave numbers accounts for the apparent local anisotropy of the moments of the derivatives found by other authors. Antonia and Mi (1993) measured the three components of the temperature dissipation rate in a turbulent heated jet and reported that the three variances were approximately equal, in conformity with local isotropy. Also, their measured temperature derivative spectra agreed well with the spectra obtained from local isotropy relations.

Intermittency of the scalar field in the inertial range has also been considered by many researchers. Sreenivasan (1991) questioned the validity of the universal hypotheses for a scalar field. The argument used is that his measured spectra of temperature fluctuations behind a heated cylinder showed a slope of -4/3 in the inertial range, which is different from the slope of -5/3 depicted by local isotropy theory. He also compiled data of the inertial range slope of scalar spectra from different shear flow experiments, which varied from -1.28 to about -1.63 at the highest Reynolds number considered and suggested an intermittency correction, dependent on Reynolds number, to the scalar spectrum. Jayesh et al. (1994) measured scalar spectra in grid-generated turbulence with and without a mean scalar gradient at a Reynolds number of about 70, based on the integral scale. The scalar spectra showed an inertial range with a slope of -5/3, although the velocity spectra had a scaling exponent of -1.34, and it was about -1.3 in the case of uniform scalar field only when the scalar was introduced farther downstream of the grid; the same conclusion has been reached by Mydlarski and Warhaft (1998). Sreenivasan (1996) argued that, based on results by Jayesh et al. (1994), the Corrsin-Obukhov constant may be better estimated from grid-turbulence experiments than from shear flows, because in the latter the scaling exponent of -5/3 is attainable only at much higher Reynolds numbers (Re_λ>1000). Moreover, Sreenivasan (1996) pointed out that, in shear flows, the streamwise velocity spectra have a slope of -5/3 at lower Reynolds numbers than the transverse velocity spectra or the scalar spectra do and suggested that, for the scalar spectrum to have a -5/3-law inertial range, all components of the velocity must first reach a -5/3 exponent. Antonia et al. (1996), in a turbulent wake of a heated cylinder, considered the second order structure functions of the temperature and the sum of the second order functions of the three velocity components which they interpreted as representing the structure function of the turbulent kinetic energy. Their measurements, at Re_λ of up to 230, showed that both structure functions had similar distributions with their inertial ranges displaying a 2/3-law dependence. This suggests that, in their flow, local isotropy was satisfied at the moderate Reynolds numbers considered and that the Corrsin-Obukhov constant could be evaluated from these structure functions without the requirement of very high Reynolds number as suggested by Sreenivasan (1996). The same conclusions have also been reached by Antonia et al. (1997), who derived a more general form of the KOC scaling laws. Mydlarski and Warhaft (1998) measured the transverse temperature structure functions and found that the second order function had a 2/3 dependence which reflected the -5/3 slope they found in the spectra measured, and that, for their highest Reynolds number, the skewness of the transverse temperature difference was almost independent of the probe spacing within the inertial range. They also showed that, in the inertial range and for the same Reynolds number and separation distance, the pdf of the longitudinal velocity difference was less flared than that of the longitudinal temperature difference, indicating that in the inertial range the scalar field is more intermittent than that of the velocity.

The refined similarity hypotheses for a scalar field have been tested only recently. Hosokawa (1994) proposed an extension of the refined similarity hypotheses for a passive scalar. His extension agreed with the data of Antonia et al. (1994) and Thoroddsen and Van Atta (1992), which supported the refined similarity hypotheses. Zhu et al. (1995) considered the conditional structure functions in a heated jet and in the atmospheric surface layer and their results were consistent with the refined similarity hypotheses. They also reported statistics of the stochastic variables V and V_θ and found that they were independent of the local Reynolds number when the latter was larger than 50, in support of the refined similarity hypotheses. Stolovitzky et al. (1995) proposed expressions for the conditional scalar differences in terms of the surrogate scalar dissipation. They showed that the refined similarity hypotheses were consistent with the evolution equation of the scalar and that the expressions of the similarity hypotheses derived for the scalar differences agreed with their measurements in a heated turbulent wake. Mydlarski and Warhaft (1998) reported that the correlation between the temperature difference and $(r\epsilon_r)^{-1/6}(r\epsilon_{\theta r})^{1/2}$ was high, in support of the refined similarity for passive scalars.

2.2 Probability Distribution Functions of Scalars in Turbulent Flows

Lundgren (1967) and Monin (1968) independently derived a hierarchy of conservation equations for the one-point and the two-point pdf for an incompressible turbulent flow, starting from the Navier-Stokes equations. The key for this method is the definition of a "fine-grained" pdf, as the Dirac function $\delta(A(x_i,t)-B)$, that takes a non-zero value only when the random variable B (independent of the spatial coordinates x_i and time t) is equal to the physical variable A. The pdf can be seen as the mean of $\delta(A(x_i,t),t)$, taken over the ensemble of all initial and boundary conditions.

Although the finite dimensional probability equations are not closed, they have an advantage over the moments equations due to the fact that the convective transport term appears in closed form. Some closures have been proposed for statistically homogeneous (Fox, 1971, 1974; Lundgren, 1972) and nonhomogeneous (Lundgren, 1969) turbulence. Lundgren (1969) developed relaxation models in which the pressure term in the pdf equation was approximated by a relaxation term and obtained analytical solutions for simple flows, which produced satisfactory results.

Dopazo and O'Brien (1974), Pope (1976) and Dopazo (1976) derived transport equations for the scalar joint pdf (the joint pdf of a pair of scalars such as temperature and concentration) and the one-point velocity-scalar joint pdf (Pope, 1985) that describe scalar mixing in turbulent flows. The hierarchy of these equations was found to be better suited for reactive flows than its moments counterpart, because it treats them without approximation regardless how complicated the reactions are. Unfortunately, no set of equations in the hierarchy is closed at any level, mainly due to the molecular mixing terms, namely the conditional expectation of the scalar dissipation that is directly connected to the rate of chemical reaction. The "conditionally Gaussian" assumption was adopted for the evolution of the one-point scalar pdf in homogeneous turbulence and in a turbulent shear flow, to approximate the diffusion term (Dopazo and O'Brien, 1974, 1975; Dopazo, 1976). The key of this model is that the conditional expectations entering the molecular diffusion term are assumed to be Gaussian. The modeled equations in this case were found to produce satisfactory results for the moments of the scalar and the shape of the scalar pdf when applied to passive scalar mixing in isotropic turbulence, but the model failed to predict higher scalar moments when discontinuous initial mean scalar fields, such as the δ-function, were encountered. Pope (1976) proposed a closure model relating the conditional expectation of the scalar dissipation to turbulent characteristics and the integral of a function that Pope himself postulated. The modeled equation in this case produced a good approximation of the evolution of the scalar pdf but failed to relax the pdf to a Gaussian asymptotic state. Considering that the models described above failed to relax the scalar pdf from arbitrary initial conditions, Dopazo (1979) conceived a model that surmounted the relaxation problem. This model contained functions of the scalar pdf, integrated over the scalar space. Unfortunately, the nonlinear and integral nature of the resulting scalar pdf conservation equation permits neither analytical nor numerical solutions for multi-dimensional scalar space.

It is noteworthy to mention that the above models failed to relax the scalar pdf towards a Gaussian distribution, because, in homogeneous velocity and temperature fields, the conditional expectation of the scalar dissipation term entering the balance equation of the scalar pdf has a form of a negative diffusion term that makes the differential equation highly unstable.

Chen et al. (1989) developed a conservation equation for a scalar-scalar spatial gradient joint probability distribution with reaction in homogeneous isotropic turbulence. They proposed a closure that employs a mapping technique that maps the evolution of the scalar field to an initial Gaussian scalar field so as to relax the scalar pdf to a Gaussian distribution. The limitation of this model is that it does not account for the change in the variance of the scalar gradient which is required for local scaling. Gao (1991) applied this technique to the evolution of a passive scalar pdf in homogeneous turbulence. Gao's (1991) analysis was extended by Gao and O'Brien (1991) to include multispecies advection in homogeneous turbulence and by Jiang and Jivi (1992) for binary and trinary scalar mixing. Solutions to the modeled scalar pdf equations yielded pdf that relaxed to Gaussian ones. O'Brien and Jiang (1991) implemented the same closure method to the evolution of a passive scalar pdf in homogeneous turbulence with an initial binary scalar field. Their solution led the scalar pdf to relax to a Gaussian distribution but the asymptotic conditional scalar dissipation rate had no resemblance to the Gaussian solution. They have also proved that, for the homogeneous case, the conditional scalar dissipation rate would not depend on the scalar, if the scalar pdf were Gaussian. The mapping closure technique was also used by Valiño (1995) in conjunction with the Monte-Carlo code, for multispecies mixing in homogeneous turbulence, and resulted in scalar pdf that relaxed to Gaussian ones. Fox (1995) developed and tested a spectral relaxation model, in which the scalar spectrum relaxed to its fully developed form starting from any initial arbitrary shape in both forced and decaying isotropic turbulence. Fox (1997) improved his previous model (Fox, 1995) to account for the effect of the small scale fluctuations on the scalar pdf and its dissipation. Its purpose was to study the scalar and the scalar dissipation statistics as they develop to their steady states.

Eswaran and Pope (1988) performed a direct numerical simulation (DNS) of the turbulent mixing of a passive scalar in isotropic turbulence with an initial scalar pdf consisting of a double δ-function. They reported that the scalar pdf reached a Gaussian asymptotic state. The conditional scalar dissipation, which, in their case, was mainly responsible for the evolution of the scalar pdf, initially exhibited a parabolic shape, at intermediate times it became flat, while at later times it adopted a reversed parabolic shape. Their simulation of the scalar variance-scalar dissipation correlation showed that, initially, the conditional expectation of the scalar dissipation was dependent on the scalar but, at longer times, it reached a zero asymptotic value, supporting the claim that, if the scalar pdf were to become Gaussian, the conditional expectation of the scalar dissipation would be independent of the scalar. Nomura and Elghobashi (1992) conducted a DNS of a passive scalar mixing layer in isotropic and homogeneous sheared turbulence. Their results of the estimated conditional expectation of the scalar dissipation rate in both flows showed that the latter retained a parabolic shape throughout the development of the scalar mixing layer.

Anselmet et al. (1991) conducted an experiment in a weakly heated turbulent boundary layer to investigate the interdependence between the temperature fluctuations variance and their dissipation rates. They represented the temperature dissipation rate by its streamwise component only. Their temperature-temperature dissipation correlations and their joint pdf revealed that the temperature dissipation was strongly dependent on the temperature fluctuations close to the wall and in the outer region of the boundary layer, where the scalar pdf are non-symmetrical due to the intermittent nature of the flow at those regions, but the dependence became very weak at intermediate locations, where the scalar pdf were Gaussian. They also reported measurements of the conditional expectation of the temperature dissipation and found that the latter adopted a constant value only where the temperature fluctuations were symmetrical, i.e. the temperature pdf was Gaussian. Anselmet et al. (1994) repeated these measurements in the same flow as well as in a heated jet using a temperature probe consisting of four temperature wires which allowed them to measure the three components of the scalar dissipation. Spectral and joint-pdf analysis of their measurements revealed that the temperature and its dissipation rate were well correlated and that the conditional expectation of the temperature dissipation depended on the temperature when the temperature fluctuations were not symmetrically distributed. The sign of the correlation followed that of the skewness of the temperature fluctuations. They suggested that, in these flows, the scalar-scalar dissipation correlations had contributions from motions with scales between the integral length scale and the Taylor microscale. Mi et al. (1995) reported measurements in a heated round jet using a set of parallel temperature wires. They argued that the symmetry of the scalar pdf is not a sufficient condition for the scalar-scalar dissipation rate independence as reported by Anselmet et al. (1994), but the flow has to be locally isotropic as well. Their conditional expectation of the temperature dissipation displayed strong peaks in regions with strong temperature fluctuations, near the interface of cold and warm fluid, and it became independent of the temperature fluctuations, in regions with weak activity, where local isotropy prevailed. Jayesh and Warhaft (1992) measured the conditional expectation of temperature dissipation in grid-generated turbulence and found it to maintain a parabolic shape with a sharp minimum along the wind tunnel for the case of an initial constant mean temperature gradient. Accordingly, they found the temperature variance-temperature dissipation correlation to be non-zero. This correlation was close to zero when an initial uniform mean temperature field was employed, but the conditional expectation of the temperature dissipation showed an opposing trend by manifesting a dependency on the scalar variance. Jayesh and Warhaft (1992) associated this discrepancy to the way heating was introduced to the flow. Kailasnath et al. (1993) measured the conditional expectation of scalar dissipation across the wake of a heated cylinder, in the atmospheric boundary layer and in a dyed water jet. Their measurements showed that this quantity was non-uniform in all three cases. It displayed a peak on the positive side of the temperature fluctuations and a larger peak on the positive side for the wake and for the atmospheric boundary layer, but, for the water jet, this quantity had only one peak located on the positive side of the temperature fluctuations. They interpreted their results as an experimental indication that the small scales cannot be locally isotropic but they are influenced by the large structures of the flow.

An important aspect of the conditional expectation of the scalar dissipation, other than being directly related to scalar mixing, is that it is solely responsible for the evolution of the scalar pdf in homogeneous flows. The scalar pdf were thought to follow Gaussian distributions for homogeneous turbulent flows (Tavoularis and Corrsin, 1981a; Kerr, 1985; Eswaran and Pope, 1988; and others). Measurements in thermal convection at high Rayleigh numbers by Castaing et al. (1989) showed temperature fluctuations with pdf having exponential tails in the so called "hard turbulence regime". This result motivated Sinai and Yakhot (1989) to derive a pdf equation for the diffusion of a passive scalar in a random velocity field. An exact closed form solution for the limit of infinite time, obtained by assuming a parabolic shape for the conditional expectation of the scalar dissipation, gave a scalar pdf that exhibited tails that were broader than Gaussian. Valiño and Dopazo (1994) extended Senai and Yakhot's (1989) work to include the time evolution of the scalar pdf using a balance equation for the flatness factor of the scalar fluctuations and assuming a parabolic shape for the conditional expectation of the scalar dissipation and found that the pdf showed exponential tails as the time increased. Yakhot (1989) showed that the scalar pdf would have exponential distribution for thermal convection, if an artificially induced instability were introduced to the thermal boundary layer even at low Rayleigh numbers (soft turbulence). Pumir et al. (1991) and Holtzer and Pumir (1993) developed a one-dimensional model based on a Fourier transform of the scalar pdf advected by turbulence and undergoing molecular mixing. Their model predicted that the scalar pdf would have exponential tails if the scalar were subject to a mean scalar gradient. Metais and Lesieur (1992) used a large eddy simulation of an isotropic and stably stratified flow and predicted that, not only the pdf of the temperature derivatives, but also the pdf of the temperature fluctuations would have exponential tails. They estimated the kurtosis of the temperature variance to be 4, different from the Gaussian value of 3. Gollub et al. (1991) presented measurements for the temperature field in a stirred fluid (oscillating grid flow) in the presence of a steady mean temperature gradient. They reported that the pdf of the temperature fluctuations was Gaussian when the Reynolds number was below a "transition Reynolds number", but, at higher Reynolds numbers, the pdf had pronounced exponential tails and a kurtosis that increased with increasing Reynolds number. Thoroddsen and Van Atta (1992) conducted an experiment in a stably stratified grid-generated turbulence with a linear mean temperature field. Their measurements revealed that, while the pdf of the temperature gradients and those of the second derivatives displayed exponential tails, the pdf of the temperature fluctuations were Gaussian. Jayesh and Warhaft (1991, 1992) measured the pdf of passive temperature fluctuations in isotropic, grid-generated turbulence. The measured scalar pdf showed pronounced exponential tails when the temperature field was subject to a constant mean temperature gradient and when Re_L (Reynolds number based on the integral length scale) was above a critical value, but the pdf were Gaussian when an initial uniform mean temperature field or a thermal mixing layer was introduced to the flow. In contrast, Mydlarski and Warhaft (1998) presented pdf of temperature fluctuations, in their high Reynolds number grid turbulence with a mean temperature gradient, that were sub-Gaussian. They attributed the difference in the scalar pdf from those reported by Jayesh and Warhaft (1991,1992) to the scalar integral scale which, in the latter study, was small enough to allow for temperature excursions to occur and thus produce exponential tails in the scalar pdf. Kerstein and McMurtry (1994 b) showed that the form of the scalar pdf depended strongly on the statistics of the advecting velocity field. Ching and Tu (1994) conducted a two-dimensional numerical simulation of passive scalar advection with and without a mean temperature gradient and Ching and Tsang (1997) conducted a numerical study of random advection of a passive scalar. These authors found that the scalar pdf had exponential tails even in the case in which the mean salar gradient was zero and that the shape of the scalar pdf depended on a parameter representing the ratio of diffusion time to velocity correlation time. A more comprehensive work on the scalar pdf is the one provided by Jaberi et al. (1996). They used a linear eddy model in stationary turbulence as well as DNS in decaying and forced turbulence for the evolution of scalar pdf by varying the initial scalar field, the distributions of the velocity and scalar length scales and the initial concentration of the small scalar scales. Their study revealed that the statistics and the pdf of the scalar depended greatly on the initial conditions, namely that, when the initial scalar integral scales were composed of different sizes larger than the velocity integral scales or when the initial scalar field had a large concentration of small scales, the scalar pdf would evolve towards distributions flatter than Gaussian. Moreover, the same DNS showed that an initial linear mean scalar field was not a sufficient condition for non-Gaussian scalar pdf to occur even at Re_L larger than that suggested by Jayesh and Warhaft (1991,1992). Overholt and Pope (1996) conducted a DNS study of a passive scalar subjected to a mean scalar gradient in isotropic stationary turbulence. Their simulation resulted in a scalar pdf that was nearly Gaussian at Reynolds numbers larger than that suggested by Jayesh and Warhaft (1991,1992).

In non-homogeneous shear flows with a non-zero mean scalar gradient, other unclosed terms, specifically the conditional expectations of the velocity conditional upon scalar, enter the scalar pdf evolution equation. These terms have been given little attention in the literature, because they are expected to be linear for jointly-Gaussian velocity-scalar joint pdf. Sahay and O'Brien (1993) assumed that these terms could be modeled as an odd-order polynomial in grid-generated turbulence with a mean scalar gradient and suggested that they may have an effect on the conditional expectation of the scalar dissipation. Tong and Warhaft (1995) suggested that the conditional expectation of the velocity fluctuations would be linear in the scalar, although their measurements departed slightly from linearity, which they attributed to contaminations of the hot wire by flow reversal. Overholt and Pope (1996) found in their numerical simulation that the conditional expectation of the velocity fluctuation was linear in the scalar. Furthermore, they suggested that in their flow this linearity and the independence of the conditional expectation of the scalar dissipation from the scalar are two sufficient conditions for the scalar pdf to be Gaussian.

2.3 Limitations of Previous Literature and Objectives of the Present Study

The previous literature review has shown that most of the experimental studies associated with Kolmogorov scaling laws and inherent corrections due to intermittency have been conducted in two categories of flows. First, in inhomogeneous flows, such as turbulent jets, the atmospheric surface layer and turbulent wakes. In these flows, the large scales are highly irregular and intermittent and the requirements of very high Reynolds numbers in these flows may be extreme if one is to isolate and study the fine structure without the effect of large scale inhomogeneity. Second, in grid-turbulence. Although in such a flow configuration, high Reynolds numbers have been obtained (Mydlarski and Warhaft, 1996), the isotropy of the turbulent eddies trivializes statistics of the transverse derivatives and structure functions. The experimental studies listed in the literature survey have concentrated on measurements of the longitudinal velocity derivatives and structure functions. These are obtained by invoking Taylor "frozen flow" approximation with which the streamwise spatial velocity derivatives and differences are obtained from their temporal counterparts. Many researchers (Lumley, 1965; Frisch, 1995; Sreenivasan and Antonia, 1997) have expressed a concern regarding the applicability of Taylor's hypothesis for high turbulent intensity flows and in the inertial subrange.

Measurements of the transverse velocity derivatives and structure functions and their variations with Reynolds number have not been as extensive as the longitudinal ones. Only a few studies, including those by Tavoularis and Corrsin (1981 b), who measured the transverse velocity derivative in a uniformly sheared turbulent flow at a single, moderate, Reynolds number and by Mestayer (1982) in a boundary layer at a single Reynolds number and, finally, the numerical simulation of homogeneous shear flow of Pumir (1996), who reported the skewness of the transverse velocity derivatives for Re_λ<100. Boratav and Pelz (1997) evaluated the anomalous exponents from both the longitudinal and the transverse structure functions in their numerical simulation of an unforced turbulent flow at Re_λ of about

100, and suggested that the exponents evaluated from the longitudinal structure functions differed considerably from the exponents evaluated from the transverse ones. It is unfortunate that computational means are limited to low Reynolds numbers (Re_λ<200) when structure functions and velocity derivatives, be it longitudinal or transverse, are considered.

While this work was in progress, similar measurements by Garg and Warhaft (1998) were published. Their maximum Re_λ was 390, which was lower than the highest Re_λ studied here. The present measurements will be compared to their work throughout the course of this report.

In this work, measurements of the longitudinal and transverse velocity derivatives and differences were performed in a uniformly sheared, nearly homogeneous turbulent flow for Reynolds numbers varying from about 140 to about 660. The near homogeneity of the large scales of this flow makes the requirement of high Reynolds number less severe than in inhomogeneous turbulent flows.

For a scalar advected by grid-generated turbulence, one has to impose a non-zero mean scalar gradient to study the statistics of the scalar derivatives, because, in the absence of a mean scalar gradient, the odd order moments would vanish due to symmetry. The case of a scalar advected by grid-generated turbulence in the presence of a constant mean scalar gradient has been investigated by many researchers, but, in this case, the turbulent kinetic energy is decaying whereas the scalar variance is growing with distances from the origin. This means that the velocity and scalar fields evolve differently, so that comparison between the states of local isotropy of the velocity and the scalar fine structures may not be appropriate. In contrast, in homogeneous shear flow, with a mean scalar gradient, the turbulent kinetic energy and the scalar variance have similar balance equations and grow nearly at the same rate, allowing for a better comparison between the states of local isotropy of the velocity and scalar fluctuation fields. Such a flow was studied by Tavoularis and Corrsin (1981 a, b) but at a single Reynolds number and without measuring inertial-range statistics. In the present work, scalar derivative statistics for varying Reynolds number will be reported in uniformly sheared flow with a uniform temperature gradient and results of the longitudinal and transverse scalar difference statistics will be presented.

The literature review showed that there have been numerous numerical studies related to the pdf formulation of scalar advection. These have focused mainly on the expectation of the scalar dissipation conditional upon the scalar. However, only a few experimental studies are available in the literature. These were conducted in non-homogeneous turbulent shear flows (Anselmet et al., 1991, 1994; Kailasnath et al., 1993; Mi at al., 1995) and in grid-generated turbulence (Jayesh and Warhaft, 1992) and the results of the conditional scalar dissipation rate in the above studies are somewhat conflicting. In the present study, measurements of the joint statistics of the scalar and its dissipation rate will be done and the results may serve as a bridge between those obtained in non-homogeneous flows and those obtained in grid-generated turbulence. The scalar dissipation rate will be estimated from its streamwise component which was found to be a good approximation in homogeneous turbulence (Kailasnath et al., 1993; Jayesh and Warhaft, 1992).

The evolution of the scalar pdf for uniform mean scalar and mean velocity fields is solely controlled by the conditional expectation of the scalar dissipation, but, in shear flows with non-uniform mean scalar gradient, other terms such as the expectations of the velocity conditional upon the scalar enter the scalar pdf evolution equation. Other than the results by Tong and Warhaft (1995), no measurements of the conditional velocity statistics have been reported. Tong and Warhaft (1995) presented measurements of the conditional expectation of the velocity in a heated jet but it seems that, in some regions of the flow, their hot-wire measurements were contaminated by flow reversal. In this report, the statistics of the conditional expectation of the velocity fluctuations will be presented and their contribution to the evolution of the scalar pdf will be determined.

The models developed for the pdf formulation of scalar mixing have focused on the model's ability to relax the scalar pdf to a Gaussian state in stationary isotropic turbulence without the presence of a mean scalar gradient. Under such conditions, there would be no effect of the velocity field on the mixing. Fox (1996) developed a model for the velocity-conditioned scalar pdf which includes the effects of anisotropy and of the mean velocity gradient on the mixing. The modeled equation was applied in homogeneous sheared turbulence in the presence of a mean temperature gradient and was shown that, unlike the case of isotropic turbulence with a mean scalar gradient, the velocity-scalar correlation vector was affected by the velocity field. The present research would be a suitable test for the validity of this model.

Chapter 3

Statistical Definitions

The flow characteristics in turbulent flows are random, which makes a deterministic approach impossible and necessitates the use of a statistical approach. The statistical approach does not attempt to predict the values of a random variable; instead, the theory aims at determining the probability that random variables would take specified values.

The definitions described below can be found in the review by Pope (1985), but some of the symbols have been changed to follow those used in most other publications.

3.1 Distribution Function

The distribution function $P_\theta(\psi)$ of a random variable, θ, is by definition the probability that $\psi \leq \theta$, i.e;

$$P_\theta(\psi)=\wp(\theta \leq \psi) \tag{3.1}$$

$P_\theta(\psi)$ is a non-decreasing function of ψ that increases from 0 to 1 as ψ varies from $-\infty$ to $+\infty$.

3.2 Probability Density Function

The probability density function (pdf) $p_\theta(\psi)$ of a random variable, θ, is defined as the derivative of the distribution function as

$$p_\theta(\psi) = \frac{dP_\theta(\psi)}{d\psi} \tag{3.2}$$

Since $P_\theta(\psi)$ is a non-decreasing function of ψ, $p_\theta(\psi)$ cannot be negative, i.e;

$$p_\theta(\psi) \geq 0 \tag{3.3}$$

Other obvious properties of $p_\theta(\psi)$ are

$$p_\theta(-\infty) = p_\theta(+\infty) = 0 \tag{3.4}$$

$$\int_{-\infty}^{\infty} p_\theta(\psi)d\psi = 1 \tag{3.5}$$

$$P(\psi \leq \theta < \psi + d\psi) = p_\theta(\psi)d\psi \tag{3.6}$$

3.3 Moments and Correlations

The mean or the expected value, $<\theta>$, is defined as

$$<\theta> = \int_{-\infty}^{\infty} \psi \, p_\theta(\psi)d\psi \tag{3.7}$$

The n^{th} central moment is defined as

$$\mu_n = <\theta^n> = \int_{-\infty}^{\infty} (\psi - <\theta>)^n \, p_\theta(\psi) d\psi \tag{3.8}$$

The variance is the second central moment of θ and its square root is referred to as the standard deviation or the root mean square of the random variable θ. The "skewness factor" indicating the degree of symmetry of a distribution is defined as

$$S = \frac{\mu_3}{\mu_2^{3/2}} \tag{3.9}$$

and the "flatness factor" or kurtosis is defined as

$$F = \frac{\mu_4}{\mu_2^{2}} \tag{3.10}$$

Let $X(\theta)$ be an integrable function of θ ; then, $<X>$ is defined as

$$<X(\theta)> = \int_{-\infty}^{\infty} X(\psi) p_\theta(\psi) d\psi \tag{3.11}$$

In the case of a stationary (the statistical properties do not depend on a shift of the time origin) and ergodic (time averages are equal to ensemble averages) random process, the mean can be computed as

$$\bar{\theta} = \lim_{T \to \infty} \frac{1}{2T} \int_{-T}^{T} \theta(t) dt \tag{3.12}$$

For a stationary and ergodic random process, the autocorrelation function is defined as

$$R_\theta(\tau) = \lim_{T \to \infty} \frac{1}{2T} \int_{-T}^{T} \theta(t+\tau)\theta(t) dt \tag{3.13}$$

3.4 Spectra

The one dimensional "frequency spectrum" is defined as the Fourier transform of the autocorrelation function, i.e.

$$F_{\theta}(f) = \int_{-\infty}^{\infty} R_{\theta}(\tau) e^{-j2\pi f\tau} dt \,, \qquad j=\sqrt{-1} \tag{3.14}$$

Taylor's "frozen flow" approximation is the assumption that a fluctuating property remains "frozen" (i.e. unchanged) while a fluid volume is convected past a measuring probe. This permits the substitution of time derivatives by streamwise space derivatives, as

$$\frac{\partial(...)}{\partial x_1} \approx -\frac{1}{\overline{U_1}}\frac{\partial(...)}{\partial t} \tag{3.15}$$

This assumption, also referred to as Taylor' hypothesis, can be justified only for low turbulence intensity (Tavoularis, 1986). It may further be used to evaluate the streamwise one-dimensional wave-number spectrum from the frequency spectrum, as

$$E_{1\theta}(\kappa_1) = \frac{\overline{U_1}}{2\pi} F_{\theta}(f) \tag{3.16}$$

where κ_1 is the streamwise wave-number, defined as

$$\kappa_1 = \frac{2\pi f}{\overline{U_1}} \tag{3.17}$$

3.5 Integral Length Scales

The integral length scales represent the order of magnitude of the size of entities with relative motions contributing the most to the turbulent kinetic energy (energy-containing eddies). The streamwise Eulerian integral length scale, $L_{11,1}$, can be determined from the corresponding integral time scale, T_{11}, as

$$L_{11,1} = \overline{U}_1 T_{11} \tag{3.18}$$

where

$$T_{11} = \int_0^\infty \frac{\overline{u_1(t)\ u_1(t+\tau)}}{\overline{u_1^2}} d\tau \tag{3.19}$$

Integral length scales for temperature fluctuations can be defined by analogy to the above equation.

3.6 Taylor and Corrsin Microscales

The Taylor microscale, was originally defined as a unique scalar for isotropic turbulence. In non-isotropic turbulence, one may define a tensorial Taylor microscale, as

$$\begin{aligned} \lambda_{ii} &= \left[\frac{\overline{u_i^2}}{\overline{(\partial u_i / \partial x_i)^2}}\right]^{1/2} && i \text{ not summed} \\ \lambda_{ij} &= \left[\frac{2\overline{u_i^2}}{\overline{(\partial u_i / \partial x_j)^2}}\right]^{1/2} && i \neq j \end{aligned} \tag{3.20}$$

Using Taylor's approximation, the streamwise Taylor microscale, λ_{11}, can be estimated as

$$\lambda_{11} \approx \overline{U_1} \left[\frac{\overline{u_1^2}}{\overline{(\partial u_1 / \partial t)^2}} \right]^{1/2} \tag{3.21}$$

The streamwise "Corrsin microscale" for the fluctuating temperature field is defined as

$$\lambda_{\theta_1} = \left[\frac{2\overline{\theta^2}}{\overline{(\partial \theta / \partial x_1)^2}} \right]^{1/2} \tag{3.22}$$

Using Taylor's hypothesis, the streamwise Corrsin microscale can be estimated from the mean square temporal derivative of temperature as

$$\lambda_{\theta_1} \approx \overline{U_1} \left[\frac{2\overline{\theta^2}}{\overline{(\partial \theta / \partial t)^2}} \right]^{1/2} \tag{3.23}$$

3.7 Kolmogorov, Corrsin-Obukhov and Batchelor Microscales

Turbulent kinetic energy dissipates into heat by the viscous action at the smallest scales of the flow. The size of these "dissipative eddies" is comparable to the "Kolmogoroff microscale", defined as

$$\eta = \left(\frac{\nu^3}{\epsilon} \right)^{1/4} \tag{3.24}$$

where ν is the kinematic viscosity and ϵ is the dissipation rate of the turbulent kinetic energy.

The "Corrsin-Obukhov microscale", corresponding to the smallest temperature fluctuation scale for a Prandtl number of the order of one (Holzer and Siggia, 1994), is given by

$$\eta_\theta = \left(\frac{\gamma}{\nu}\right)^{3/4} \eta = (Pr)^{-3/4} \eta \tag{3.25}$$

where γ is the thermal diffusivity.

In the case of large Prandtl or Schmidt numbers, the part of the scalar power spectrum corresponding to very high wave numbers is referred to as the "viscous diffusive" subrange. The smallest scale in that subrange is called the "Batchelor microscale" (Holzer and Siggia, 1994) and it is defined as

$$\eta_B = \left(\frac{\gamma}{\nu}\right)^{1/2} \eta = (Pr)^{-1/2} \eta \tag{3.26}$$

3.8 Joint Probability Density Functions

The joint distribution function $P_{u\theta}(U,\psi)$ of the random variables u and θ is defined as the probability that $U \le u$ and $\psi \le \theta$ as

$$P_{u\theta}(U,\psi) = \wp(U \le u \;,\; \psi \le \theta) \tag{3.27}$$

The joint pdf of u and θ is given by

$$p_{u\theta}(U,\theta) = \frac{\partial^2}{\partial U \partial \psi} P_{u\theta}(U,\psi) \tag{3.28}$$

Let $Y(U,\psi)$ be an integrable function of u and θ; then its mean is defined as

$$<Y(u,\theta)> = \int_{-\infty}^{\infty}\int_{-\infty}^{\infty} Y(U,\psi)p_{u\theta}(U,\psi)dUd\psi \tag{3.29}$$

Similarly, the covariance $<u\theta>$ is defined as

$$<u\theta> = \int_{-\infty}^{\infty}\int_{-\infty}^{\infty}(U-<u>)(\psi-<\theta>)p_{u\theta}(U,\psi)dUd\psi \tag{3.30}$$

where the brackets designate an average or expectation.

For two jointly stationary and ergodic random processes u and θ, the cross-correlation function is defined as

$$R_{u\theta} = \lim_{T\to\infty}\frac{1}{2T}\int_{-T}^{T}\psi(t+\tau)U(t)dt \tag{3.31}$$

3.9 Conditional Probabilities

The conditional probability of the event A, conditioned upon the event B, is defined as

$$\wp(A|B) = \frac{\wp(AB)}{\wp(B)} \tag{3.32}$$

where $\wp(AB)$ is the joint probability of the joint event A and B. For the random variables u and θ and considering the events

$$\begin{aligned} A &= u \leq U \\ B &= \psi \leq \theta \leq \psi + \Delta\psi \end{aligned} \tag{3.33}$$

equation (3.32) becomes

$$\wp(u \le U | \psi \le \theta \le \psi + \Delta\psi) = \frac{\int_{-\infty}^{U} \int_{\psi}^{\psi+\Delta\psi} p_{u\theta}(U,\psi) dU d\psi}{\int_{\psi}^{\psi+\Delta\psi} p_{\theta}(\psi) d\psi} \tag{3.34}$$

In the limit when $\Delta\psi \to 0$, one gets

$$P_{u|\theta}(U|\psi) = \wp(u \le U | \theta = \psi) = \frac{\int_{-\infty}^{U} p_{u\theta}(U,\psi) dU}{p_{\theta}(\psi)} \tag{3.35}$$

The conditional pdf $p_{u|\theta}(U|\psi)$ is the derivative of the above equation with respect to U, namely

$$p_{u|\theta}(U|\psi) = \frac{p_{u\theta}(U,\psi)}{p_{\theta}(\psi)} \tag{3.36}$$

One can regard $p_{u|\theta}(U|\psi)dU$ as the probability that $U \le u \le U+dU$ when $\theta = \psi$, and from which the joint pdf $p_{u\theta}(U,\psi)$ is recovered as

$$p_{u\theta}(U,\psi) = p_{u|\theta}(U|\psi) p_{\theta}(\psi) \tag{3.37}$$

$p_u(U)$ and $p_\theta(\psi)$ are called the marginal pdf's of u and θ, respectively.

If $Y(U,\psi)$ is an integrable function of u and θ, the conditional mean of $Y(U,\psi)$ is given by

$$\langle Y(U,\psi) | \theta = \psi \rangle = \int_{-\infty}^{\infty} Y(U,\psi) P_{u|\theta}(U|\psi) dU \tag{3.38}$$

The unconditional mean of $Y(U,\psi)$ can be computed as

$$\begin{aligned}
<Y(U,\psi)> &= \int_{-\infty}^{\infty}\int_{-\infty}^{\infty} Y(U,\psi)p_{u\theta}(U,\psi)dUd\psi \\
&= \int_{-\infty}^{\infty}\int_{-\infty}^{\infty} Y(U,\psi)p_{\theta}(\psi)p_{u|\theta}(U|\psi)dUd\psi \\
&= \int_{-\infty}^{\infty} p_{\theta}\left\{\int_{-\infty}^{\infty} p_{u|\theta}(U|\psi)Y(U,\psi)dU\right\}d\psi \\
&= \int_{-\infty}^{\infty} p_{\theta}(\psi)<Y(U,\psi)|\theta=\psi>d\psi
\end{aligned} \tag{3.39}$$

where $<Y(U,\psi)|\theta=\psi>$ is the conditional expectation of the function $Y(U,\psi)$, conditioned upon the random variable θ.

In the next Chapter, terms such as $<Y(U,\psi)\delta(\theta-\psi)>$, where δ is Dirac's function, will often be encountered. These will be reduced following the above procedure as follows

$$\begin{aligned}
<Y(U,\psi)\delta(\theta-\psi)> &= \int_{-\infty}^{\infty} p_{\theta}(\psi')<Y(U,\psi)\delta(\theta-\psi)|\theta=\psi'>d\psi' \\
&= \int_{-\infty}^{\infty} p_{\theta}(\psi')\delta(\psi'-\psi)<Y(U,\psi)|\theta=\psi'>d\psi' \\
&= p_{\theta}(\psi)<Y(U,\psi)|\theta=\psi>
\end{aligned} \tag{3.40}$$

Chapter 4

Mathematical Description of the Flow

4.1 The Velocity Field

4.1.1 Equation for the Means and Fluctuations

The Navier-Stokes equation applied to a viscous, incompressible fluid in the absence of body forces is given by

$$\frac{\partial U_i}{\partial t} + U_j \frac{\partial U_i}{\partial x_j} = -\frac{1}{\rho} \frac{\partial P}{\partial x_i} + \nu \frac{\partial^2 U_i}{\partial x_j \partial x_j} \tag{4.1}$$

and the continuity equation corresponding to the conservation of mass is given by

$$\frac{\partial U_j}{\partial x_j} = 0 \tag{4.2}$$

where U_i is the instantaneous local velocity, t is the time, x_i is the Cartesian coordinate system, ρ is the fluid density, P is the instantaneous pressure, ν is the kinematic viscosity and the indices $i, j = 1, 2, 3$ follow the summation convention.

Following Reynolds decomposition, one may decompose the instantaneous velocity and instantaneous pressure as

$$U_j = \overline{U}_j + u_j \tag{4.3}$$

$$P = \overline{P} + p \tag{4.4}$$

where $\overline{U}_j$ and $\overline{P}$ represent the mean values of the velocity and pressure, respectively, and u_j and p are the velocity and pressure fluctuations.

Substituting equations (4.3) and (4.4) in equation (4.1) and averaging the resulting equation, one gets the mean momentum equation as

$$\frac{\partial \overline{U}_i}{\partial t} + \overline{U}_j \frac{\partial \overline{U}_i}{\partial x_j} = -\frac{1}{\rho}\frac{\partial \overline{P}}{\partial x_i} + \nu \frac{\partial^2 \overline{U}_i}{\partial x_j \partial x_j} - \frac{\partial \overline{u_i u_j}}{\partial x_j} \tag{4.5}$$

where $\overline{u_i u_j}$ is called the Reynolds (or turbulent) stress tensor (per unit mass).

The momentum equation for the velocity fluctuations may be obtained by subtracting equation (4.5) from equation (4.1) as

$$\frac{\partial u_i}{\partial t} + \overline{U}_j \frac{\partial u_i}{\partial x_j} + u_j \frac{\partial \overline{U}_i}{\partial x_j} + u_j \frac{\partial u_i}{\partial x_j} = -\frac{1}{\rho}\frac{\partial P}{\partial x_i} + \nu \frac{\partial^2 u_i}{\partial x_j \partial x_j} + \frac{\partial \overline{u_i u_j}}{\partial x_j} \tag{4.6}$$

4.1.2 Balance Equation for the Turbulent Kinetic Energy

Turbulent kinetic energy per unit mass is defined as

$$k = \frac{1}{2}\,\overline{u_i u_i} = \frac{1}{2}\,(\overline{u_1^2} + \overline{u_2^2} + \overline{u_3^2}) \tag{4.7}$$

An equation for this quantity is obtained by multiplying equation (4.6) by u_i and averaging and omitting all vanishing terms as

$$\frac{\partial k}{\partial t} + \overline{U}_j \frac{\partial k}{\partial x_j} = -\overline{u_i u_j}\,\frac{\partial \overline{U}_i}{\partial x_j} - \frac{\partial}{\partial x_j}\,\overline{u_j\left(\frac{p}{\rho}+k\right)} + \nu\,\overline{u_i \frac{\partial^2 u_i}{\partial x_j \partial x_j}} \tag{4.8}$$

4.1.3 Form of the Turbulent Kinetic Energy in USF

In stationary, uniformly sheared, nearly homogeneous turbulence, the velocity components $\overline{U}_2$ and $\overline{U}_3$ vanish, the streamwise mean velocity $\overline{U}_1$ varies in the transverse direction x_2 only and the turbulence is nearly homogeneous in x_2 and x_3. Applying these assumptions to equation (4.8) and omitting all negligible terms (Tavoularis and Corrsin, 1981 a) one gets

$$\overline{U_1}\,\frac{dk}{dx_1} \approx -\overline{u_1 u_2}\,\frac{d\overline{U_1}}{dx_2} - \epsilon \tag{4.9}$$

where ϵ is the mean dissipation rate of the turbulent kinetic energy, equal to

$$\epsilon = \frac{1}{2}\nu\,\overline{\left(\frac{\partial u_i}{\partial x_j} + \frac{\partial u_j}{\partial x_i}\right)\left(\frac{\partial u_i}{\partial x_j} + \frac{\partial u_j}{\partial x_i}\right)} \tag{4.10}$$

4.2 Scalar Transport Equations

4.2.1 Instantaneous Scalar Balance Equation

Turbulence transports contaminants such as heat, chemical species and particles in much the same way as momentum. Consider the transport of a passive scalar (for example, temperature in flow with small amounts of heat so that the velocity field is not altered) in a turbulent flow of an essentially constant density fluid. The conservation equation of such a scalar requires that the total rate of change of the scalar balances its molecular diffusion, as

$$\frac{\partial T}{\partial t} + U_j\frac{\partial T}{\partial x_j} = \gamma\frac{\partial^2 T}{\partial x_j \partial x_j} \tag{4.11}$$

where γ is the molecular diffusivity. Equation (4.11) describes the instantaneous temperature field as well as any other transported passive scalar. Following Reynolds decomposition one may decompose the instantaneous velocity and temperature as

$$U_j = \overline{U_j} + u_j \tag{4.12}$$

$$T = \overline{T} + \theta \tag{4.13}$$

where $\overline{T}$ and $\overline{U_j}$ represent the mean values of the temperature and velocity, respectively, and θ and u_j designate the temperature and velocity fluctuations. Substitution of equations (4.12) and (4.13) in equation (4.11) yields

$$\frac{\partial(\overline{T} + \theta)}{\partial t} + (\overline{U_j} + u_j)(\frac{\partial \overline{T}}{\partial x_j} + \frac{\partial \theta}{\partial x_j}) = \gamma \frac{\partial^2 \overline{T}}{\partial x_j \partial x_j} + \gamma \frac{\partial^2 \theta}{\partial x_j \partial x_j} \tag{4.14}$$

4.2.2 Balance Equation for the Mean Scalar

Ensemble averaging equation (4.14), and omitting all vanishing fluctuating quantities, one may obtain the balance equation for the mean temperature field as

$$\frac{\partial \overline{T}}{\partial t} + \overline{U_j}\frac{\partial \overline{T}}{\partial x_j} = \gamma \frac{\partial^2 \overline{T}}{\partial x_j \partial x_j} - \frac{\partial \overline{\theta u_j}}{\partial x_j} \tag{4.15}$$

4.2.3 Balance Equation for the Scalar Fluctuations

The balance equation for the temperature fluctuations is obtained by subtracting equation (4.15) from equation (4.14). The resulting equation is

$$\frac{\partial \theta}{\partial t} + \overline{U_j}\frac{\partial \theta}{\partial x_j} + u_j \frac{\partial \overline{T}}{\partial x_j} + \frac{\partial \theta u_j}{\partial x_j} - \frac{\partial \overline{\theta u_j}}{\partial x_j} = \gamma \frac{\partial^2 \theta}{\partial x_j \partial x_j} \tag{4.16}$$

4.2.4 Balance Equation for the Scalar Variance

Multiplying equation (4.16) by θ and averaging, one obtains a balance equation for the mean squared temperature fluctuations as

$$\frac{\partial \overline{\theta^2}}{\partial t} + \overline{U_j}\frac{\partial \overline{\theta^2}}{\partial x_j} = -2\overline{u_j\theta}\frac{\partial \overline{T}}{\partial x_j} - \frac{\partial \overline{\theta^2 u_j}}{\partial x_j} + \gamma\frac{\partial^2 \overline{\theta^2}}{\partial x_j \partial x_j} - 2\gamma\overline{\frac{\partial \theta}{\partial x_j}\frac{\partial \theta}{\partial x_j}} \tag{4.17}$$

4.2.5 Balance Equation for the Scalar Variance in USF with an Imposed Constant Mean Scalar Gradient

In addition to the assumptions made about the velocity field in USF, here it is assumed that the scalar fluctuations are homogeneous in the x_2 and x_3, the mean scalar varies linearly in x_2 and the mean temperature is nearly constant along any streamline in the streamwise direction (Tavoularis and Corrsin, 1981a). Applying these approximations to equation (4.17) and omitting the negligible terms yields

$$\overline{U_1}\frac{d\overline{\theta^2}}{dx_1} \approx -2\overline{u_2\theta}\frac{d\overline{T}}{dx_2} - 2\,\epsilon_\theta \tag{4.18}$$

where

$$\epsilon_\theta = \gamma \left(\overline{\left(\frac{\partial \theta}{\partial x_1}\right)^2} + \overline{\left(\frac{\partial \theta}{\partial x_2}\right)^2} + \overline{\left(\frac{\partial \theta}{\partial x_3}\right)^2} \right) \tag{4.19}$$

The main conclusion of these derivations is that, when comparing equations (4.9) and (4.18), one notices that the balance equations for the turbulent kinetic energy and the scalar variance are similar in form and, presumably, the velocity and the scalar field may evolve in the same manner allowing for a comparison between the state of the fine structure of the scalar field to that of the velocity.

4.3 Pdf Formulation

4.3.1 The Scalar Pdf

Equation (4.17), the balance equation for the temperature fluctuation variances, gives rise to non-closed terms, such as the turbulent transport terms. In this so called moments formulation, these terms have to be modeled in order to solve the equation. Several models associated with this method generally rely on gradient transport approximations. Although these models were successful in treating simple flows, such as passive scalar mixing in homogeneous turbulence, they were found to be inaccurate in treating turbulent reactive flows. Density variations and chemical reactions in these flows were found to be easily accommodated in a pdf formulation and the closure problem associated with the pdf method is not more difficult than that for a scalar mixing without reaction.

The method of deriving a pdf conservation equation was introduced by Lundgren (1967). Adopting Lundgren's technique, one can arrive at a conservation equation for the pdf of a scalar mixed by turbulence as follows.

First a "fine-grained" one-point scalar probability density function, namely the scalar pdf in one realization of the flow, is defined as

$$\rho(\psi, x_p, t) = \delta[\theta(x_p, t) - \psi] \tag{4.20}$$

where δ is the Dirac function and ψ is called the sample space of the random variable $\theta(x,t)$; the ψ-space is also referred to as the scalar or temperature space.

Then, the one-point pdf is defined as the average of the "fine-grained" pdf as

$$p(\psi, x_p, t) = \langle\rho(\psi, x_p, t)\rangle = \langle\delta[\theta(x_p, t) - \psi]\rangle \tag{4.21}$$

4.3.2 Transport Equation for the Scalar Pdf

For the remainder of the derivation, $p(\psi,x,t)$ will be denoted by p. Taking the time derivative of equation (4.21) (Lundgren, 1967) yields

$$\begin{aligned} \frac{\partial p}{\partial t} &= \langle\frac{\partial}{\partial t}\delta(\theta-\psi)\rangle \\ &= \langle\frac{\partial\theta}{\partial t}\frac{\partial\delta(\theta-\psi)}{\partial\theta}\rangle \\ &= \langle-\frac{\partial\theta}{\partial t}\frac{\partial\delta(\theta-\psi)}{\partial\psi}\rangle \end{aligned} \tag{4.22}$$

The last step in equation (4.22) follows because an infinitesimal change in θ of $d\theta$ has the same effect on the δ-function as a change in ψ of $d\psi = -d\theta$.

Substituting for $\partial\theta/\partial t$ from equation (4.16) into equation (4.22), one gets

$$\frac{\partial p}{\partial t} = \left\langle \overline{U}_j \frac{\partial \theta}{\partial x_j} \frac{\partial \delta(\theta-\psi)}{\partial \psi} \right\rangle + \left\langle u_j \frac{\partial \overline{T}}{\partial x_j} \frac{\partial \delta(\theta-\psi)}{\partial \psi} \right\rangle + \left\langle \frac{\partial (\theta u_j)}{\partial x_j} \frac{\partial \delta(\theta-\psi)}{\partial \psi} \right\rangle$$
$$- \left\langle \frac{\partial \overline{\theta u_j}}{\partial x_j} \frac{\partial \delta(\theta-\psi)}{\partial \psi} \right\rangle - \left\langle \gamma \frac{\partial^2 \theta}{\partial x_j \partial x_j} \frac{\partial \delta(\theta-\psi)}{\partial \psi} \right\rangle \tag{4.23}$$

The detailed derivations provided in appendix (A) lead to the following balance equation for the temperature fluctuations pdf

$$\frac{\partial p}{\partial t} + \overline{U}_j \frac{\partial p}{\partial x_j} + \frac{\partial}{\partial x_j}[\langle u_j | \theta=\psi \rangle\, p] + \frac{\partial \overline{\theta u_j}}{\partial x_j} \frac{\partial p}{\partial \psi} = \gamma \frac{\partial^2 p}{\partial x_j \partial x_j} - \frac{\partial^2}{\partial \psi^2}[\langle \epsilon_\theta | \theta=\psi \rangle\, p]$$
$$+ \frac{\partial \overline{T}}{\partial x_j} \frac{\partial}{\partial \psi}[\langle u_j | \theta=\psi \rangle\, p] \tag{4.24}$$

where

$\langle u_j | \theta=\psi \rangle$ and $\langle \epsilon_\theta | \theta=\psi \rangle$ are the conditional expectations of the velocity fluctuations and the scalar dissipation rate respectively.

$\frac{\partial p}{\partial t} + \overline{U}_j \frac{\partial p}{\partial x_j}$ is the total rate of change of the temperature pdf.

$\frac{\partial}{\partial x_j}[\langle u_j | \theta=\psi \rangle\, p]$ is the turbulent transport of the temperature pdf in physical space.

$\frac{\partial \overline{\theta u_j}}{\partial x_j} \frac{\partial p}{\partial \psi}$ is the transport of the temperature pdf by the gradient of the turbulent fluxes in the ψ-space.

$\gamma \frac{\partial^2 p}{\partial x_j \partial x_j}$ is the molecular diffusion of the temperature pdf in the physical space.

$-\frac{\partial}{\partial \psi^2}[\langle \epsilon_\theta | \theta=\psi \rangle\, p]$ is the molecular diffusion of the temperature pdf in ψ-space.

$\frac{\partial \overline{T}}{\partial x_j}[\langle u_j | \theta=\psi \rangle\, p]$ is the turbulent transport of the temperature pdf in ψ-space.

The last term accounts for the production of the scalar by the action of the turbulent velocity on the mean scalar field.

One should recall that the term $\overline{\theta u_j}$ in equation (4.24) can be expressed in terms of probabilities as

$$\overline{\theta u_j} = \int_{-\infty}^{\infty} \psi < u_j | \theta = \psi > p(\psi, x_p, t) d\psi$$

4.3.3 Form of the Scalar Pdf Equation in Uniformly Sheared Turbulence with an Imposed Constant Mean Scalar Gradient

To identify the terms in equation (4.24) that are to be measured and assess their contributions to the evolution of the temperature fluctuations pdf in this study, equation (4.24) has to be implemented for the temperature mixing in a uniformly sheared turbulence with a constant mean scalar gradient. In this flow configuration, one can invoke the flow assumptions mentioned above. Then, after omitting negligible terms, the transport equation for the scalar pdf, equation (4.24), reduces to

$$\begin{aligned} \overline{U_1}\frac{\partial p}{\partial x_1} + \frac{\partial}{\partial x_1}[< u_1 | \theta = \psi > p] + \frac{\partial \overline{\theta u_1}}{\partial x_1}\frac{\partial p}{\partial \psi} &= - \frac{\partial^2}{\partial \psi^2}[< \epsilon_\theta | \theta = \psi > p] \\ &+ \frac{\partial \overline{T}}{\partial x_2}\frac{\partial}{\partial \psi}[< u_2 | \theta = \psi > p] \end{aligned} \tag{4.25}$$

At this stage, it is important to point out that for a homogeneous flow with a zero mean scalar gradient, the scalar pdf evolves solely under the effect of the conditional scalar dissipation. Equation (4.25) shows that for a sheared flow with a non-zero mean temperature gradient, other terms, presumably with important effects, enter the evolution equation of the scalar field, mainly the last term of equation (4.25) which represents the production of the scalar fluctuations. Moreover, for an isotropic flow with a mean temperature gradient, the second and third terms on the left-hand side of equation (4.25) are absent which may suggest that the scalar pdf and the conditional expectation of the scalar dissipation rate may evolve differently in this flow.

Chapter 5

Experimental Facility and Instrumentation

5.1 The Flow Facility

The wind-tunnel (fig. 5.1), in which the experiments were conducted was constructed at the University of Ottawa and was described by Ferchichi (1991). The flow of air was filtered by fiberglass filters (Farr, model KB-HIE-40) and passed through a diffuser, a settling chamber across which turbulence reducing screens were installed, and a 16 to 1 contraction. A shear generator was installed immediately following the contraction (fig. 5.2). The shear generator comprised a set of 12 separate channels, each 25.4 mm high, separated by aluminum plates, about 150 mm long. Screens with varying resistances were attached across each channel so as to produce a uniform shear. A flow separator, consisting of 12 parallel plates, 610 mm long, aligned with those of the shear generator, was inserted into the flow in order to make the larger scales of the flow uniform on the transverse plane. The test section was 305 mm high, 457 mm wide and 5180 mm long. It provided 4 slots for insertion of grids and other devices normal to the flow direction. Probes were mounted on a traversing mechanism providing transverse displacements with a minimum traverse of about 0.25mm. The traversing mechanism was attached to a hand-driven belt so that measurements could be taken at different streamwise stations. The side walls of the second half of the test section diverged slightly to compensate for boundary layer growth. To increase the flow velocity, a diffuser of 5° angle and a length of 3 m was placed at the exit of the test section for some tests.

5.2 Heating system

The heating system, shown in fig. 5.3, consisted of a wooden frame that could be inserted normal to the flow into the slots provided in the wind-tunnel test section. Across the vertical walls of the frame, 47 heating elements (Nicrome 60) were stretched. The heating elements were 0.8 mm wide, 0.08 mm thick and 6.3 mm apart and were heated in pairs by variable voltage sources to produce the desired initial mean temperature profile. The heating elements were kept stretched using springs attached to their ends. The heating system was introduced into the flow at a distance of 0.61 m upstream of the first test section (fig. 5.4) to allow for higher temperature variances downstream in the test section. A copper heating plate was mounted inside the top of the wind tunnel to prevent heat losses and to allow for better transverse homogeneity of the temperature fluctuations.

5.3 Hot wire instrumentation

In the present work, several hot wire probes, all having tungsten sensors of 5 μm diameter, were used. These included single hot wires (DANTEC model 55P14) with nominal lengths of about 0.6 mm, which were used for one-point, streamwise velocity measurements and a pair of single-wire sensors, with nominal lengths of about 0.9 mm, mounted on a traversing mechanism (fig. 5.5) for two-point, streamwise velocity measurements. The traversing mechanism included two micrometers having a 0.01 mm precision, used to place the two hot wires probes normal to the flow at the desired transverse separation distances. A specially made, parallel-wire probe (AUSPEX), with two sensors having a nominal length of about 0.9 mm and separated by a 0.6 mm distance, was used for the measurements of the transverse derivatives of the streamwise velocity. Simultaneous measurements of the streamwise and the transverse velocity components were done using a specially made probe (fig. 5.6) consisting of two-sub-miniature cross wires having a length of 0.7 mm and a cold wire of about 0.5 mm. Each pair of wires was separated by a nominal distance of about 1 mm. It was realized, however, that the cold wire signal was contaminated by the heat conducted from the cross wires to the probe body. For this reason, the cold wire on the three-wire was not used in the final measurements, but a special probe holder was designed on which an independent cold wire was mounted in the vicinity of the cross wires at a distance of about 1 mm. In the heated flow, the cold wire signal was used to correct the hot wire outputs for their temperature sensitivity.

The hot wires were operated in a constant temperature mode by a multi-channel anemometer unit (AA Lab Sys, model AN-1003). Each channel had built-in low pass filters with cut-off frequencies ranging from 380 Hz to 14 kHz, built-in signal conditioning, consisting of amplifiers with gains ranging form 1 to 20 and DC voltage offsets from -12V to +12 V, and a frequency compensation unit to allow for optimal frequency response of the hot wires. When higher cut-off frequencies were required, the anemometer's filters were bypassed and home-made filters, based on the second order Butterworth design (fig. 5.7), were used. The hot wires were calibrated in the wind tunnel against a pitot tube. The difference between total and static pressures was measured with a pressure transducer that was calibrated against a Meriam micromanometer.

5.4 Temperature Measuring Instruments

Thermistors were used to measure the mean temperature of the heated flow. These were glass-coated, mini-probes (Fenwall Electronics, 2000 Ω), operated by a home-made electronic circuit which could provide individual signals as well as direct measurements of the temperature difference by subtracting the conditioned outputs of the thermistors (fig. 5.8). The thermistors were calibrated in the calibration jet against a mercury thermometer with a 0.1 K precision.

In the heated flow, cold wire (1 μm diameter, 100% Platinum) probes were used to measure temperature fluctuations. A single cold wire of about 0.5 mm in length was used for the one-point measurements of temperature fluctuations. A set of two cold wires, similar to the one mentioned above, were mounted on the traversing mechanism described in section

5.3, and the spacing between the cold wires was adjusted to the desired distance for two-point temperature fluctuation measurements. Simultaneous measurements of velocity and temperature fluctuations were performed with the triple-wire probe described in section 5.3 using the independent cold wire. All cold wires were operated by a home-made electronic circuit (fig. 5.9), comprising a constant current source, low-pass filters with cut-off frequencies that could be selected at 1, 2, 5 and 10 kHz, and amplifiers with selectable gains of 1000, 2000, 5000 and 10000. The circuitry was DC powered by batteries to minimize the contamination of the signals by the 60 Hz line frequency.

5.5 Calibration Jet

Calibrations of thermistors and cold-wires and measurements of directional and temperature sensitivities of the hot-wires were made in a calibration jet (DISA, model 55D90). Compressed air from the supply lines was fed to a pressure control unit (DISA, model 55D44) after which it passed through an air filter, a pressure regulator and a sonic nozzle to produce a steady, constant flow rate. The flow then passed through screens and flow straighteners before exiting through an axisymmetric nozzle. A home-made, motor driven probe positioning system was added to the unit. The jet air temperature was adjusted by a home-made electric heating system, which was installed before the jet unit. A swivelling mechanism rotating in two perpendicular planes was installed at the exit of the jet nozzle for measurements of the hot wire directional sensitivity.

5.6 Data Acquisition System

Raw analog signals obtained from the measuring instruments were digitized using a 16-bit analog-to-digital converter (IOTECH, model 488/16) with analog input voltage ranges selectable as ±1V, ±2V±, ±5V and ±10V. Up to 16 single-ended or 8 differential analog inputs could be sampled simultaneously at a sampling frequency of up to 100 kHz per channel. The digitized data were transferred to the hard disk of a personal computer and then transferred to a CD-ROM for long term storage.

5.7 Digital Filtering

Non-recursive digital low-pass filters were designed to further eliminate the undesirable high frequency noise part of the probe signals. These are known to have a zero phase shift and they preserve the signal waveform up to the desired cut-off frequency. Therefore, no errors are introduced in estimating the skewness and flatness of the original signal (Tavoularis and Corrsin, 1981 b). A low pass, non-recursive digital filter was constructed as

$$y_m = b_0 x_m + \sum_{n=1}^{N} b_n (x_{m-n} + x_{m+n}) \tag{5.1}$$

where y_m and x_m are the output and input signals and b_0 and b_n are the Fourier coefficients of the filter's transfer function, defined as

$$b_o = \frac{\Delta t}{\pi}\int_0^{\pi/\Delta t} H(\omega)d\omega$$

$$b_n = \frac{\Delta t}{\pi}\int_0^{\pi/\Delta t} H(\omega)\cos(n\omega\Delta t)d\omega \qquad n=1,\ 2,\ldots,\ N \tag{5.2}$$

For an ideal low pass filter, the transfer function $H(\omega)$ is

$$H(\omega)=\begin{cases}1 & if\ \ \omega\le\omega_c\\ 0 & if\ \ \omega>\omega_c\end{cases} \tag{5.3}$$

where $\omega_c=2\pi f_c$ and f_c is the cut-off frequency. To achieve a smooth transfer function, a "Hanning window" ω_n, defined as

$$\omega_n = \frac{1}{2}\left(1+\cos\frac{n\pi}{N}\right) \tag{5.4}$$

was used and, therefore, the above equations were reduced to

$$y_m = b_0 x_m + \sum_{n=1}^{N} b_n \omega_n\ (x_{m-n}+x_{m+n}) \tag{5.5}$$

and

$$b_0 = \frac{\omega_c \Delta t}{\pi}$$

$$b_n = \frac{\sin(n\omega_c\Delta t)}{n\pi} \tag{5.6}$$

The number of coefficients n was chosen to be 256.

Chapter 6

Measurement Procedure and Resolution

6.1 Calibration of the Hot Wire Probes

Hot wire anemometry has been used extensively in measurements of mean velocities and velocity fluctuations in turbulent air flows. A hot wire is a thin cylinder, which is heated electrically. In the presence of a fluid flow, the rate of heat transfer from the wire varies in response to changes of the instantaneous velocity of the flow. This can be related to the instantaneous changes of voltage across the hot wire through the well known "King's law". A modified semi-empirical form of King's law is

$$E^2 = (A + BU^n)(T_w - T_a) \tag{6.1}$$

where T_w and T_a are the temperatures of the wire and of the flow, respectively, U is the instantaneous flow velocity normal to the wire and A, B and n are constants to be determined from calibration. E is the voltage output of the constant temperature bridge, representing the voltage across the hot wire, and is given by

$$E = iR_w \tag{6.2}$$

where i the current flowing into the hot wire and R_w is the wire operating resistance to be chosen such that the wire temperature T_w is about 473 K, which is maintained constant in the constant temperature mode by a feedback circuit. The choice of R_w can be determined from the linear relationship between the wire resistance and its temperature as

$$R_w = R_a[1 + \alpha_w(T_w - T_a)] \tag{6.3}$$

where α is the wire resistivity obtained by measuring the resistance of the hot wire at different temperatures (see fig. 6.1 for a typical R-T relationship).

Calibrations of single wires were obtained by placing them in the unobstructed tunnel in which the turbulence intensity was lower than 0.5%, in the vicinity of a pitot tube and normal to the flow. Plots of the outputs from the hot wires and the pitot tube were then least square fitted according to equation (6.1) and the exponent n was optimized to yield the minimum r.m.s. error deviation from the fitted data.

In the cross wire arrangement, where both wires are inclined with respect to the flow (fig. 6.2), an effective cooling velocity, U_{ef}, is defined as the hypothetical flow velocity normal to the wire that would produce the same cooling as the actual flow velocity. This velocity is given by

$$\begin{aligned} U_{ef_1} &= \sqrt{(U sin\theta_1 - V cos\theta_2)^2 + W^2} \\ U_{ef_2} &= \sqrt{(U sin\theta_1 + V cos\theta_2)^2 + W^2} \end{aligned} \tag{6.4}$$

where U, V and W are the instantaneous velocities defined with respect to the probe axis such that U is parallel to the probe axis, V is normal to this axis on a plane parallel to the two wires and W is normal to the plane of the wires. θ_1 and θ_2 are the wire inclinations with respect to the probe axis. When the probe is aligned approximately with the mean flow direction and the turbulence intensity is small, one gets

$$\begin{aligned} U_{ef_1} &= U\sin\theta_1 - V\cos\theta_2 \\ U_{ef_2} &= U\sin\theta_1 + V\cos\theta_2 \end{aligned} \tag{6.5}$$

The calibration jet was used to experimentally determine the orientations of the cross-wires. This was achieved by varying the angular position of the cross-wire probe with respect to the jet axis (fig. 6.3). An expression relating the jet inclination with respect to the probe axis φ and the hot wire angles θ_1 and θ_2 was derived as

$$\tan(\pi/2 - \theta_i) = \frac{\dfrac{1}{U_j}\left[\dfrac{E_i^2 - A_i}{B_i}\right]^{1/n_i} - \cos\varphi_i}{\sin\varphi_i} \tag{6.6}$$

where U_j is the jet velocity. For each jet inclination φ, θ_1 and θ_2 were evaluated using equation (6.6) and average values of θ_1 and θ_2 were found to be 42.15° and 44.23° respectively for the specific probe used. These values are measurably different from the ideal ±45°.

The modified King's law for the two wires leads to expressions for the effective cooling velocities U_{ef_1} and U_{ef_1}, as

$$U_{ef_1} = \left[\frac{\left(\frac{E_1^2}{T_{w_1} - T_a} \right) - A_1}{B_1} \right]^{\frac{1}{n_1}}$$

$$U_{ef_2} = \left[\frac{\left(\frac{E_2^2}{T_{w_2} - T_a} \right) - A_2}{B_2} \right]^{\frac{1}{n_2}} \tag{6.7}$$

from which the instantaneous velocities U and V can be obtained as

$$U = \frac{U_{ef_1}\cos\theta_2 + U_{ef_2}\cos\theta_1}{\sin(\theta_1 + \theta_2)}$$

$$V = \frac{U_{ef_2}\sin\theta_1 - U_{ef_1}\sin\theta_2}{\sin(\theta_1 + \theta_2)} \tag{6.8}$$

Finally, from equation (6.8), the mean and fluctuating velocities were computed using Reynolds decomposition.

The cross-wires were calibrated against a pitot tube in the wind tunnel with all obstructions removed to provide a low turbulence air stream (the turbulent intensity was less than 0.5%). Typical calibration curves for the hot wires are shown in fig. 6.4.

6.2 Temperature Measurements

The thermistors used for measuring the mean temperature of the flow were calibrated in the heated jet at temperatures ranging from 294 K to 313 K versus a mercury thermometer with 0.1 K resolution. In that range, the thermistor voltage outputs varied linearly with the mean jet temperature. Typical calibration curves for two thermistors are shown in fig. 6.5.

Temperature fluctuations were measured with the cold wires described in the previous Chapter. A systematic study was conducted to determine the maximum current intensity fed to the cold wires at which the sensitivity to mean velocity changes was negligible. It was found that a current level of about 0.4 mA, the cold wire showed no apparent sensitivity to the mean velocity (fig. 6.6) . The cold wires were calibrated in the heated jet against a previously calibrated thermistor. Typical calibration curves of the cold wires are shown in fig. 6.7.

6.3 Resolution

A turbulent flow contains motions of different scales which may be characterized by the integral length scale, representing the typical size of the most energetic eddies, the Taylor microscale, which may be loosely regarded as the threshold scale, at which the dissipation of turbulent kinetic energy becomes significant, and the Kolmogorov microscale, representing sizes of eddies entirely dominated by viscous actions. To study the fine structure of a turbulent flow, the wire size and its frequency response must be chosen such that it resolves scales corresponding to the Kolmogorov microscale.

6.3.1 Velocity Measurement Resolution

Using the balance equation of the turbulent kinetic energy developed in section (4.1), the dissipation rate of the turbulent kinetic energy along the centerline of the wind tunnel can be written as

$$\epsilon(x_1) = -\overline{u_1 u_2}\,\frac{d\overline{U}_1}{dx_2} - \overline{U}_c\,\frac{dk}{dx_1} \tag{6.8}$$

where $\overline{U}_c$ is the centerline speed. Preliminary measurements performed for centerline speeds of 7 m/s and 13 m/s, indicated that the shear constant $k_s = (1/\overline{U}_c)d\overline{U}_1/dx_2$, was about 7 s^{-1}. Karnik and Tavoularis (1989) measurements suggested that $k \approx 0.91\overline{u_1^2}$ and $\overline{u_1u_2} \approx -0.3\overline{u_1^2}$. Based on these estimates, the dissipation was estimated for each measurement location along the tunnel centerline by fitting exponential laws to the growth of the streamwise turbulent intensity. The Taylor microscale was estimated from the isotropic relation as

$$\lambda_{11} = \sqrt{15\nu\frac{(u')^2}{\epsilon}} \tag{6.9}$$

and, finally, the Kolmogorov microscale was estimated as

$$\eta = \left(\frac{\nu^3}{\epsilon}\right)^{\frac{1}{4}} \tag{6.10}$$

These estimates suggested that, for the centerline speed of 7 m/s, the Taylor microscale λ_{11} was about 4.7 mm and nearly constant along the centerline of the wind tunnel, whereas the Kolmogorov microscale η decreased from 0.21 mm at $x_1/h = 0$ to about 0.13 mm at $x_1/h = 11$. Accordingly, the Kolmogorov frequency, $f_k = \overline{U}_c/2\pi\eta$, increased from about 5.5 kHz to 8.7 kHz. For the centerline speed of 13 m/s, λ_{11} was nearly constant, with a value of about 3.4 mm, η decreased from about 0.14 mm at $x_1/h = 0$ to about 0.08 mm $x_1/h = 11$ and f_k increased from 15.5 kHz to about 25 kHz.

6.3.1.1 Spatial Resolution

Clearly, the 0.6 mm long single hot-wire is much larger than the estimated Kolmogorov scales reported above and it may introduce some errors in measurements of quantities related to the fine structure. However, a further decrease in the wire length introduces other errors due to heat conduction to the prongs and to non-uniform heating of the wire. Plots provided by Wyngaard (1969) suggested that, for $\overline{U}_c = 7$ m/s, $\overline{(\partial u_1/\partial x_1)^2}$ would be underestimated by 5% at $x_1/h = 0$ to about 10% at $x_1/h = 11$ and, for the case of 13 m/s, it would be underestimated by 10 % at $x_1/h = 0$ to about 20 % at $x_1/h = 11$. The above estimates indicate that the measured streamwise Taylor microscale would be overestimated by less that 10% in the worst case.

The streamwise velocity derivatives were evaluated using Taylor's "frozen flow" hypothesis which may be applied in low turbulent intensity flows. Heskestad (1965) provided an approximate correction to the streamwise velocity derivative when invoked from its temporal counterpart as

$$\overline{\left(\frac{\partial u_1}{\partial x_1}\right)^2} = \frac{1}{\overline{U}^2}\frac{1}{\left(1+\overline{u_1^2}/\overline{U}^2+\overline{u_2^2}/\overline{U}^2+\overline{u_3^2}/\overline{U}^2\right)}\overline{\left(\frac{\partial u_1}{\partial t}\right)^2} \tag{6.11}$$

In this particular study, the highest turbulence intensity was $u_1'/\overline{U}_c = 16\%$, for the case with $\overline{U}_c = 13$ m/s and at $x_1/h = 11$. Using the fact that, in this particular flow, $u_2' \approx 0.65u_1'$ and $u_3' \approx 0.5u_2'$, then the above equation suggests that the maximum error in estimating the mean squared streamwise derivative using Taylor's approximation, would be less that 4%.

For the transverse velocity derivatives, the parallel wires had a length of 0.9 mm and were spaced by a distance of 0.6 mm. The wire length was chosen to be larger than the single wire used for the one-point measurements, because, according to Wyngaard (1969), an increase in the length of the wires can only improve the transverse derivative measurements. According to the estimates of Wyngaard (1969), $\overline{(\partial u_1/\partial x_2)^2}$ may be underestimated, for $\overline{U}_c = 7$ m/s, by 10% at $x_1/h = 0$ to about 20% at $x_1/h = 11$, and for $\overline{U}_c = 13$ m/s, it would be underestimated by 20% at $x_1/h = 0$ to about 35% at $x_1/h = 11$.

In view of the above, spatial corrections to $\overline{(\partial u_1/\partial x_1)^2}$ and $\overline{(\partial u_1/\partial x_2)^2}$ will be applied according to the method of Wyngaard (1969). Unfortunately, there are no available methods to correct the skewness and flatness of the streamwise and transverse velocity derivatives. But, Derksen and Azad (1983) estimated the skewness, $S_{\partial u_1/\partial x_1}$, and flatness, $F_{\partial u_1/\partial x_1}$, of the streamwise velocity derivative obtained from signals of hot wires of different sizes in a turbulent boundary layer and suggested that $S_{\partial u_1/\partial x_1}$ and $F_{\partial u_1/\partial x_1}$ were nearly invariant with the hot wire length, l_w for $2.9 < l_w/\eta < 20$. Moreover, Garg and Warhaft (1998) showed that the measured transverse derivative skewness, $S_{\partial u_1/\partial x_2}$, maintained nearly a constant value for up to $\Delta x_2/\eta = 10$.

6.3.1.2 Temporal Resolution

The above estimates suggested that, for $\overline{U}_c = 7$ m/s, the maximum Kolmogorov frequency, f_k, was about 8.7 kHz. The Nyquist criterion depicts that the sampling frequency should be at least 17.4 kHz. Accordingly, the signals from the single wire and the parallel wires were low-pass filtered at 14 kHz and sampled at a rate of 50 kHz. For $\overline{U}_c = 13$ m/s, the maximum f_k was about 25 kHz, the signals from the single wire were low pass filtered at a frequency of 38 kHz and sampled at a sampling frequency of 100 kHz, but to conform with the sampling frequency limitations of the analog to digital converter, the signals form the parallel wires were low-pass filtered at 25 kHz and sampled at a sampling frequency of 50 kHz. About 100 records, each consisting of 400 000 data points for the single wire and 262 144 data points for the parallel wires, were sampled. Each record had a duration of about 5 seconds corresponding to roughly 800 times the integral time scale which ensured good statistical representation of the large scales of the flow.

6.3.2 Temperature Measurement Resolution

The heating system was inserted into the flow at a position about 0.61 m upstream of the test section to allow the development of relatively high temperature fluctuations in the test section. The possible effects of the heating system on the velocity field were investigated. To achieve measurable temperature differences and to avoid element vibrations, one had to maintain the centerline speed below 7 m/s. At the centerline speed of about 6.6 m/s, a constant mean temperature gradient $\partial\overline{T}/\partial x_2$ of about 7.8 K/m was produced at $x_1/h = 0.5$. Under these conditions, the Taylor microscale was estimated to be about 5.2 mm and the Kolmogorov microscale was found to decrease from about 0.20 mm at $x_1/h = 3$ to about 0.16 mm at $x_1/h = 8$. The Corrsin-Obukhov microscale, corresponding to the dissipative scales of the temperature variance and defined as $\eta_\theta = (\mathrm{Pr})^{-3/4}\eta$, decreased from 0.26 mm to about 0.21 mm at the locations mentioned above. Accordingly, the Kolmogorov frequency for temperature $f_{k_\theta} = \overline{U}_c/2\pi\eta_\theta$ increased from 4 kHz to about 4.9 kHz. The rate of destruction of temperature fluctuations was estimated from the balance equation (4.18) using an exponential fit to the growth of preliminary measurements of the temperature variance along the centerline. Then the Corrsin microscale was estimated using the isotropic expression

$$\lambda_{\theta_1} = \sqrt{\frac{6\gamma\overline{\theta^2}}{\epsilon_\theta}} \tag{6.12}$$

to be about 3 mm and nearly constant along the wind tunnel centerline.

6.3.2.1 Spatial Resolution

When using the 0.5 mm long cold wire, $\overline{(\partial\theta/\partial x_1)^2}$ would be underestimated by about 10% (Wyngaard, 1971) and as a result, the Corrsin microscale, λ_{θ_1}, would be overestimated by about 5%. Browne and Antonia (1987) conducted an experiment to study the effect of the cold wire length on the statistics of the temperature fluctuations and their derivatives. They suggested that, to eradicate the effects of end conduction on these statistics, the cold wire must have a length to diameter ratio l_w/d_w larger than 1500. For $d_w = 1\,\mu\mathrm{m}$, $l_w/d_w = 1500$ requires a wire with a length of 1.5 mm, which would result in an error in of about 38% in estimating $\overline{(\partial\theta/\partial x_1)^2}$ (Wyngaard, 1971). Further reducing the diameter of the cold wire to increase l_w/d_w would make it very fragile and extremely hard to handle and repair. Mydlarsky and Warhaft (1998) commented that the spatial resolution of the cold wire has the predominant contribution to the uncertainty in estimating temperature derivative statistics and used a cold wire with l_w/d_w of about 560. In view of this, the present choice of $l_w/d_w = 500$ seemed to be reasonable for this type of study.

The transverse temperature derivative, $\partial\theta/\partial x_2$, and differences, $\Delta\theta(x_2)$, were measured by placing two cold wires of nearly the same length and resistance on the traversing system described in section (5.3) in the heated flow parallel to the mean temperature gradient, $\partial\overline{T}/\partial x_2$. The cold wires were separated by a distance, d, of about 0.5 mm for the transverse derivative estimate. Therefore, d/η_θ would vary from about 1.9 to about 2.4, which are in the ranges of d/η_θ suggested by Antonia and Mi (1993), Anselmet et al. (1994) and Tong and Warhaft (1994).

6.3.2.2 Temporal Resolution

According to the above estimates, the maximum Kolmogorov frequencies for the velocity and temperature were 4 kHz and 4.9 kHz respectively. To satisfy the Nyquist criterion, the cross-wire signals were low-pass filtered at a cut-off frequency of 8 kHz, the cold wire signal was low-pass filtered at 10 kHz and all signals were sampled at a frequency of 20 kHz. The sampled cold wire signals were further low-pass filtered using a digital filter (section 5.7) at a cut-off frequency of 5 kHz prior to processing. At this cut-off frequency, the signal-to-noise ratio, s^2/n^2, where n is the cold wire signal in the unheated flow, varied from 47 to about 90. To ensure good statistical representation of the large scales of the flow, 60 records of 262 144 data points were collected.

Chapter 7

Measurements of the Fine Structure of the Velocity Field

7.1 The Mean Velocity Field

Measurements of velocity derivatives and structure functions were conducted at two mean centerline velocities, 7.3 m/s and 13.0 m/s. The latter centerline speed was achieved by installing a diffuser at the exit of the wind tunnel test section, as described in Section 5.1. Measurements were performed at positions corresponding to $x_1/h = 0, 2, 4, 6, 8, 10$ and 11, where h is the wind tunnel height, equal to 0.305 m. Fig. 7.1 shows typical transverse profiles of the mean velocity $\overline{U}_1$. These exhibited good linearity except at far downstream distances where the effects of boundary layer growth on the walls of the wind tunnel were noticeable. Fig. 7.2 displays the shear constant $k_s = 1/\overline{U}_c \, d\overline{U}_1/dx_2$, for each centerline speed and at the streamwise positions mentioned above. This plot suggests that k_s was roughly constant and equal to about 7.07 ± 0.19 m^{-1}, independently of the centerline speed and of the streamwise position. This also shows that the addition of the diffuser had no significant effect on the value of k_s.

7.2 The Turbulent Stresses

Fig. 7.3 shows transverse profiles of the streamwise r.m.s. turbulent fluctuations. The observed variation in $u_1'/\overline{U}_c$ increased with increasing centerline speed and downstream position. At its worse, near the tunnel exit, the variation was less than 30 % in the core of the wind tunnel; thus, the flow may be assumed to be nearly homogeneous in the transverse direction. The downstream development of the turbulent stresses for both centerline speeds is shown in fig. 7.4. Exponential fits to the data gave, for $\overline{U}_c$ = 7.3 m/s,

$$\frac{\overline{u_1^2}}{\overline{U}_c^2} \approx 0.0033e^{0.19x_1/h} \tag{7.1}$$

and, for $\overline{U}_c$ = 13.0 m/s,

$$\frac{\overline{u_1^2}}{\overline{U}_c^2} \approx 0.0030e^{0.20x_1/h} \tag{7.2}$$

which are within 5 % from each other. The measured Taylor microscale, λ_{11}, turbulent Reynolds number, Re_λ, and Kolmogorov microscale, η, are provided in table 7.1. The same table provides the turbulent kinetic energy dissipation rate.

7.3 Spectral Measurements

For clarity, all plots have been presented for a few selected values of Re_λ, namely, 172, 311, 476 and 578. Fig. 7.5 shows typical streamwise one-dimensional velocity spectra, normalized by Kolmogorov's variables. The data show a reasonable collapse at all Re_λ in both the inertial and dissipative ranges. A sizable inertial range is noticeable that extends over about one wavenumber decade at $Re_\lambda = 173$ to about two wavenumber decades at $Re_\lambda = 580$. These spectra are in good agreement with one-dimensional spectra measured in other turbulent flows (Monin and Yaglom, 1975; Frisch, 1995; Mydlarski and Warhaft, 1996). Fig. 7.6 shows one-dimensional dissipation spectra, $(\kappa\eta)^2 E_l/(\epsilon\nu^5)^{1/4}$. They all show a peak in the range between 0.25 and 0.27 at about $\kappa\eta = 0.15$, which is close to values reported by Monin and Yaglom (1975).

For a closer examination of the spectra in the inertial range, Fig. 7.7 plots the Kolmogorov constant $C_{l\kappa}=E_l/(\epsilon^{2/3}\,\kappa^{-5/3})$. Although none of the spectra reached an extensive plateau, as would be the case if the -5/3 law applied, fig.7.7 suggests that, as Re_λ increases, the slope of the spectra in the inertial range is approaching -5/3. Sreenivasan (1991) suggested a modified form of the energy spectrum in the inertial subrange as

$$E_1 = C'_{1\kappa}\epsilon^{2/3}\kappa^{-5/3}(\kappa\eta)^{5/3-\alpha} \tag{7.3}$$

where $C'_{l\kappa}$ is a coefficient dependent on Re_λ and α is the slope of the measured spectra in the inertial range also dependent on Re_λ. Following the method of Mydlarski and Warhaft (1996), $C'_{l\kappa}$ was plotted vs. $\kappa\eta$ for different values of α and the "optimal" α was selected as the value resulting in the longest range of $\kappa\eta$ having a nearly constant $C'_{l\kappa}$. Fig. 7.8 shows the variation of the "optimal" values of 5/3-α, which may be fitted by the curve $120Re_{\lambda}^{-1.2}$. The optimal α differed from the Kolmogorov value of 5/3 by 8 % at $Re_{\lambda} = 300$, by 5 % at $Re_{\lambda} = 480$ and decreased to 3 % at the highest $Re_{\lambda} = 660$. Fig. 7.9 shows sample plots of $C'_{1\kappa}$ as a function of $\kappa\eta$. For Re_{λ} larger than 480, these values are close to values reported by Monin and Yaglom (1975), Sreenivasan (1995) and Mydlarski and Warhaft (1996) at comparable Re_{λ} and supports previous findings, that $C'_{1\kappa}$ approaches a constant value as Re_{λ} increases. For comparison, $C'_{1\kappa} = 0.70$ at $Re_{\lambda} = 300$, $C'_{1\kappa} = 0.65$ at $Re_{\lambda} = 480$ and $C'_{1\kappa} = 0.60$ at $Re_{\lambda} = 580$.

7.4 Velocity Derivative Statistics

First, the pdf of the normalized streamwise velocity fluctuations are presented in fig. 7.10. These are nearly Gaussian with a skewness of -0.04 and a flatness of 2.91.

Fig. 7.11 is a plot of the ratio $\overline{(\partial u_1/\partial x_1)^2}/\overline{(\partial u_1/\partial x_2)^2}$. The variances of both velocity partial derivatives have been corrected for the wire length and wire spacing using Wyngaard's (1969) estimates. This ratio, plotted for both centerline speeds, fluctuated between 0.45 and 0.55 for Re_{λ} increasing from 140 to 660 . This ratio is close to the locally isotropic value of 0.5, but substantially larger than the value of 0.22 reported by Tavoularis and Corrsin (1981 b). The reasons for this difference have yet not yet been identified.

In contrast to the pdf of the velocity fluctuations, the pdf of the streamwise velocity derivative are highly non-Gaussian, as demonstrated in fig. 7.12. For all Reynolds numbers examined, including cases not shown in fig. 7.12, the pdf of $\partial u_1/\partial x_1$ displayed two main features. Firstly, their tails are very broad and nearly exponential in form, becoming progressively steeper as Re_λ increases, with the negative tails being more flared than the positive ones. Secondly, the peaks of these pdf seem to shift toward positive values of $\partial u_1/\partial x_1$ and to become sharper as Re_λ increases. The sharpness of these peaks is an indication of intermittency of the fine structure and consistent with the expectation that the internal intermittency increases as Re_λ increases. Because the tails of these pdf are associated with large and rare fluctuations of $\partial u_1/\partial x_1$ and, hence, with the dissipative scales, their distribution would indicate the degree of intermittency of such scales. Their tails may be fitted by the exponential expression

$$p(z_1) = e^{-\beta_1 z_1} \tag{7.4}$$

where $z_1 = (\partial u_1/\partial x_1)/(\partial u_1/\partial x_1)'$. Fig. 7.13 shows that values of β_1 determined from the positive tails were somewhat higher than values determined from the negative ones, but both showed a monotonic decrease with Re_λ. The systematic decrease in β_1 as Re_λ increases is consistent with the expected increase in the internal intermittency. Figs. 7.12 and 7.13 clearly show that the asymmetry of the pdf of the streamwise velocity derivative becomes more pronounced as Re_λ increases. This asymmetry may be better seen in fig. 7.14 in which the pdf have been multiplied by the cube of the normalized derivative.

Figs. 7.15 and 7.16 show the measured values of the skewness $S_{\partial u_1/\partial x_1}$ and the flatness $F_{\partial u_1/\partial x_1}$ of the streamwise velocity derivative for different Re_λ at two centerline speeds, $\overline{U}_c = 7.3$ m/s and $\overline{U}_c = 13.0$ m/s. Although the trends are similar for both centerline speeds, the magnitudes of the measured $S_{\partial u_1/\partial x_1}$ and $F_{\partial u_1/\partial x_1}$ do not collapse. This may be partly due to experimental errors and partly to small differences in the large scales of the flow. As seen in fig. 7.15, the measured skewness $S_{\partial u_1/\partial x_1}$ is non-zero and negative. Note that a non-zero $S_{\partial u_1/\partial x_1}$ is not a violation of Kolmogorov's similarity hypothesis, but its non-constancy for different Re_λ would be (Frisch, 1995). Fig. 7.15 shows that $S_{\partial u_1/\partial x_1}$ varies only slowly with Re_λ, increasing from about 0.37 to about 0.43 in the range of Re_λ between 140 and 660. The measured skewness falls within the range of data collected by Sreenivasan and Antonia (1997) from numerous experimental and numerical studies. A power law fit to the present data suggested that $S_{\partial u_1/\partial x_1}$ varies as $Re_\lambda^{0.1}$. The exponent 0.1 is not far from the value of 0.07 obtained by Frisch (1995) from the measurements of Gagne (1987).

Compared to $S_{\partial u_1/\partial x_1}$, $F_{\partial u_1/\partial x_1}$ shows a stronger dependence on Re_λ and increases with increasing Re_λ (fig. 7.16), consistent with the fact the internal intermittency should increase as Re_λ increases. The measured $F_{\partial u_1/\partial x_1}$, which increased from about 5.5 to about 7.7 in the range of Re_λ investigated in this study, falls within the range of various measurements reported by Sreenivasan and Antonia (1997). A fit to the data of fig. 7.16 suggested that $F_{\partial u_1/\partial x_1}$ varies as $Re_\lambda^{0.18}$. The exponent 0.18 is close to the values obtained by Frisch (1995), namely 0.15 from the data of Anselmet et al. (1984) and 0.18 from the data of Gagne (1987).

Up to this point, it has been shown that, for the range of Re_λ studied, the reported pdf and the statistics of the streamwise velocity derivative $\partial u_1/\partial x_1$ are consistent with numerous experimental and numerical studies. No comparison was made with the measurements of Garg and Warhaft (1998), because their measured $S_{\partial u_1/\partial x_1}$ and $F_{\partial u_1/\partial x_1}$ showed considerable scatter and no systematic trends with Re_λ.

Next, the focus will be on the transverse velocity derivative statistics. Fig. 7.17 shows the pdf of $\partial u_1/\partial x_2$ at the same Re_λ as those used for the pdf of $\partial u_1/\partial x_1$. Some features found in the pdf of $\partial u_1/\partial x_1$, in particular the exponential tails and the increasing sharpness of the peak as Re_λ increases, are also encountered in the pdf of $\partial u_1/\partial x_2$. However, there are also some differences. The positive tails of the pdf of $\partial u_1/\partial x_2$ are more flared than the negative ones, the peaks of these pdf are shifted towards the negative values of $\partial u_1/\partial x_2$ and the shape of the these pdf becomes more symmetrical as Re_λ increases. Exponential fits to the tails of these pdf using the expression

$$P(z_2) = e^{-\beta_2 z_2} \tag{7.5}$$

where $z_2 = (\partial u_1/\partial x_2)/(\partial u_1/\partial x_2)'$, provided β_2 for the negative tails which were higher than those the positive tails (fig. 7.18). A decrease in β_2 with increasing Re_λ was also noticeable, but not as pronounced as the increase in the exponent β_1. The asymmetry of these pdf may also be seen in fig. 7.19 which shows that the positive peak was always higher than the corresponding negative peak in the range of Re_λ studied and, to a lesser extent, that the asymmetry seems to become less pronounced as Re_λ increases. The measured skewness and flatness of $\partial u_1/\partial x_2$ are shown in figs.7.20 and 7.21 respectively. Along with the present measurements of $S_{\partial u_1/\partial x_2}$, the values measured by Tavoularis and Corrsin (1981b), Garg and Warhaft (1998) and Pumir (1996) were also included. As shown in fig. 7.20, the values of $S_{\partial u_1/\partial x_2}$ were positive for the range of Re_λ reported in this study. The signs of the skewnesses of $\partial u_1/\partial x_1$ or $\partial u_1/\partial x_2$ have been explained by the phenomenological model of Tavoularis and Corrsin (1981 b), according to which, for positive $\partial\overline{U}_1/\partial x_2$, a "ramp-like" structure of u_1 develops, causing $S_{\partial u_1/\partial x_1}$ to be negative and $S_{\partial u_1/\partial x_2}$ to be positive. Note that, according to this model, the presence of non-zero mean velocity gradient is essential for a non-zero $S_{\partial u_1/\partial x_2}$. This was confirmed by Ferchichi and Tavoularis (1998) who measured a nearly zero $S_{\partial u_1/\partial x_2}$ in grid-generated turbulence.

Since a non-zero $S_{\partial u_1/\partial x_1}$ is not inconsistent with local isotropy hypotheses, then

$S_{\partial u_1/\partial x_2}$ would be a better measure of deviation from local isotropy. Fig. 7.20 shows that $S_{\partial u_1/\partial x_2}$ decreases from about 0.7 to about 0.34 as Re_λ increases from 140 to 660, indicating that the fine structure may be tending towards local isotropy. The main conclusion here is that the skewness of $\partial u_1/\partial x_2$ evolves differently with Re_λ from the skewness of $\partial u_1/\partial x_1$: the latter increases with increasing Re_λ while the former decreases. Fit to each set of data suggested that, $S_{\partial u_1/\partial x_2}$ decreased roughly as $Re_\lambda^{-0.8\pm0.2}$, which is consistent with Garg and Warhaft (1998) result. It is important to mention that the change in $S_{\partial u_1/\partial x_2}$ is quite significant (almost reduced by half for Re_λ varying form 140 to about 660), and that its dependence on Reynolds number cannot be accounted for by experimental uncertainty.

Fig. 7.21 displays the measured flatness of the transverse velocity derivative $F_{\partial u_1/\partial x_2}$, together with the values obtained by Tavoularis and Corrsin (1981 b) and by Garg and Warhaft (1998). The measurements of the latter authors indicated that $F_{\partial u_1/\partial x_2}$ decreased as Re_λ increased for low values of Re_λ, but for the highest Re_λ considered, $F_{\partial u_1/\partial x_2}$ seemed to approach a constant. The present measurements seem to suggest that $F_{\partial u_1/\partial x_2}$ consistently increases with Re_λ, but at a slower rate than $F_{\partial u_1/\partial x_1}$ does. A power law fit to the data was $F_{\partial u_1/\partial x_2} \propto Re_\lambda^{0.11}$, although a power law may not be appropriate in this case, as the data in fig. 7.21 show that $F_{\partial u_1/\partial x_2}$ tends towards a constant value.

7.5 Inertial Range Statistics and Structure Functions

Figs. 7.22 and 7.23 are plots of the pdf of the streamwise and transverse velocity differences $\Delta u_1(x_1)$ and $\Delta u_1(x_2)$, respectively, at $Re_\lambda = 578$ for $r/\eta = 21$, 76, 142 and 210 (*r* is the separation distance measured in the x_1 or x_2 directions). These figures show that, for small separation distances, the pdf have extended tails, similar to those seen in the derivative pdf, but, at larger r/η, they approach the Gaussian shape. It is interesting to see that, for the pdf of $\Delta u_1(x_1)$, the positive tails decay faster towards the Gaussian than the negative ones do, while the opposite can be observed for the pdf of $\Delta u_1(x_2)$.

Fig. 7.24 is a plot of the normalized second order longitudinal velocity structure function $D^2_{u_1u_1}(x_1)/(r\varepsilon)^{2/3}$ as a function of r/η for $Re_\lambda = 172, 311, 476$ and 578. In conformity with the normalized spectra shown in fig. 7.9, fig 7.24 shows that the inertial range widens as Re_λ increases. For the highest Re_λ examined, the normalized second order structure function seems to suggest that the Kolmogorov constant C_2 is about 2.2, close to the values of 2.25 reported by Boratav and Pelz (1997) and 1.95 reported by Anselmet et al. (1984), but somewhat higher than the value of 1.85 reported by Garg and Warhaft (1998) for a lower Reynolds number. Since $C_\kappa = 0.76C_2$ (C_κ is the Kolmogorov constant for a three-dimensional spectrum) and $C_{1\kappa} = 0.327C_\kappa$ (Monin and Yaglom, 1975), the present value of C_2=2.2 suggests that $C_{1\kappa}$=0.55 consistent with the value of $C_{1\kappa}$ of about 0.6 reported in Section (7.3) at the same $Re_\lambda = 578$. Shown in fig. 7.25 is the normalized second order transverse velocity structure function $D^2_{u_1u_1}(x_2)/(r\varepsilon)^{2/3}$. Although the number of data points plotted was not as large as that for the longitudinal velocity structure function, the data seem to indicate that $D^2_{u_1u_1}(x_2)/(r\varepsilon)^{2/3}$ reached nearly a constant value of about 4 in the inertial range. Note that, at $Re_\lambda = 311$, this value is about 3.5, compared to the value of 3.0 reported by Garg and Warhaft (1998) at nearly the same Re_λ.

Fig. 7.26 is a plot of the normalized third order longitudinal velocity structure function $D^3_{u_1u_1}(x_1)/(r\varepsilon)$ versus r/η. According to Kolmogorov scaling, this quantity should be constant and equal to -4/5 in the inertial range. Fig. 7.26 suggests that, as Re_λ increases, this function approaches this value. The same trend was also observed by Garg and Warhaft (1998). Fig. 7.27 shows the skewness of the longitudinal velocity difference $S_{\Delta u_1(x_1)}$, whose locally isotropic value in the inertial range should be constant (Kolmogorov, 1941). Indeed this quantity was nearly constant, with an average value of about -0.21, close to the value -0.18, reported by Garg and Warhaft (1998).

Fig. 7.28 is a plot of the normalized third order transverse velocity structure function $D^3_{u_1u_1}(x_2)/(r\varepsilon)$. In accordance with the results of Garg and Warhaft (1998), the present measurements indicate that this quantity was non-zero throughout the range of Re_λ used in this study, and it contained a narrow range of constancy, which widened with increased Re_λ. The similarity hypotheses requires that such a function must vanish (Garg and Warhaft, 1998). The skewness of the transverse velocity difference $S_{\Delta u_1(x_2)}$, shown in fig. 7.29, also possesses a nearly constant range.

The flatnesses of the streamwise and transverse velocity differences $F_{\Delta u_1(x_1)}$ and $F_{\Delta u_1(x_2)}$, shown in figs. 7.30 and fig. 7.31, monotonically decreased with increasing r/η for all Re_λ, from the values of the corresponding derivative flatnesses for small r/η to the Gaussian value of 3 for large r/η. Both $F_{\Delta u_1(x_1)}$ and $F_{\Delta u_1(x_2)}$ show an increase with increasing Re_λ, not only in the dissipative range, but in the inertial range as well. This seems to suggest that the flow motions in the inertial range are intermittent, but not as strongly as those in the dissipative range. To further elaborate on the variations of $F_{\Delta u_1(x_1)}$ and $F_{\Delta u_1(x_2)}$ in the inertial range, their values, at selected r/η have been plotted versus Re_λ in figs. 7.32 and 7.33. The shapes of the curves that correspond to values of r/η in the inertial range imply that the inertial range intermittency becomes more pronounced as either r/η or Re_λ increases.

Finally, the second, third, fourth, fifth and sixth order normalized structure functions, $D^p_{u_1u_1}(x_2)/(r\varepsilon)^{p/3}$, where p is the order of the structure function, have been plotted at Re_λ = 578 for the longitudinal and transverse directions, in figs. 7.34 and 7.35, respectively. Both figures indicate that, if a correction to the exponents $p/3$ were required, it would only be necessary for p greater than 4. To find this correction, all structure functions were replotted in figs. 7.36 and 7.37, respectively, by replacing the exponents $p/3$ by ξ_p such that they would be constant in the inertial range. The optimum exponents ξ_p resulting from the longitudinal and transverse structure functions are plotted in fig. 7.38, together with values of ξ_p reported by Anselmet et al. (1984), Boratav (1997) and She and Lévêque (1994) (note that the latter authors' model anticipates that $\xi_p = p/9 + 2 - 2(2/3)^{p/3}$). There seems to be a reasonable agreement between the present estimates of ξ_p and the above studies. Note that the values of ξ_p resulting from the odd-order structure functions have not been used in the literature, because possible symmetries existing in the mean field may affect their values. For this reason, odd-order structure functions are not shown in fig. 7.38. It is clear form fig. 7.38 that the present and previous data are in close agreement with Kolmogorov's (1941) scaling law, $\xi_p = p/3$, for $p \le 4$ but they deviate from that law for $p = 6$.

Chapter 8

Measurements of the Scalar Pdf, the Scalar-Scalar Dissipation and Velocity-Scalar Joint Statistics and the Scalar Derivative Statistics

8.1 The Mean Velocity Field

The heating system described in section 5.2 was inserted at a position $2h$ upstream of the test section, which resulted in relatively large temperature fluctuations while permitting a reasonable transverse homogeneity in the test section. A relatively low centerline speed (about 6.6 m/s) was chosen for the scalar mixing study because of limitations on the current input to the heating elements and to avoid distortion of the velocity field due to heating element vibrations that were observed at higher centerline speeds. At $\overline{U}_c = 6.6$ m/s, heating of the elements individually, at rates varying from 720 W to about 5 W, produced an initial constant mean temperature gradient $\partial\overline{T}/\partial x_2 = 7.8$ K/m at a position of $x_1/h = 0.5$ with a centerline mean temperature rise, $\overline{T}_c = 1.37$ K. Under such relatively low overheats, buoyancy effects are negligible and the temperature can be treated as a passive scalar. Measurements of the velocity statistics, velocity-temperature joint statistics and pdf and temperature dissipation statistics were taken in the heated flow along the centreline at positions $x_1/h = 3$, 4.7, 6.3, and 8. The velocity signals were corrected for the mean and fluctuating temperature according to equation 6.7.

Fig. 8.1 shows typical transverse profiles of the mean velocity at different downstream locations. The measured mean velocity displayed good linearity with k_s equal to about 6.0 ± 0.15 m^{-1}. This value was lower than that obtained in Chapter 7. The difference may be attributed mostly to the presence of the heating system which acted as a shear-reducing screen, resulting in lower k_s values (Tavoularis and Karnik, 1989).

8.2 The Turbulent Stresses

Fig. 8.2 shows the transverse profiles of the transverse and streamwise r.m.s. turbulent fluctuations $u_1'/\overline{U}_c$ and $u_2'/\overline{U}_c$. The transverse variations in $u_1'/\overline{U}_c$ and $u_2'/\overline{U}_c$ were less than 30% in the core of the wind tunnel. Fig. 8.3 is a plot of the transverse profiles of the shear stress correlation coefficient $\rho = \overline{u_1 u_2}/u_1' u_2'$. This coefficient displayed good transverse homogeneity and reached an asymptotic value of about -0.45. Based on the above results one may assume that the velocity is nearly homogeneous and that the heating and the obstruction by heating ribbons did not have undesirable effects on the velocity field. The downstream developments of the turbulent intensities, $\overline{u_1^2}/\overline{U}_c^2$ and $\overline{u_2^2}/\overline{U}_c^2$ are shown in fig. 8.4.

Exponential fits to the data gave

$$\frac{\overline{u_1^2}}{\overline{U}_c^2} \approx 0.0040e^{0.14x_1/h}$$
$$\frac{\overline{u_2^2}}{\overline{U}_c^2} \approx 0.0014e^{0.14x_1/h} \tag{8.1}$$

both growing at the same rate, but slower than those corresponding quantities in the absence of the heating system (equations 7.1 and 7.2). The difference is accounted for by the difference in the shear constant k_s. Fig. 8.5 is a plot of the centerline development of the shear stress correlation coefficient ρ. The data suggests that ρ was nearly constant along the tunnel centerline, equal to about -0.45.

8.3 The Integral Length Scales

Measurements of the integral length scales $L_{11,1}$ and $L_{22,1}$ are plotted in fig. 8.6. Exponential fitting to $L_{11,1}$ gave

$$L_{11,1} = 0.020e^{0.11x_1/h} \tag{8.2}$$

Fig. 8.7 shows the values of $L_{22,1}/L_{11,1}$ at different downstream locations. This ratio was roughly constant with a value of about 0.37, not very different from the value of 0.33 reported by Tavoularis and Corrsin (1981a).

8.4 The Velocity Pdf

Figs. 8.8 and 8.9 display the pdf of the streamwise and transverse velocity fluctuations, respectively. These were nearly Gaussian with skewness and flatness of -0.08 and 2.93, and -0.02 and 3.03, respectively, which were closer the Gaussian than the corresponding values of -0.22 and 3.1, and 0.16 and 3.2 reported by Tavoularis and Corrsin (1981 a).

8.5 The Mean Temperature Field

Fig. 8.10 shows the transverse profiles of the mean temperature at different downstream locations. The mean temperature displayed good linearity with a nearly constant mean temperature gradient $\partial \overline{T}/\partial x_2$ of about 7.8 K/m in the core of the wind tunnel, which was lower than the value 9.5 K/m in the experiments of Tavoularis and Corrsin (1981 a).

8.6 The Temperature Fluctuations and Temperature-Velocity Covariances

Fig. 8.11 shows the transverse profiles of the normalized temperature fluctuations. Transverse profiles of the correlation coefficients $\rho_{u_1\theta} = \overline{u_1\theta}/u_1'\theta'$ and $\rho_{u_2\theta} = \overline{u_2\theta}/u_2'\theta'$, are shown in fig. 8.12. The normalized temperature fluctuations and the correlation coefficients displayed good homogeneity, which improved as the distance downstream from the heating elements increased. Measurements of the normalized mean temperature variance $\overline{\theta^2}/\overline{T}_c^{\,2}$ along the tunnel centerline are shown in fig. 8.13. This quantity decayed up to $x_1/h = 2$, but further downstream, it grew steadily. Exponential fit to the data of fig. 8.13 gave

$$\frac{\overline{\theta^2}}{\overline{T}_c^{\,2}} = 0.0164 e^{0.16 x_1/h} \tag{8.3}$$

indicating that the turbulence intensities and the temperature variance grew at nearly the same rate. Centreline measurements of $\rho_{u_1\theta}$ and $\rho_{u_2\theta}$ are shown in fig. 8.14. As opposed to ρ, a small increase in absolute values of $\rho_{u_1\theta}$ and $\rho_{u_2\theta}$ (with the increase in $\rho_{u_1\theta}$ being more pronounced) is observed as the downstream distance increased. This result is consistent with the results of Tavoularis and Corrsin (1981 a). At $x_1/h = 8$, corresponding to $Re_\lambda = 253$, the values of $\rho_{u_1\theta}$ and $\rho_{u_2\theta}$ were 0.56 and -0.50, respectively, comparable to the values of 0.59 and -0.45 reported by Tavoularis and Corrsin (1981 a) at nearly the same Reynolds number.

8.7 The Temperature Integral Length Scales

Fig. 8.15 shows the variation of $L_{\theta,1}/L_{11,1}$ at different downstream locations. This ratio was roughly constant along the tunnel centerline and equal to 0.74, close to the value of 0.76 reported by Tavoularis and Corrsin (1981 a) suggesting that the velocity and temperature integral length scales grew at nearly the same rate. Further measurements of the Taylor microscale, the Corrsin microscale and the Kolmogorov microscale are included in table 8.2.

8.8 The Scalar Pdf

Fig. 8.16, shows the pdf of the scalar fluctuations at Re_λ = 184, 200, and 253, corresponding to x_i/h = 3, 4.7 and 8. The central portions of these pdf were very close to the normal distribution but their tails departed slightly from normality. The measured skewness and flatness shown in fig. 8.17, were found to be -0.19 ± 0.06 and 3.15 ± 0.08, respectively, not very different from the Gaussian values of S_θ = 0.0 and F_θ = 3.0 reported by Tavoularis and Corrsin (1981 a) at comparable Re_λ.

As noted in the literature survey, there has been some controversy about the shape of the tails of the scalar pdf. Experimentally, exponential tails of the scalar pdf have been observed when the scalar is subjected to a constant mean temperature gradient (Gollab et al., 1991, in a stirred fluid; Jayesh and Warhaft, 1991 and 1992, in grid turbulence; Castaing et al., 1989, in high Rayleigh number convection). The main conclusion of these experimental studies is that there exists a transitional Reynolds number, above which the tails of the scalar pdf would change from Gaussian to exponential. Jayesh and Warhaft (1992) suggested that the transitional Reynolds number Re_L (based on the integral length scale) must be larger than 70. In the present study, although Re_L was much greater than this value (for example, at Re_λ = 253, Re_L = 2380), the scalar pdf was essentially Gaussian, in agreement with the findings of Tavoularis and Corrsin (1981 a) in uniformly sheared flow, Thoroddsen and Van Atta (1992) in a stably stratified flow and Overholt and Pope (1996) in a numerical simulation. The lack of exponential tails in the scalar pdf cannot be attributed to the limited temperature range across the tunnel, because the present mean scalar profile extended over nearly ± 10 scalar standard deviations on either side of the measuring point. It may be relevant to mention that Jaberi et al. (1996) have concluded that the scalar pdf depends on the initial conditions and, if a constant mean scalar gradient is imposed, the long-time pdf would become Gaussian, in agreement with the present findings.

8.9 Joint Statistics of the Scalar and its Dissipation

Local isotropy requires the correlation between the scalar and its destruction rate to be zero. The corresponding correlation coefficient is defined as (Eswaran and Pope, 1988)

$$\rho_{\theta^2\varepsilon_\theta} = \frac{\overline{(\theta^2-\overline{\theta^2})(\varepsilon_\theta-\langle\varepsilon_\theta\rangle)}}{\left[\overline{(\theta^2-\overline{\theta^2})^2}\right]^{1/2}\left[\overline{(\varepsilon_\theta-\langle\varepsilon_\theta\rangle)^2}\right]^{1/2}} \tag{8.4}$$

The thermal destruction rate was estimated from the locally isotropic expression as $\varepsilon_\theta = 3\gamma\overline{(\partial\theta/\partial x_1{}^2)}$. Fig. 8.18 shows that the measured correlation were less than 0.02 for all Re_λ investigated suggesting that θ^2 and ε_θ are essentially statistically independent. Further insight into the statistical independence of θ and ε_θ can be inferred by evaluating the coherence of θ and ε_θ defined as

$$C_{\theta\varepsilon_\theta} = \frac{E_{1\theta\varepsilon_\theta}}{\sqrt{E_{1\theta}\,E_{1\varepsilon_\theta}}} \tag{8.5}$$

where $E_{1\theta}$ and $E_{1\varepsilon_\theta}$ are the one dimensional spectra of θ and ε_θ respectively. This has been evaluated and plotted for $Re_\lambda = 200$ and 253, up to frequencies equal to twice the frequency corresponding to the Taylor microscale (fig. 8.19), thus covering the inertial range, if any. The measured coherence was less than 0.02 within the examined frequency range, suggesting that θ and ϵ_θ are essentially independent in this flow configuration. Alternatively, one may consider the joint pdf of θ and ϵ_θ, $p(\theta, \epsilon_\theta)$. Statistical independence of θ and ϵ_θ requires that

$$p(\theta,\epsilon_\theta) = p(\theta)p(\epsilon_\theta) \tag{8.6}$$

Fig. 8.20 displays the pdf of ϵ_θ and indicates that high probability of ϵ_θ corresponds to values of ϵ_θ near the average, whereas, large fluctuations in ϵ_θ (up to 25 times its standard deviation), which constitute the long tail in its pdf, occur with low probability. Iso-probability contours of $p(\theta, \epsilon_\theta)$ at $Re_\lambda = 253$ are displayed in fig. 8.21a. These contours are nearly symmetrical with respect to the mean of the scalar fluctuations, suggesting that the fluid is well mixed and that the scalar dissipation gets nearly equal contributions from both the negative and positive scalar fluctuations. Fig. 8.21b is a plot of contours of the product of the pdf $p(\theta)p(\epsilon_\theta)$. No significant difference can be observed between figs. 8.21a and fig. 8.21b, which seems to validate equation 8.6 and hence, to suggest the independence of θ and ϵ_θ

Another quantity of interest in this thesis is the conditional expectation of the scalar dissipation, conditional upon the scalar $<\epsilon_\theta|\theta>$, which is a term in the transport equation of the scalar pdf (equation 4.24) that needs to be modeled. Fig. 8.22 shows the normalized conditional expectation of the scalar dissipation for $Re_\lambda = 200$ and 253. The data seem to suggest that, for $|\theta/\theta'| < 2$, this parameter is within $\pm$ 10% from one. Its constancy seems to improve as Re_λ increases, which may be attributed to the fact that the transverse homogeneity of the temperature fluctuations improves downstream of the heating elements. The figure also displays substantial scatter for values of $|\theta/\theta'| > 2$. Then, it is reasonable to conclude that the conditional expectation of the scalar dissipation is independent of the scalar, in agreement with the independence tests performed above.

The independence between ϵ_θ and θ has been observed in non-homogeneous turbulent flows in regions where the flow is well mixed. Anselmet et al. (1994) found that, for a heated turbulent boundary layer and a heated jet, when the scalar pdf was symmetrical with a skewness $S_\theta \approx 0$, ϵ_θ and θ were independent. Moreover, Mi et al. (1996) evaluated the joint statistics of ϵ_θ and θ in a heated jet and reported that the θ-ϵ_θ independence requires not only the scalar pdf to be symmetrical, but also the flow to be locally isotropic as well. The present measurements are in agreement with these studies as well as with the finding of Overholt and Pope (1996), who also reported that $<\epsilon_\theta|\theta>$ was nearly constant, independent of the scalar, when subjected to a constant mean transverse temperature gradient. The latter authors referred to the work of Miller et al. (1995), who demonstrated that, when the scalar has a Gaussian distribution in the presence of a mean temperature gradient, the conditional expectation of the scalar dissipation is independent of the scalar. The measurements of $<\epsilon_\theta|\theta>$ reported by Jayesh and Warhaft (1992) displayed a V-shape with the scalar. According to Mi et al (1996), the dependence of ϵ_θ on θ found by Jayesh and Warhaft (1992) is due to departure from local isotropy.

8.10 Velocity-Scalar Joint Statistics

The conditional expectations of the velocity fluctuations conditional upon the scalar $<u_1|\theta>$ and $<u_2|\theta>$, appearing in the transport equation of the scalar pdf (equation 4.24), have received little attention experimentally and theoretically. Figs. 8.23 and 8.24 display these terms, respectively, normalized by the corresponding r.m.s. values. If u_1-θ and u_2-θ were jointly normal, then these normalized quantities should be straight lines with slopes equal to the correlation coefficients $\rho_{u_1\theta}$ and $\rho_{u_2\theta}$, respectively. Figs. 8.23 and 8.24 suggest that $<u_1|\theta>$ and $<u_2|\theta>$ are nearly linear in θ, especially in the central portion of the figures, but they depart slightly from linearity at high values of $|\theta/\theta'|$. Small deviations from Gaussianity are also observed in the iso-probability contours of u_1-θ joint pdf (fig. 8.25) and u_2-θ joint pdf (fig. 8.26). Fits to figs. 8.23 and 8.24 at $Re_\lambda = 253$, provided the slopes 0.53 and -0.47 respectively, which are close to the evaluated correlations $\rho_{u_1\theta} = 0.56$ and $\rho_{u_1\theta} = -0.50$ at the same location. Similar conclusions have been reached by Venkataramani and Chevray (1979) in their experiment in a heated grid-generated turbulence with a constant mean temperature gradient, Tong and Warhaft (1994) in a heated jet and Overholt and Pope (1996) in a numerical simulation. Finally Sahay and O'Brien (1993) showed that, in their modeled pdf equation in heated grid-turbulence with a constant mean temperature gradient, if $<u_1|\theta>$ and $<u_2|\theta>$ are linear in θ and the pdf of the temperature fluctuations is Gaussian, then the conditional expectation of the scalar dissipation $<\epsilon_\theta|\theta>$ would be independent of θ. Although the present configuration is different from that used by Sahay and O'Brien (1993), their findings seem to apply to the present flow as well.

8.11 Statistics of Scalar derivatives and Differences

In contrast to the pdf of the temperature fluctuations which is nearly Gaussian, the pdf of their derivatives $\partial\theta/\partial x_1$ and $\partial\theta/\partial x_2$, plotted in figs. 8.27 and 8.28, respectively, show strong departures from the Gaussian pdf. Both pdf display a very sharp peak and exponential-like tails, which are indicative of internal intermittency of the scalar field. The difference between the two pdf resides in their asymmetry: the pdf of $\partial\theta/\partial x_1$ has a negative tail which is more flared than the positive one, whereas the opposite is observed in the pdf of $\partial\theta/\partial x_2$. Holzer and Siggia (1994) suggested an exponential fit to the tails of their streamwise scalar derivative pdf as

$$P(\partial\theta/\partial x_1) = \exp\left(-\beta|\partial\theta/\partial x_1|^{\alpha}\right) \tag{8.7}$$

Because these authors considered isotropic turbulence, the pdf of $\partial\theta/\partial x_1$ was symmetrical with a skewness of zero and β and α were the same for the negative and positive tails. In the present case, the streamwise and transverse scalar derivative pdf had asymmetrical tails, thus requiring two different fits to the same pdf. Such fittings to the tails of the pdf of $\partial\theta/\partial x_1$ suggested that $\beta = 1.9$ and $\alpha = 0.78$ for the negative tail and $\beta = 2.1$ and $\alpha = 0.82$ for the positive tail, which are measurably different from the values 2.50 and 0.66 reported by Holzer and Siggia (1994). Moreover, fitting to the tails of the pdf of $\partial\theta/\partial x_2$, gave $\beta = 1.98$ and $\alpha = 0.87$ for the negative tail and $\beta = 1.93$ and $\alpha = 0.72$ for the positive tail, which are also different from the Holzer and Siggia (1994) values mentioned above.

The asymmetry of the pdf of $\partial\theta/\partial x_1$ and $\partial\theta/\partial x_2$ is shown more clearly in figs. 8.29 and 8.30, in which the pdf have been multiplied by $z_{i\theta}^3 = [(\partial\theta/\partial x_i)/(\partial\theta/\partial x_i)']^3$, $i = 1, 2$, respectively. It is reminded that the area under those curves corresponds to the skewness of the scalar derivative $S_{\partial\theta/\partial x_i}$. These figures clearly show the asymmetry of the scalar derivative pdf, with the area of the negative lobe being larger than the area of the positive lobe for the pdf of $\partial\theta/\partial x_1$, while the opposite is observed for the pdf of $\partial\theta/\partial x_2$. This suggests that $S_{\partial\theta/\partial x_1}$ gets significant contributions from large and rare negative fluctuations of $\partial\theta/\partial x_1$, while $S_{\partial\theta/\partial x_2}$ gets significant contributions from large and rare positive fluctuations of $\partial\theta/\partial x_2$. Within the narrow range of Re_λ investigated, the measured skewness $S_{\partial\theta/\partial x_1}$, shown in fig. 8.31, was nearly constant, equal to -1.0. This value is very close to the value of -0.95 reported by Tavoularis and Corrsin (1981 b) at comparable Re_λ and falls within the scatter of data of $S_{\partial\theta/\partial x_1}$ compiled by Sreenivasan and Antonia (1997) in different shear flows. The existence of such a non-zero skewness is evidence of local anisotropy. Fig. 8.32 shows that the flatness of $\partial\theta/\partial x_1$, was nearly 19 within the Re_λ range covered. Note that, at a comparable Re_λ, the flatness of the streamwise velocity derivative $F_{\partial u_1/\partial x_1}$ was about 6.3, much smaller than $F_{\partial\theta/\partial x_1}$, suggesting that the scalar field is more intermittent than the velocity field. The measured $F_{\partial\theta/\partial x_1}$ is slightly higher than the value of 15 reported by Tavoularis and Corrsin (1981 b) but compares well with the data reported by Sreenivasan and Antonia (1997).

Statistics of $\partial\theta/\partial x_2$ were determined at a single location on the centerline of the wind tunnel, at which $Re_\lambda = 200$. The evaluated skewness of the transverse scalar derivative $S_{\partial\theta/\partial x_2}$ was 1.47, comparable to measurements in other shear flows (Tavoularis and Corrsin, 1981 b; Sreenivasan et al., (1977); Mestayer, 1982). It is pointed out, however, that values of $S_{\partial\theta/\partial x_2}$ measured in grid turbulence with a constant mean scalar gradient were higher than those obtained in shear flows. Tong and Warhaft (1994), Holzer and Siggia (1994) and Pumir (1994) found this skewness to be about 1.9, independently of Re_λ. Tong and Warhaft (1994) suggested that the high values of $S_{\partial\theta/\partial x_2}$ in shearless turbulent flows are associated with the strong correlation between u_2 and θ in such flows. The flatness of the transverse scalar derivative $F_{\partial\theta/\partial x_2}$ at $Re_\lambda = 200$ was about 13.0, comparable to the values of 11.0 reported by

Tavoularis and Corrsin (1981 b) and 10.0 reported by Mestayer (1982) in a turbulent boundary layer at Re_λ = 616. At a comparable Re_λ, $F_{\partial u_1/\partial x_2}$ was found to be about 8.0, considerably smaller than $F_{\partial\theta/\partial x_2}$ confirming previous observations that the scalar field is more intermittent than the velocity field.

Fig. 8.33 is a plot of the compensated frequency spectra of the streamwise velocity, $f^n E_1(f)$, and the temperature fluctuations, $f^{n\theta} E_{1\theta}(f)$, at $Re_\lambda = 253$. The values of n and n_θ were chosen such that the plots presented the longest possible plateau, which presumably extends over the inertial range. The most suitable values of n and n_θ were found to be about 1.50 and 1.24, respectively. Figs. 8.34 and 8.35 are plots of the pdf of the streamwise and transverse scalar differences, respectively, for varying separations r/η. It can be seen from these figures that, even for relatively large separation distances, the pdf have sharp peaks and exponential-like tails, consistently with the expected intermittency of the scalar field in the inertial range. This is corroborated by the plots of the flatness of the scalar difference, $F_{\Delta\theta(x_1)}$ and $F_{\Delta\theta(x_2)}$ (figs. 8.36 and 8.37 respectively), which decreased from the flatnesses of the corresponding derivatives to about 3 at large separation distances. This suggests that the scalar internal intermittency becomes more pronounced as the separation distance decreased. Note that, for all r/η, the measured flatness of the streamwise scalar difference was higher than that of the transverse scalar difference. Finally, figs. 8.38 and 8.39 show the variations of the skewness of the streamwise and transverse scalar differences $S_{\Delta\theta(x_1)}$ and $S_{\Delta\theta(x_2)}$ for varying r/η. These decreased monotonically with r/η and they seem to approach zero as r becomes comparable to the integral length scale. The same trends were also observed by Mydlarski and Warhaft (1998).

Chapter 9

Conclusions and Recommendations for Future Research

9.1 Conclusions

The present thesis is an experimental study related to the statistics of the fine structure of the velocity and the scalar fields in uniformly sheared turbulence with an imposed mean scalar gradient. Measurements of the streamwise and transverse velocity derivatives and differences and structure functions were presented. Measurements of the scalar pdf, scalar-scalar dissipation joint statistics and scalar-velocity joints statistics for use in the pdf formulation of scalar mixing in turbulent flows were also reported. Also, statistics of the streamwise and transverse scalar derivatives and differences were included. The measurements of quantities related to the velocity fine structure were done for Re_λ ranging from 140 to 660. The heating system, introduced into the flow, produced a constant mean temperature gradient of about 7.8 K/m and the Re_λ achieved in this case, varied from 184 to 253. The main conclusions of this study are as follows.

- The measured streamwise and transverse velocity derivative skewnesses were non-zero. The streamwise velocity derivative skewness was negative and varied only slowly with Re_λ. In contrast, the transverse velocity derivative skewness was positive and decreased with increasing Re_λ for the range of Re_λ investigated.
- The measured flatnesses of the streamwise and transverse velocity derivatives increased with increasing Re_λ, with the latter increasing at a slower rate.
- The Kolmogorov constant evaluated from the one dimensional spectrum and from the longitudinal second order structure function resulted in nearly the same value.
- The skewnesses of the transverse and the longitudinal velocity differences were nearly constant in the inertial range for Re_λ between 470 and 660.
- The flatnesses of the transverse and longitudinal velocity differences showed systematic increase with increasing Re_λ and separation distances in the inertial range.
- The measured structure functions of orders up to six suggested that intermittency corrections to Kolmogorov's scaling may only be required for structure functions of orders higher than 4.
- The pdf of the scalar fluctuations was nearly Gaussian for all Re_λ investigated.
- The joint statistics of the scalar and its dissipation rate suggested that the dissipation rate was essentially independent of the scalar.
- The normalized expectations of the velocity fluctuations conditioned upon the scalar were nearly linear in the scalar with slopes corresponding to the measured turbulent

velocity-scalar correlations.

- The measured skewness of the streamwise and transverse scalar derivatives were non-zero.
- The scalar field was found to be more intermittent than the velocity field in both the dissipative range as well as in the inertial range.

9.2 Recommendations for Future Research

- Measurements of the transverse velocity derivatives in uniformly sheared turbulence at much higher Re_λ to study their asymptotic behaviour would be very useful for comparison of the streamwise and transverse velocity derivative statistics. This may be accomplished by designing a shear generator for a wind tunnel with a flow rate larger than the ones used in this study.
- A systematic study should be conducted to investigate the effects of the hot wire size and spacing on the measured transverse derivative statistics.
- Some improvements to the heating system such that scalar studies could be conducted at higher Re_λ.
- Different scalar fields could be introduced into the flow to study the effect of initial conditions on the scalar pdf. Moreover, the case of a uniform scalar field would be useful if one is to investigate the effect of the mean shear on the scalar mixing.

Bibliography

ANSELMET, F., GAGNE, Y., HOPFINGER, E.J. and ANTONIA, R.A., 1984 *High-order velocity structure functions in turbulent shear-flows.* J. Fluid Mech. **140**, 63.

ANSELMET, F., DJERIDI, H. and FULACHIER, L., 1991 *Joint statistics between a passive scalar and its dissipation in a turbulent boundary layer.* In Proceedings of the 8th Symposium on Turbulent Shear Flow, Munich, 27-3.

ANSELMET, F., DJERIDI, H. and FULACHIER, L., 1994 *Joint statistics between a passive scalar and its dissipation in turbulent flows.* J. Fluid Mech. **280**, 173.

ANTONIA, R.A., BROWNE, L.W.B., and SHAH, D.A., 1989 *Instantaneous dissipations of turbulent energy and temperature in a wake.* Phys. Fluids A **1**, 1374.

ANTONIA, R.A., HOPFINGER, E.J., GAGNE, Y. and ANSELMET, F., 1984 *Temperature structure functions in turbulent shear flows.* Phys. Rev. A **30**, 2704.

ANTONIA, R.A., ZHU, Y., ANSELMET, F. and OULD-ROUIS, M., 1996 *Comparison between the sum of second-order velocity structure functions and the second-order temperature structure function.* Phys. Fluids **8**, 3105.

ANTONIA, R.A., SATYAPRAKASH, B.R. and HUSSAIN, A.K.M.F .,1982 *Statistics of fine-scale velocity in turbulent plane and circular jets.* J. Fluid Mech. **119**, 55.

ANTONIA, R.A. and MI, J., 1993 *Temperature dissipation in a turbulent round jet.* J. Fluid Mech. **250**, 531.

ANTONIA, R.A., DJERIDI, L. and SPALART, P.R., 1994 *Anisotropy of the dissipation* *tensor in a turbulent flow*. Phys. Fluids **6**, 2475.

ANTONIA, R.A., OULD-ROUIS, M., ANSELMET, F. and ZHU, Y., 1997 *Analogy between predictions of Kolmogorov and Yaglom*. J. Fluid Mech. **332**, 395.

ANTONIA, R.A. and BROWNE, L.W.B., 1986 *Anisotropy of the temperature dissipation in a turbulent wake*. J. Fluid Mech. **163**, 393.

BATCHELOR, G.K. and TOWNSEND, A.A., 1949 *The nature of turbulent motion at large wave-numbers*. Proc. Roy. Soc. Lond. A **199**, 238.

BATCHELOR, G.K., 1959 *Small-scale variation of convected quantities like temperature in turbulent fluid*. J. Fluid Mech. **5**, 113.

BENZI, R., BIFERALE, L., CILIBERTO, M.V. and TRIPICCONE, R., 1995 *On the intermittent energy transfer at viscous scales in turbulent flows*. Europhys. Lett. **32**, 709.

BENZI, R., CILIBERTO, S., TRIPICCIONE, R., BAUDET, C., MASSAIOLI, F. and SUCCI, S., 1993 *Extended self similarity in turbulent flows*. Phys. Rev. E **48**, 29.

BORATAV, O.N. and PELZ, R.B., 1997 *Structures and structure functions in the inertial range of turbulence*. Phys. Fluids **9**, 1400.

BORATAV, O.N., 1997 *On recent intermittency models of turbulence*. Phys. Fluids **9**, 1206.

BRIGGS, J., 1992 *Fractals: The Pattern of Chaos*. Simon and Schuster, New York.

BROWNE, L.W.B., and ANTONIA, R.A., 1987 *The effect of wire length on temperature statistics in a turbulent wake*. Exp. Fluids **5**, 426.

BUDWIG, R., TAVOULARIS, S. And CORRSIN, S., 1985 *Temperature fluctuations and heat flux in grid generated isotropic turbulence with streamwise and transverse mean-temperature gradients*. J. Fluid Mech. **153**, 441.

CASTAING, B., GUNARATNE, G., HESLOT, F., KADANOFF, L., LIBCHABER, A., THOMAE, S., WU, X.Z., ZALESKI S. and ZANETTI, G., 1989 *Scaling of hard thermal turbulence in Rayleigh-Benard convection*. J. Fluid Mech. **204**, 1.

CHEN, S., DOOLEN, G.D., KRAICHNAN, R.H. and SHE, Z.S., 1993 *On statistical correlations between velocity increments and locally averaged dissipation in homogeneous turbulence*. Phys. Fluids A **5**, 458.

CHEN, H., CHEN, S. and KRAICHNAN, R.H., 1989 *Probability distribution of a stochastically advected scalar field*. Phys. Rev. Lett. **63**, 2657.

CHING, E.S.C. and TSANG, Y.K., 1997 *passive scalar conditional statistics in a model of random advection*. Phys. Fluids **9**, 1353.

CHING, E.S.C. and TU, Y., 1994 *Passive scalar fluctuations with and without a mean gradient: A numerical study*. Phys. Rev. E **49**, 1278.

CORRSIN, S., 1962 *Turbulent dissipation fluctuations*. Phys. Fluids **5**, 1301.

CORRSIN, S., 1951 *On the spectrum of isotropic temperature fluctuations in isotropic turbulence*. J. Appl. Phys. **22**, 469.

DERKSEN, R.W. and AZAD, R.S., 1983 *An examination of hot-wire length correction*. Phys. Fluids **26**, 1751.

DOPAZO, C., 1975 *Probability density function approach for a turbulent axisymmetric heated jet*. Phys. Fluids **18**, 397.

DOPAZO, C. and O'BRIEN, E.E., 1975 *Functional formulation of nonisothermal turbulent reactive flows*. Phys. Fluids **17**, 1968.

DOPAZO, C. and VALIÑO, L., 1994 *Pdf approach and stochastic models of the turbulent* *mixing of inert and reactive statistically homogeneous scalar fields*. Transport Theory and Statistical Physics **23** (1-3), 339.

DOPAZO, C. and O'BRIEN, E.E., 1974 *An approach to the autoignition of a turbulent mixture.* Acta Astron. **1**, 1239.

DOPAZO, C., 1976 *A probabilistic approach to turbulent mixing of reactive scalars.* Third Symposium on Atmospheric Turbulence, Diffusion and Air Quality. American Meteorological Society, Boston.

DOPAZO, C., 1979 *Relaxation of initial probability density functions in the turbulent convection of scalar fields.* Phys. Fluids **22**, 20.

DOPAZO, C., 1976 *A probabilistic approach to the turbulent flame theory.* Acta Astron. **3**, 853.

DOWLING, D.R., 1991 *The estimated scalar dissipation rate in gas-phase turbulent jets.* Phys. Fluids A **3**, 2229.

ESWARAN, V. and POPE, S.B., 1988 *Direct numerical simulations of the turbulent mixing of a passive scalar.* Phys. Fluids **31**, 506.

FERCHICHI, M., 1991 *Evolution of a Thermal Mixing Layer in Uniformly Sheared Turbulent Flow*. M.A.Sc. Thesis, Department of Mechanical Engineering, University of Ottawa.

FERCHICHI, M. and TAVOULARIS, S., 1998 *A Selection of Test Cases for the Validation of Large-Eddy Simulations of Turbulent Flows: Decaying Grid Turbulence*. AGARD-AR-345, 61. Canada Communication Group Inc. Québec, Canada.

FOX, R.L., 1974 *The multipoint distribution function hierarchy for compressible turbulent* *flows.* Bull. Am. Phys. Soc. **19**, 93.

FOX, R.L., 1971 *Solution for turbulent correlations using multipoint distribution functions.* Phys. Fluids **14**, 1804.

FOX, R.O., 1997 *The Lagrangian spectral relaxation model of the scalar dissipation in homogeneous turbulence.* Phys. Fluids **9**, 2364.

FOX, R.O. 1996 *On velocity-conditioned scalar mixing in homogeneous turbulence.* Phys. Fluids **8**, 2678.

FOX, R.O., 1995 *The spectral relaxation model of the scalar dissipation rate in homogeneous turbulence.* Phys. Fluids 7, 1082.

FRISCH, U., SULEM, P.L. and NELKIN, M., 1978 *A simple dynamical model of intermittent fully developed turbulence.* J. Fluid Mech. **87**, 719.

FRISCH, U., 1995 *Turbulence: The Lagacy of A.N. Kolmogorov.* Cambridge University Press.

GAO, F., 1991 *Mapping closure and non-Gaussianity of the scalar probability density functions in isotropic turbulence.* Phys. Fluids **A 3**, 2438.

GAO, F. and O'BRIEN, E.E., 1991 *A mapping closure for multispecies Fickian diffusion.* Phys. Fluids **A 3**, 956.

GARG, S. and WARHAFT, Z., 1998 *On the small scale structure of simple shear flow.* Phys. Fluids **10**, 662.

GIBSON, C.H., FRIEHE, C.A. and McConnell S.O., 1977 *Structure of sheared turbulent fields.* Phys. Fluids **20**, S156.

GIBSON, C.H. and MASIELLO, P.J., 1972 *Observations of the variability of dissipation* *rates of turbulent velocity and temperature fields.* In Statistical Models and Turbulence, edited by M. Rosenblatt and C. Van Atta, Springer-Verlag, Berlin.

GIBSON, C.H., 1968 *Fine structure of scalar fields mixed by turbulence.* Phys. Fluids **11**, 2305.

GIBSON, C.H., STEGEN, G.R. and WILLIAMS, R.B., 1970 *Statistics of the fine structure of turbulent velocity and temperature fields measured at high Reynolds number.* J. Fluid Mech. **41**, 153.

GOLLUB, J.P., CLARKE, J., GHARIB, M., LANE, B. and MESQUITA, O.N., 1991 *Fluctuations and transport in a stirred fluid with a mean gradient.* Phys. Rev. Lett. **67**, 3507.

GURVICH, A.S., 1967 *Probability distribution of the square of the temperature difference between two points of a turbulent flow.* Soviet Physics-Doklady **12**, 17.

GURVICH, A.S. and YAGLOM, A.M., 1967 Breakdown of eddies and probability distributions for small scale turbulence. Phys. Fluids **10**, 559.

HESKESTAD, G., 1965 *A generalized Taylor hypothesis with application for high Reynolds number turbulent shear flows.* J. Applied Mech. 65-APM-G 1.

HOLZER, M. and SIGGIA, E.D., 1994 *Turbulent mixing of a passive scalar.* Phys. Fluids **6**, 1820.

HOLZER, M. and PUMIR, A., 1993 *Simple models of non-Gaussian statistics for a turbulently advected passive scalar*. Phys. Rev. E **47**, 202.

HOSOKAWA, I., 1994 *Probability distribution function of the temperature increment in isotropic turbulence*. Phys. Rev. E **49**, 4775.

HOSOKAWA, I. And YAMAMOTO, K., 1992 *Evidence against the Kolmogorov refined* *simalarity hypothesis.* Phys. Fluids A **4**, 457.

JABERI, F.A., MILLER, R.S., MADNIA, C.K. and GIVI, P., 1996 *Non-Gaussian scalar statistics in homogeneous turbulence.* J. Fluid Mech. **313**, 241.

JAYESH and WARHAFT, Z., 1991 *Probability distribution of a passive scalar in grid-generated turbulence.* Phys. Rev. Lett. **67**, 3503.

JAYESH, TONG, C. and WARHAFT, Z., 1994 *On temperature spectra in grid turbulence.* Phys. Fluids **6**, 306.

JAYESH AND WARHAFT, Z., 1992 *Probability distribution, conditional dissipation, and transport of passive temperature fluctuations in grid-generated turbulence.* Phys. Fluids A **4**, 2292.

JIANG, T.L. and GIVI, P., 1992 *Binary and Trinary scalar mixing by Fickian Diffusion - Some mapping closure results.* Phys. Fluids A **4**, 1028.

JIMENEZ, J., WRAY, A.A., SAFFMAN, P.G. and ROGALLO, R.S., 1993 *The structure of intense vorticity in homogeneous isotropic turbulence.* J. Fluid Mech. **255**, 65.

KAILASNATH, P., SREENIVASAN, K.R. and STOLOVITZKY, G., 1992 *Probability density of velocity increments in turbulent flows.* Phys. Rev. Lett. 68, 2766.

KAILASNATH, P., SREENIVASAN, K.R. and SAYLOR, J.R., 1993 *Conditional scalar dissipation rates in turbulent wakes, jets, and boundary layers.* Phys. Fluids A **5**, 3207.

KARNIK, U. And TAVOULARIS, S., 1989 *Measurements of heat diffusion from a continuous line source in a uniformly sheared turbulent flow.* J. Fluid Mech. **202**, 233.

KERR, R.M., 1985 *Higher-order derivative correlations and the alignment of small scale structures in isotropic numerical turbulence.* J. Fluid Mech., **153**, 31.

KERSTEIN, A.R. and ASHURST, W.T., 1984 *Lognormality of gradients of diffusive scalars in homogeneous, two-dimensional mixing system.* Phys. Fluids **27**, 2819.

KERSTEIN, A.R. and McMURTRY, P.A., 1994 b *Mean-field theories of random advection.* Phys. Rev. E **49**, 474.

KOLMOGOROV, A.N., 1941 *Local structure of turbulence in an incompressible fluid for very large Reynolds numbers.* Dokl. Akad. Nauk SSSR **30**, 299.

KOLMOGOROV, A.N., 1962 *A refinement of previous hypotheses concerning the local structure of turbulence in a viscous incompressible fluid at high Reynolds number.* J. Fluid Mech. **13**, 82.

KUO, A.Y.S. and CORRSIN, S., 1971 *Experiments on internal intermittency and fine structure distribution functions in fully turbulent fluid.* J. Fluid Mech. **50**, 285.

LANDAU, L.D. and LIFSHITZ, E.M., 1963 *Fluid Mechanics.* Pergamon Press, London.

LUMLEY, J.L., 1965 *Interpretation of time spectra measured in high-intensity shear flows.* Phys. Fluids **8**, 1056.

LUNDGREN, T.S., 1972 A *closure hypothesis for the hierarchy of equations for turbulent probability distribution function.* Lecture Notes In Physics **12**, 70.

LUNDGREN, T.S., 1969 *Model equation for the nonhomogeneous turbulence.* Phys. Fluids **12**, 485.

LUNDGREN, T.S., 1967 *Distribution functions in the statistical theory of turbulence.* Phys. Fluids **10**, 969.

MARINEAU-MES, S., 1997 *Fractal and Probabilistic Aaspects of Scalar Fluctuations Behind a Line Source in Turbulent Flows.* Ph.D. Thesis Proposal, Department of Mechanical

Engineering, University of Ottawa.

MENEVEAU, C. and SREENIVASAN, K.R., 1987 *Simple multifractal cascade model for fully developed turbulence*. Phys. Rev. Lett. **59**, 1424.

MESTAYER, P., 1982 *Local isotropy and anisotropy in a high-Reynolds-number turbulent boundary layer*. J. Fluid Mech. **125**, 475.

METAIS, O. and LESIEUR, M., 1992 *Spectral large-eddy simulation of isotropic and stably stratified turbulence*. J. Fluid Mech. **239**, 157.

MI, J. and ANTONIA, R.A., 1995 *General relation for stationary probability density functions*. Phys. Rev. E **51**, 4466.

MI, J., ANTONIA R.A. and ANSELMET, F., 1995 *Joint statistics between temperature and its dissipation rate components in a round jet*. Phys. Fluids **7**, 1665.

MONIN, A.S., 1968 *Equations for the finite dimensional probability distributions of a field of turbulence*. Soviet Physics-Doklady **12**, 1113.

MONIN, A.S. and YAGLOM, A.M., 1975 *Statistical Fluid Mechanics II*. M I T Press., Boston.

MYDLARSKI, L. and WARHAFT, Z., 1998 *Passive scalar statistics in high-péclet-number grid turbulence*. J. Fluid Mech. **358**, 135.

MYDLARSKI, L. and WARHAFT, Z., 1996 *On the onset of high-Reynolds-number grid generated wind tunnel turbulence*. J. Fluid Mech. **320** 331.

NOMURA, K.K. and ELGHOBASHI, S.E., 1992 *Mixing characteristics of an inhomogeneous scalar in isotropic and homogeneous sheared turbulence*. Phys. Fluids A **3**, 606.

O'BRIEN, E.E. and JIANG, T.L., 1991 *The conditional dissipation rate of an initially binary scalar in homogenous turbulence.* Phys. Fluids A **3**, 3121.

OBUKHOV, A.M., 1962 *Some specific features of atmospheric turbulence.* J. Fluid Mech. **13**, 77.

OBUKHOV, A.M., 1949 *Structure of the temperature field in turbulent flow.* Izv. Akad. Nauk SSSR, Ser. Geogr. i Geofiz. **13**, 58.

OVERHOLT, M.R. and POPE, S.B., 1996 *Direct numerical simulation of a passive scalar with imposed mean gradient in isotropic turbulence.* Phys. Fluids **8**, 3128.

PARISI, G. and FRISCH, U., 1985 *On the singularity structure of fully developed turbulence.* In Turbulence and Predictability in Geophysical Fluid Dynamics, ed. M. Ghil, R. Benzi and G. Parisi, 84.

POPE, S.B., 1976 *The probability approach to the modeling of turbulent reacting flows.* Combust. Flame **27**, 299.

POPE, S.B., 1985 *Pdf methods for turbulent reactive flows.* Prog. Energy Combust. Sci. **11**, 119.

PRASKOVSKY, A., PRASKOVSKAYA, E. and HURST, T., 1997 *Further experimental support for the Kolmogorov refined similarity hypothesis.* Phys. Fluids **9**, 2465.

PUMIR, A., 1994b *Small-scale properties of scalar and velocity differences in three-dimensional turbulence.* Phys. Fluids **6**, 3974.

PUMIR, A., SHRAIMAN, B. And SIGGIA, E.D., 1991 *Exponential tails and random advection.* Phys. Rev. Lett. **66**, 2984.

PUMIR, A., 1994a *A numerical study of the mixing of a passive scalar in three dimensions* *in the presence of a mean gradient*. Phys. Fluids **6**, 2118.

PUMIR, A., 1996 *Turbulence in homogeneous shear flows*. Phys. Fluids **8**, 3112.

SAHAY, A. and O'BRIEN, E., 1993 *Uniform mean scalar gradient in grid turbulence: Conditioned dissipation and production*. Phys. Fluids A **5**, 1076.

SHAH, D.A. and ANTONIA, R.A., 1986 *A comparison between measured and calculated thermal inertia of cold wires*. DANTEC Information **2**, 13.

SHE, Z.-S. and LÉVÊQUE, E., 1994 *Universal scaling laws in fully developed turbulence*. Phys. Rev. Lett. **72**, 336.

SHE, Z.-S., 1991 *Physical model of intermittency in turbulence. Near-dissipation-range non-Gaussian statistics*. Phys. Rev. Let. **66**, 600.

SHE, Z.S and ORSZAG, S.A., 1991 *Physical model of intermittency in turbulence: Inertial-range non-Gaussian statistics*. Phys. Rev. Lett. **66**, 1701.

SINAI, Y.G. and YAKHOT, V., 1989 *Limiting probability distributions of a passive scalar in a random velocity field*. Phys. Rev. Lett. **63**, 1962.

SREENIVASAN, K.R., 1995 *On the universality of the Kolmogorov constant*. Phys. Fluids **7**, 2778.

SREENIVASAN, K.R., TAVOULARIS, S., 1980 *On the skewness of the temperature derivative in turbulent flows*. J. Fluid Mech. **101**, 783.

SREENIVASAN, K.R., 1991 *On local isotropy of passive scalars in turbulent shear flows*. Proc. R. Soc. Lond. A **434**, 165.

SREENIVASAN, K.R., ANTONIA, R.A. And BRITZ, D.,1979 *Local isotropy and large structures in a heated turbulent jet*. J. Fluid Mech. **94**, 745.

SREENIVASAN, K.R., 1996 *The passive scalar spectrum and the Obukhov-Corrsin constant*. Phys. Fluids **8**, 189.

SREENIVASAN, K.R., ANTONIA, R.A. and DANH, H.Q., 1977 *Temperature dissipation fluctuations in a turbulent boundary layer*. Phys. Fluids **20**, 1238.

SREENIVASAN, K.R. and ANTONIA, R.A., 1997 *The phenomenology of small-scale turbulence*. Annu. Rev. Fluid Mech. **29** 435.

STOLOVITZKY, G., KAILASNATH, P. and SREENIVASAN, K.R., 1995 *Refined similarity hypotheses for passive scalars mixed by turbulence*. J. Fluid Mech. **297** 275.

TABELING, P., ZOCCHI, G., BELIN, F., MAURER, J. and WILLAIME, H., 1996 *Probability density functions, skewness and flatness in large Reynolds number turbulence*. Phys. Rev. E. **53**, 1613.

TAVOULARIS, S., 1986 *Techniques for turbulence measurements*. Encyclopedia of Fluid Mechanics. By Gulf Publishing Company, Houston, Texas.

TAVOULARIS, S. and KARNIK. U., 1989 *Further experiments on the evolution of turbulent stresses and scales in uniformly sheared turbulence*. J. Fluid Mech. **204**, 457.

TAVOULARIS, S. and SREENIVASAN, K.R., 1981 *Skewness of the temperature derivative in an asymmetrically heated wake*. Phys. Fluids **24**, 778.

TAVOULARIS, S. and CORRSIN, S., 1981a *Experiments in nearly homogenous turbulent shear flow with a uniform mean temperature gradient*. J. Fluid Mech. **104**, 311.

TAVOULARIS, S. and CORRSIN, S., 1981b *Experiments in nearly homogenous turbulent shear flow with a uniform mean temperature gradient*. J. Fluid Mech. **104**, 349.

TENNEKES, H., 1968 *Simple model for the small-scale structure of turbulence*. Phys.

Fluids **11**, 669.

THORODDSEN, S.T., 1995 *Reevaluation of the experimental support for the Kolmogorov refined similarity hypothesis*. Phys. Fluids 7, 691.

THORODDSEN, S.T. and VAN ATTA, C.W., 1992*a* *Exponential tails and skewness of density-gradient probability density functions in stably stratified turbulence*. J. Fluid Mech. **244**, 547.

THORODDSEN, S.T. and VAN ATTA, C.W., 1992b *Experimental evidence supporting Kolmogorov's refined similarity hypothesis*. Phys. Fluids A 4, 2592.

THORODDSEN, S.T. and VAN ATTA, C.W., 1996 *Experiments on density-gradient anisotropies and scalar dissipation of turbulence in a stably stratified fluid*. J. Fluid Mech. **322**, 383.

TONG, C. and WARHAFT, Z., 1995 *Passive scalar dispersion and mixing in a turbulent jet*. J. Fluid Mech. **292**, 1.

TONG, C. and WARHAFT, Z., 1994 *On passive scalar derivative statistics in grid turbulence*. Phys. Fluids **6**, 2165.

VALIÑO, L., DOPAZO, C. and ROS, J., 1994 *Quasistationary probability density functions in the turbulent mixing of a scalar field*. Phys. Rev. Lett. **72**, 3518.

VALIÑO, L., 1995 *Multiscalar mapping closure for mixing in homogeneous turbulence*. Phys. Fluids 7, 144.

VAN ATTA, C.W., 1971 *Influence of fluctuations in local dissipation rates on turbulent scalar characteristics in the inertial subrange*. Phys. Fluids 14, 1803.

VAN ATTA, C.W., 1991 *Local isotropy of the smallest scales of turbulent scalar and* *velocity fields*. Proc. Royal. Soc. Lond. A **434**, 139.

VAN ATTA, C.W., 1973 *Influence of fluctuations in local dissipation rates on turbulent scalar characteristics in the inertial subrange*. Phys. Fluids **14**, 1803.

VENKATARAMANI, K.S. and CHEVRAY, R., 1978 *Statistical features of heat transfer in grid-generated turbulence: constant gradient case*. J. Fluid Mech. **86**, 513.

WANG, L.P., CHEN, S., BRASSEUR, J.G. and WYNGAARD, J.C., 1996 *Examination of hypotheses in Kolmogorov refined turbulence theory through high-resolution simulations*. J. Fluid Mech. **309**, 113.

WYNGAARD, J.C. and TENNEKES, H., 1970 *Measurements of small scale structure of turbulence at moderate Reynolds numbers*. Phys. Fluids **13**, 1962.

WYNGAARD, J.C., 1968 *Measurements of small-scale turbulence structure with hot wires*. J. Sci. Instrum. **1**, 1105.

WYNGAARD, J.C., 1971 *Spatial resolution of a resistance wire temperature sensor*. Phys. Fluids **14**, 2052.

WYNGAARD, J.C., 1969 *Spatial resolution of the vorticity meter and other hot-wire arrays*. J. Sci. Instrum. **2**, 983.

YAGLOM, A.M., 1949 *On the local structure of a temperature field in a turbulent flow*. Dokl. Akad. Nauk. SSSR **69**, 743.

YAKHOT, V., 1989 *Probability distributions in high-Rayleigh-number* Bénard *convection*. Phys. Rev. Lett. **63**, 1965.

ZHU, Y., ANTONIA, R.A. and HOSOKAWA, I., 1995 *Refined similarity hypotheses for turbulent velocity and temperature fields*. Phys. Fluids **7**, 1637.

x_f/h	$\overline{U}_c$ (m/s)	k_s (m^{-1})	u' (m/s)	ϵ (m^2/s^3)	λ_{11} (mm)	Re_λ	η (mm)
0	7.37	7.2	0.47	2.43	4.61	140	0.20
4	7.42	7.2	0.65	3.97	4.98	209	0.18
6	7.37	7.4	0.79	5.40	5.17	264	0.16
8	7.29	7.3	0.97	7.48	5.41	339	0.15
10	7.29	6.9	1.14	9.79	5.56	410	0.14
11	7.30	6.9	1.22	11.18	5.56	438	0.14
0	13.45	7.0	0.74	9.75	3.61	172	0.14
4	13.21	7.2	1.17	18.71	4.12	311	0.12
6	13.08	6.8	1.42	25.24	4.31	395	0.11
8	12.85	7.0	1.68	34.06	4.39	476	0.10
10	12.67	7.0	2.00	46.38	4.48	578	0.10
11	12.71	6.9	2.19	51.09	4.67	660	0.09

Table 7.1: Flow characteristics for the velocity fine structure measurements.

x_1/h	$\overline{U}_c$ (m/s)	k_s (m^{-1})	u' (m/s)	θ' (°C)	ϵ (m^2/s^3)	λ_{11} (mm)	$\lambda_{1\theta}$ (mm)	Re_λ	η (mm)	η_θ (mm)
3	6.74	5.9	0.54	0.073	2.43	5.3	4.6	184	0.20	0.26
4.7	6.65	5.8	0.59	0.081	2.96	5.2	4.5	200	0.19	0.24
6.3	6.59	6.0	0.66	0.093	3.86	5.1	4.5	217	0.18	0.23
8	6.54	6.2	0.76	0.109	4.98	5.2	4.7	253	0.17	0.21

Table 8.1: Flow characteristics for the scalar mixing measurements.

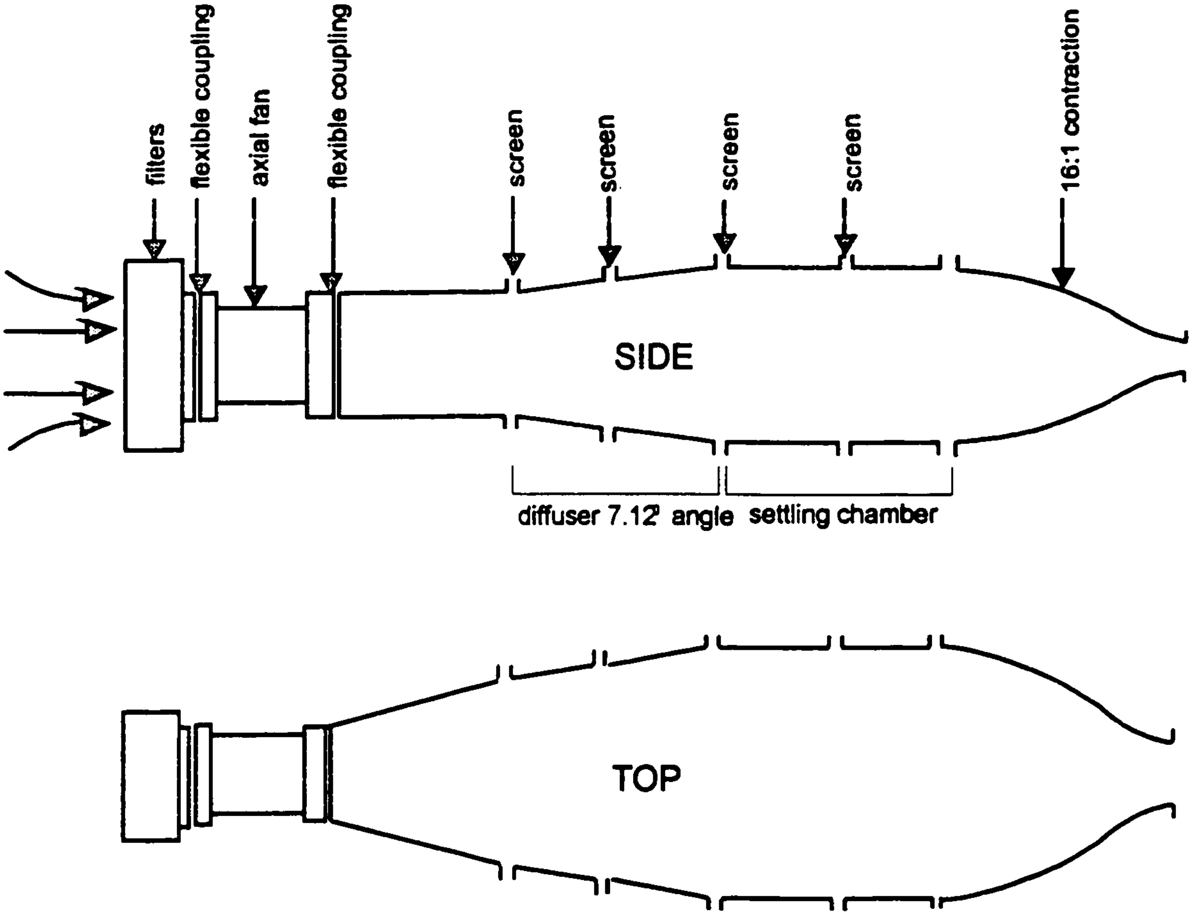

Fig. 5.1: Upstream section of wind tunnel.

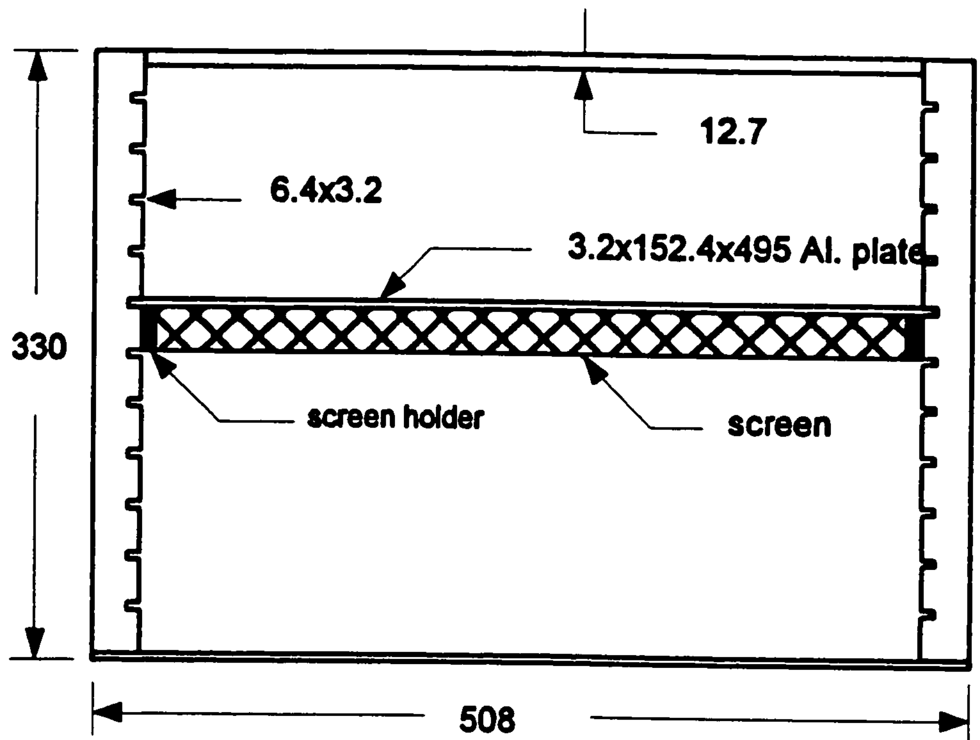

Fig. 5.2: Shear generator (dimensions in mm).

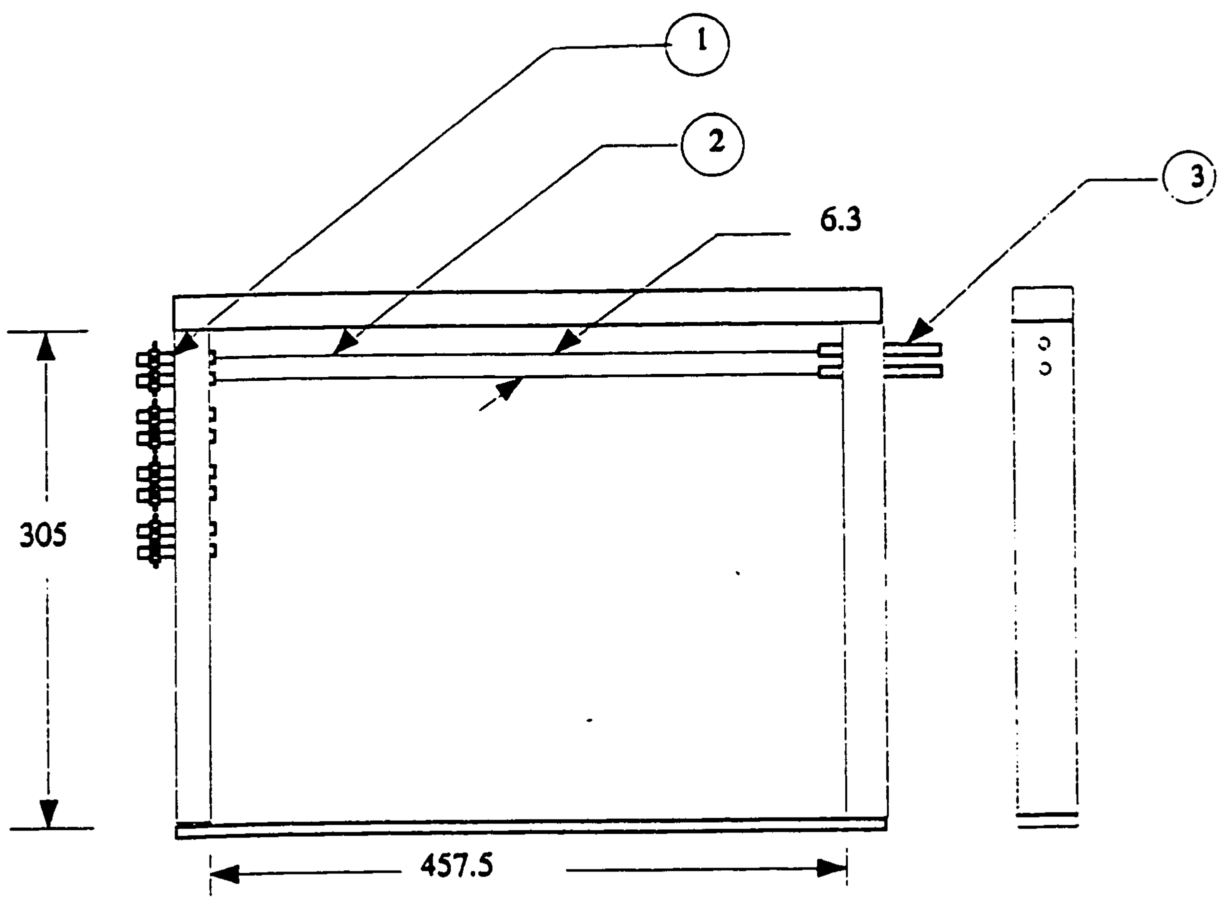

Fig. 5.3: Heating system: (1) connection of two elements in series; (2) 47 heating ribbons;

(3) springs attached to ends.

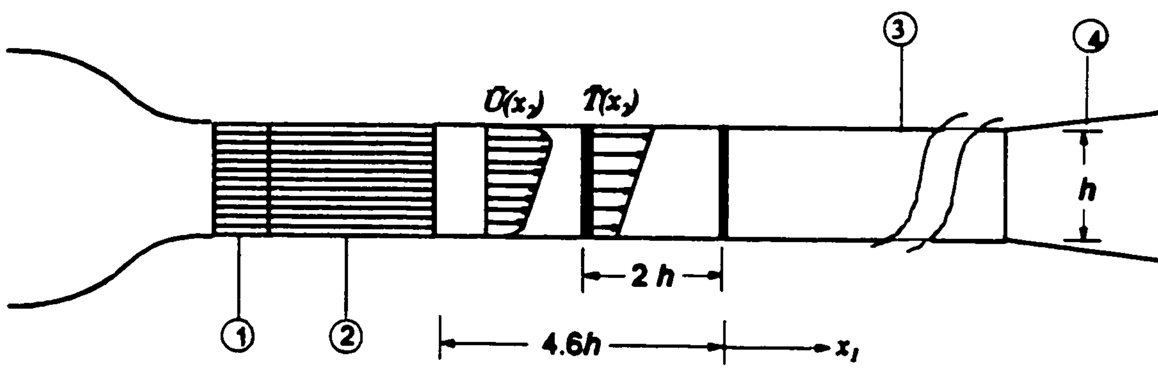

Fig. 5.4: Downstream section of wind tunnel: (1) shear generator; (2) flow separator; (3) test section; (4) optional diffuser.

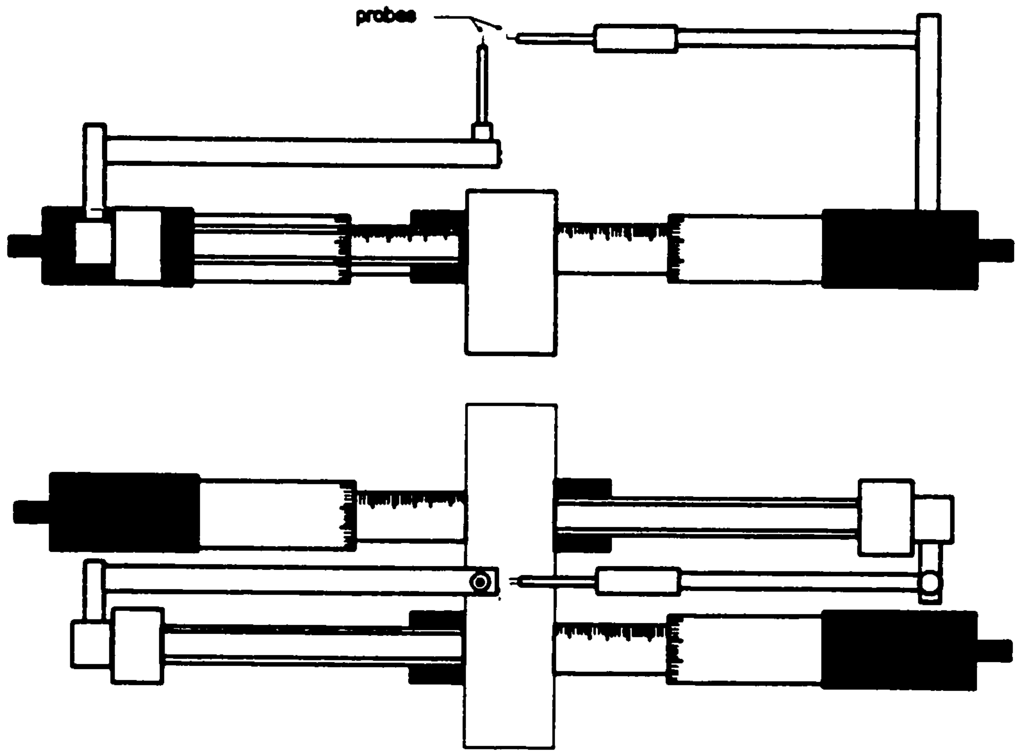

Fig. 5.5: Traversing mechanism for parallel wires.

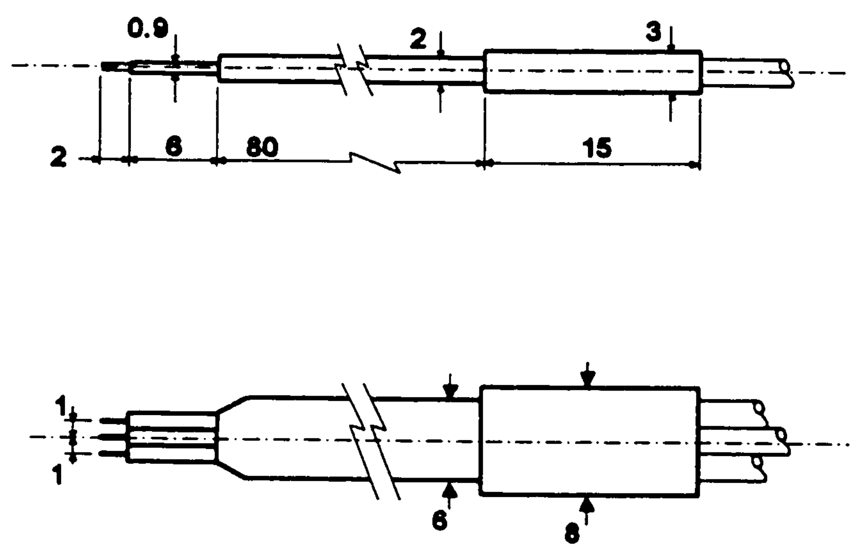

Fig. 5.6: Triple wire probe (dimensions in mm).

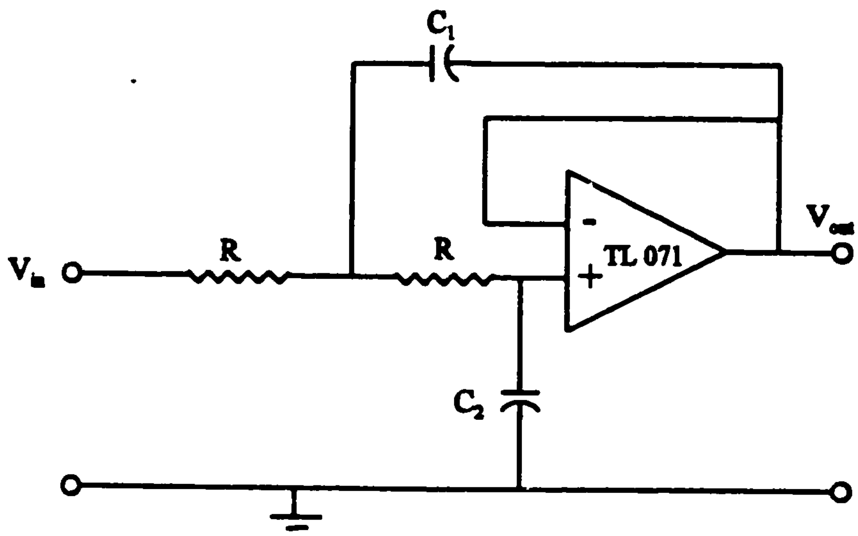

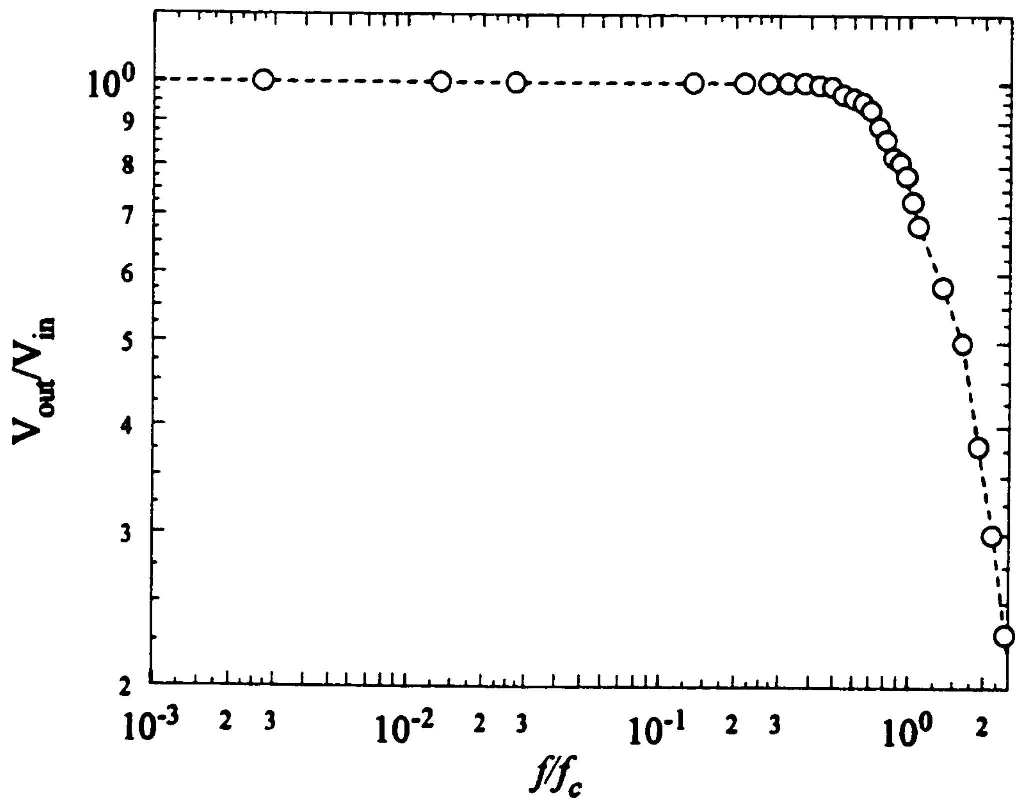

Fig. 5.7 : Butterworth second order low pass filter and its frequency response.

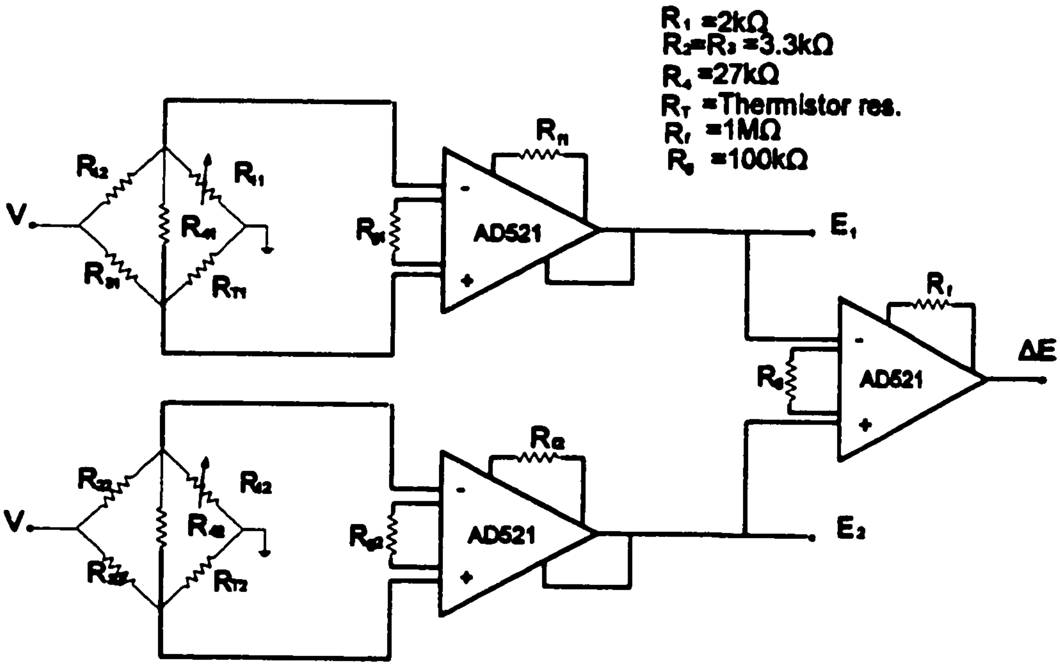

Fig. 5.8 : Thermistor circuits (Karnik, 1988).

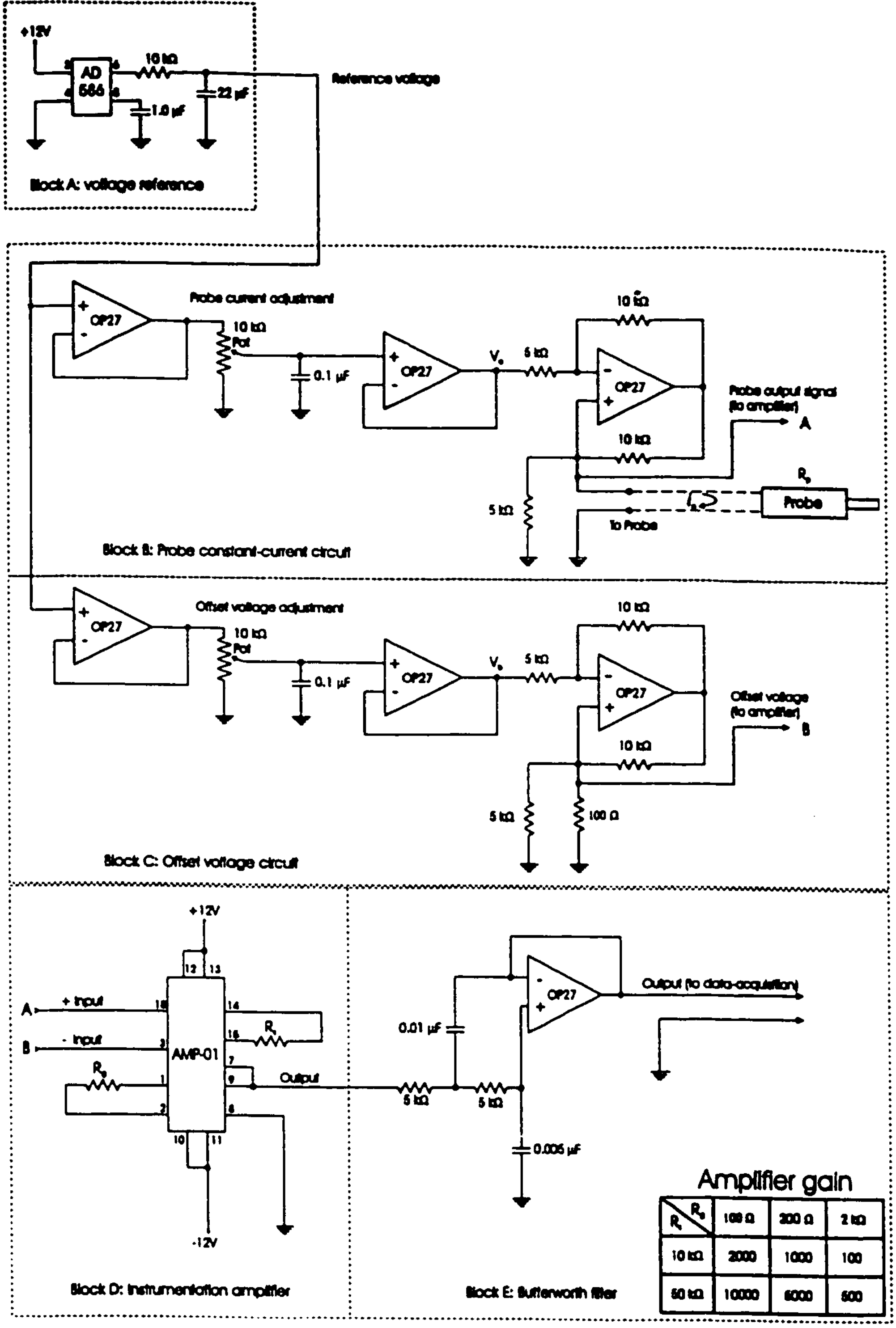

R_s \ R_g	100 Ω	200 Ω	2 kΩ
10 kΩ	2000	1000	100
50 kΩ	10000	5000	500

Fig. 5.9: Cold wire circuitry (Marineau-Mes, 1997).

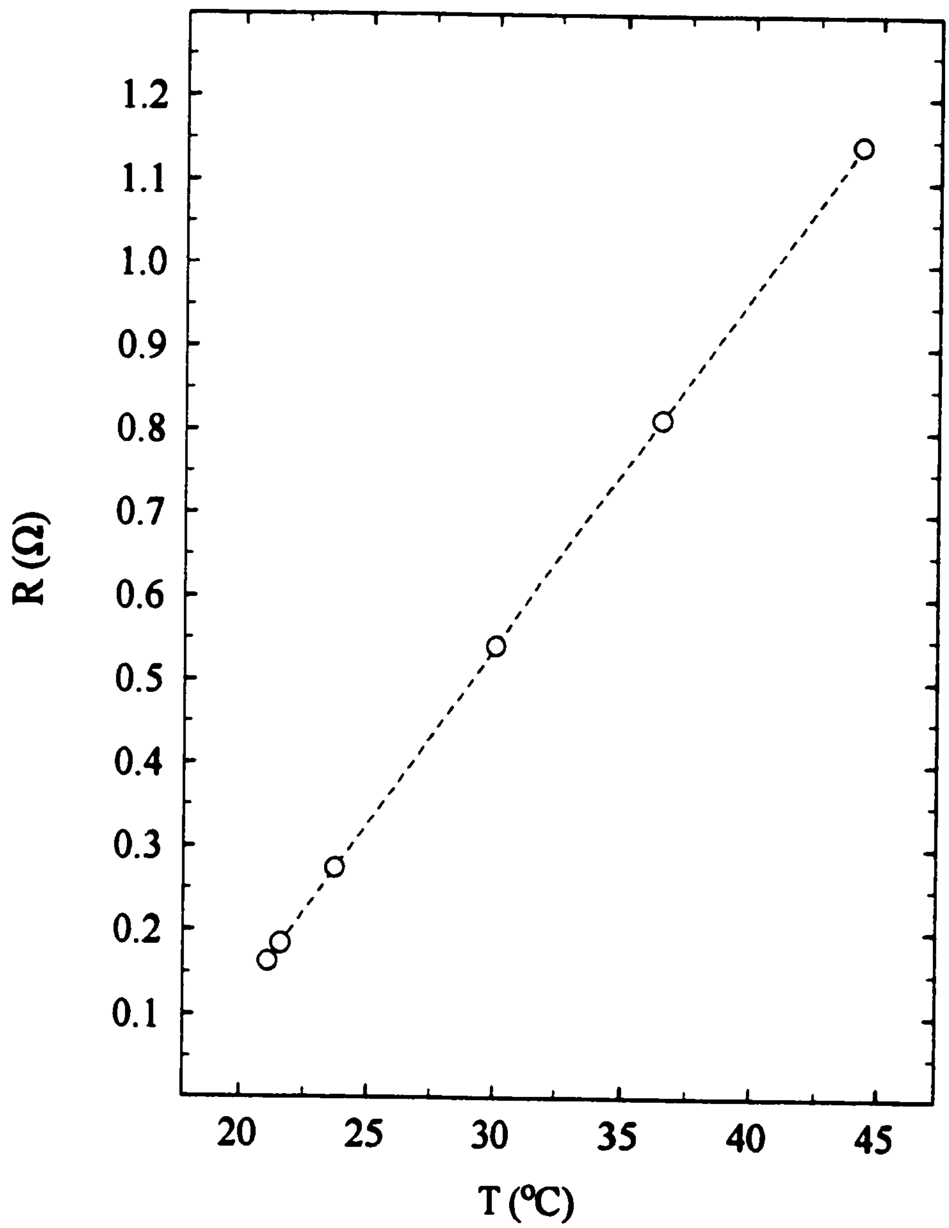

Fig. 6.1: Typical variation of hot wire resistance with temperature.

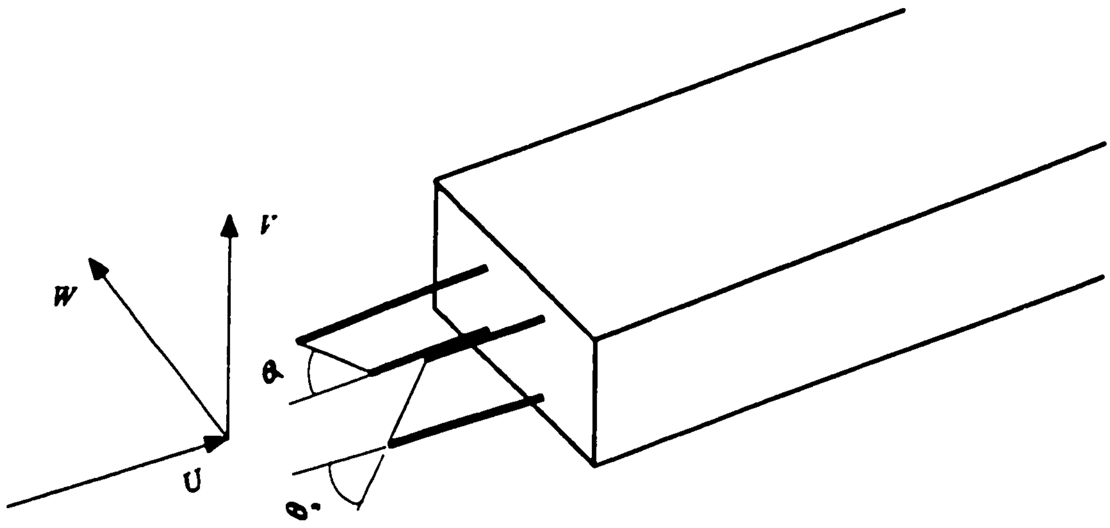

Fig. 6.2: Orientation of the cross-wires.

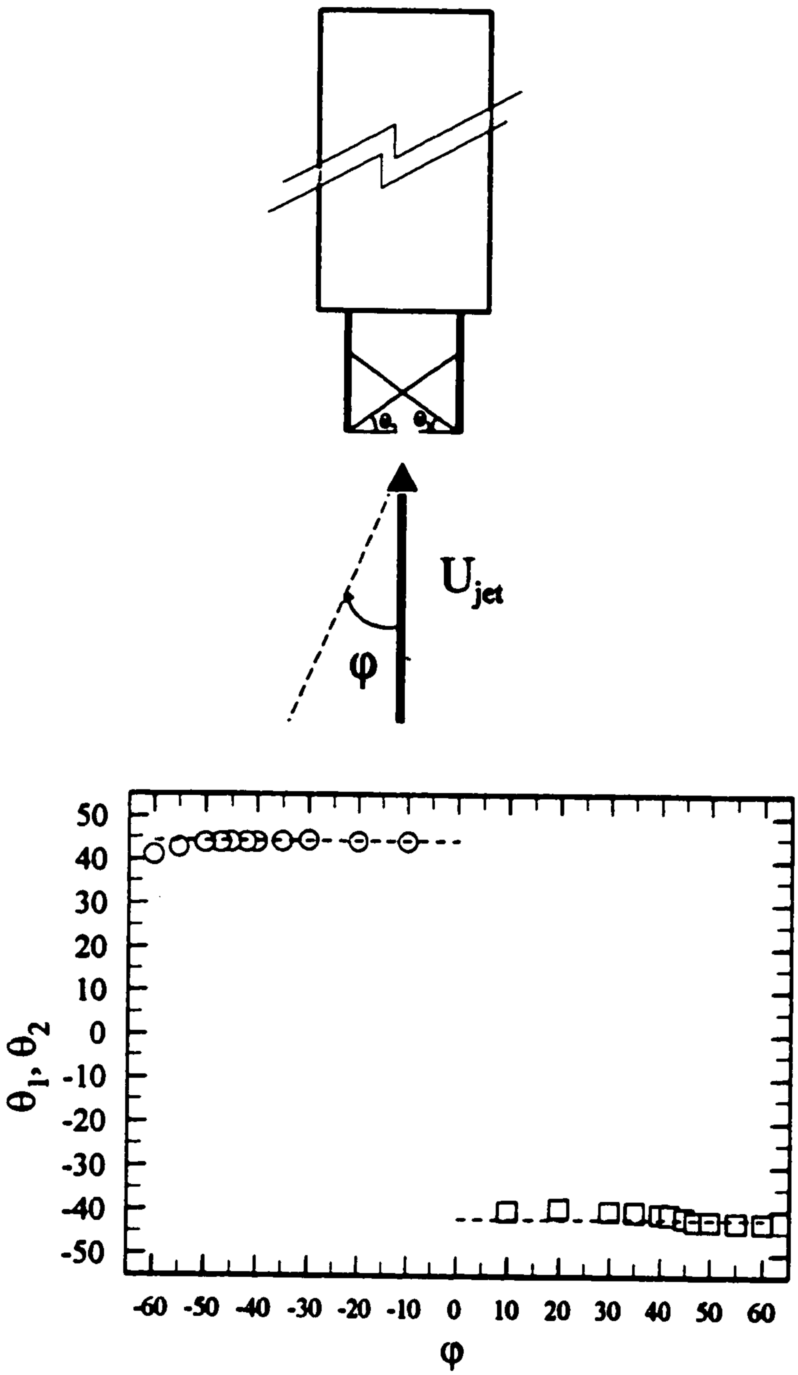

Fig. 6.3: Determination of the cross-wires angles.

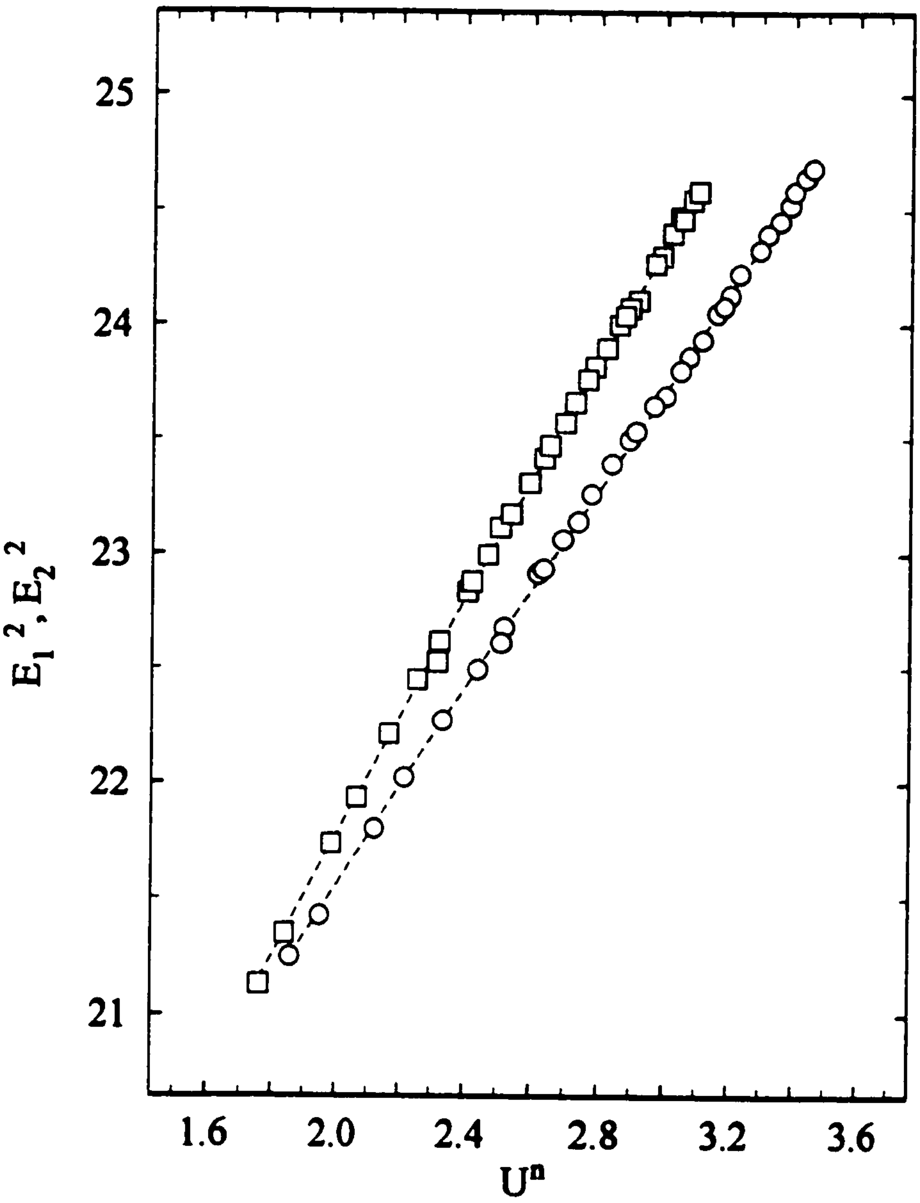

Fig. 6.4: Typical calibration curves of the cross-wires n_1=0.44; n_2=0.42.

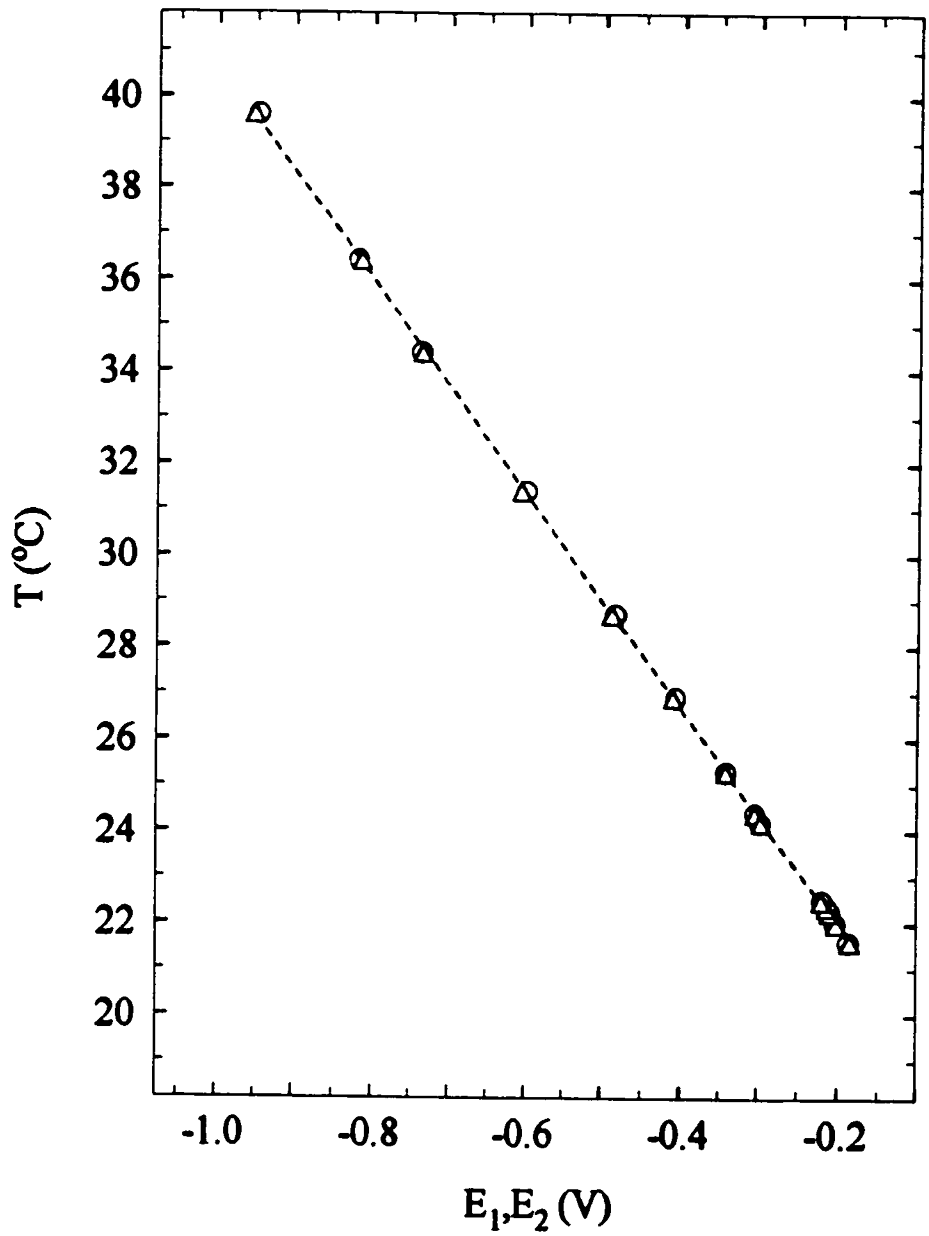

Fig. 6.5: Typical calibration curves of thermistors.

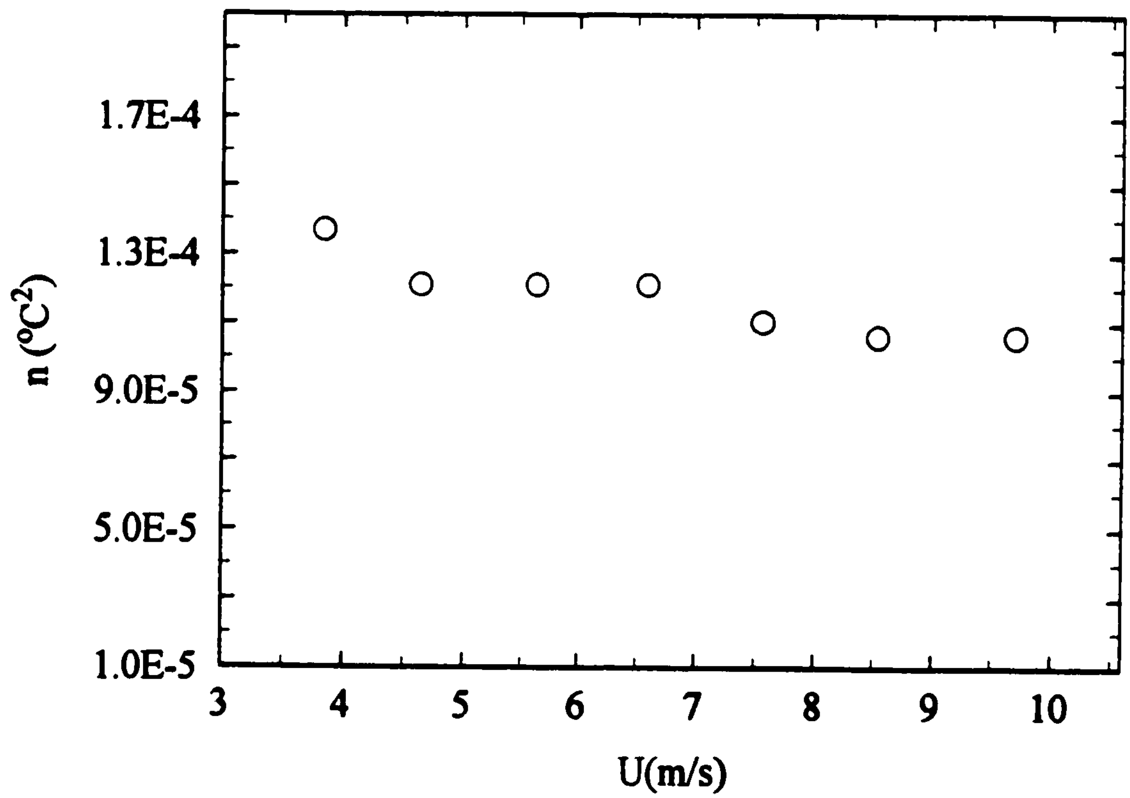

Fig. 6.6: Variations of cold wire sensitivity with mean velocity.

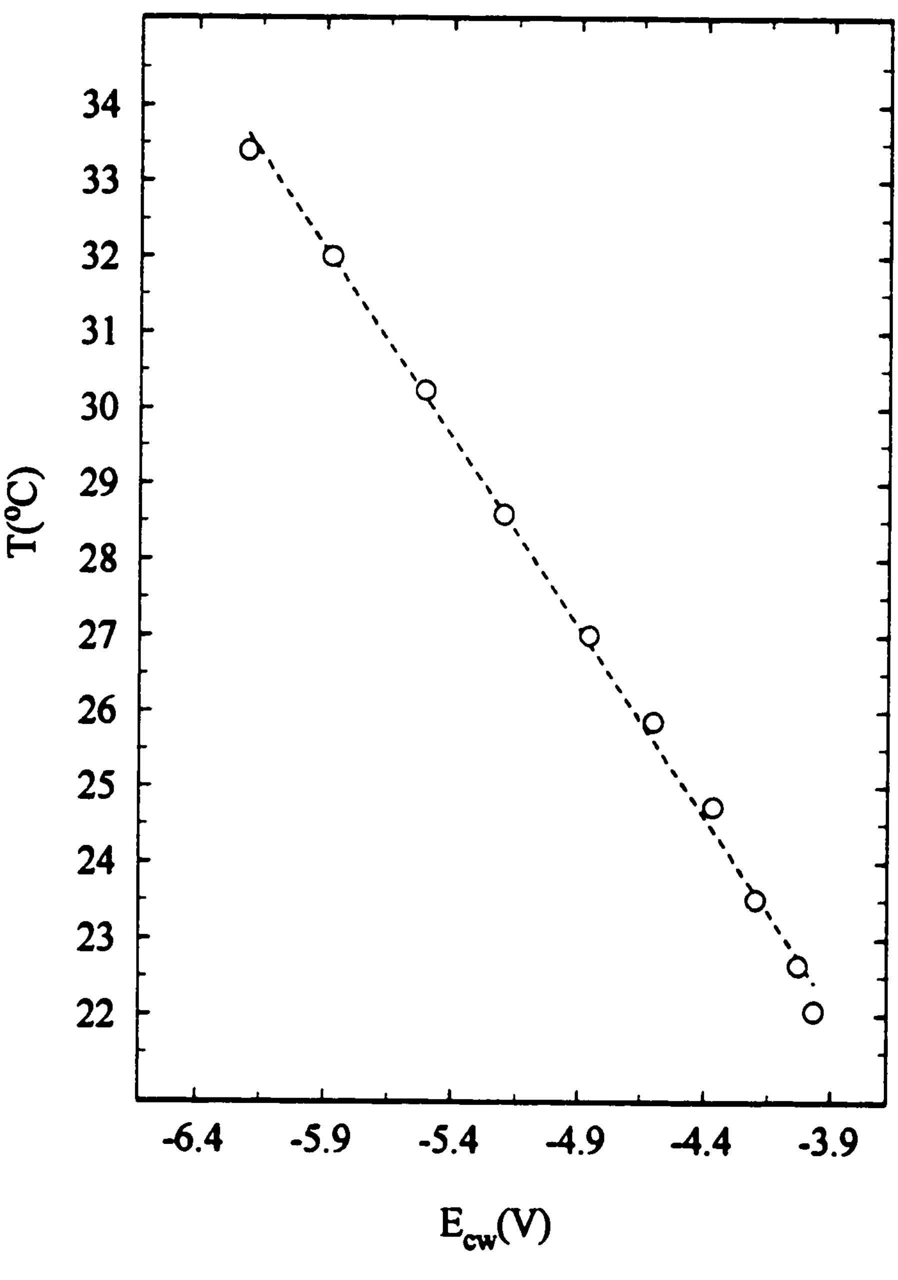

Fig. 6.7: Typical calibration curve of cold wire.

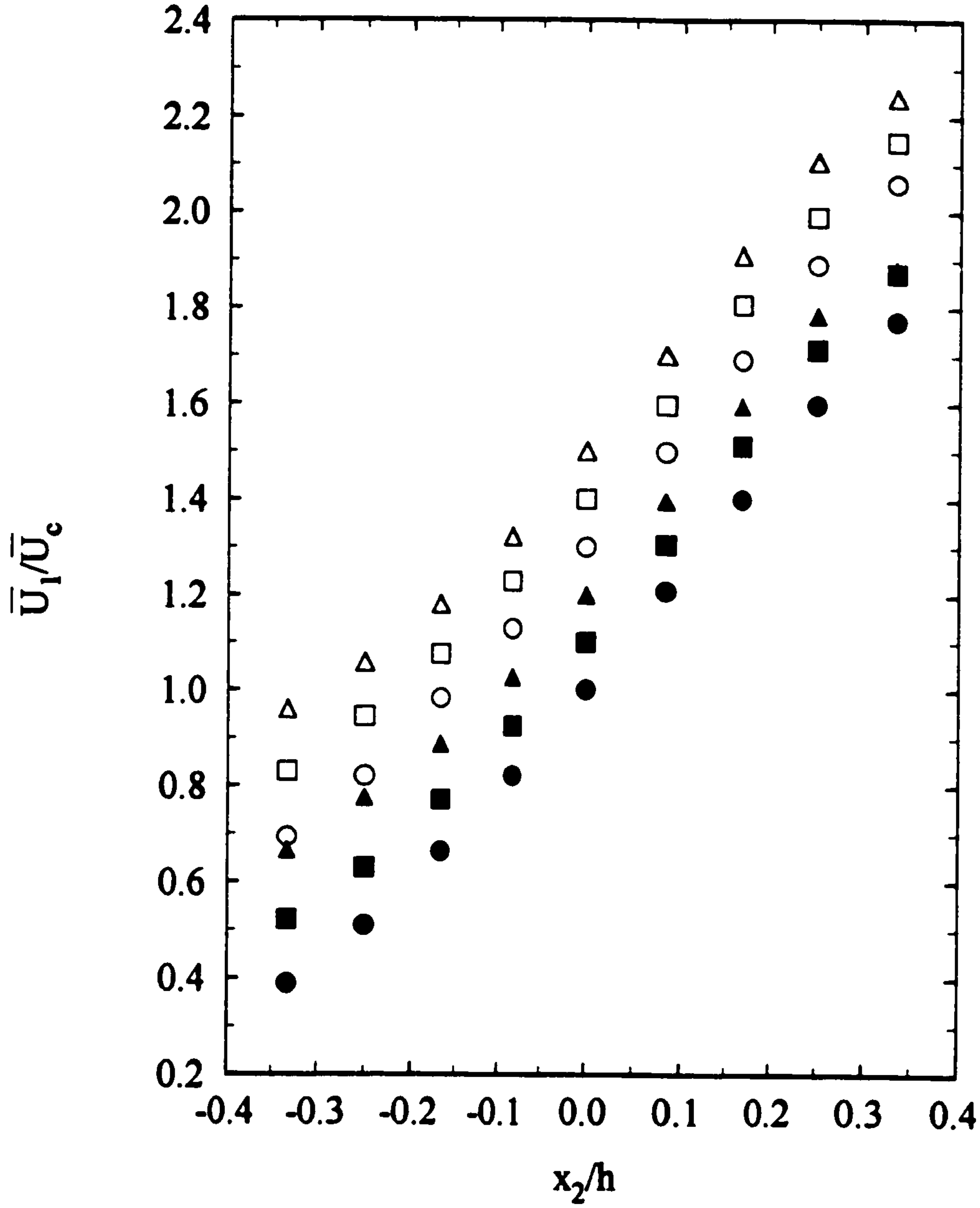

Fig. 7.1: Transverse profiles of the mean velocity. Full symbols, $\overline{U}_c$ = 7.3 m/s; empty symbols, $\overline{U}_c$ = 13.0 m/s. ○ (shifted by 0.3) and ● $x_1/h = 0$; □ (shifted by 0.4) and ■ $x_1/h = 6$ (shifted by 0.1); △ (shifted by 0.5) and ▲ $x_1/h = 11$ (shifted by 0.2).

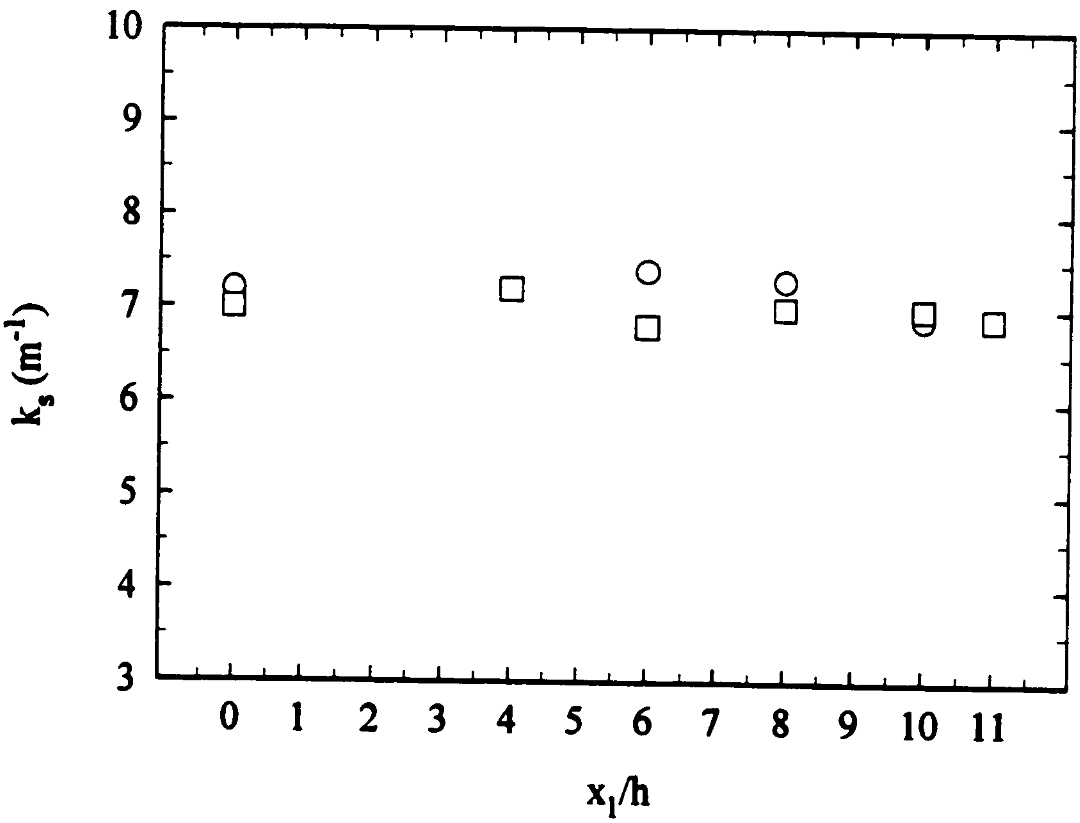

Fig. 7.2: Downstream variations of the shear constant k_s. ○ $\overline{U}_c$ = 7.3 m/s;

□ $\overline{U}_c$ = 13.0 m/s.

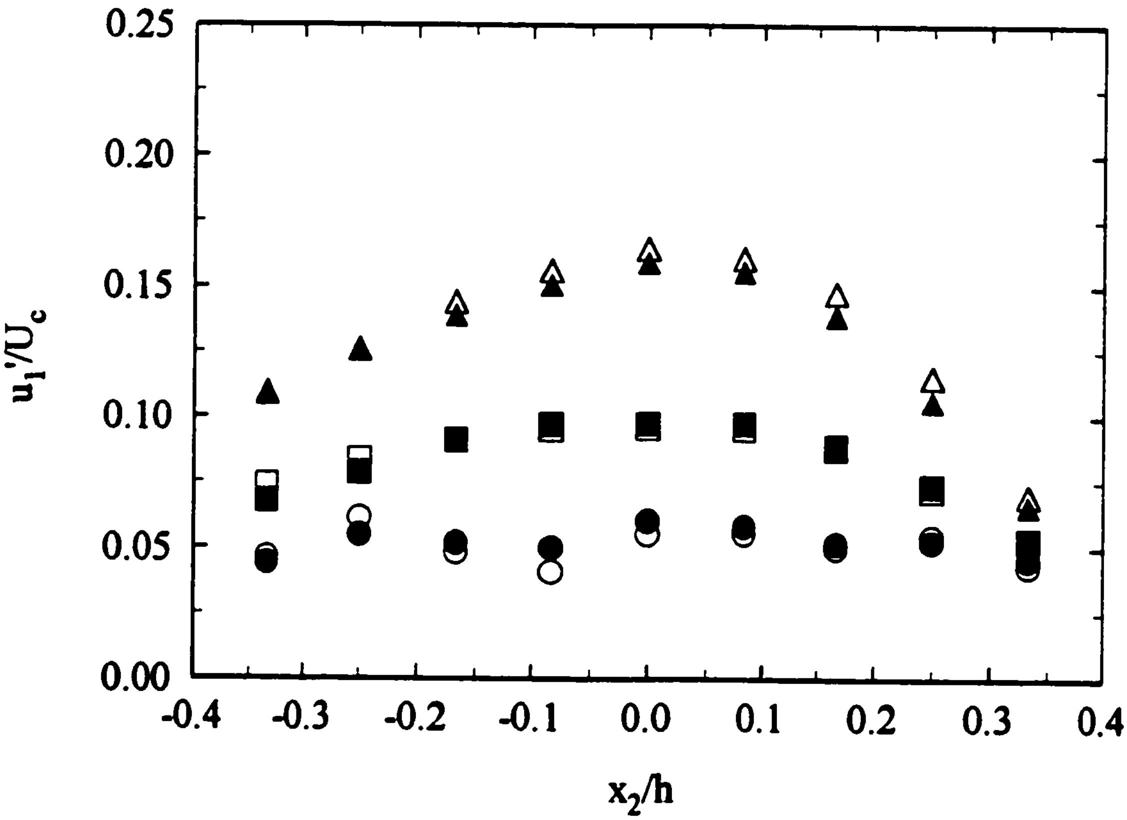

Fig. 7.3: Transverse profiles of the streamwise r.m.s. turbulent velocity.

Symbols as in fig. 7.1.

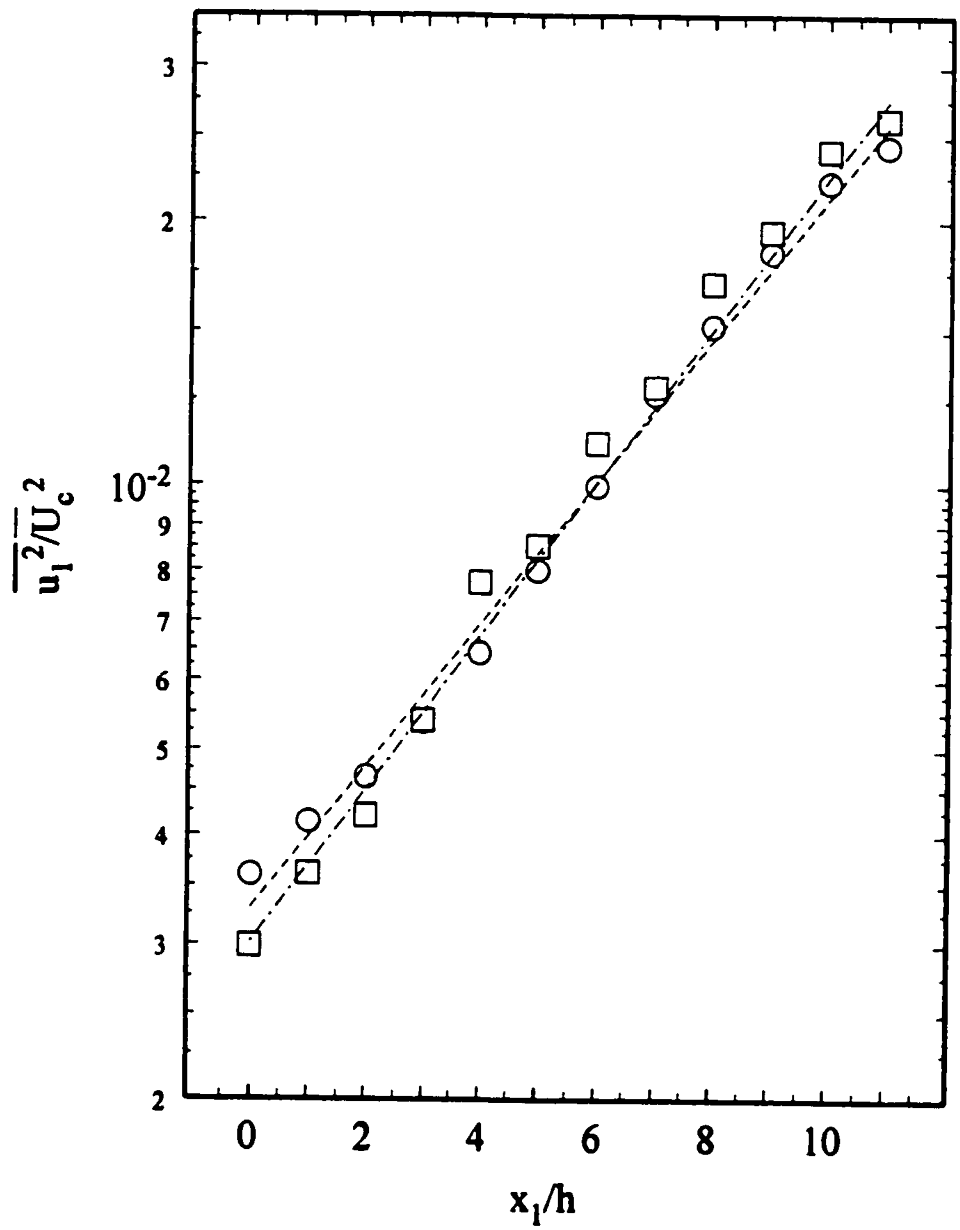

Fig. 7.4: Growth of the streamwise turbulent stress along the centreline. ○ $\overline{U}_c$ = 7.3 m/s; □ $\overline{U}_c$ = 13.0 m/s.

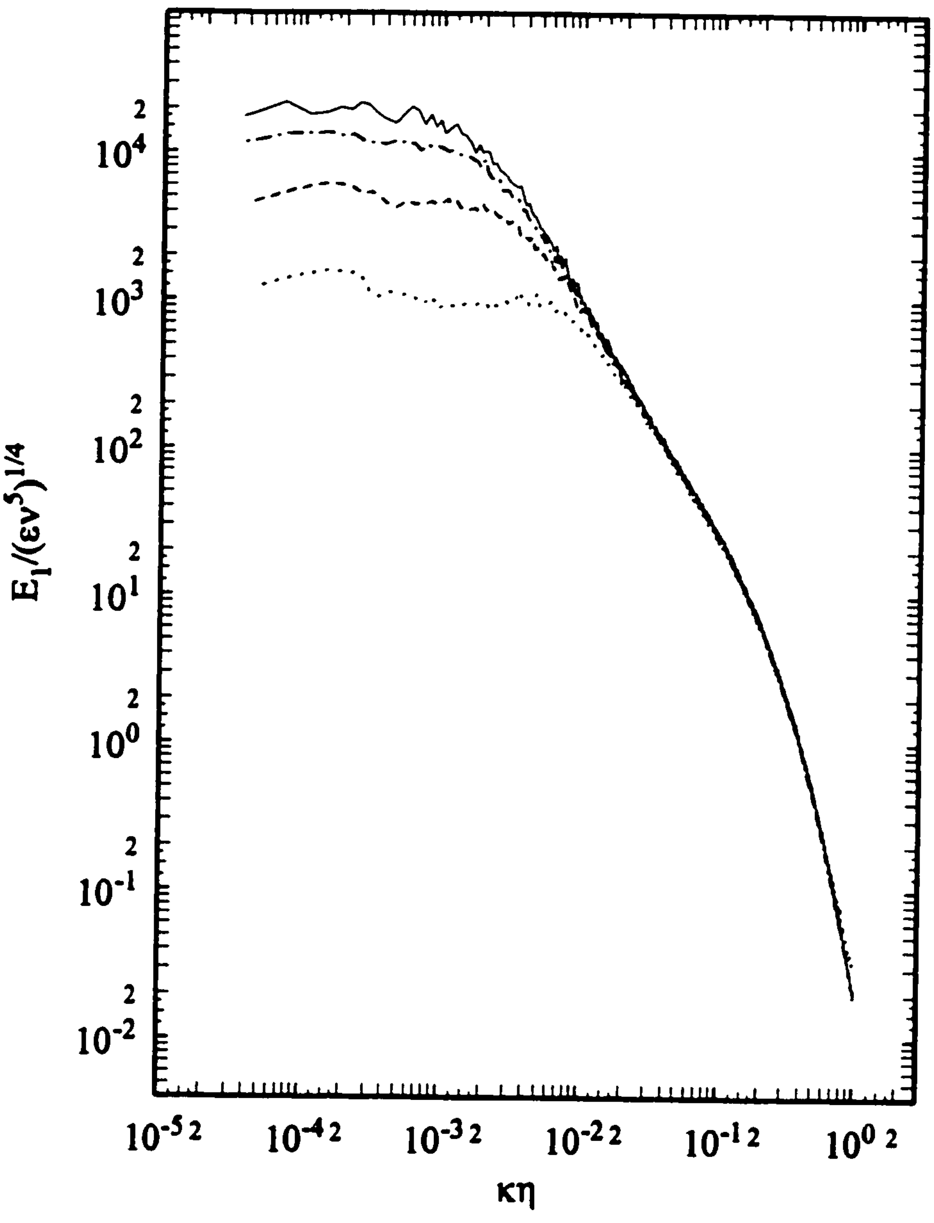

Fig. 7.5 : One-dimensional normalized spectra: . . . $Re_\lambda = 172$; - - - - $Re_\lambda = 311$; —— $Re_\lambda = 476$; ___ $Re_\lambda = 578$.

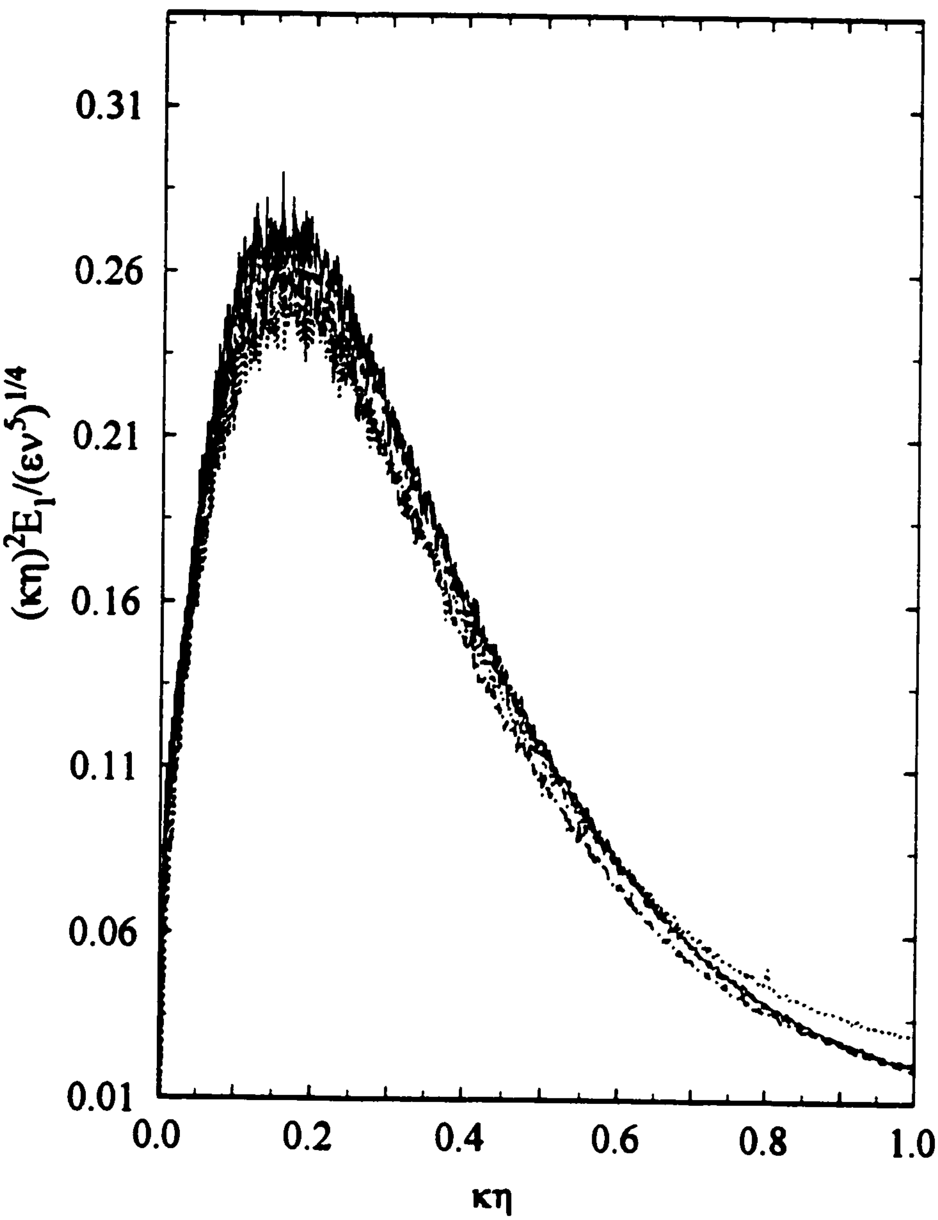

Fig. 7.6: One-dimensional normalized dissipation spectra. . . . $Re_\lambda = 172$; - - - - $Re_\lambda = 311$; ——— $Re_\lambda = 476$; ____ $Re_\lambda = 578$.

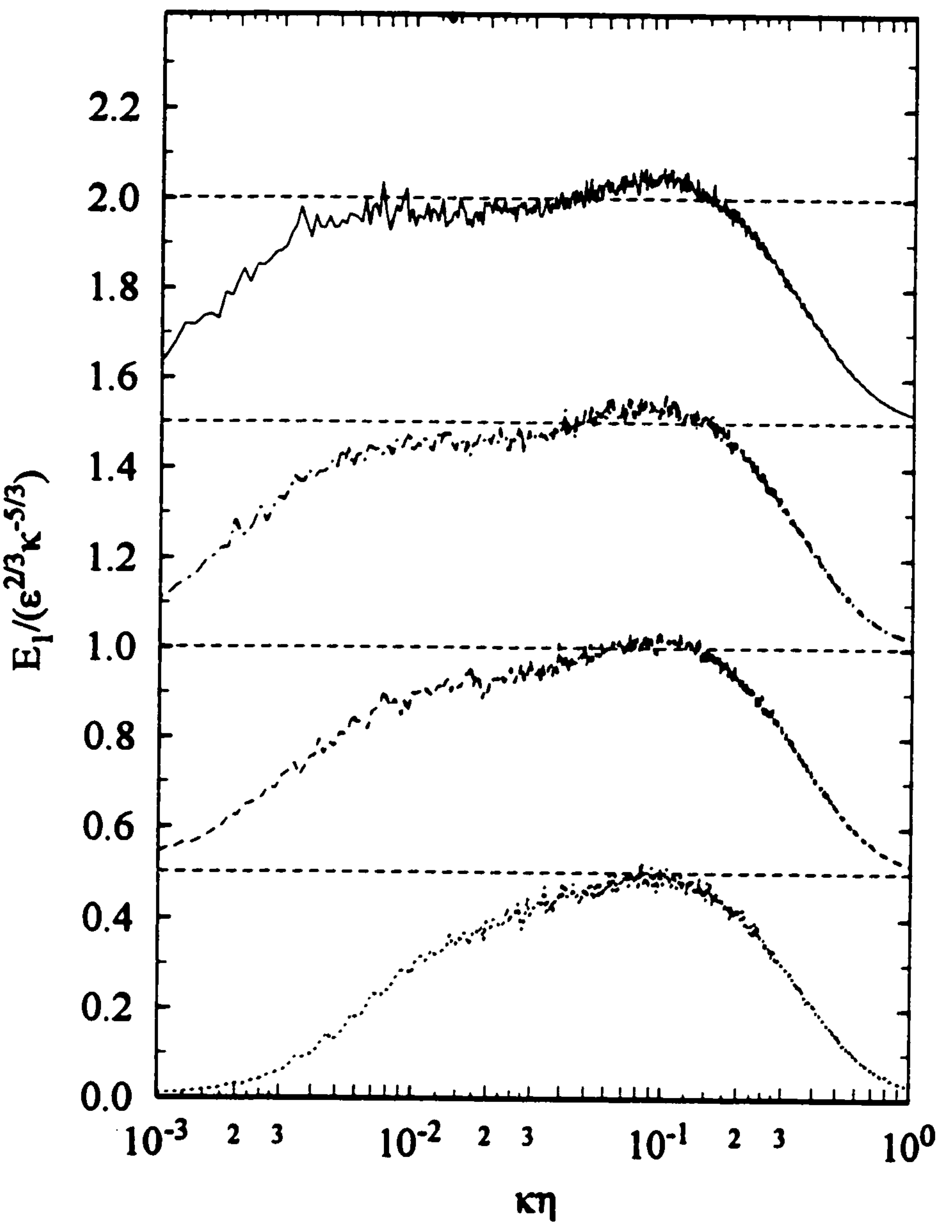

Fig. 7.7 : Variations of Kolmogorov's constant with Re_λ and r/η: .... $Re_\lambda = 172$; - - - $Re_\lambda = 311$ (shifted by 0.5); —·— $Re_\lambda = 476$ (shifted by 1.0); ___ $Re_\lambda = 578$ (shifted by 1.5).

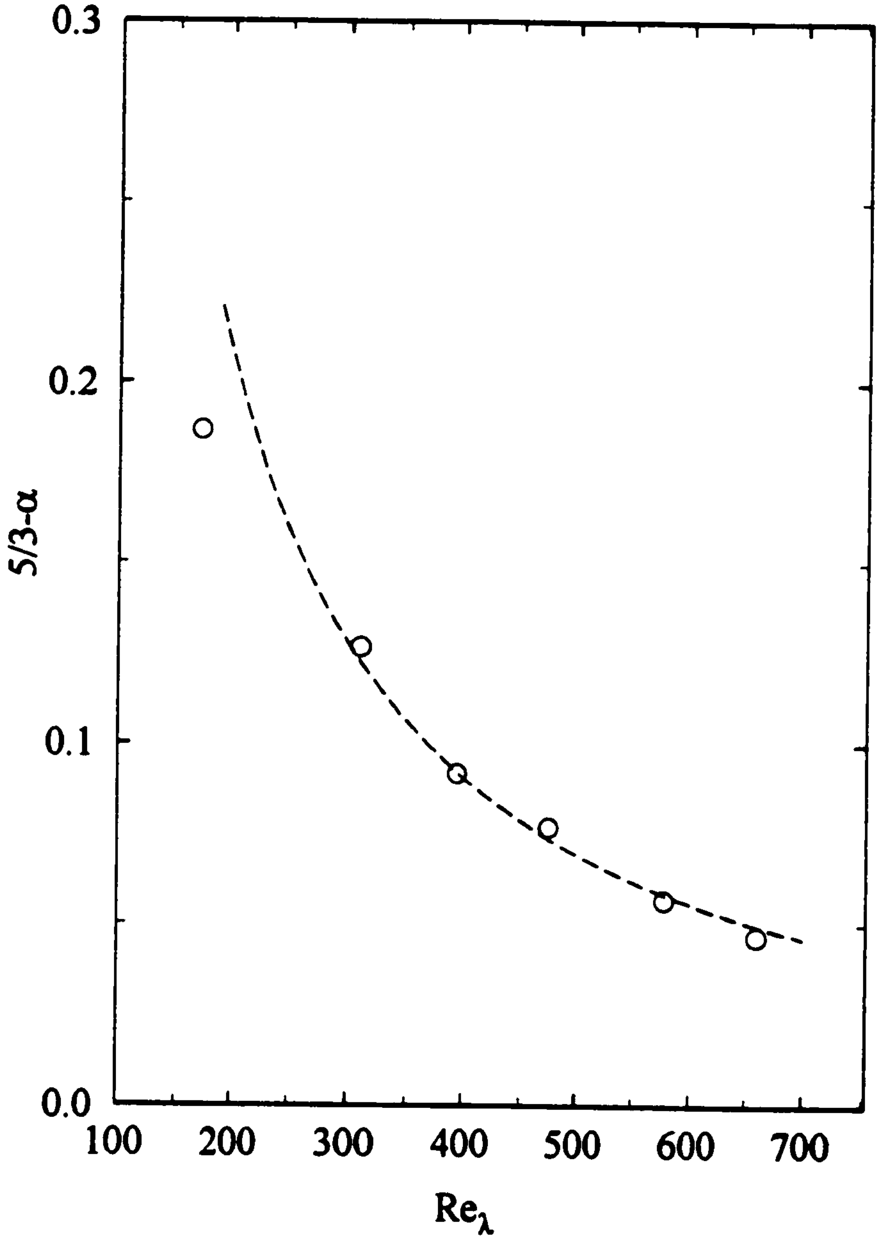

Fig. 7.8 : Variations of the parameter α with Re_λ.

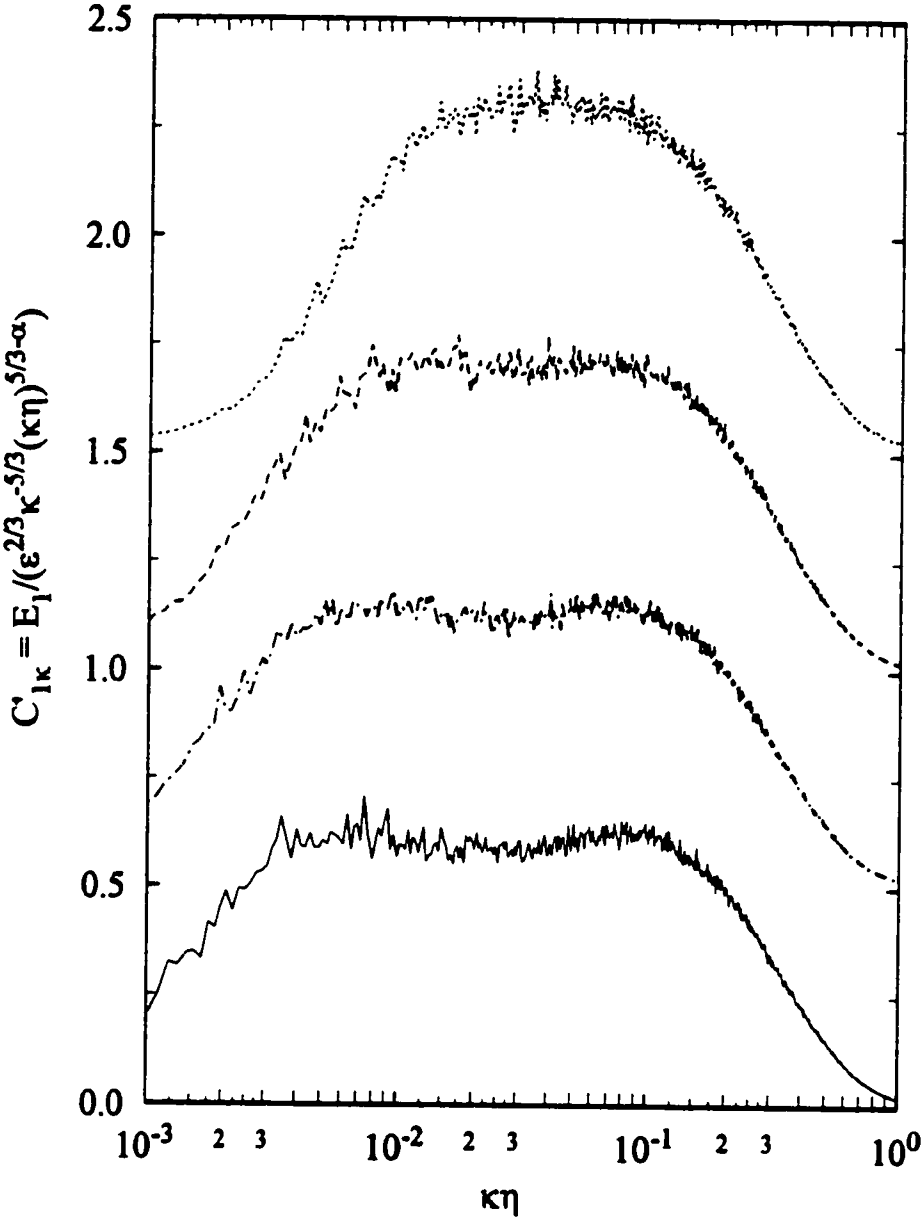

Fig. 7.9: Corrected Kolmogorov's constant: . . . $Re_\lambda = 172$ (shifted by 1.5); - - - - $Re_\lambda = 311$ (shifted by 1); ——— $Re_\lambda = 476$ (shifted by 0.5); ___ $Re_\lambda = 578$.

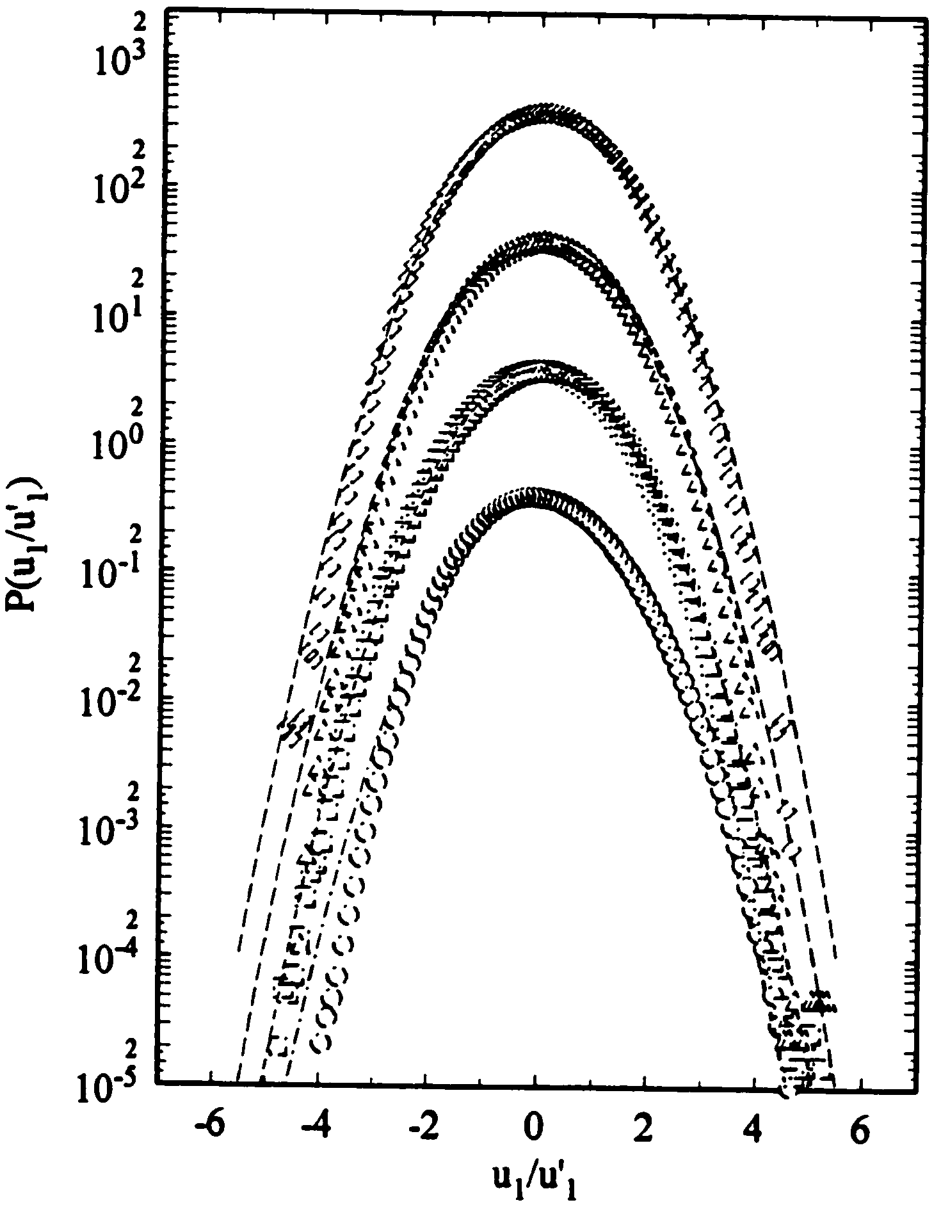

Fig. 7.10: Pdf of the normalized streamwise velocity fluctuations: ○ $Re_\lambda = 172$; □ $Re_\lambda = 311$; △ $Re_\lambda = 476$; ◇ $Re_\lambda = 578$.

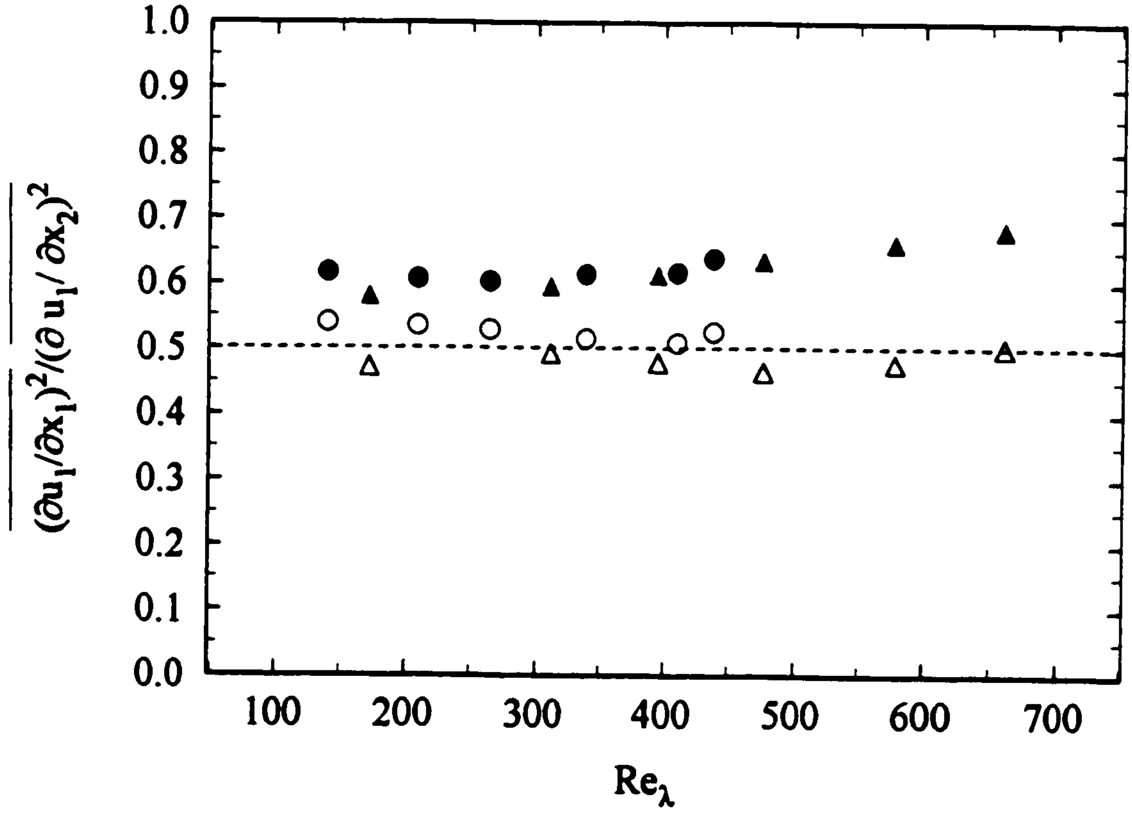

Fig. 7.11: Ratio of the variances of the velocity derivatives: ○ $\overline{U}_c = 7.3$ m/s;

△ $\overline{U}_c = 13.0$ m/s, full symbols, uncorrected.

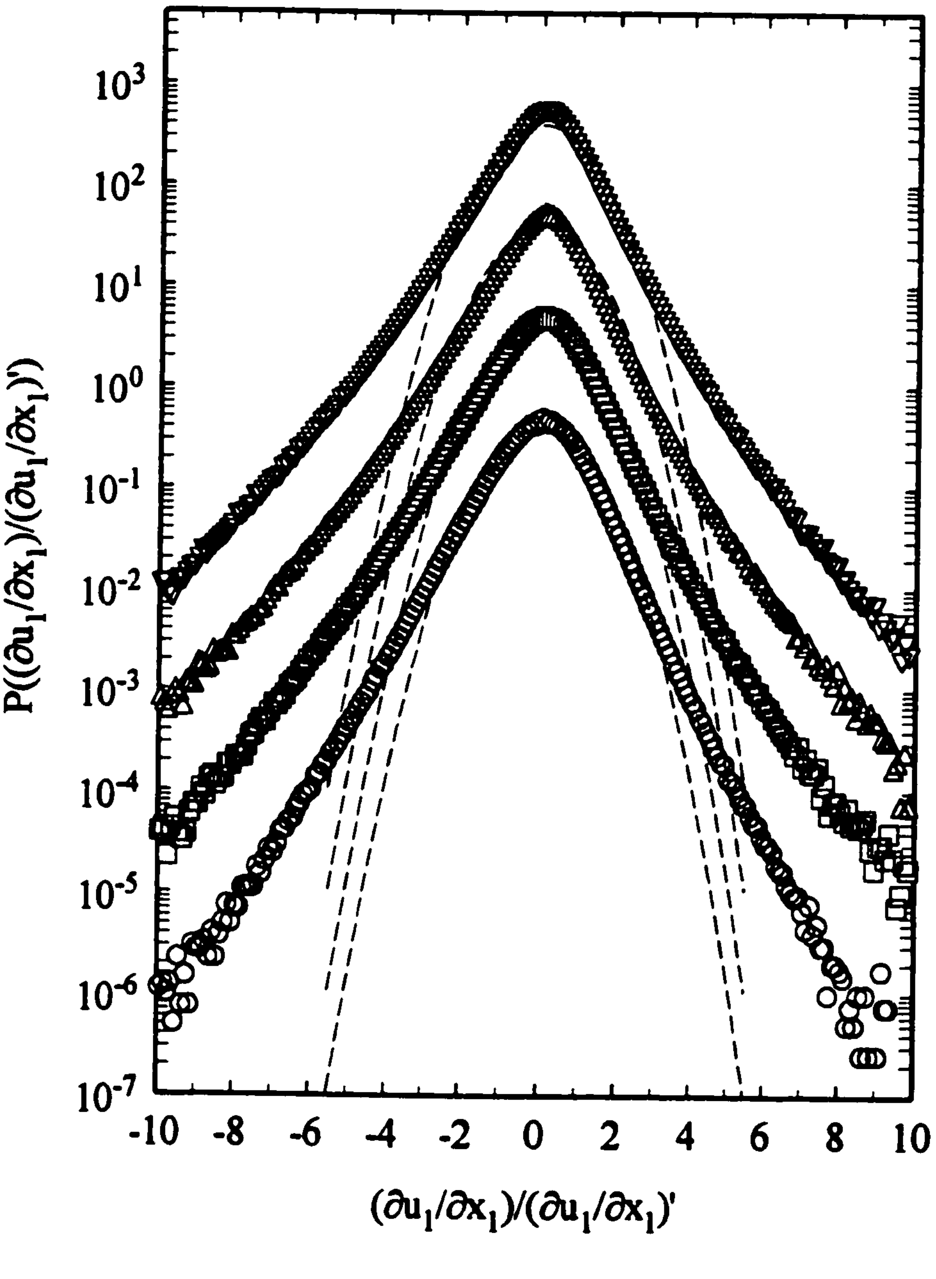

Fig. 7.12: Pdf of the normalized streamwise velocity derivative: ○ $Re_\lambda = 172$; □ $Re_\lambda = 311$; △ $Re_\lambda = 476$; ▽ $Re_\lambda = 578$.

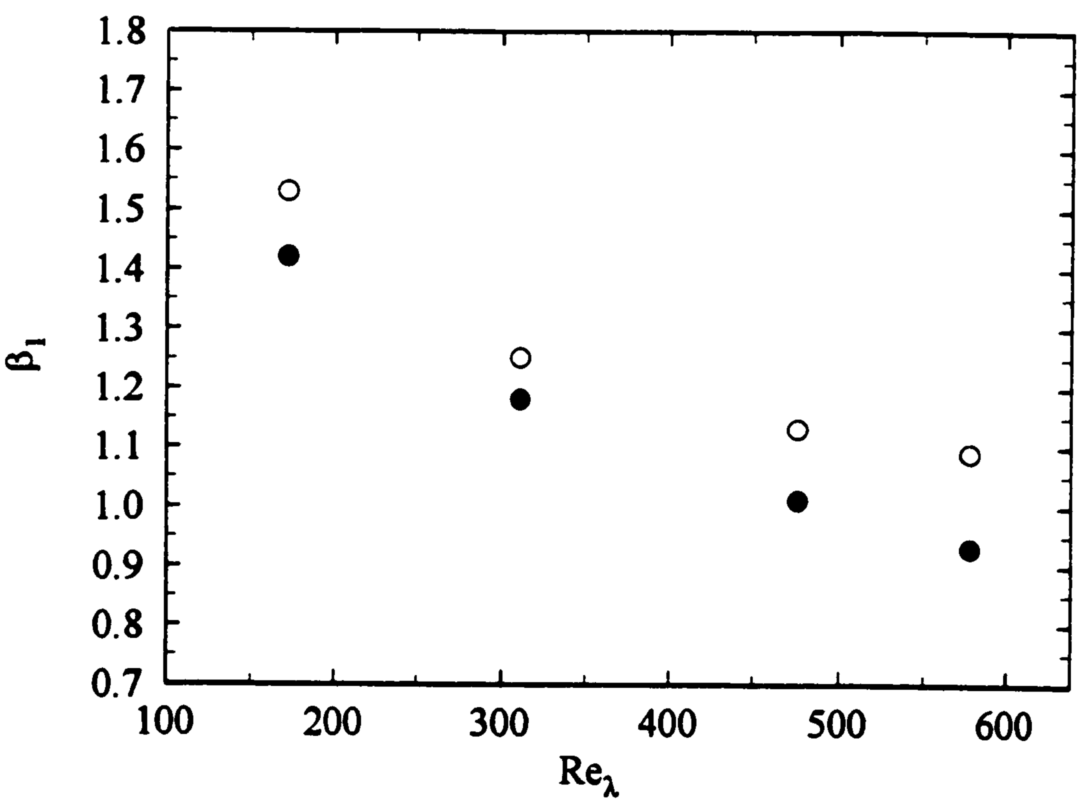

Fig. 7.13: Slope of the tails of the streamwise velocity derivative pdf : ○ positive tails;

● negative tails.

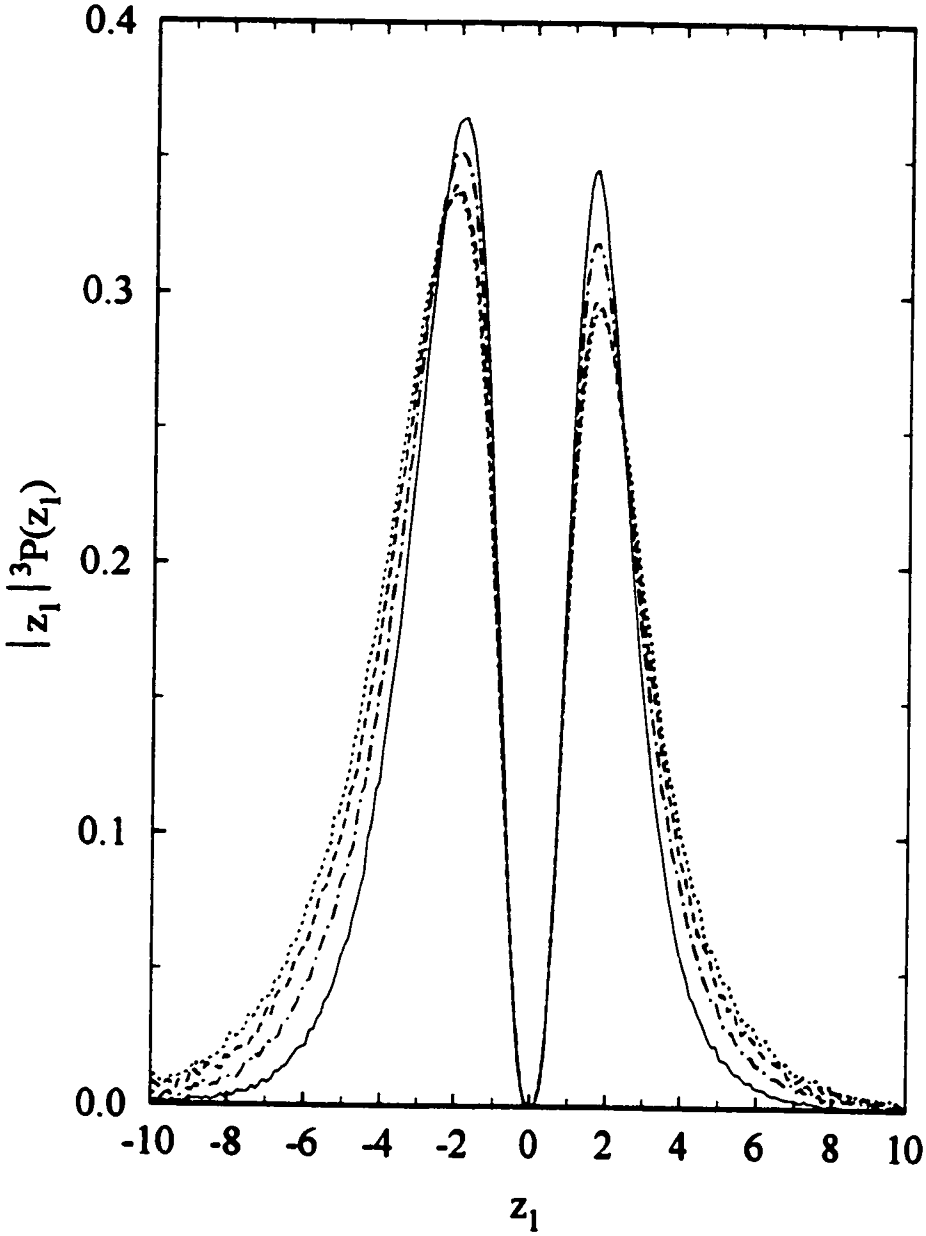

Fig. 7.14: Third moment of the pdf of the streamwise velocity derivative: —— $Re_\lambda = 172$; — — $Re_\lambda = 311$; ---- $Re_\lambda = 476$; ...... $Re_\lambda = 578$.

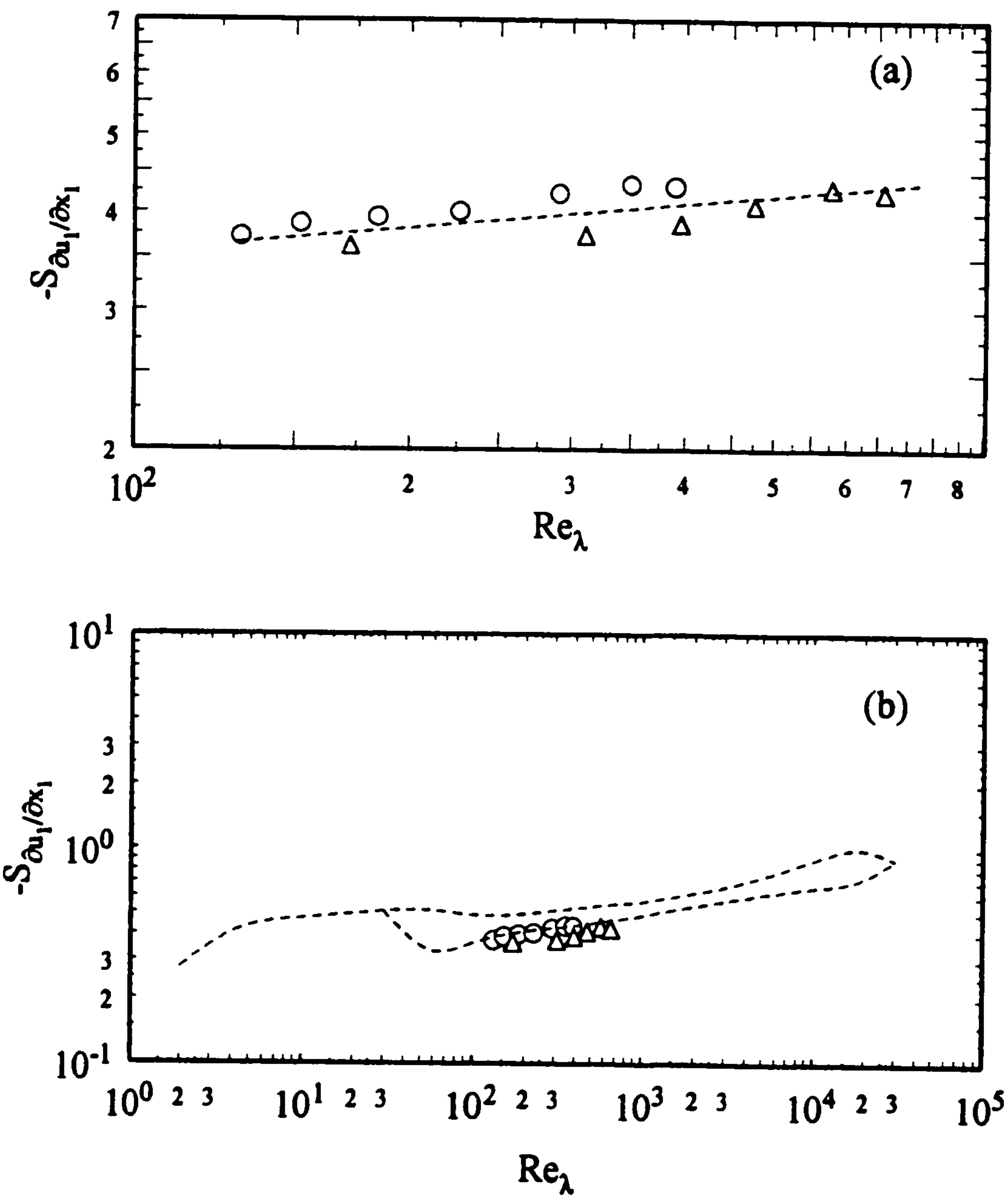

Fig. 7.15: Skewness of the streamwise velocity derivatives: (a) ○ $\overline{U}_c$ = 7.3 m/s; △ $\overline{U}_c$ = 13.0 m/s, (b) The data in (a) replotted with fig. 5 of Sreenivasan and Antonia (1997).

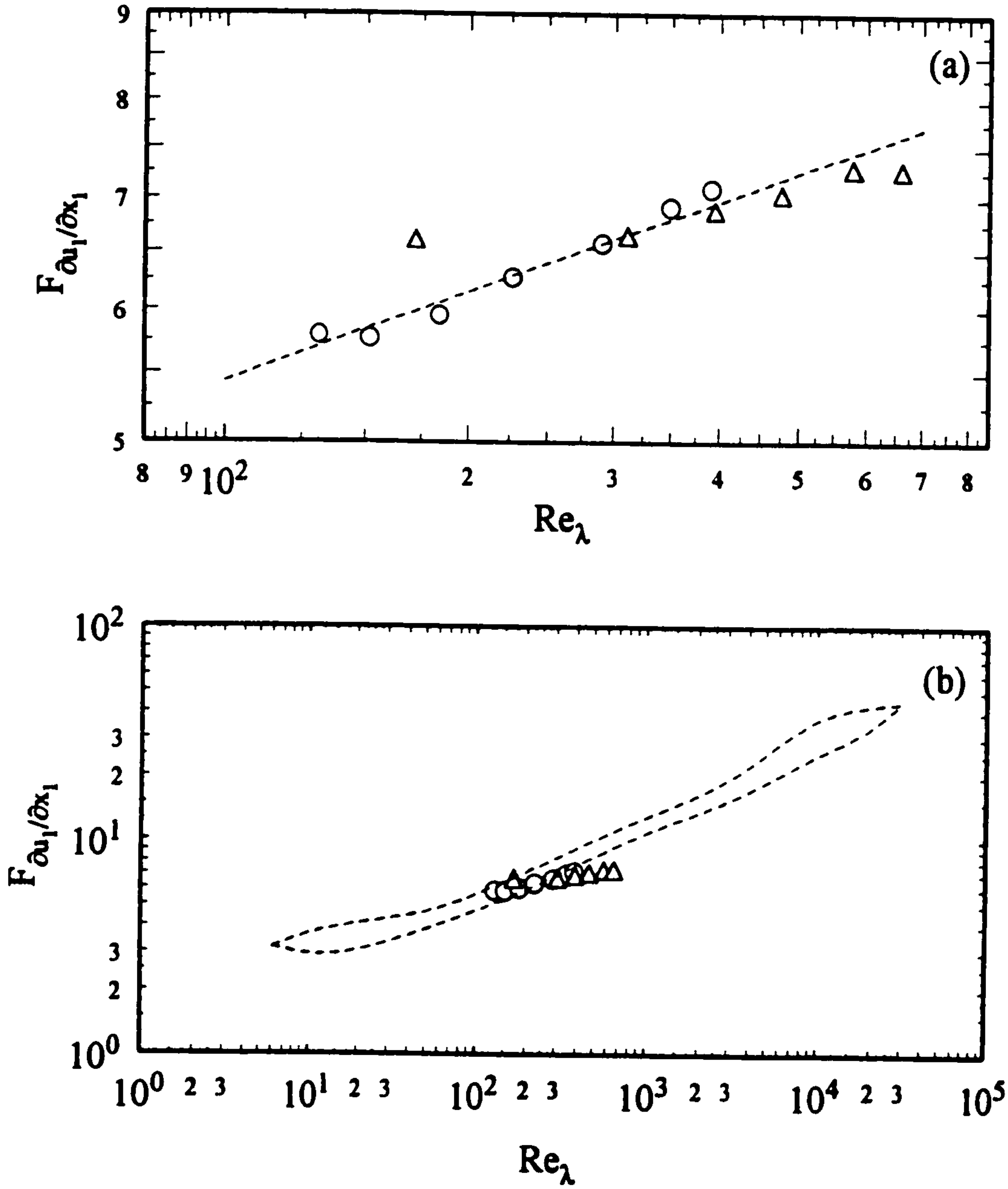

Fig. 7.16: Flatness of the streamwise velocity derivatives: (a) ○ $\overline{U}_c$ = 7.3 m/s; △ $\overline{U}_c$ = 13.0 m/s, (b) The data in (a) replotted with fig. 6 of Sreenivasan and Antonia (1997).

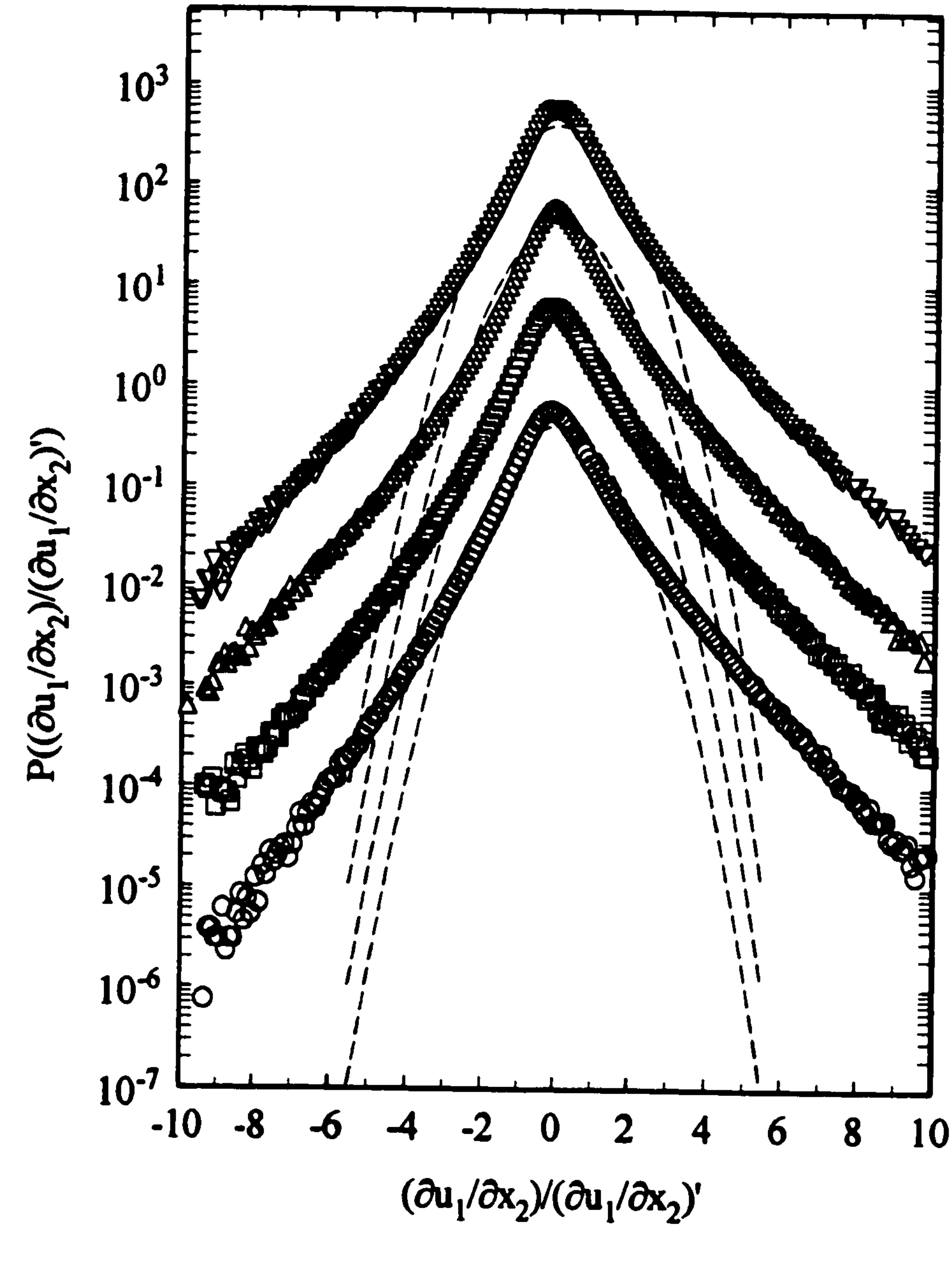

Fig. 7.17: Pdf of the normalized transverse velocity derivative: ○ $Re_\lambda = 172$; □ $Re_\lambda = 311$; △ $Re_\lambda = 476$; ▽ $Re_\lambda = 578$.

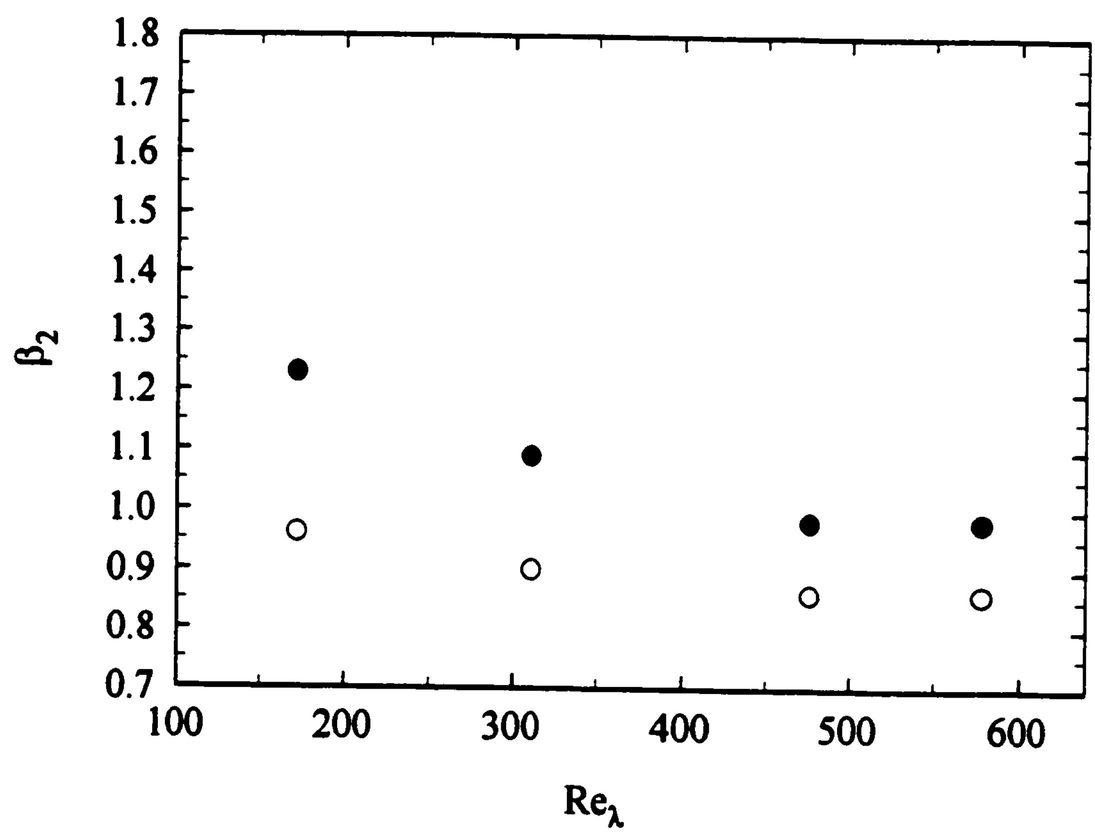

Fig. 7.18: Slope of tails of the transverse velocity derivative pdf : ○ positive tails;

● negative tails.

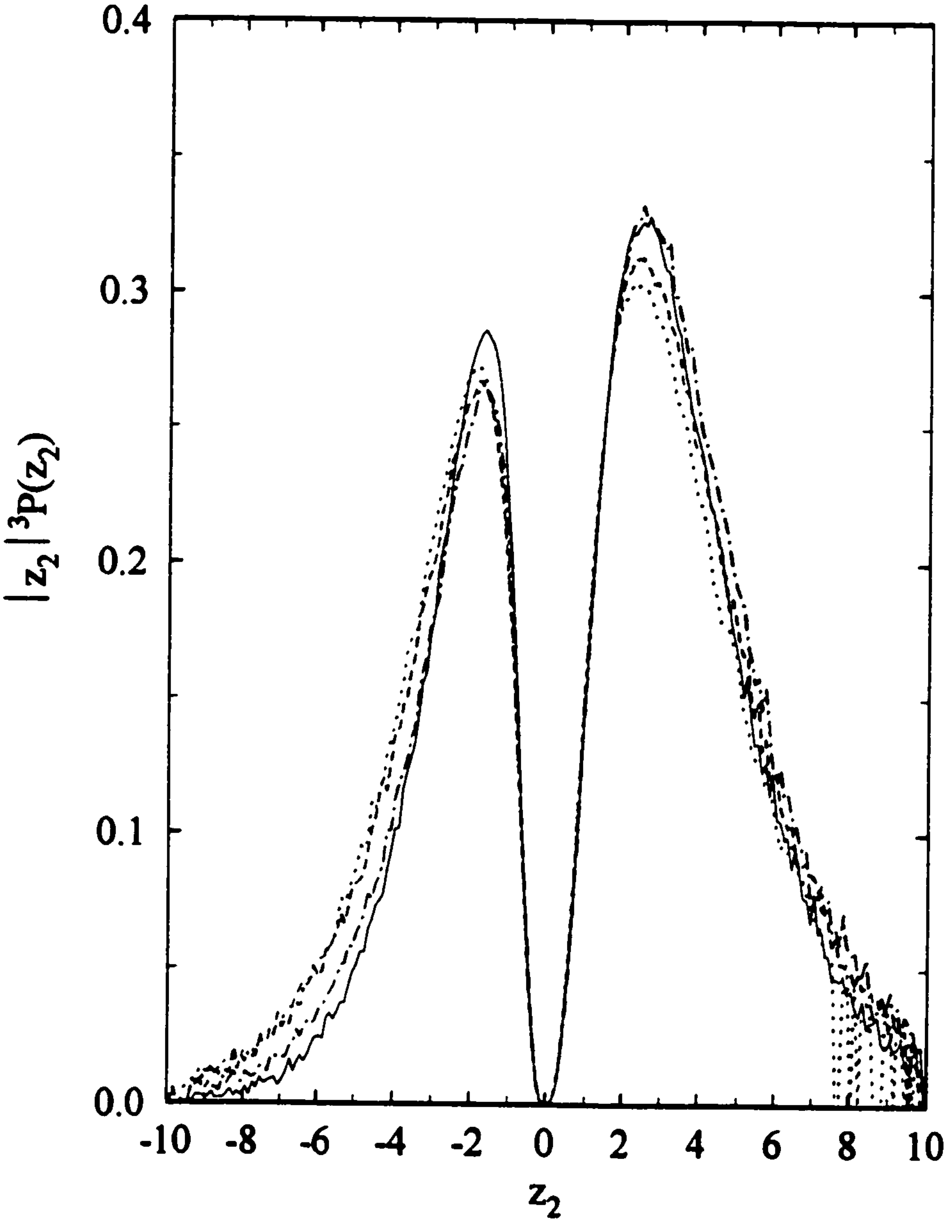

Fig. 7.19: Third moment of the pdf of the transverse velocity derivative: —— $Re_\lambda = 172$; —-— $Re_\lambda = 311$; ---- $Re_\lambda = 476$; ······ $Re_\lambda = 578$.

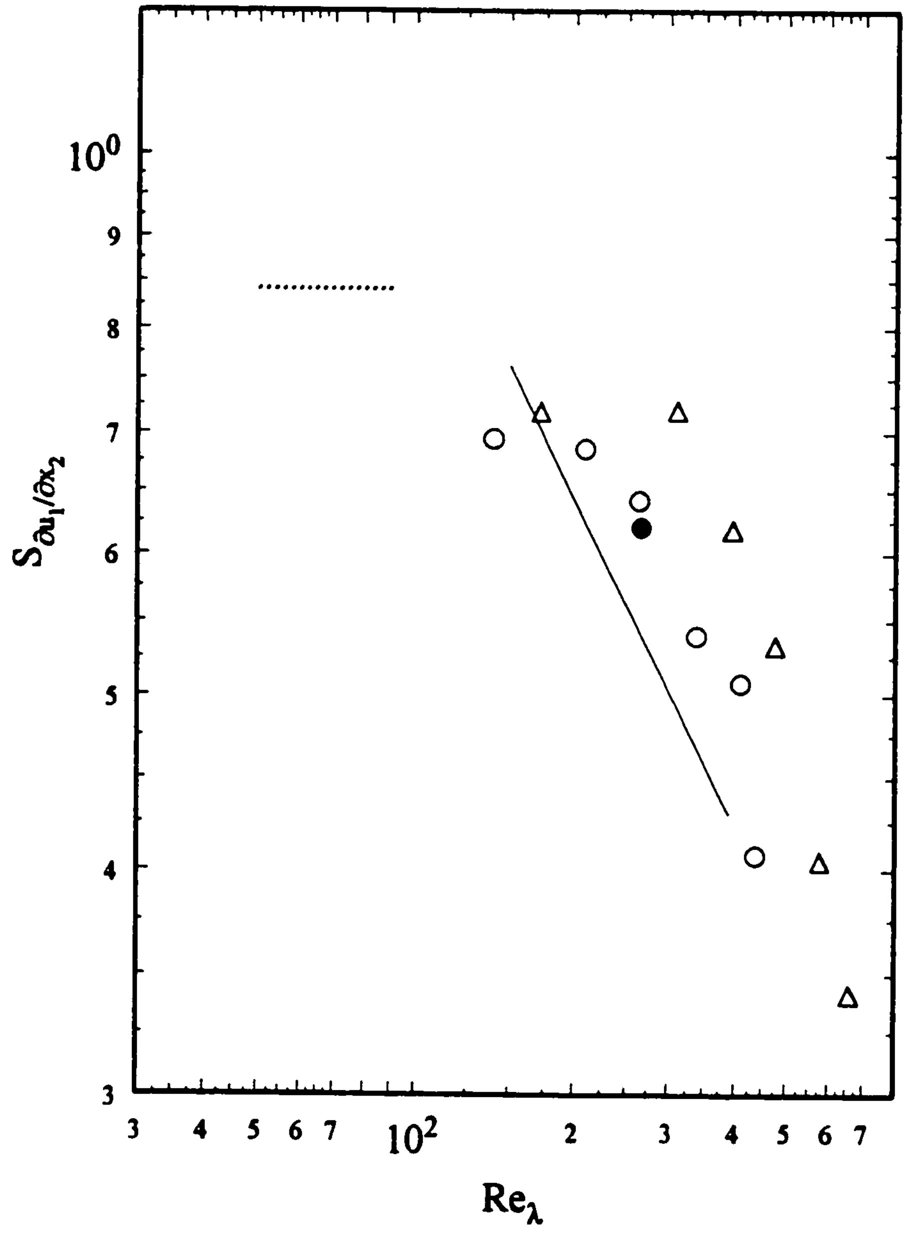

Fig. 7.20: Skewness of the transverse velocity derivatives: ○ $\overline{U}_c$ = 7.3 m/s; △ $\overline{U}_c$ = 13.0 m/s;

● Tavoularis and Corrsin (1981 b); —— Garg and Warhaft (1998); ..... Pumir (1996).

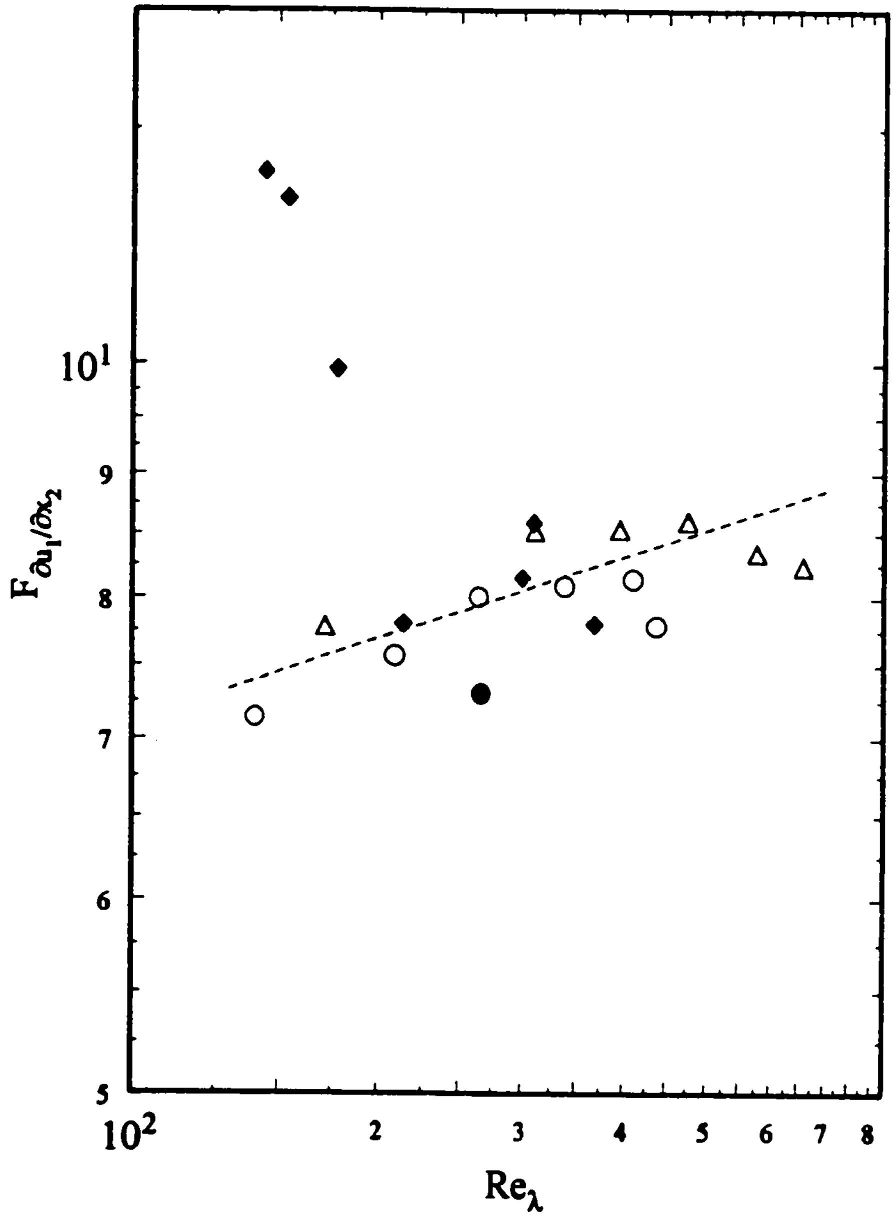

Fig. 7.21: Flatness of the transverse velocity derivatives: ○ $\overline{U}_c = 7.3$ m/s; △ $\overline{U}_c = 13.0$ m/s;

● Tavoularis and Corrsin (1981 b); ♦ Garg and Warhaft (1998).

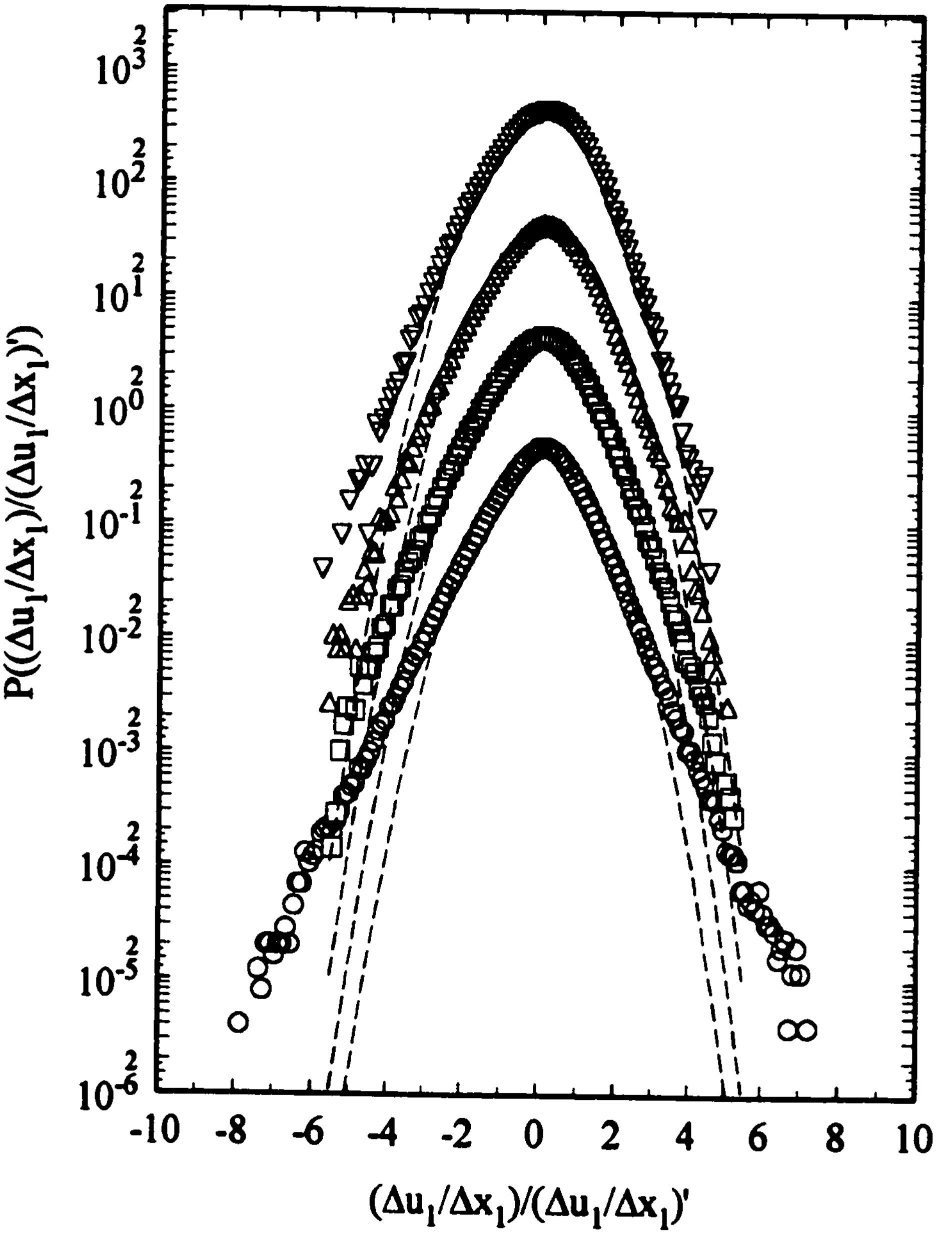

Fig. 7.22: Pdf of the normalized streamwise velocity differences at $Re_\lambda = 578$: ○ $r/\eta = 21$; □ $r/\eta = 76$; △ $r/\eta = 142$; ▽ $r/\eta = 210$.

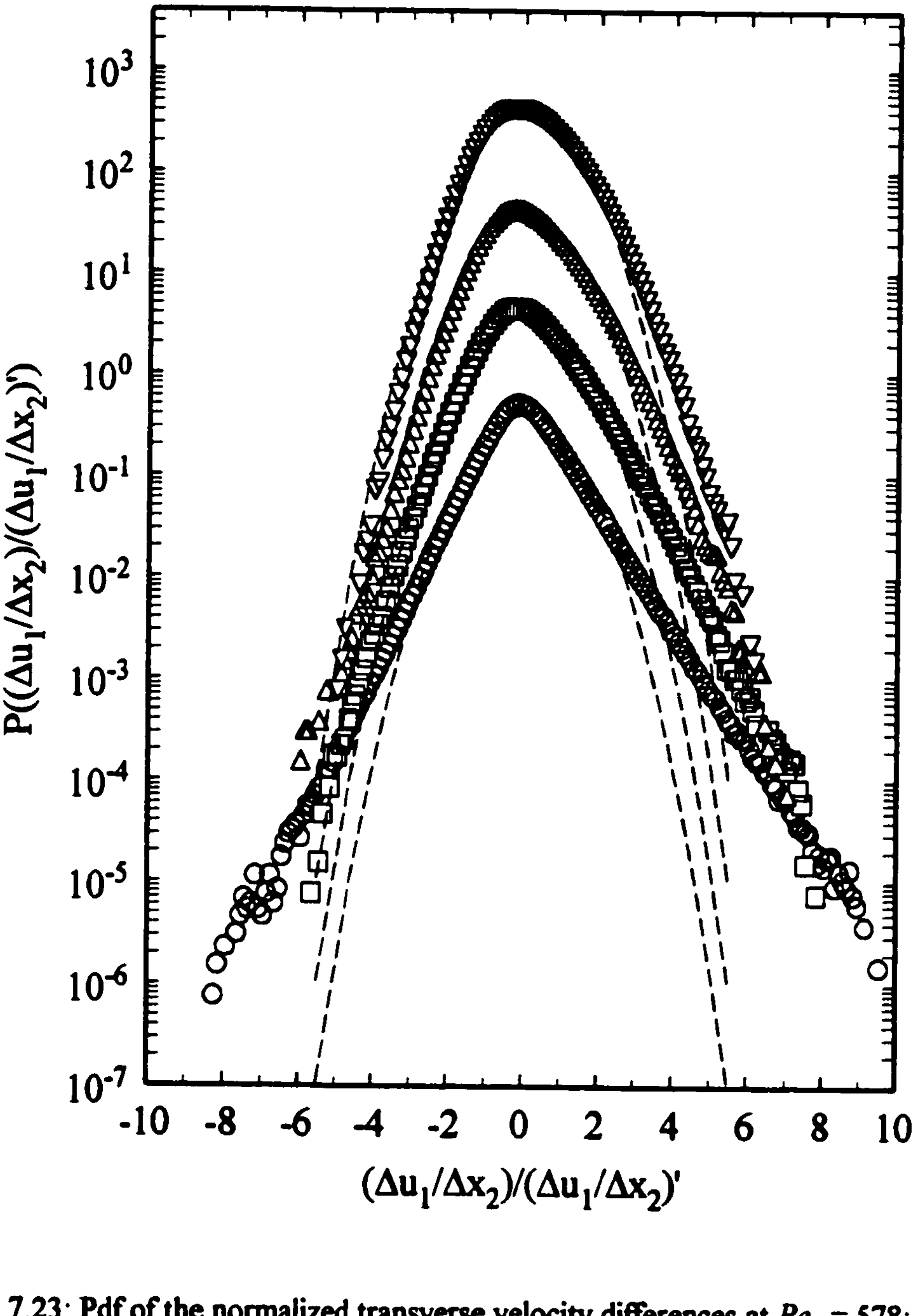

Fig. 7.23: Pdf of the normalized transverse velocity differences at $Re_\lambda = 578$: ○ $r/\eta = 21$; □ $r/\eta = 76$; △ $r/\eta = 142$; ▽ $r/\eta = 210$.

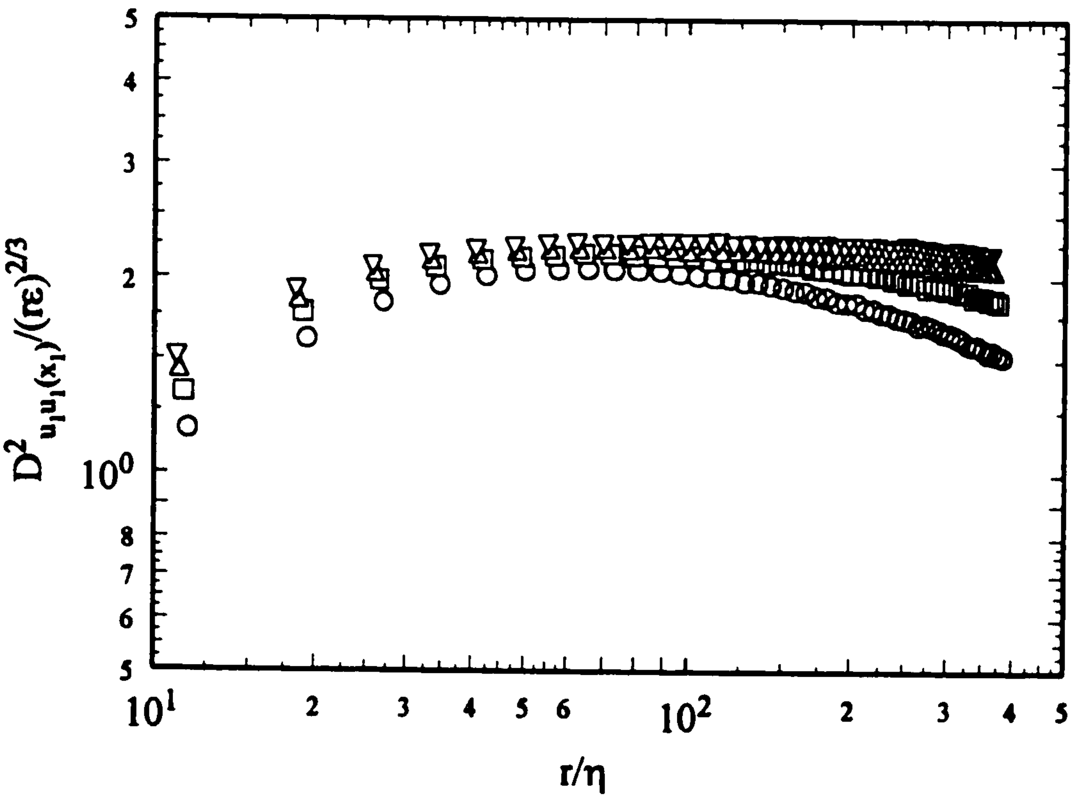

Fig. 7.24: Normalized second order longitudinal velocity structure functions: ○ $Re_\lambda = 172$; □ $Re_\lambda = 311$; △ $Re_\lambda = 476$; ▽ $Re_\lambda = 578$.

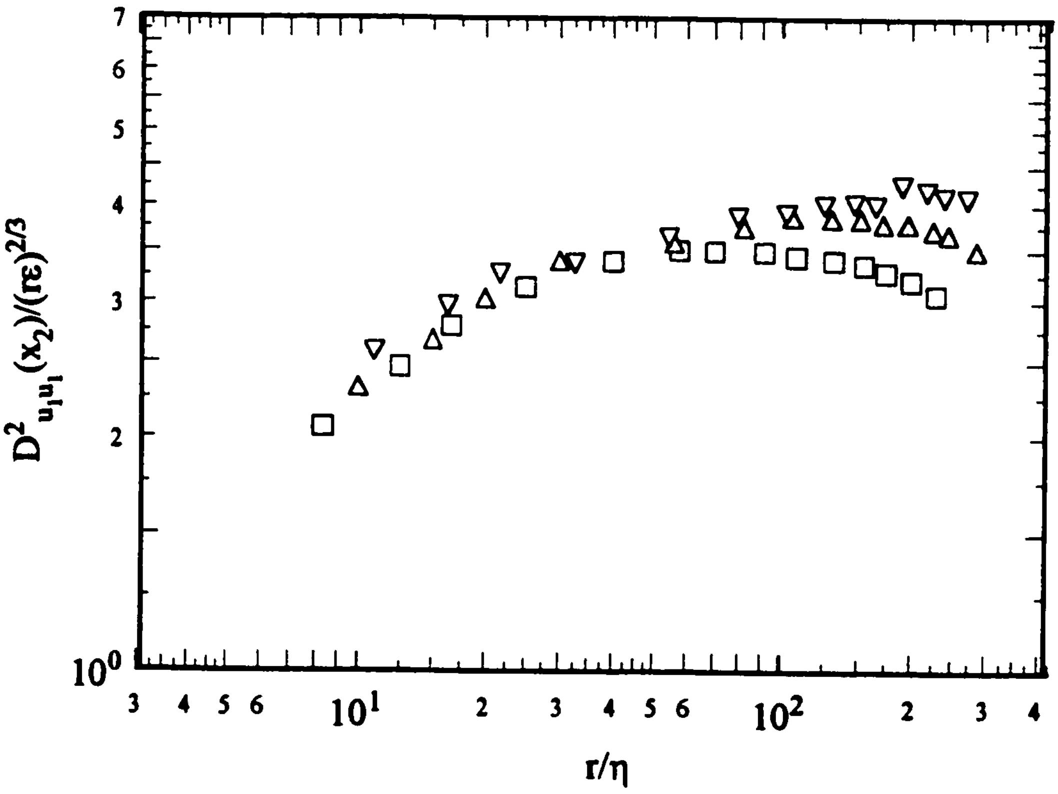

Fig. 7.25: Normalized second order transverse velocity structure functions: □ $Re_\lambda = 311$; △ $Re_\lambda = 476$; ▽ $Re_\lambda = 578$.

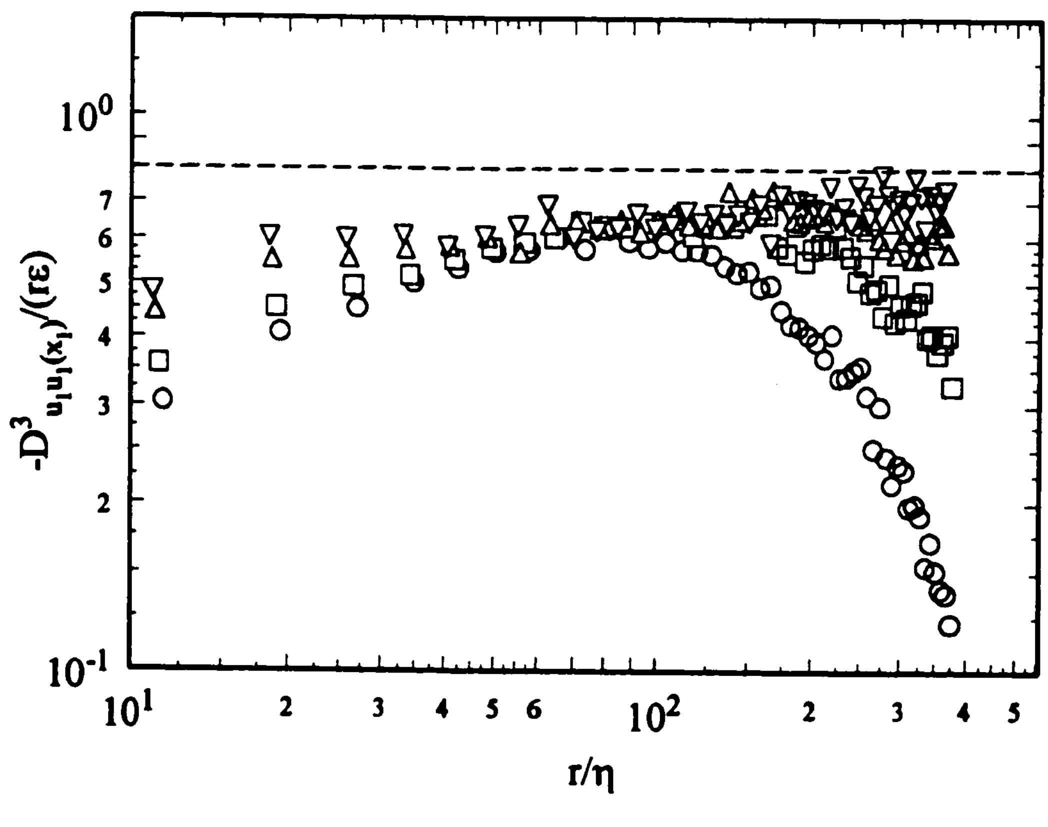

Fig. 7.26: Normalized third order longitudinal velocity structure functions: ○ $Re_\lambda = 172$; □ $Re_\lambda = 311$; △ $Re_\lambda = 476$; ▽ $Re_\lambda = 578$.

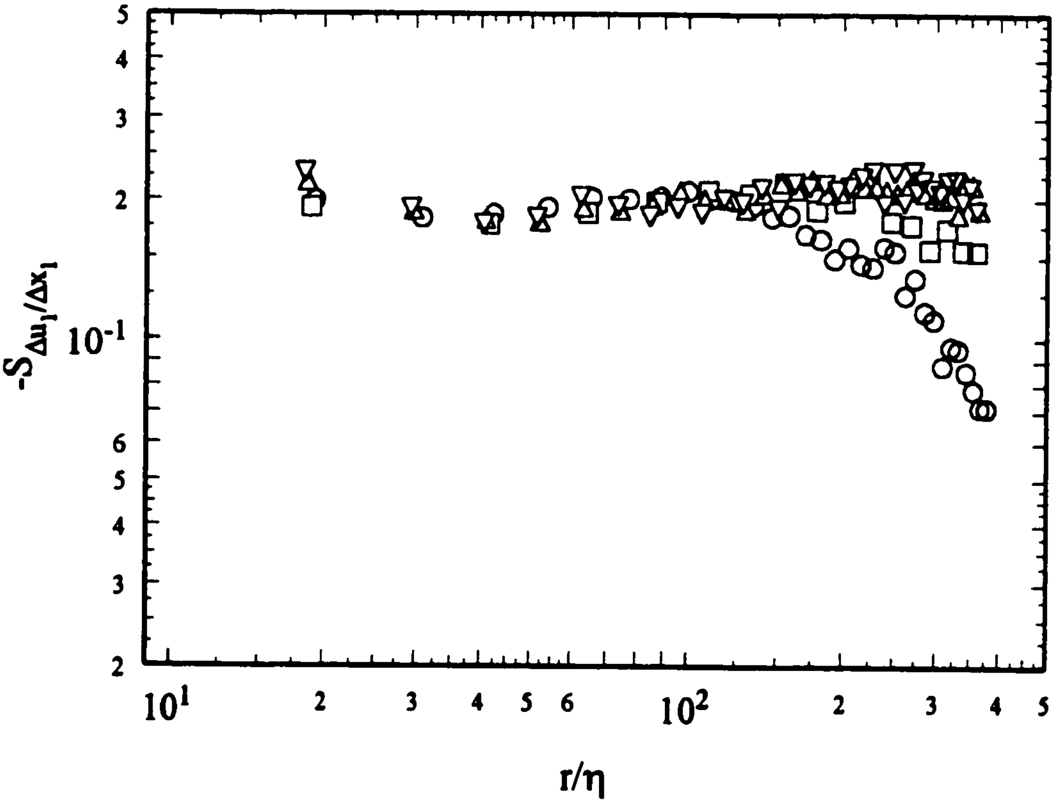

Fig. 7.27: Skewness of the longitudinal velocity difference: ○ $Re_\lambda = 172$; □ $Re_\lambda = 311$;

△ $Re_\lambda = 476$; ▽ $Re_\lambda = 578$.

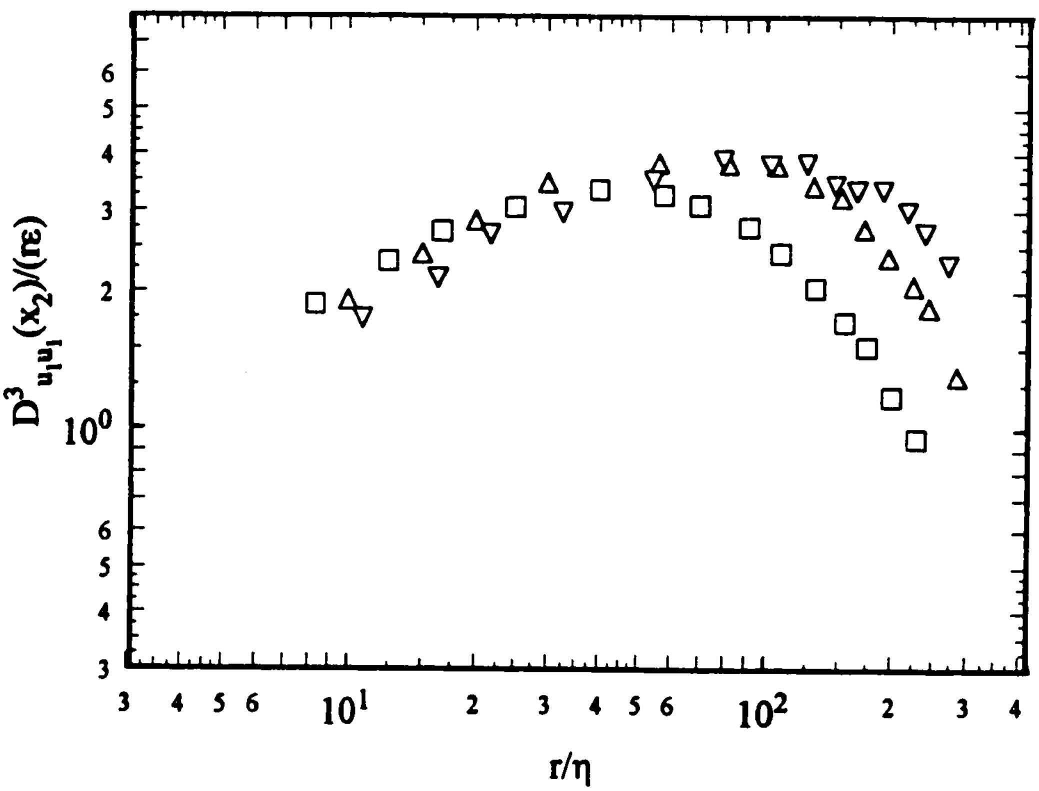

Fig. 7.28: Normalized third order transverse velocity difference: □ $Re_\lambda = 311$; △ $Re_\lambda = 476$; ▽ $Re_\lambda = 578$.

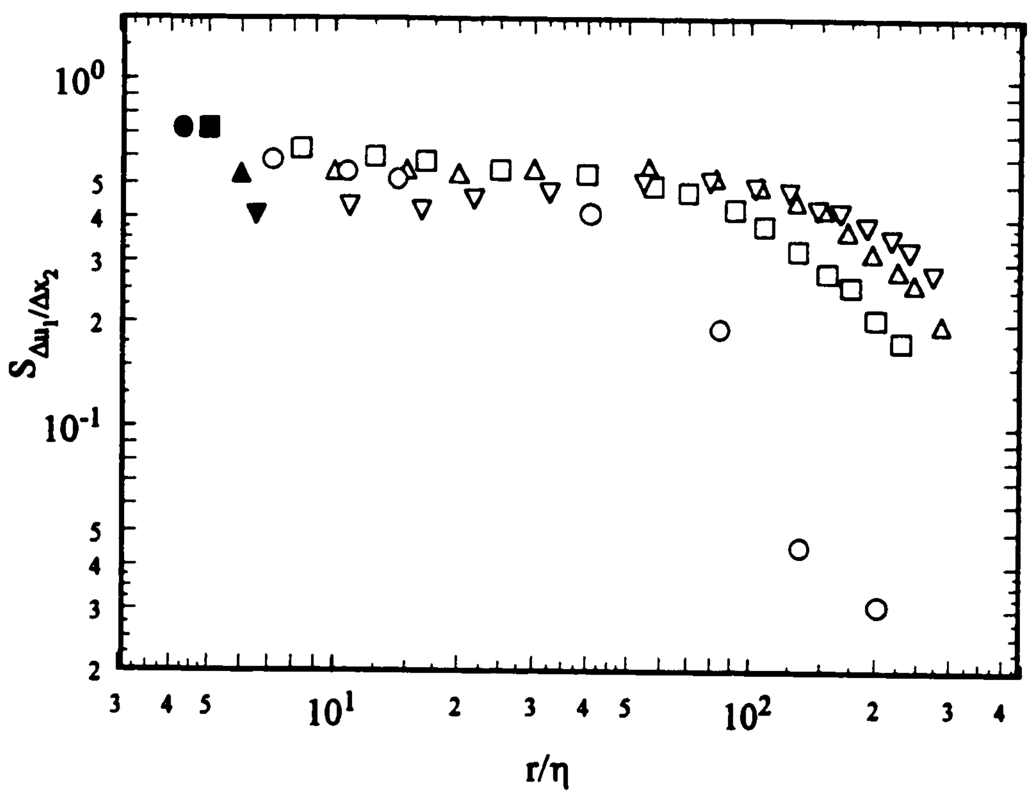

Fig. 7.29: Skewness of the transverse velocity difference: ○ $Re_\lambda = 172$; □ $Re_\lambda = 311$; △ $Re_\lambda = 476$; ▽ $Re_\lambda = 578$. Full symbols, measured with the fixed parallel hot wires.

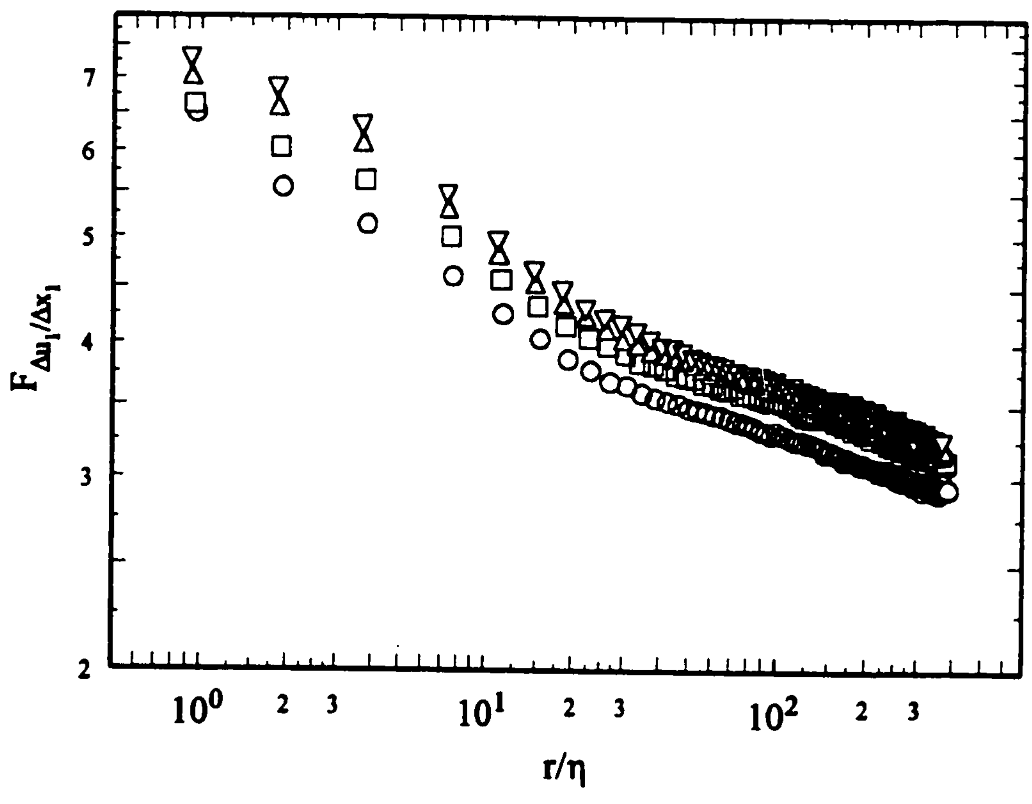

Fig. 7.30: Flatness of the longitudinal velocity difference: ○ $Re_\lambda = 172$; □ $Re_\lambda = 311$;

△ $Re_\lambda = 476$; ▽ $Re_\lambda = 578$.

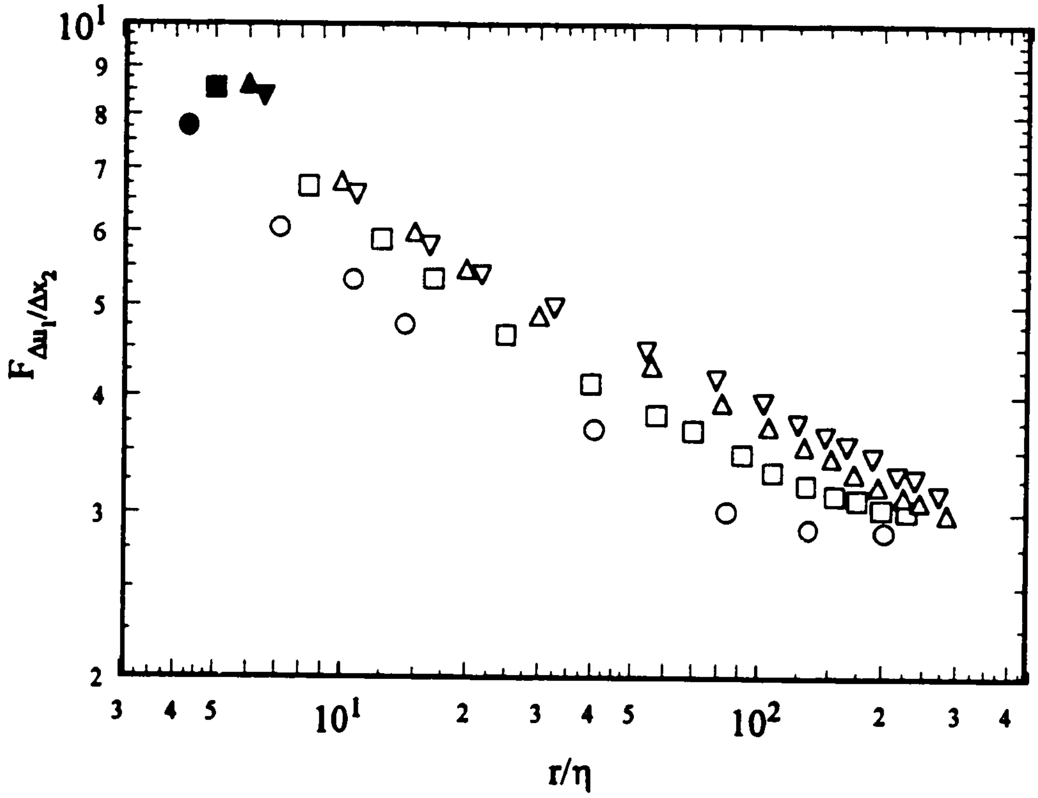

Fig. 7.31: Flatness of the transverse velocity difference: ○ $Re_\lambda = 172$; □ $Re_\lambda = 311$; △ $Re_\lambda = 476$; ▽ $Re_\lambda = 578$. Full symbols, measured with the fixed parallel hot wires.

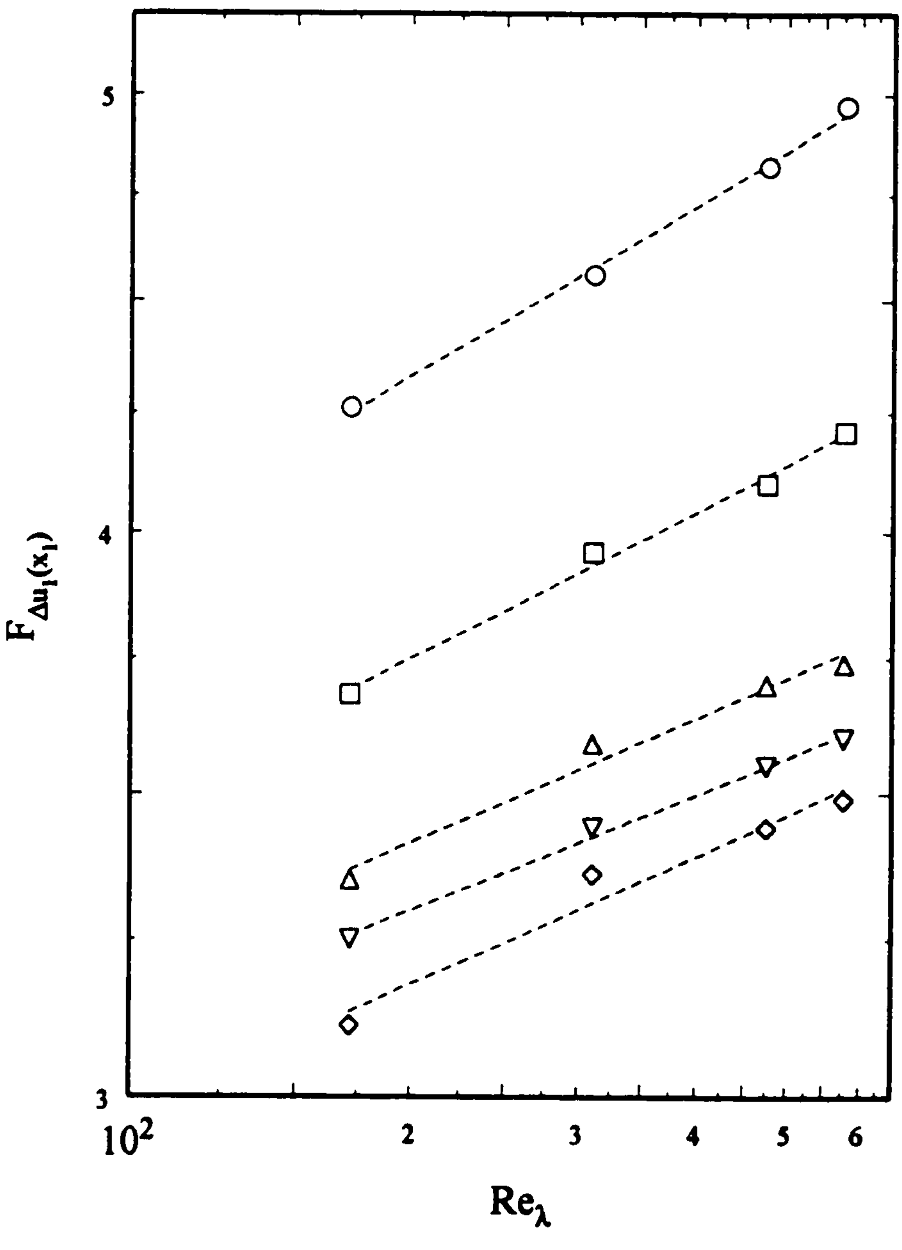

Fig. 7.32: Variations of the flatness of the longitudinal velocity difference with r/η.

○ r/η=10; □ r/η=20; △ r/η=80; ▽ r/η=120; ◇ r/η=180.

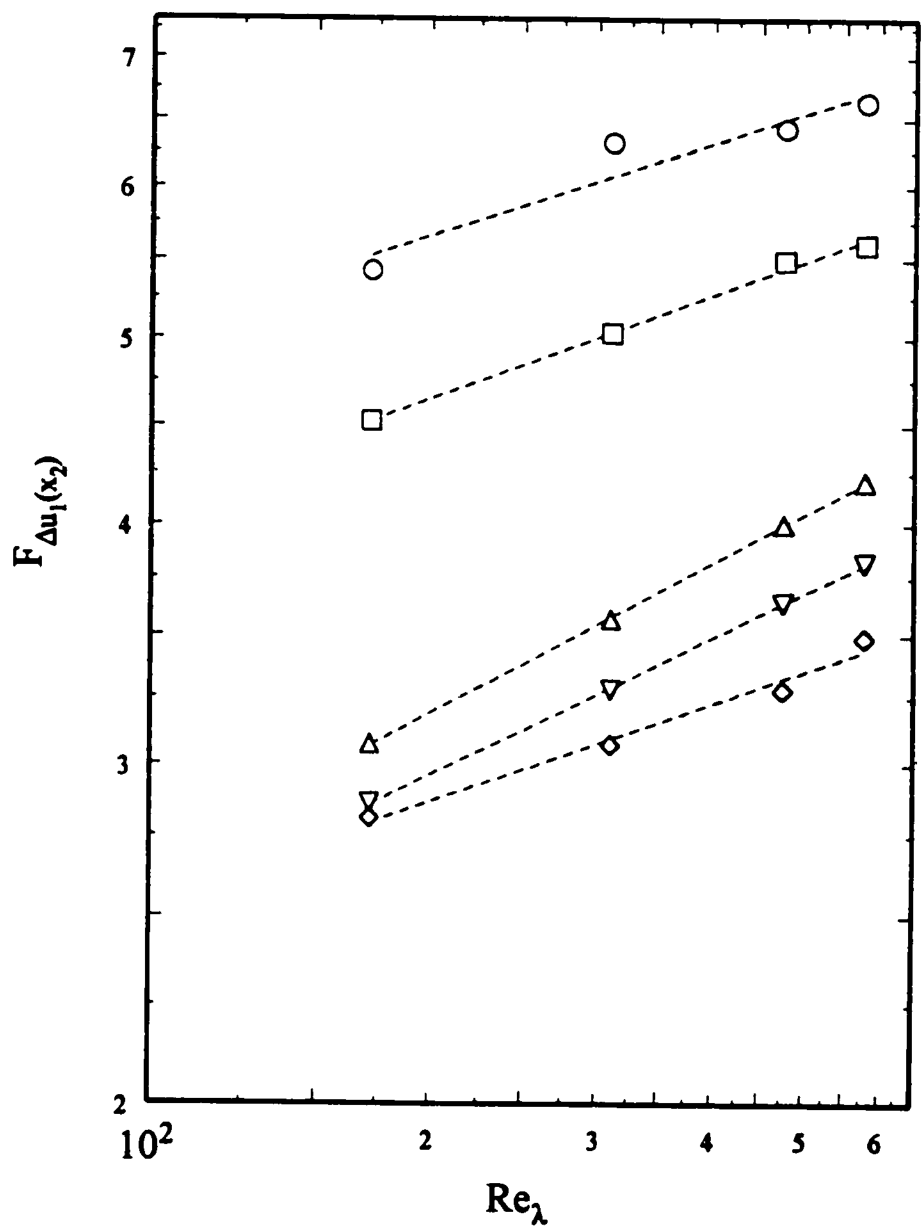

Fig. 7.33: Variations of the flatness of the transverse velocity difference with r/η.

○ r/η=10; □ r/η=20; △ r/η=80; ▽ r/η=120; ◇ r/η=180.

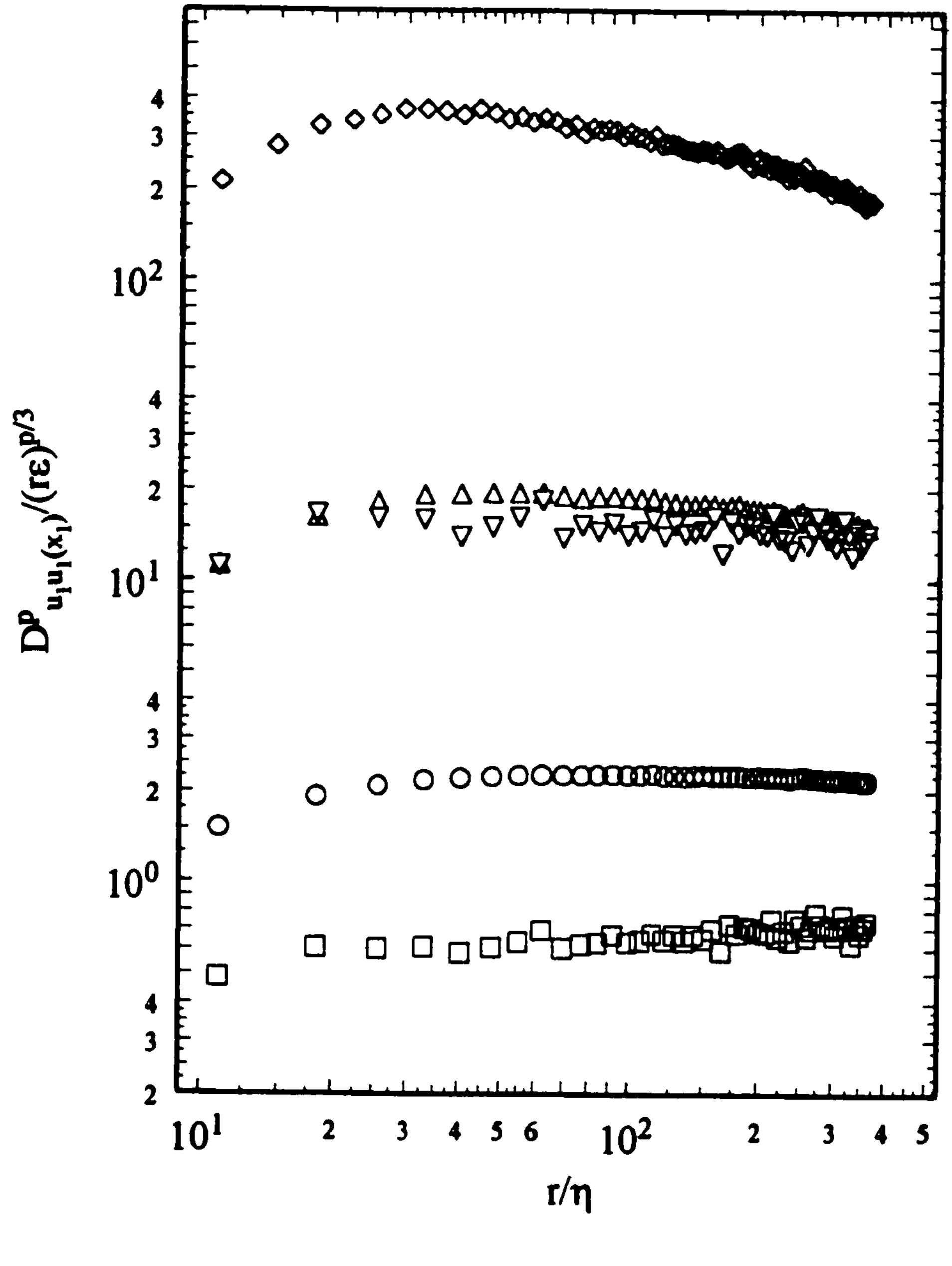

Fig. 7.34: Normalized p^{th} order longitudinal structure functions: ○p=2; □p=3; △p=4; ▽p=5; ◇p=6.

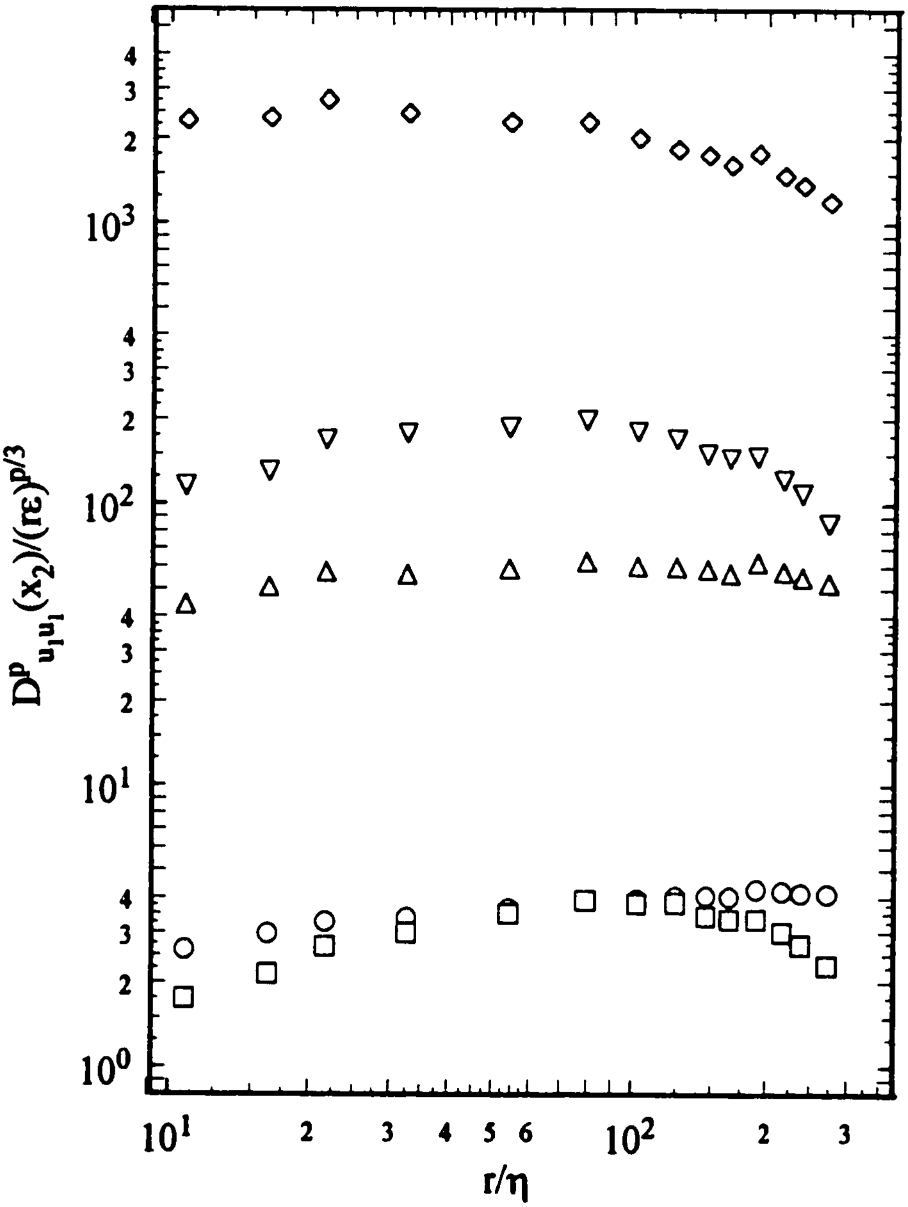

Fig. 7.35: Normalized p^{th} order transverse structure functions: ○p=2; □p=3; △p=4;

▽p=5; ◇p=6.

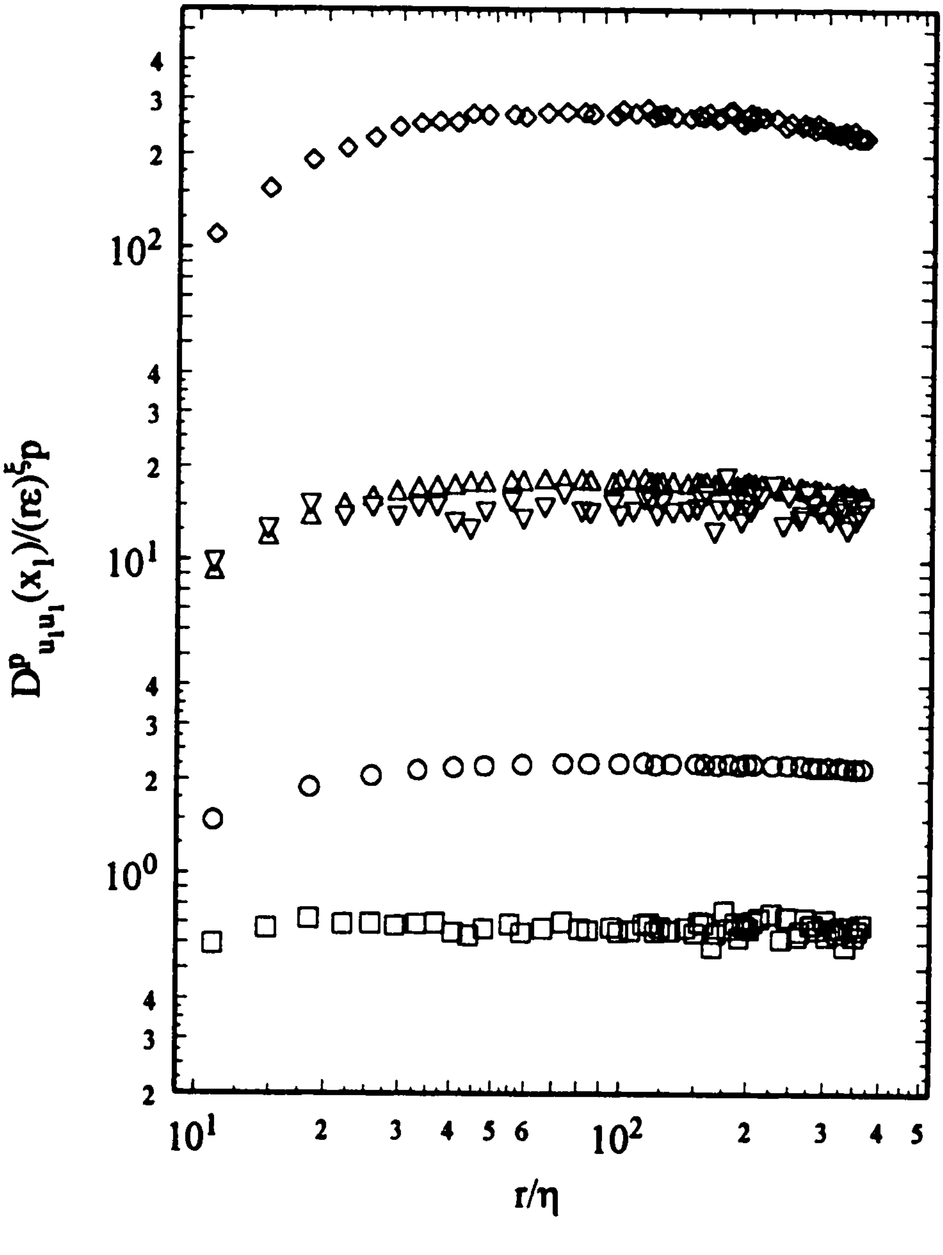

Fig. 7.36: Corrected p^{th} order longitudinal structure functions: ○p=2; □p=3; △p=4; ▽p=5; ◇p=6.

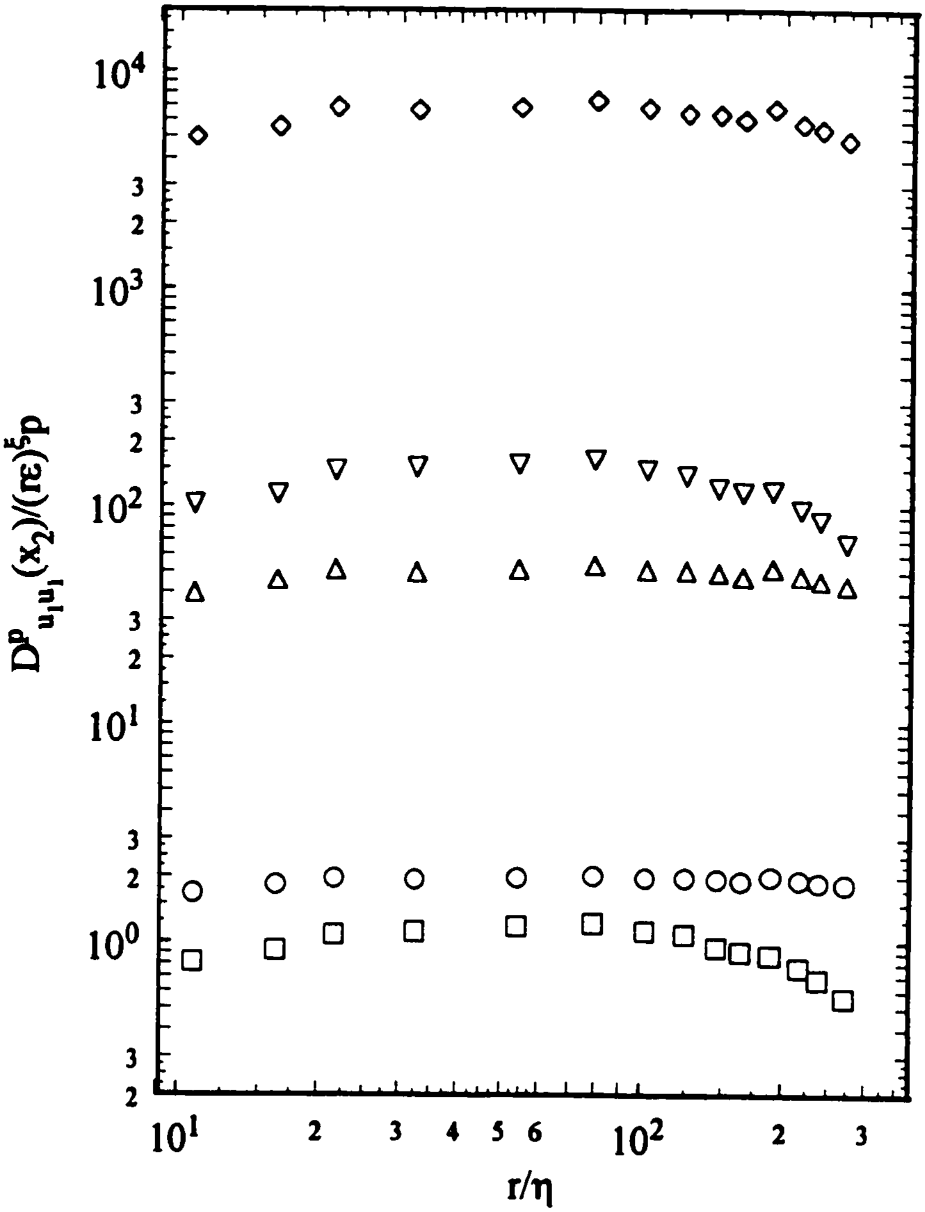

Fig. 7.37: Corrected p^{th} order transverse structure functions: ○p=2; □p=3; △p=4;

▽p=5; ◇p=6.

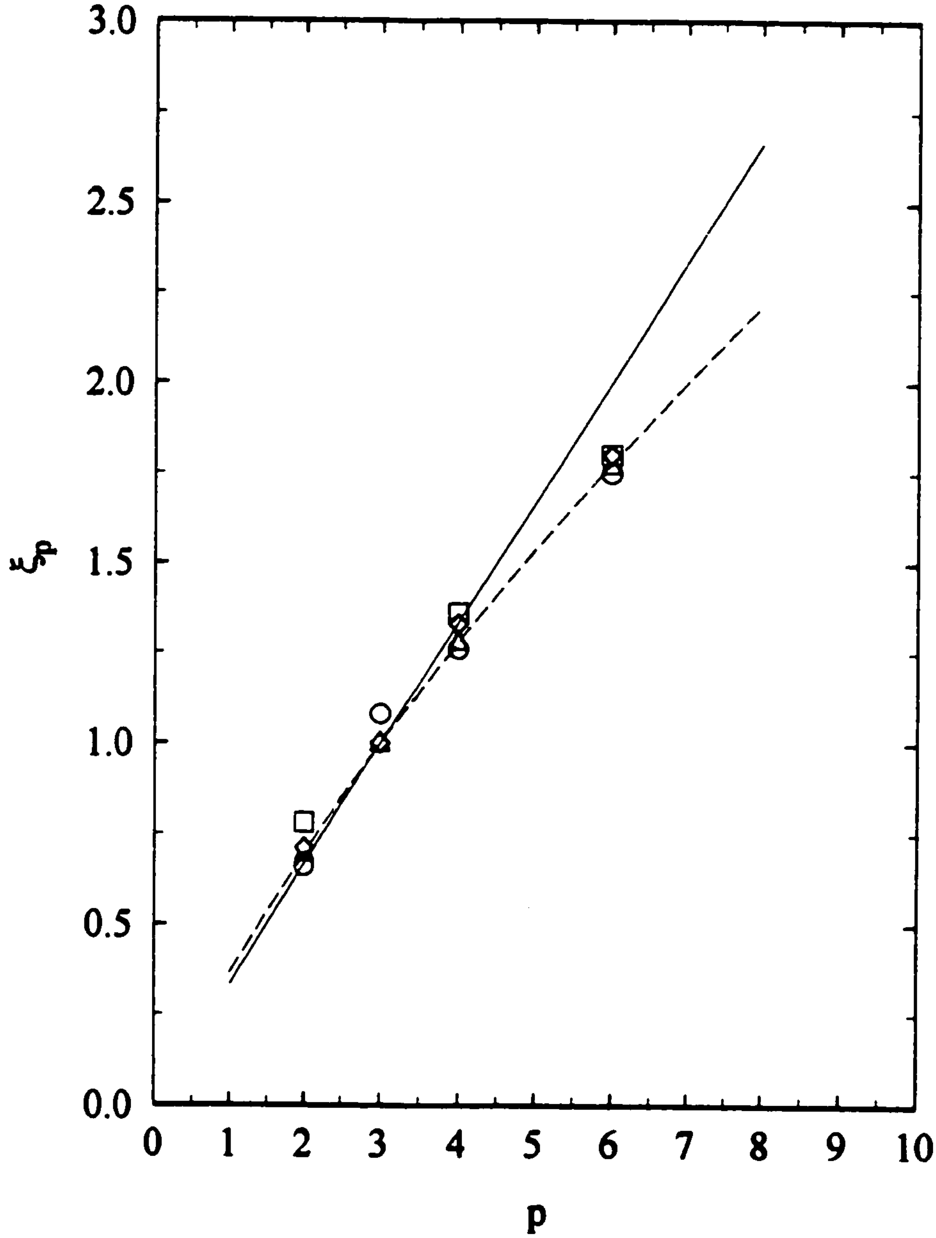

Fig. 7.38: Intermittency exponent variations with structure function order: ○ determined form the longitudinal structure function; □ determined form the transverse structure function; △ Anselmet et al. (1984); ▽ Boratav (1997); ----- She and Lévêque (1994); —— $\zeta_p = p/3$ (Kolmogorov, 1941).

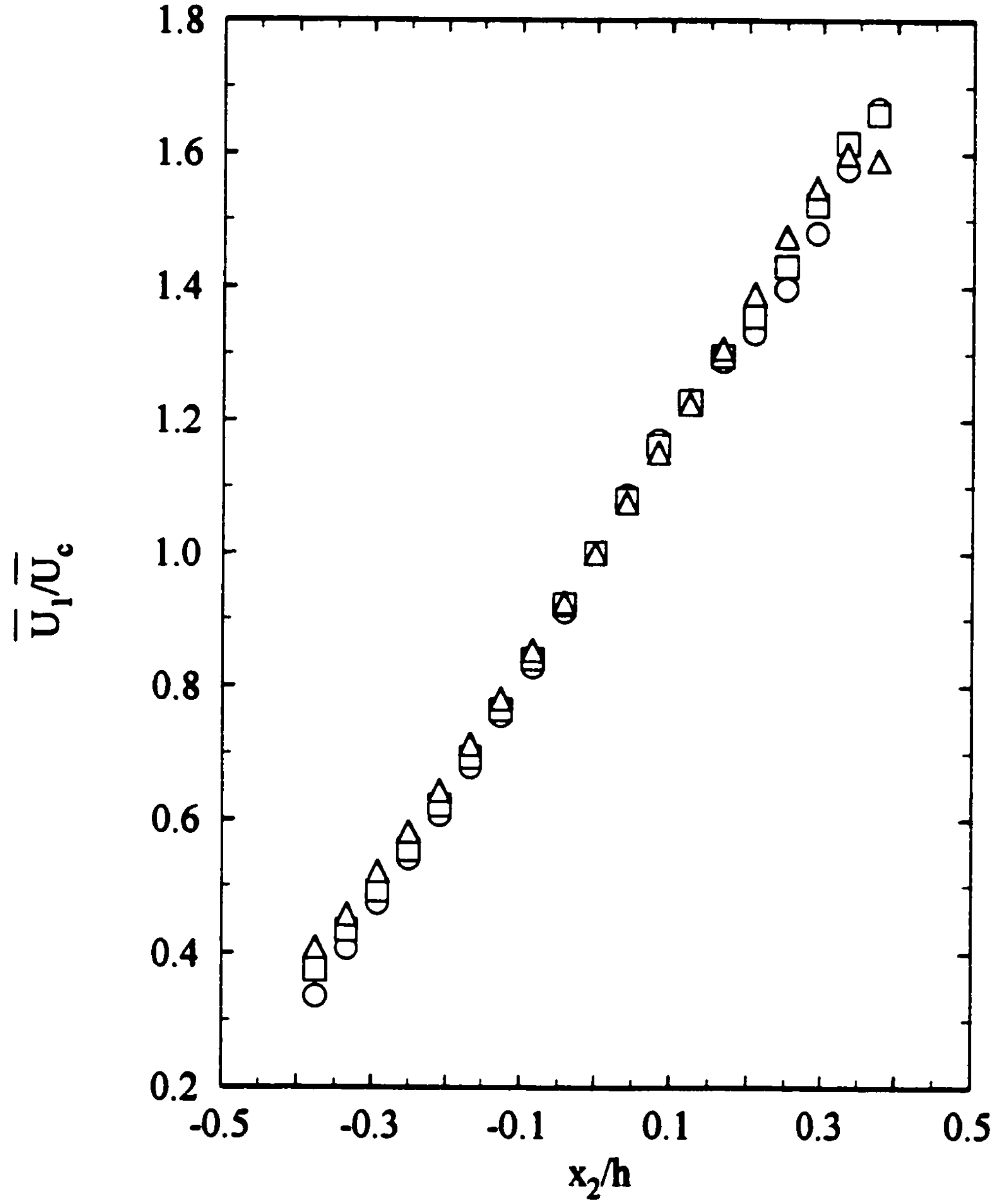

Fig. 8.1: Transverse profiles of the mean velocity in the heated flow.

○ x_1/h=3; □ x_1/h=4.7; △ x_1/h=8.

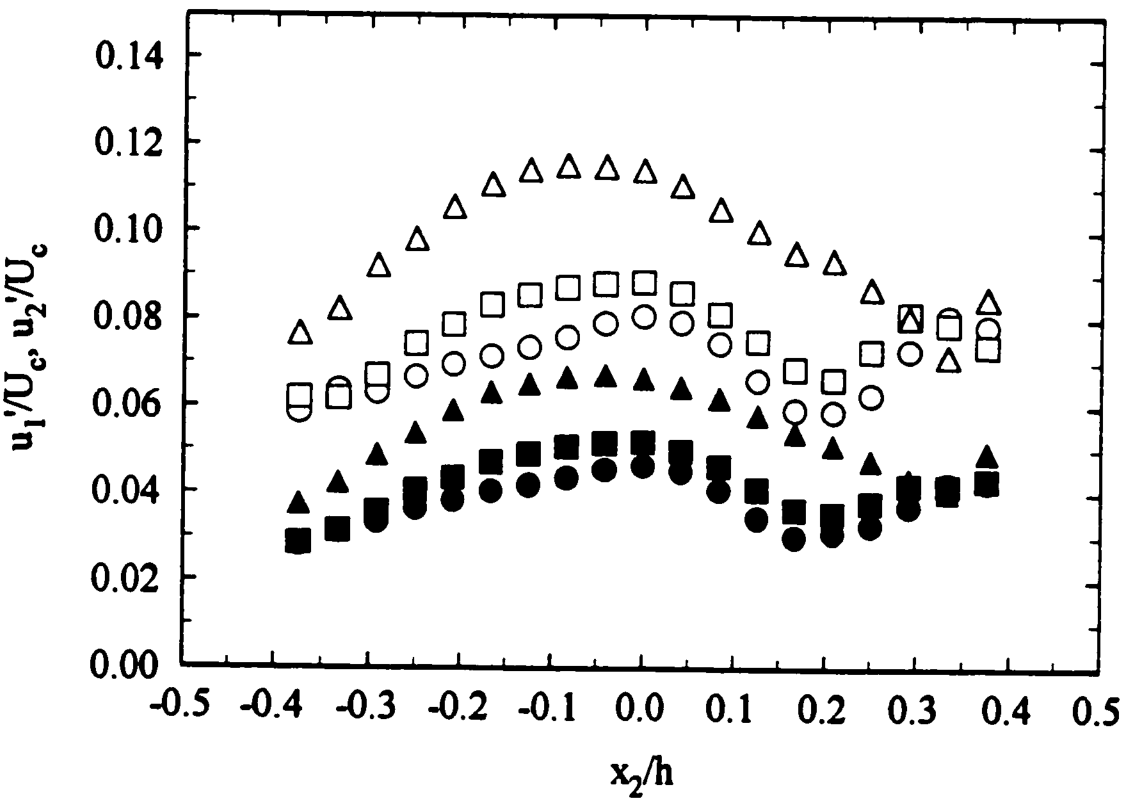

Fig. 8.2: Transverse profiles of the turbulent intensity. Full symbols, $u_2'/\overline{U}_c$, empty symbols, $u_1'/\overline{U}_c$. ○ and ● x_1/h=3; □ and ■ x_1/h=4.7; △ and ▲ x_1/h=8.

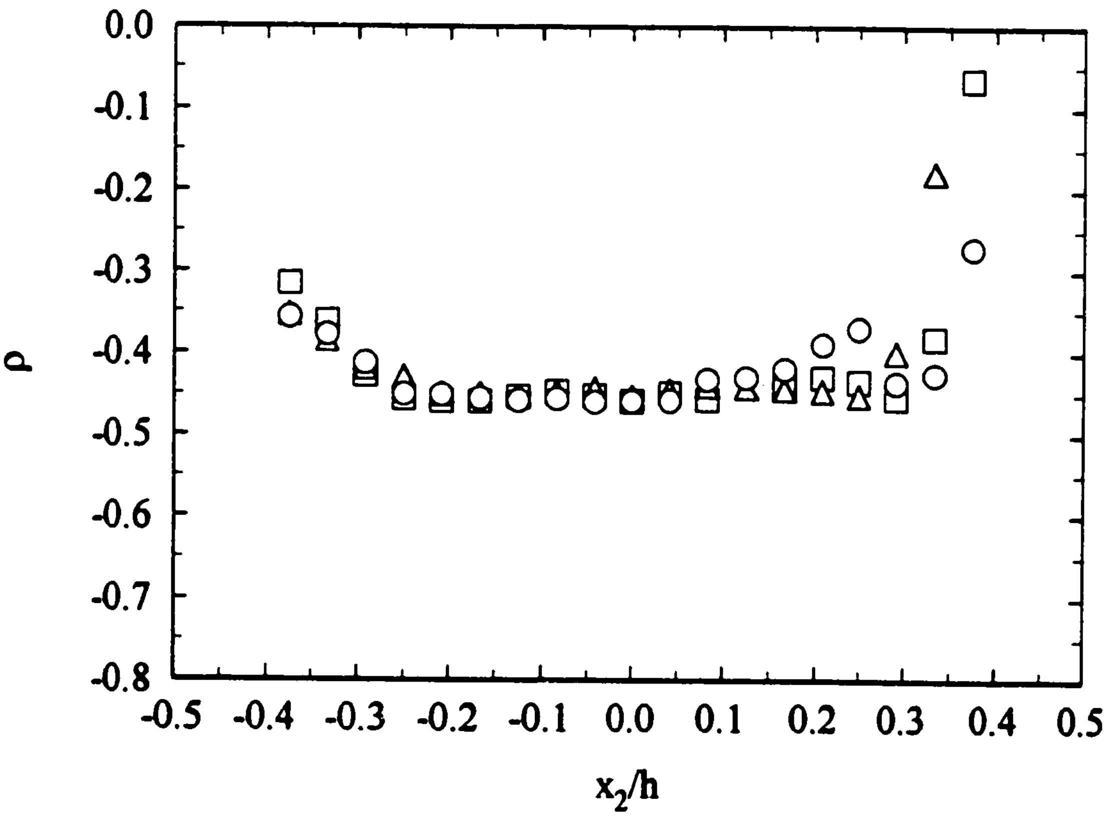

Fig. 8.3: Transverse profiles of the turbulent shear stress coefficient. ○ x_1/h=3;

□ x_1/h=4.7; △ x_1/h=8.

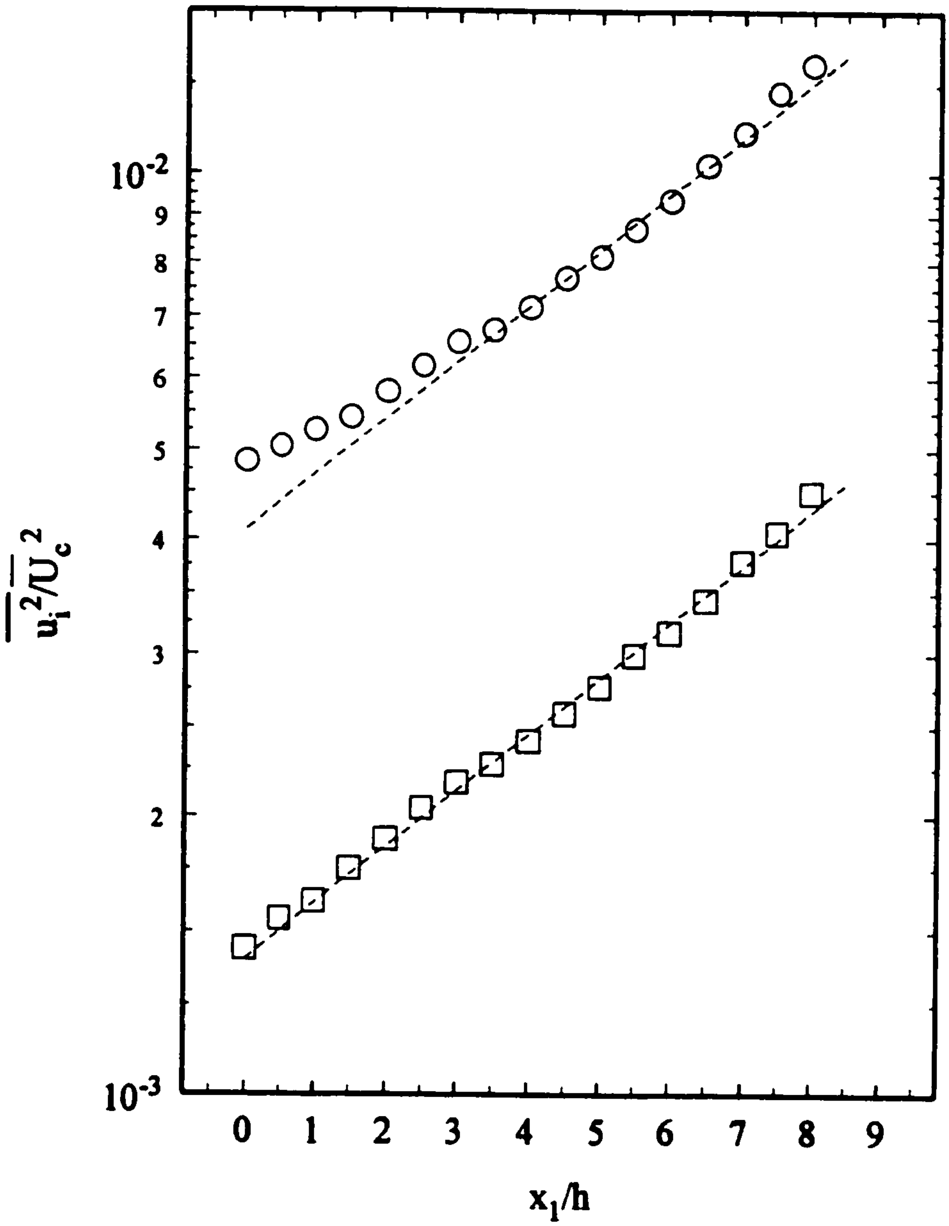

Fig. 8.4: Growth of the turbulent intensities. ○ $\overline{u_1^2}/\overline{U_c^2}$; □ $\overline{u_2^2}/\overline{U_c^2}$.

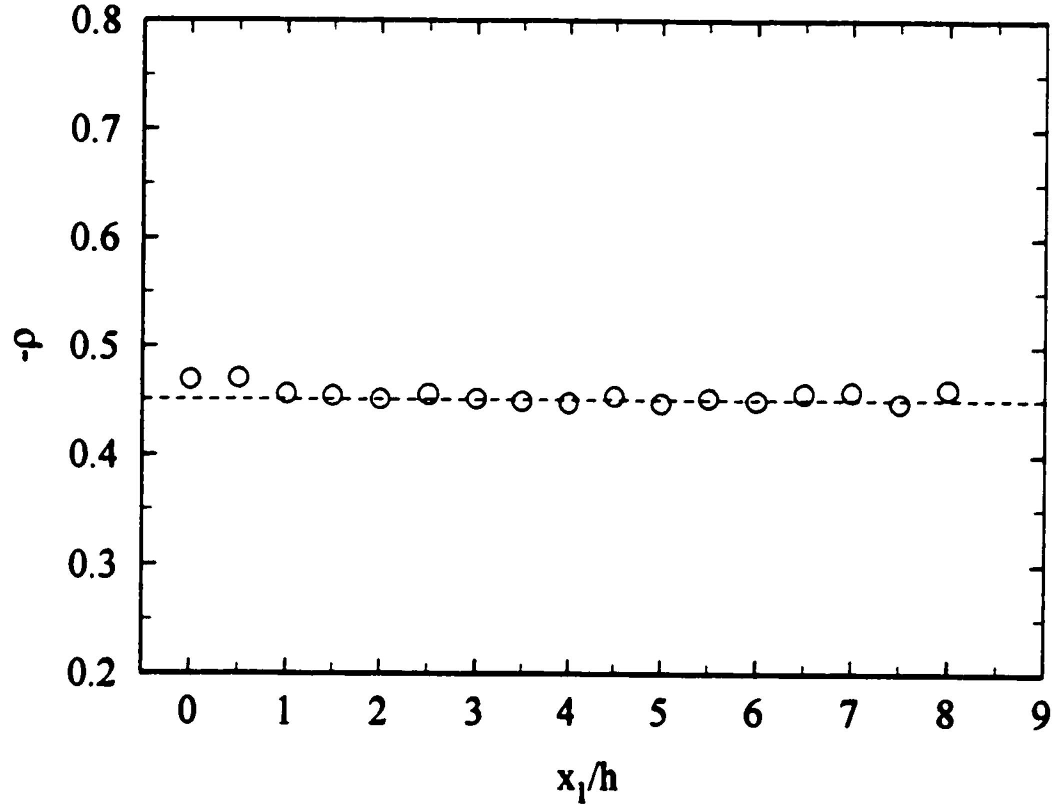

Fig. 8.5: Downstream development of the shear stress coefficient.

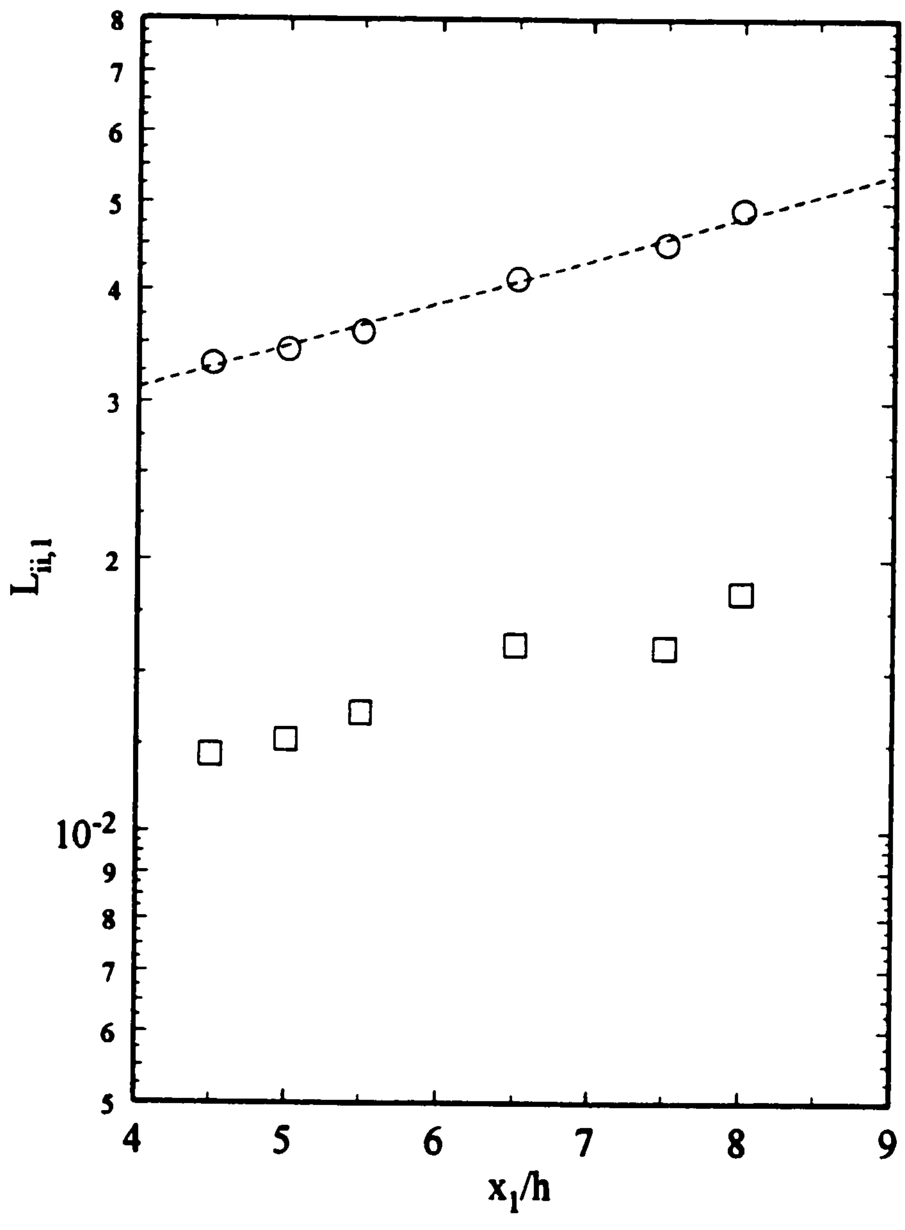

Fig. 8.6: Downstream development of the integral length scales. ○ $L_{11,1}$; □ $L_{22,1}$.

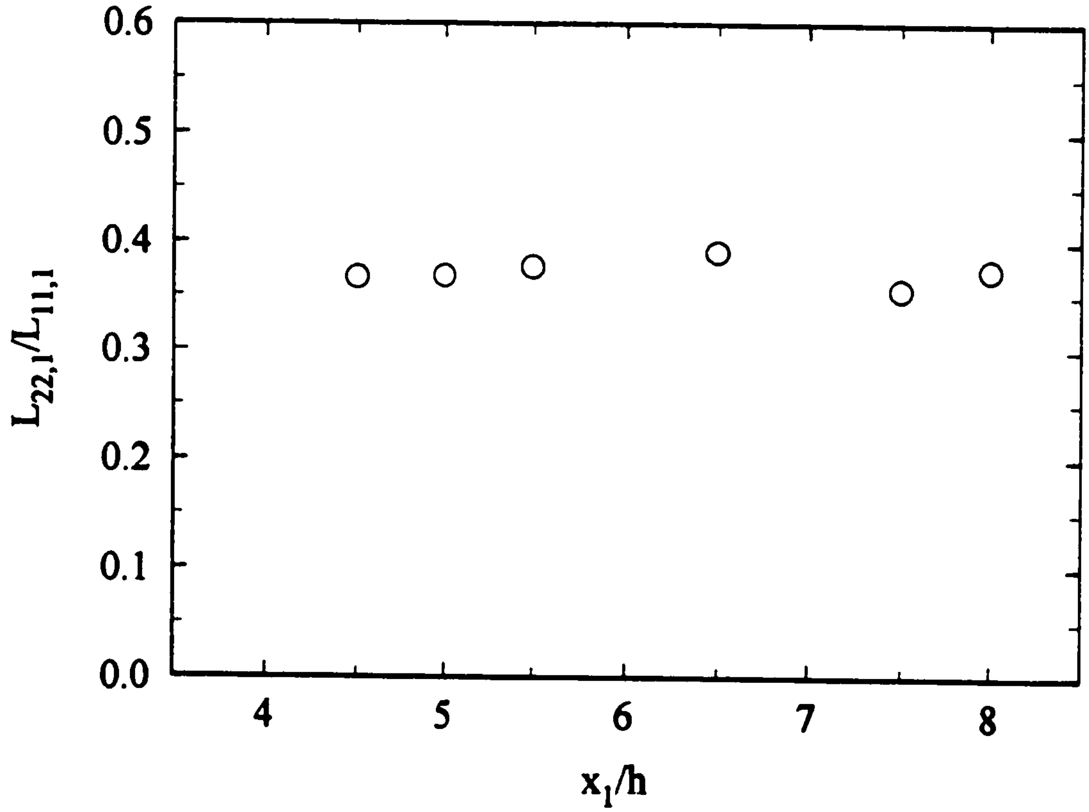

Fig. 8.7: Ratio of the integral length scales, $L_{22,1}/L_{11,1}$.

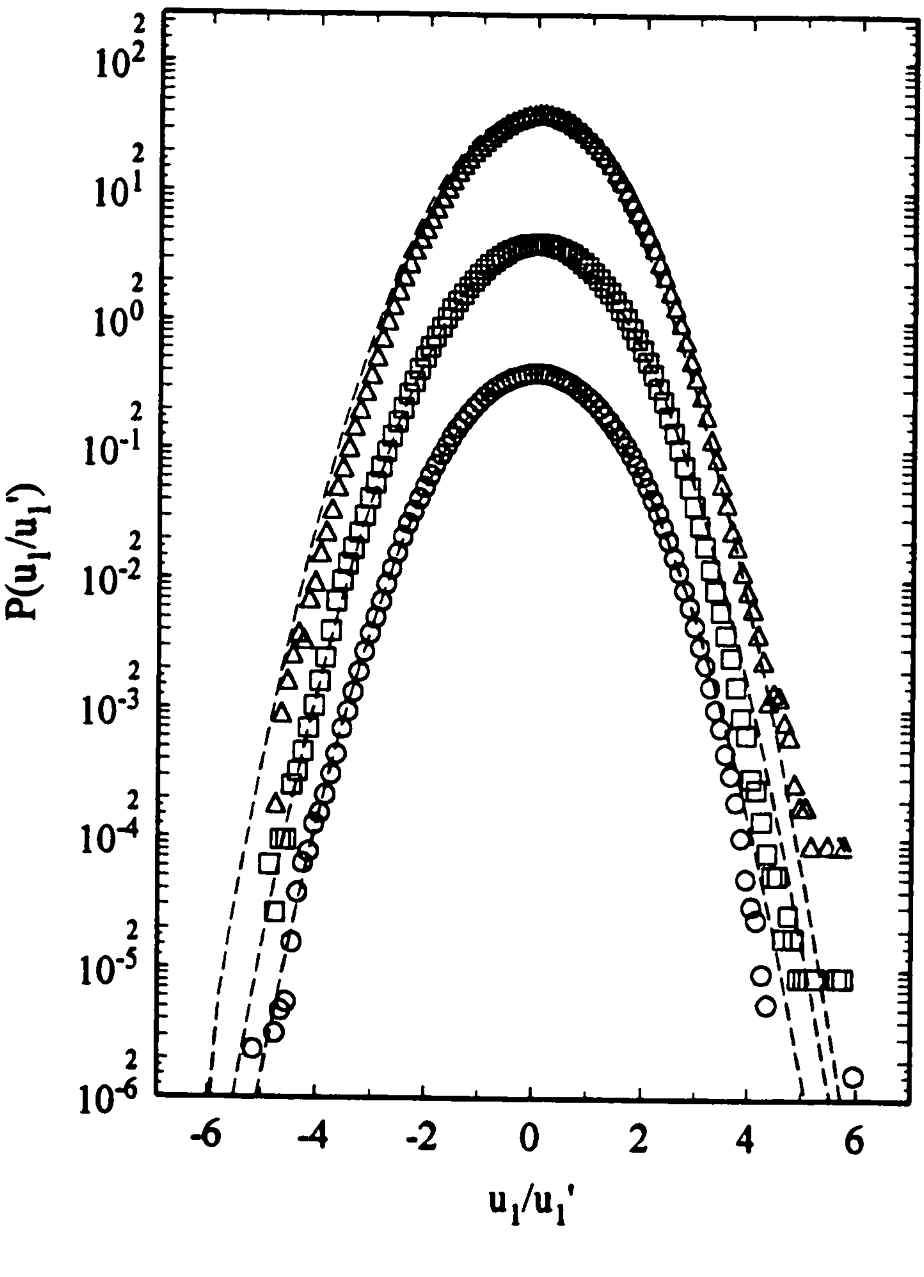

Fig. 8.8: Pdf of the streamwise velocity fluctuations. ○ $Re_\lambda = 184$; □ $Re_\lambda = 200$;

△ $Re_\lambda = 253$.

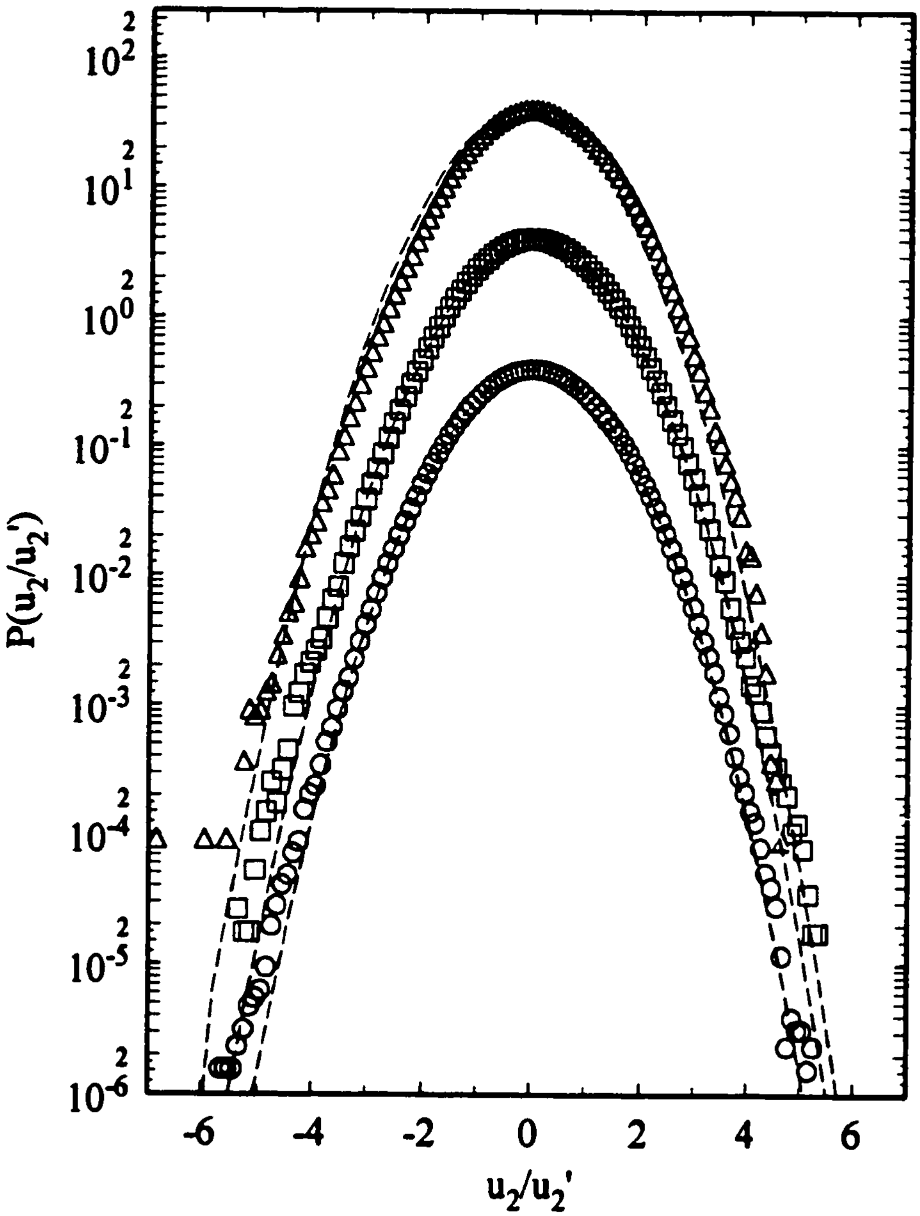

Fig. 8.9: Pdf of the transverse velocity fluctuations. ○ $Re_\lambda = 184$; □ $Re_\lambda = 200$;

△ $Re_\lambda = 253$.

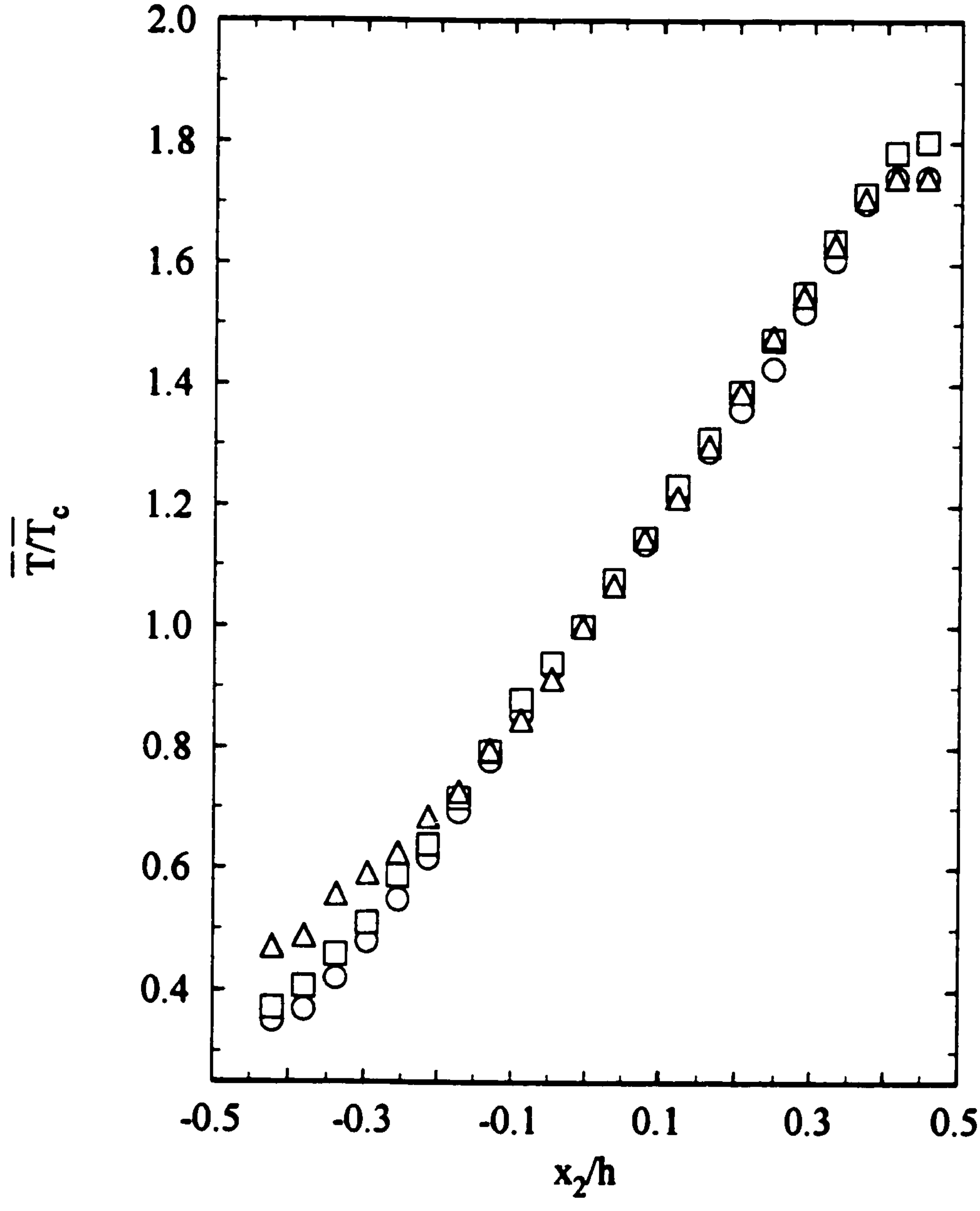

Fig. 8.10: Transverse profiles of the mean temperature rise. ○ x_1/h=3; □ x_1/h=4.7;

△ x_1/h=8.

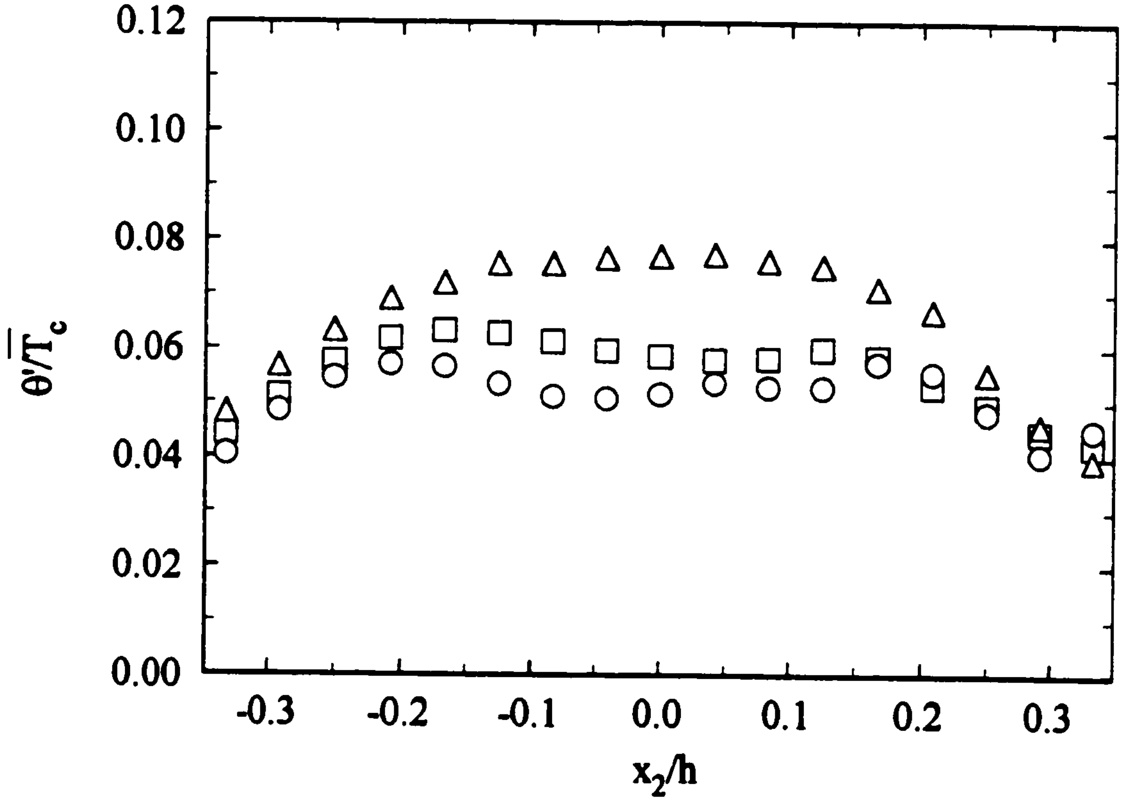

Fig. 8.11: Transverse profiles of the normalized temperature fluctuations. ○ x_1/h=3; □ x_1/h=4.7; △ x_1/h=8.

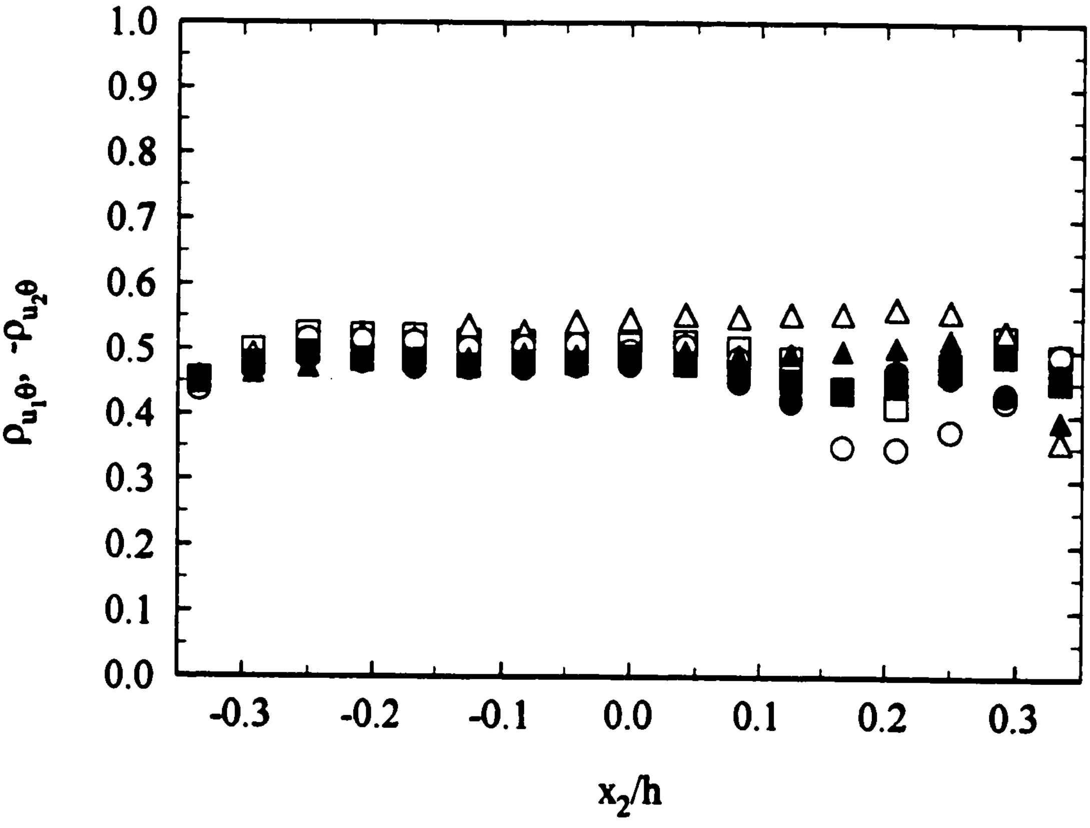

Fig. 8.12: Transverse profiles of the temperature-velocity correlations. Full symbols, $-\rho_{u_2\theta}$, empty symbols, $\rho_{u_1\theta}$. ○ and ● x_1/h=3; □ and ■ x_1/h=4.7; △ and ▲ x_1/h=8.

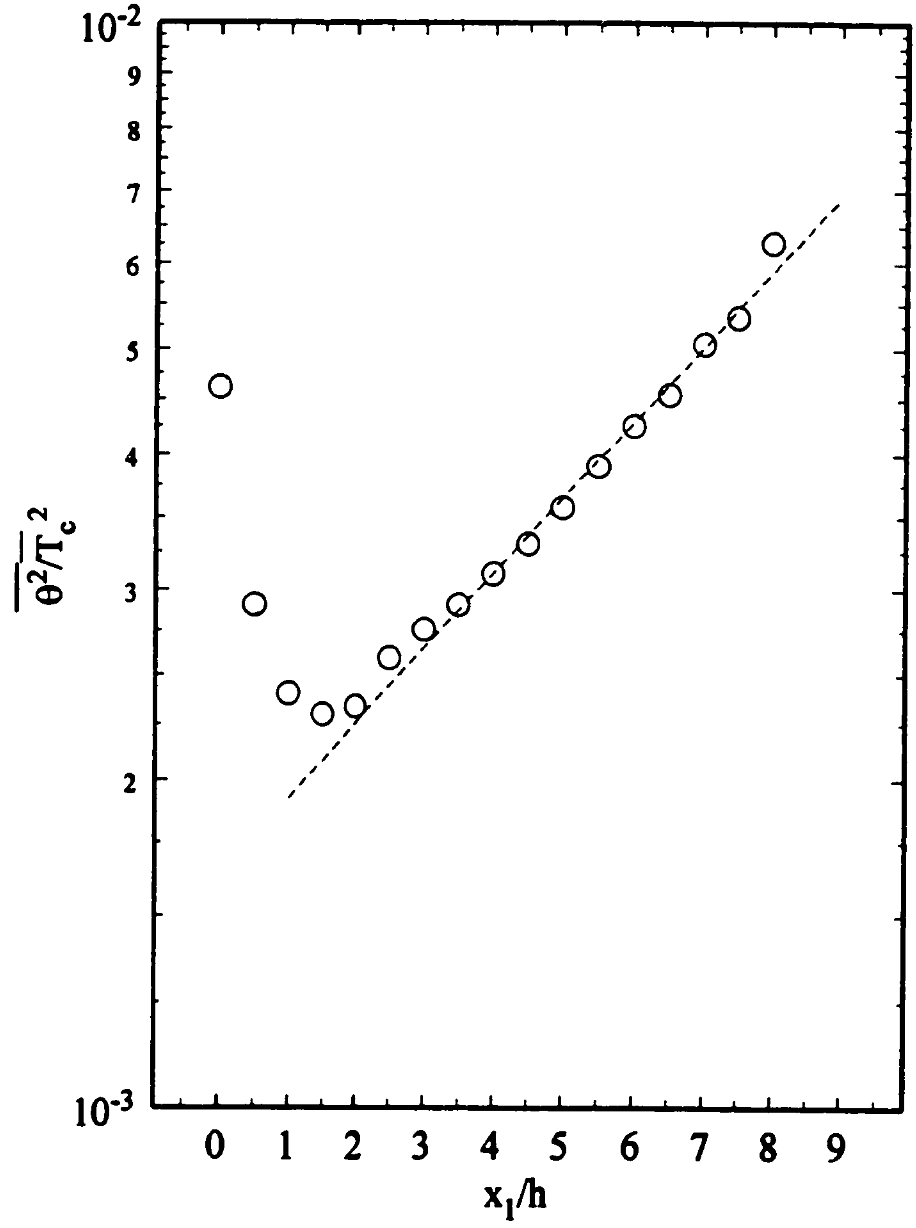

Fig. 8.13: Growth of the normalized temperature variance.

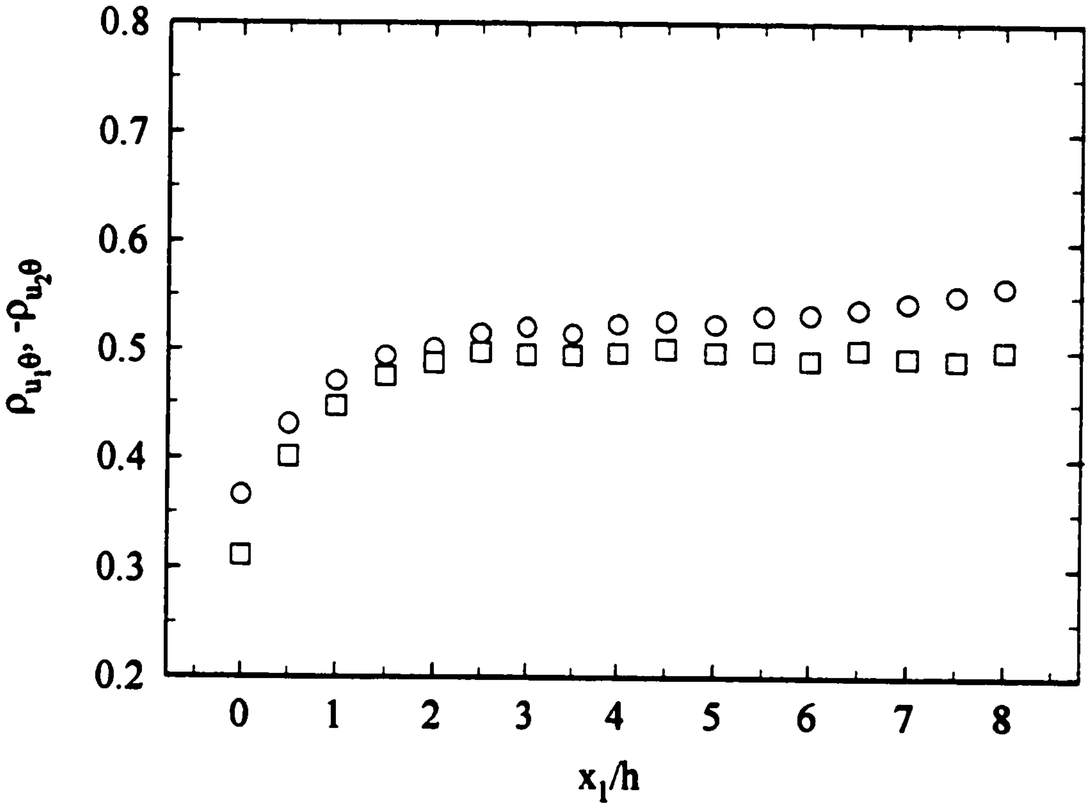

Fig. 8.14: Downstream development of the turbulent correlations. ○ $\rho_{u_1\theta}$; □ $-\rho_{u_2\theta}$.

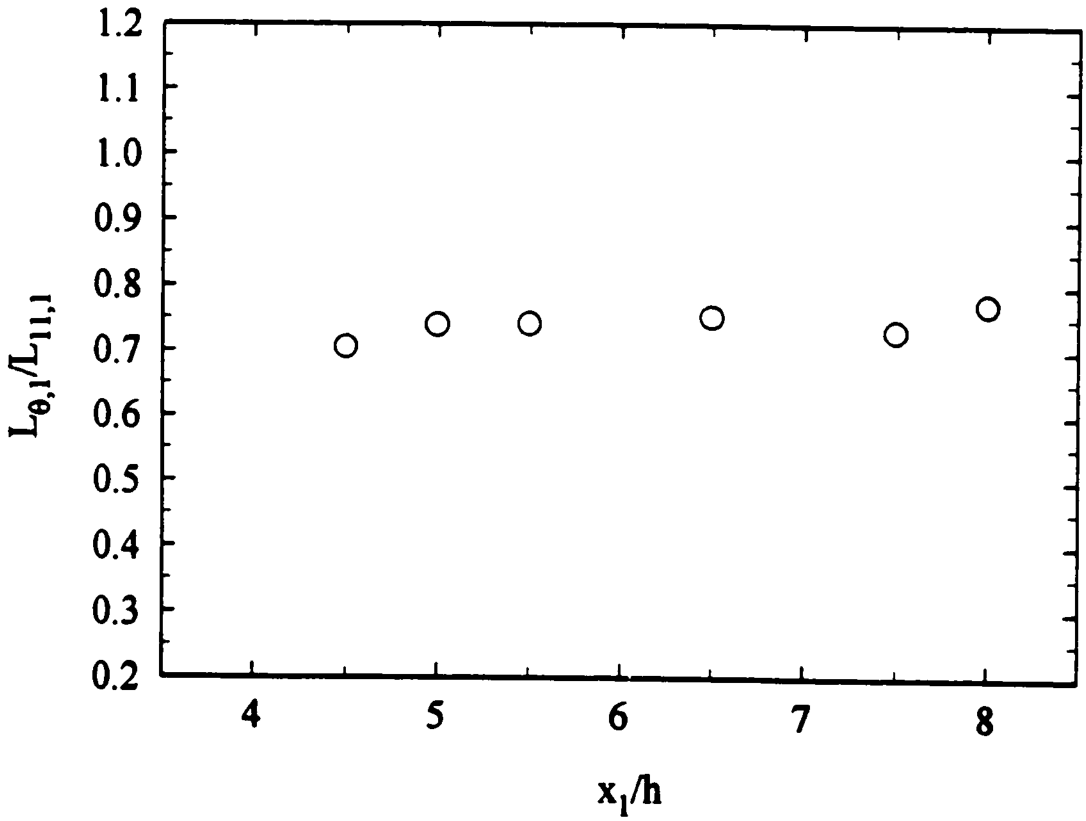

Fig. 8.15: Ratio of integral length scales, $L_{\theta,1}/L_{11,1}$.

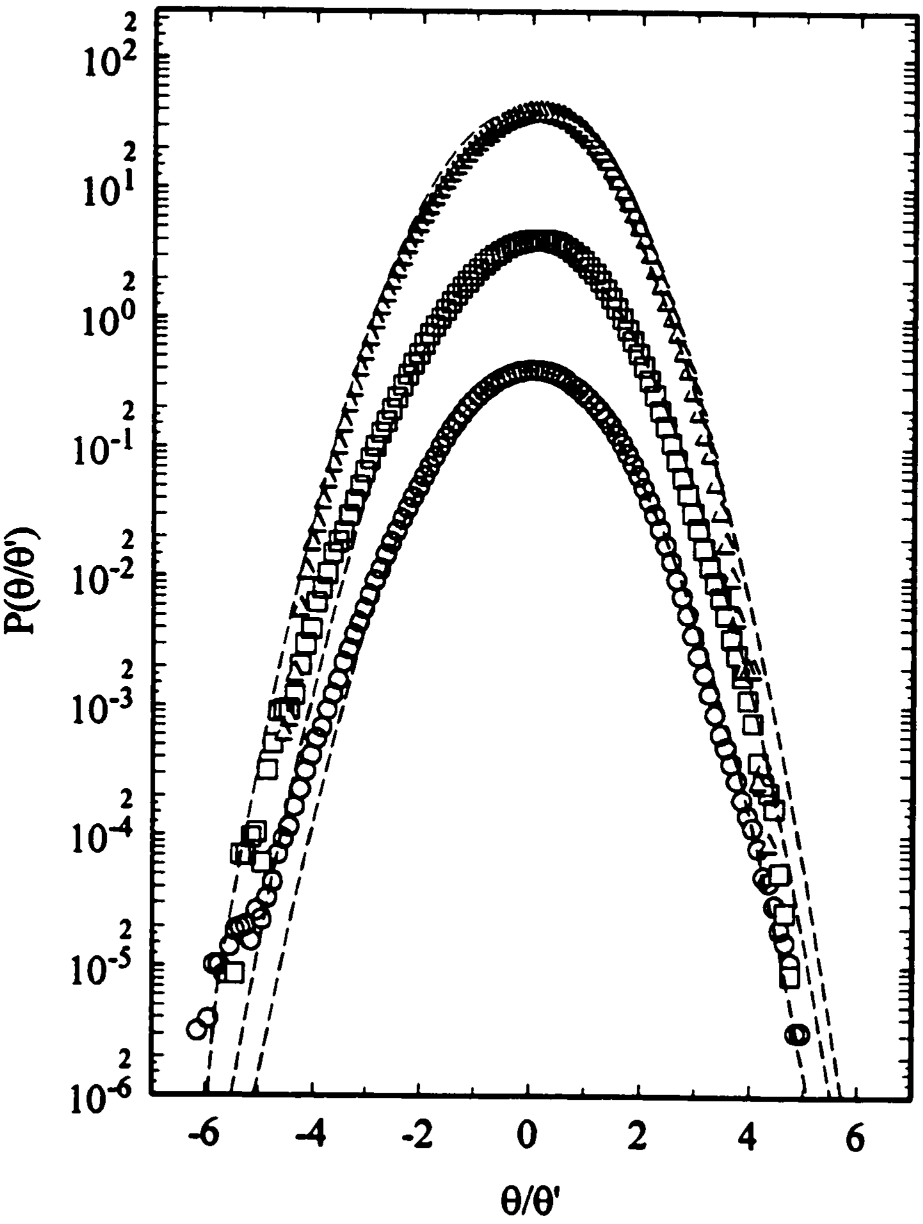

Fig. 8.16: Pdf of the temperature fluctuations. ○ $Re_\lambda = 184$; □ $Re_\lambda = 200$; △ $Re_\lambda = 253$.

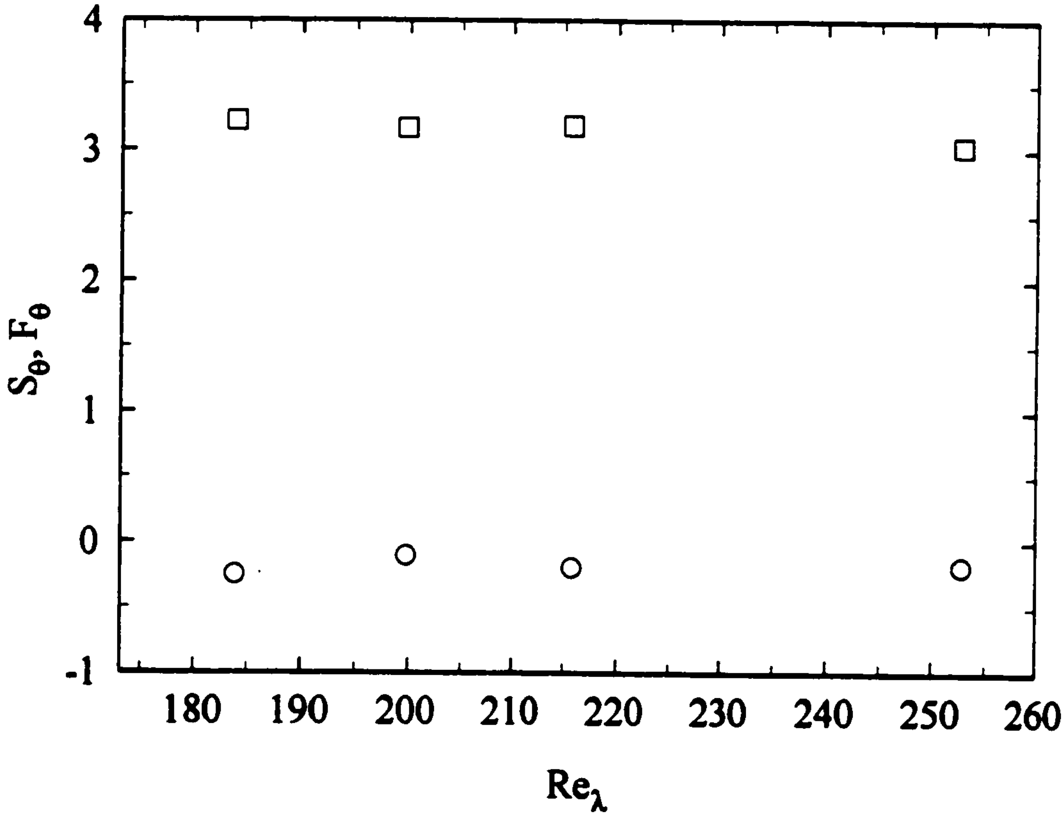

Fig. 8.17: Variations of skewness and flatness of the temperature fluctuations with Re_λ.

○ S_θ; □ F_θ

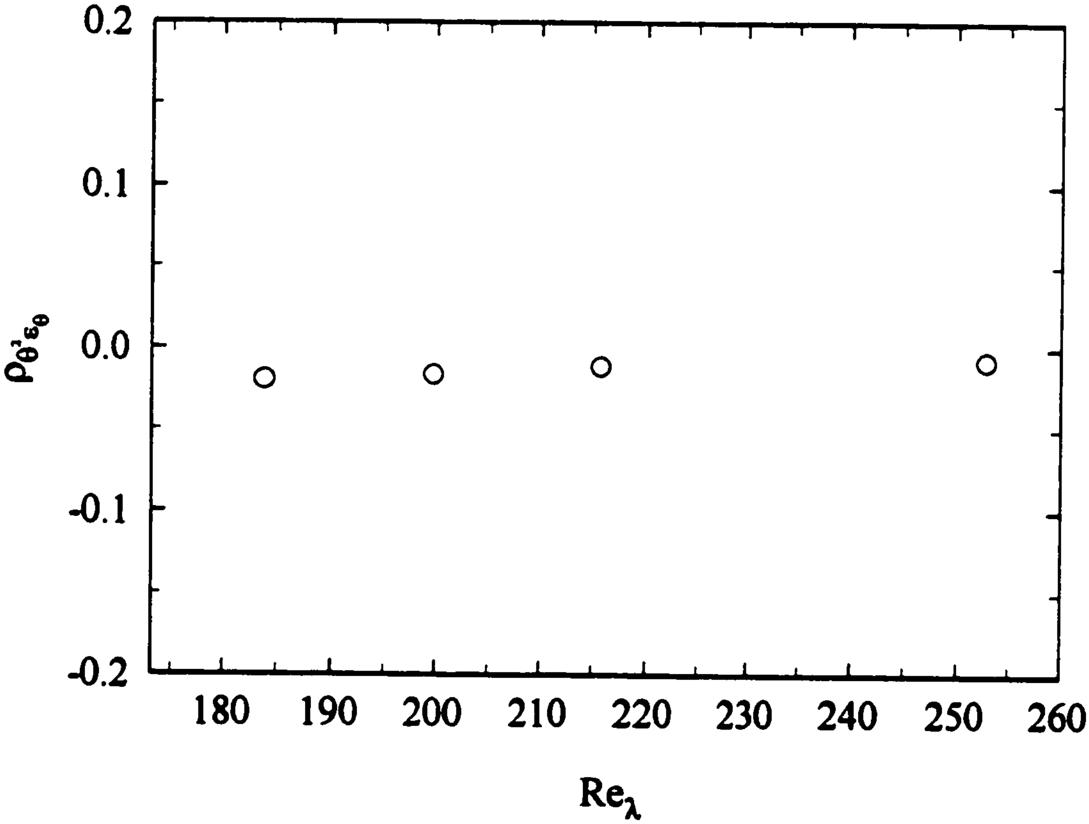

Fig. 8.18: Variations of the squared temperature-temperature dissipation correlation coefficient with Re_λ.

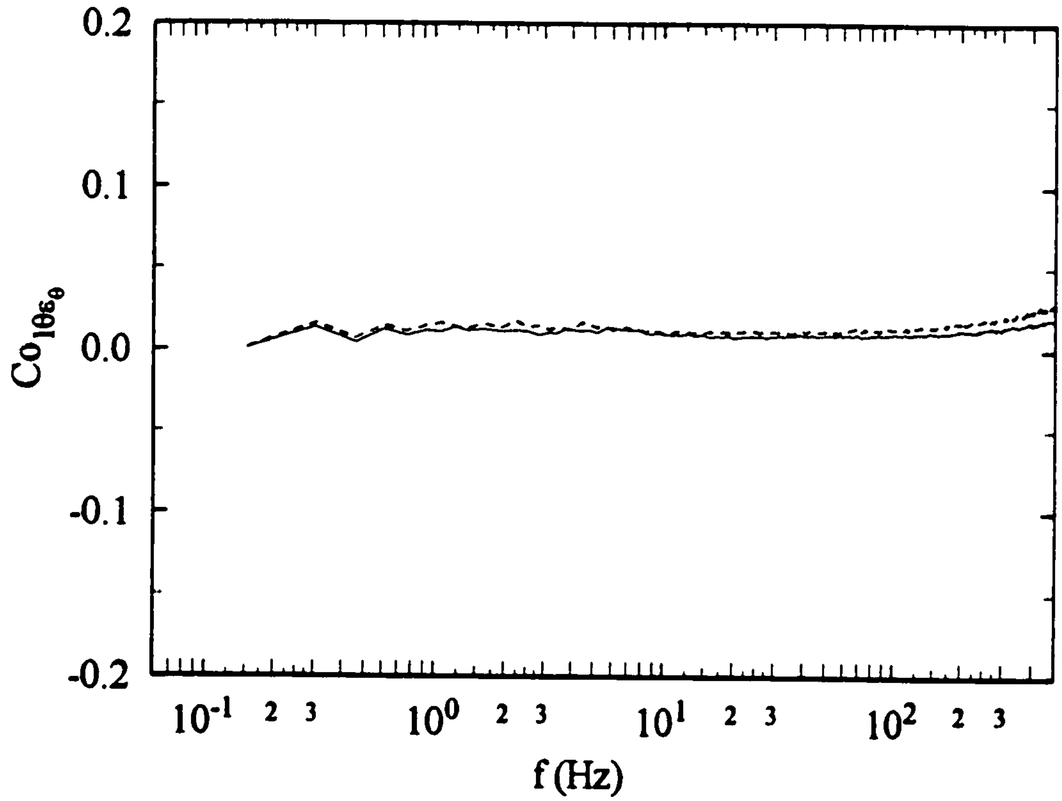

Fig. 8.19: Normalized co-spectra of the temperature-temperature dissipation.

— $Re_\lambda = 200$; --- $Re_\lambda = 253$.

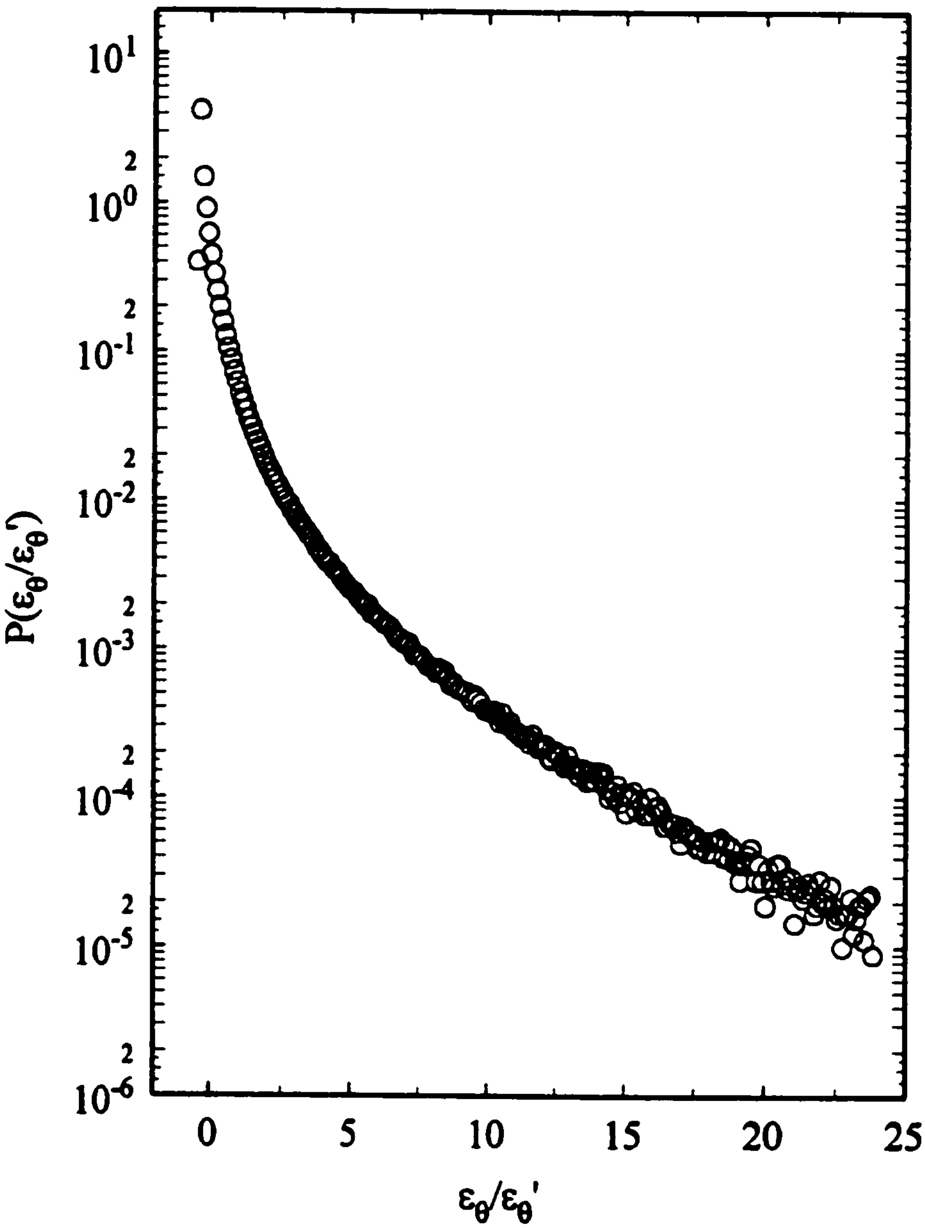

Fig. 8.20: Pdf of the scalar dissipation at $Re_\lambda = 253$.

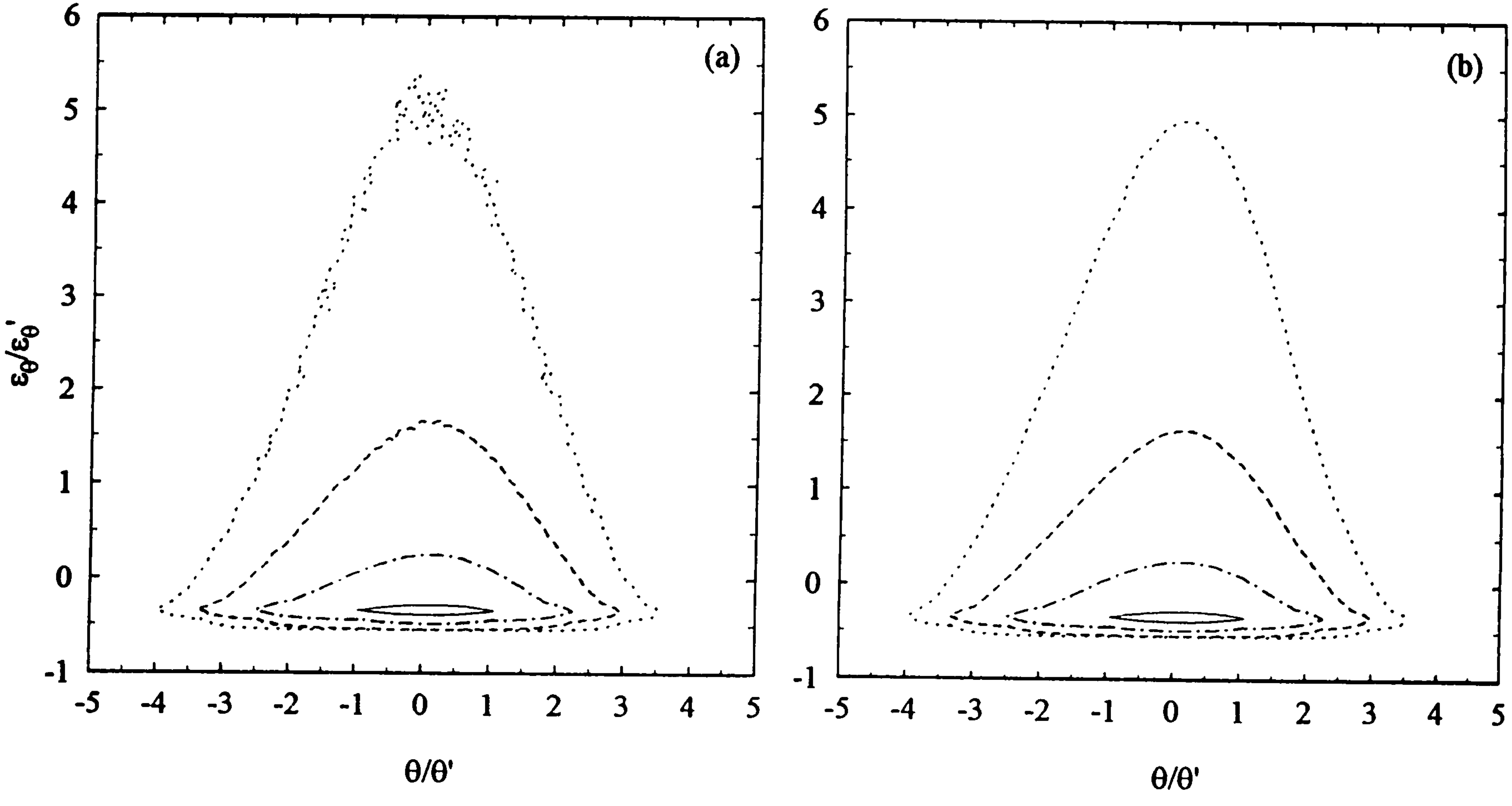

Fig. 8.21: (a) θ-ϵ_θ joint pdf contours;(b) the product of the pdf of θ and ϵ_θ

—— 1; –·– 0.1; ----0.01; ······ 0.001.

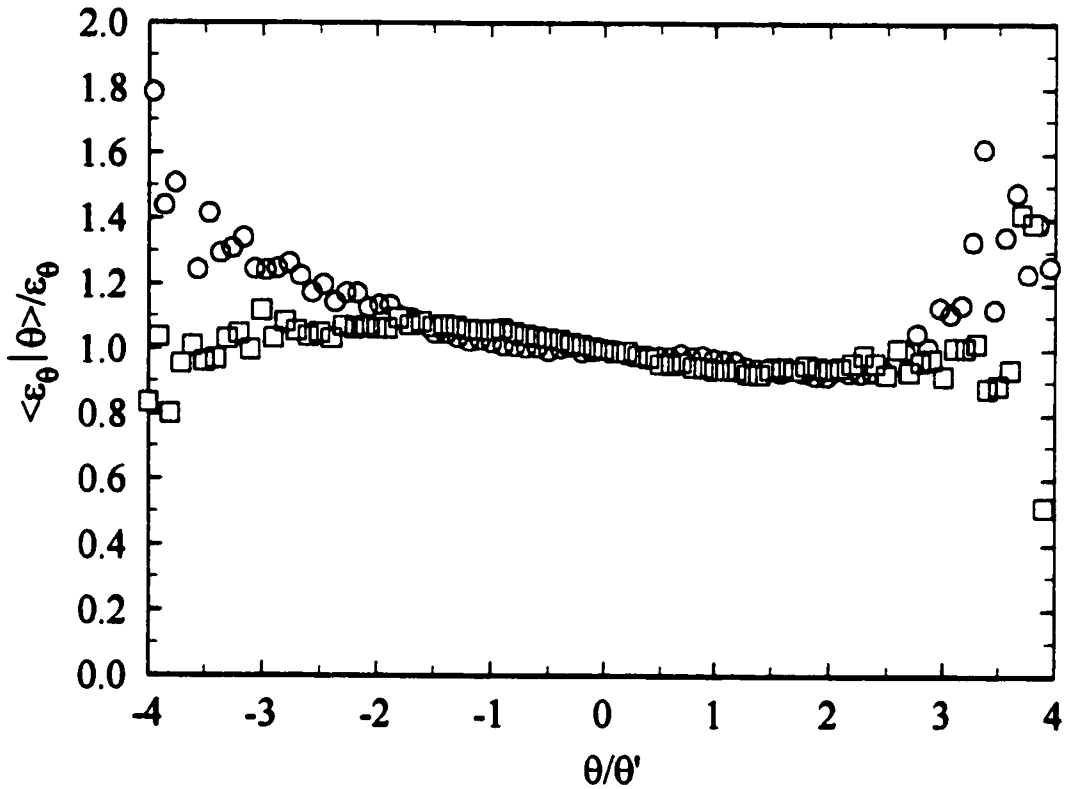

Fig. 8.22: Normalized conditional expectation of the scalar dissipation.

○ $Re_\lambda = 200$; □ $Re_\lambda = 253$.

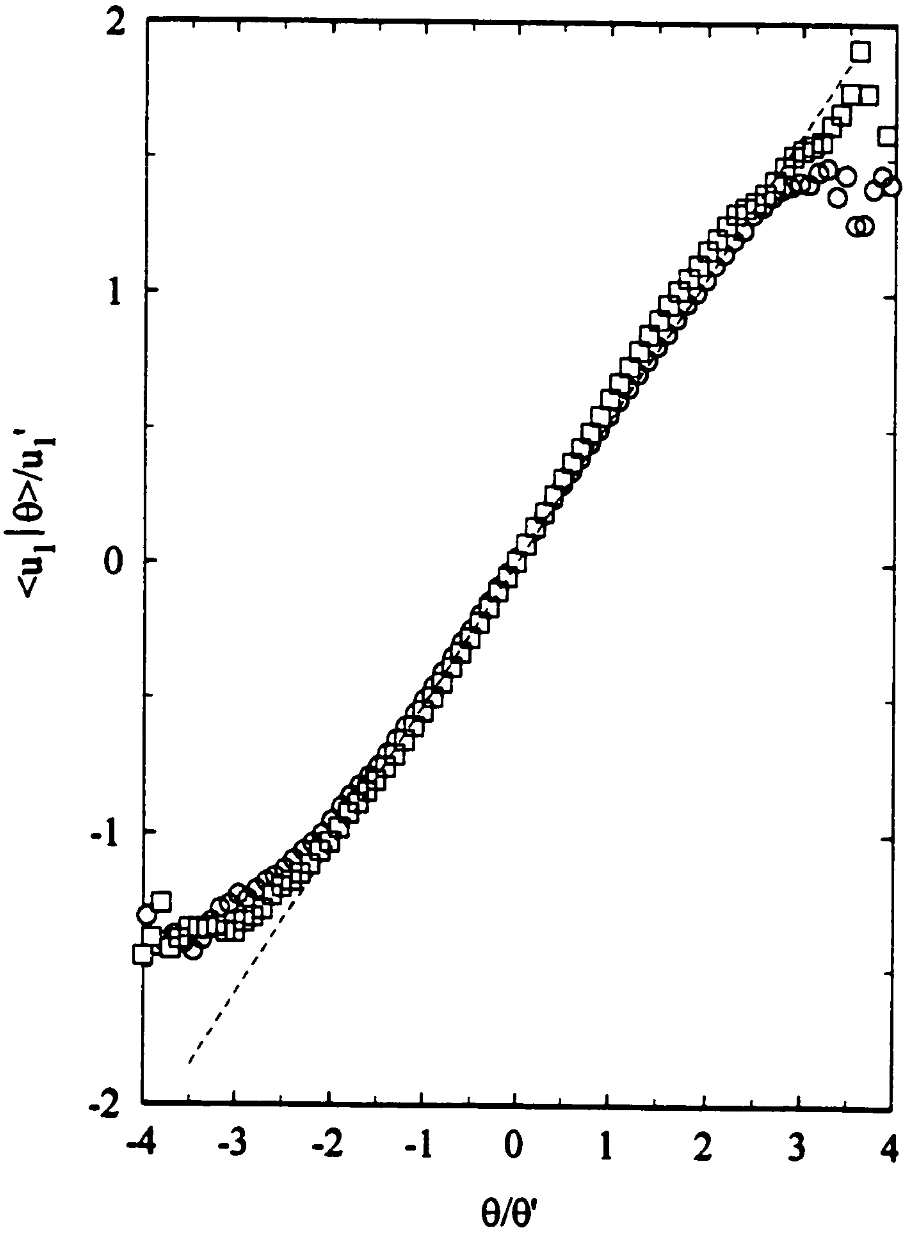

Fig. 8.23: Normalized conditional expectation of the streamwise velocity fluctuations.

○ $Re_\lambda = 200$; □ $Re_\lambda = 253$.

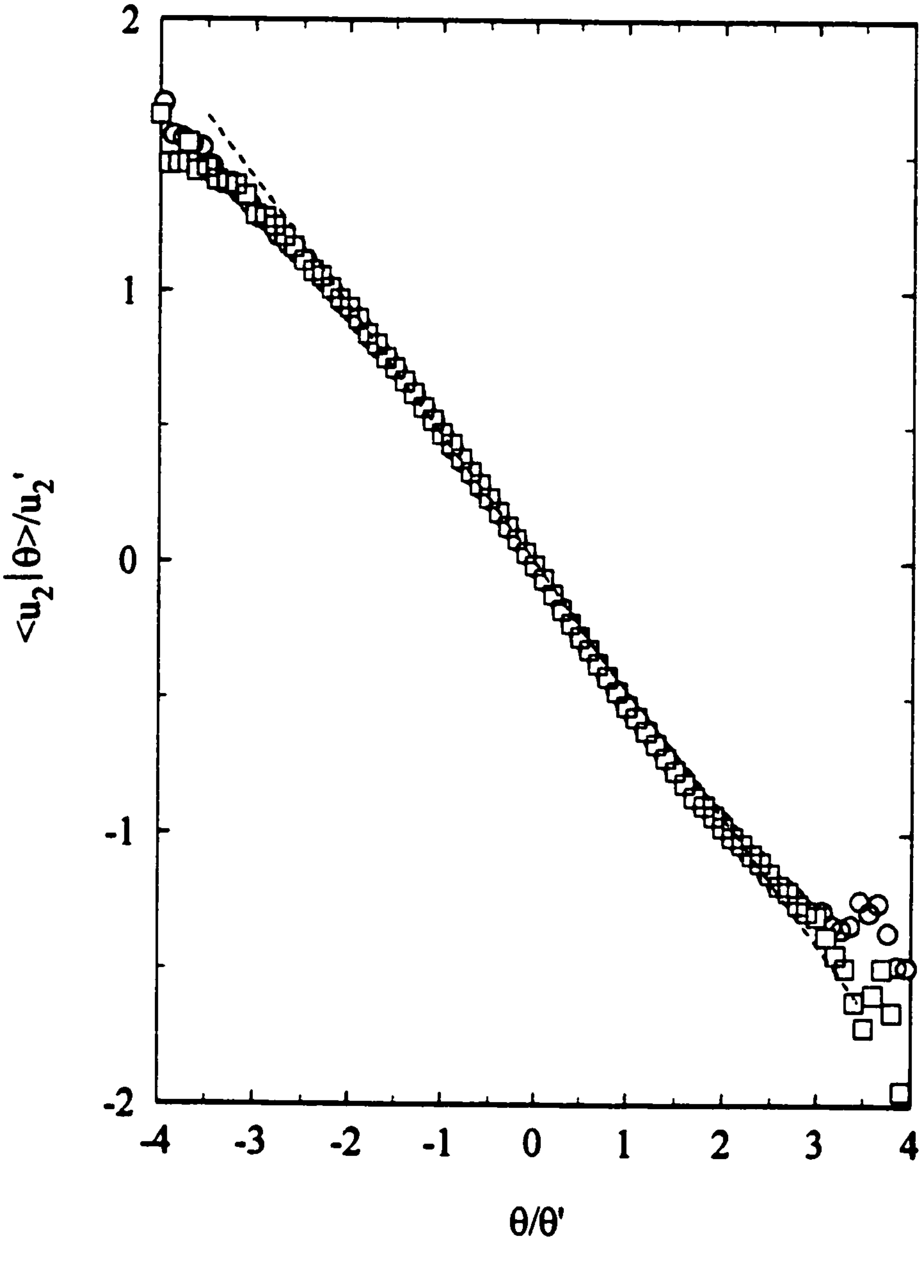

Fig. 8.24: Normalized conditional expectation of the transverse velocity fluctuations.

○ $Re_\lambda = 200$; □ $Re_\lambda = 253$.

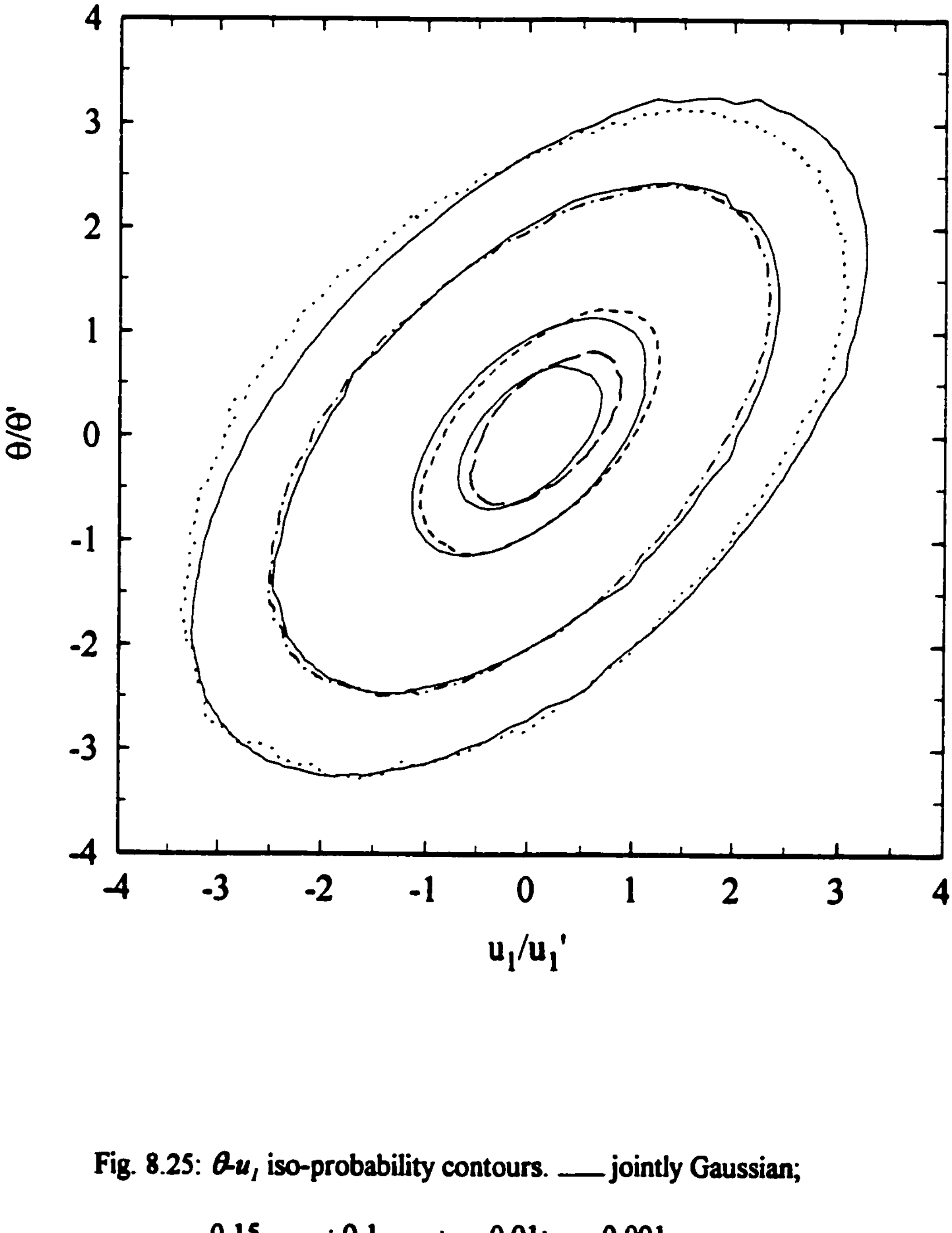

Fig. 8.25: θ-u_1 iso-probability contours. ___ jointly Gaussian;

0.15__ __; 0.1_ _ _; _._0.01; . . . 0.001.

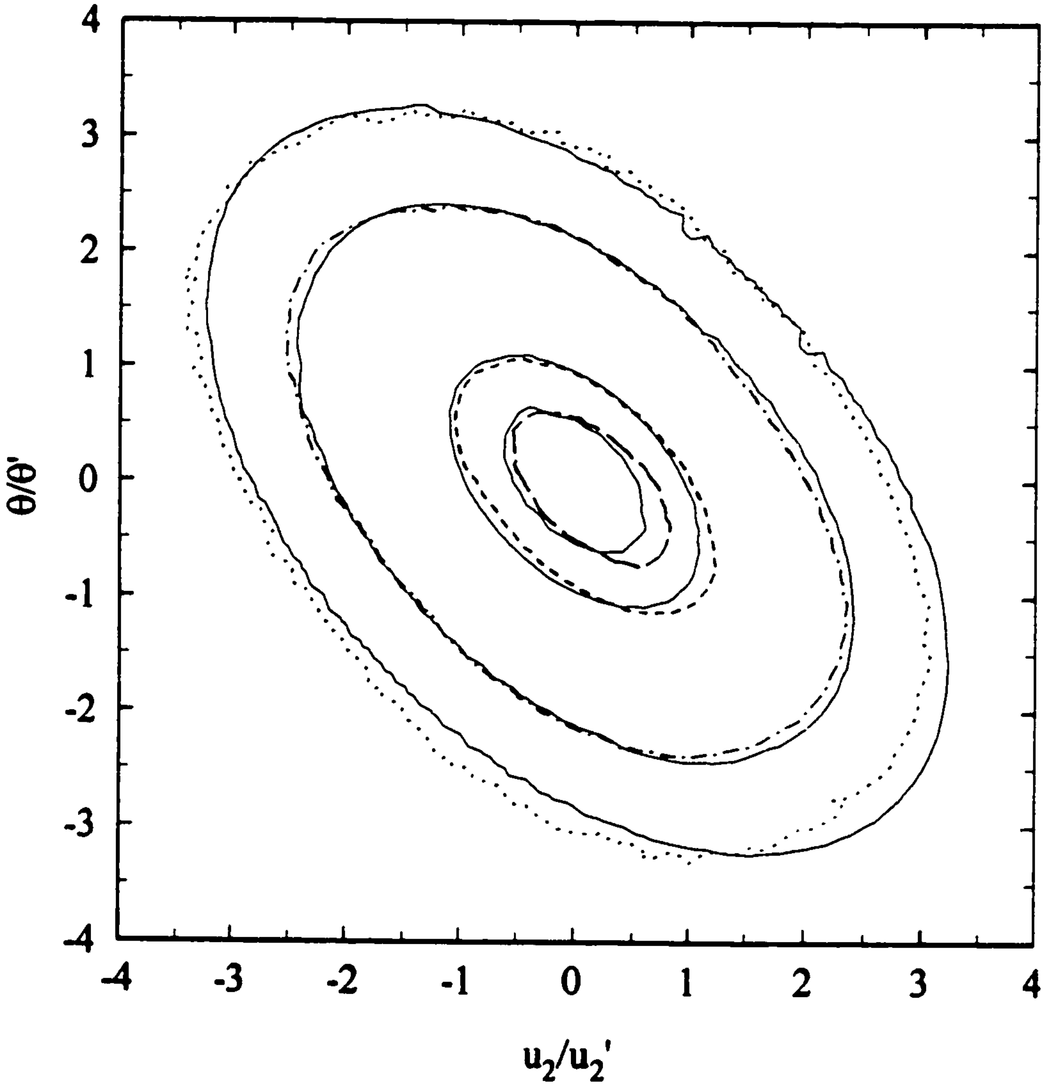

Fig. 8.26: θ-u_2 iso-probability contours. — jointly Gaussian;

__ __ 0.15; _ _ _ 0.1; _._ 0.01; . . . 0.001.

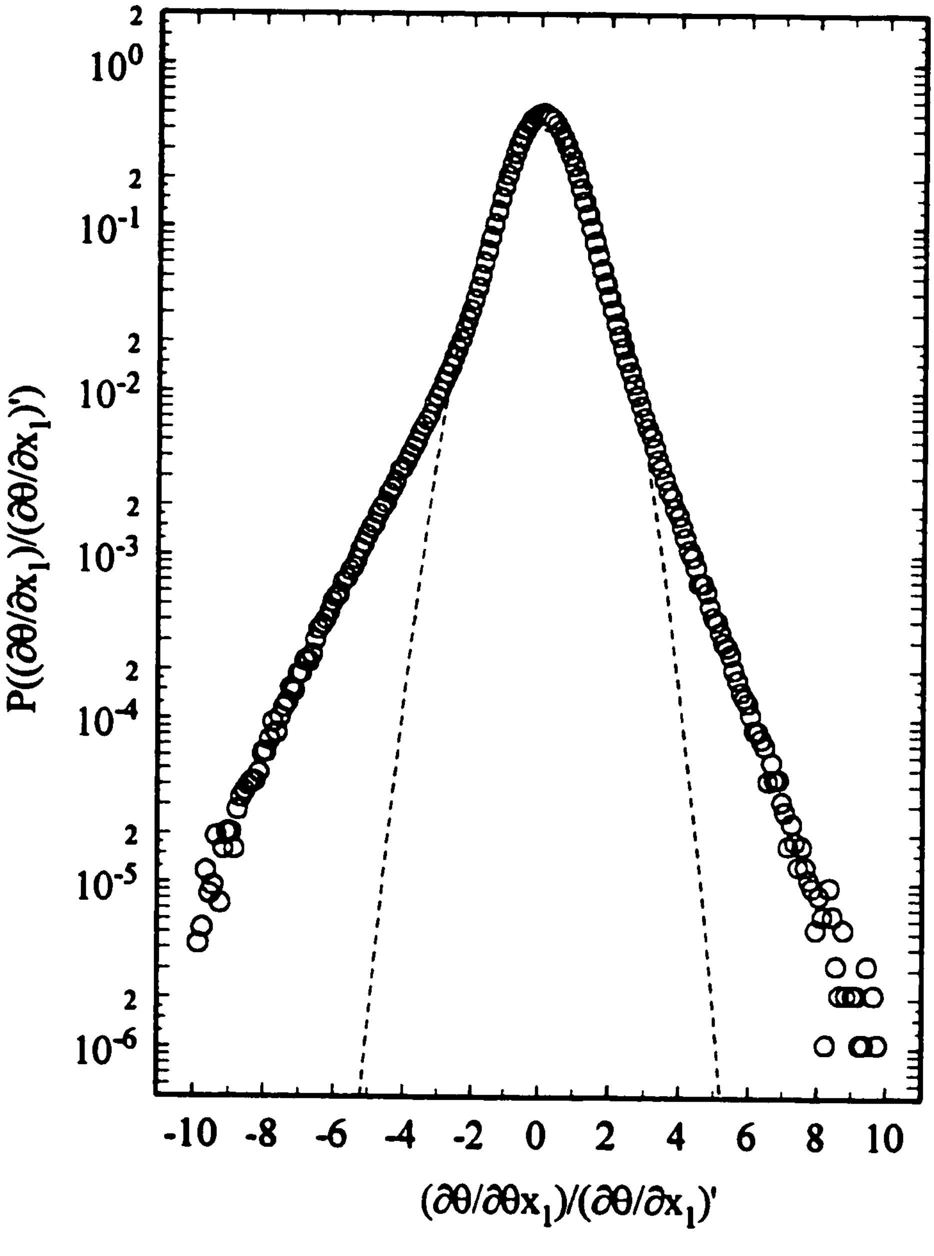

Fig. 8.27: Pdf of the streamwise scalar derivative at $Re_\lambda = 253$.

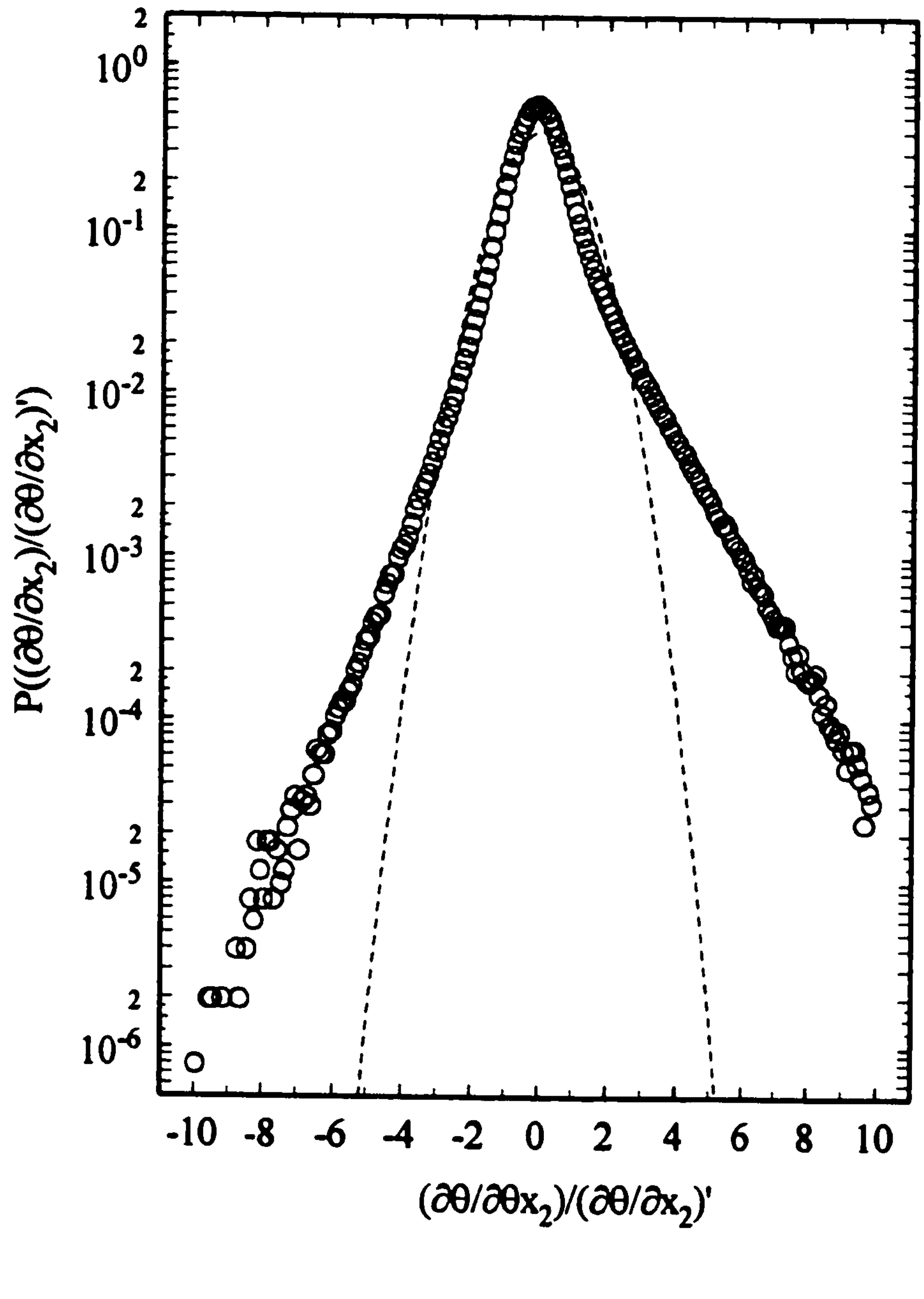

Fig. 8.28: Pdf of the transverse scalar derivative at $Re_\lambda = 200$.

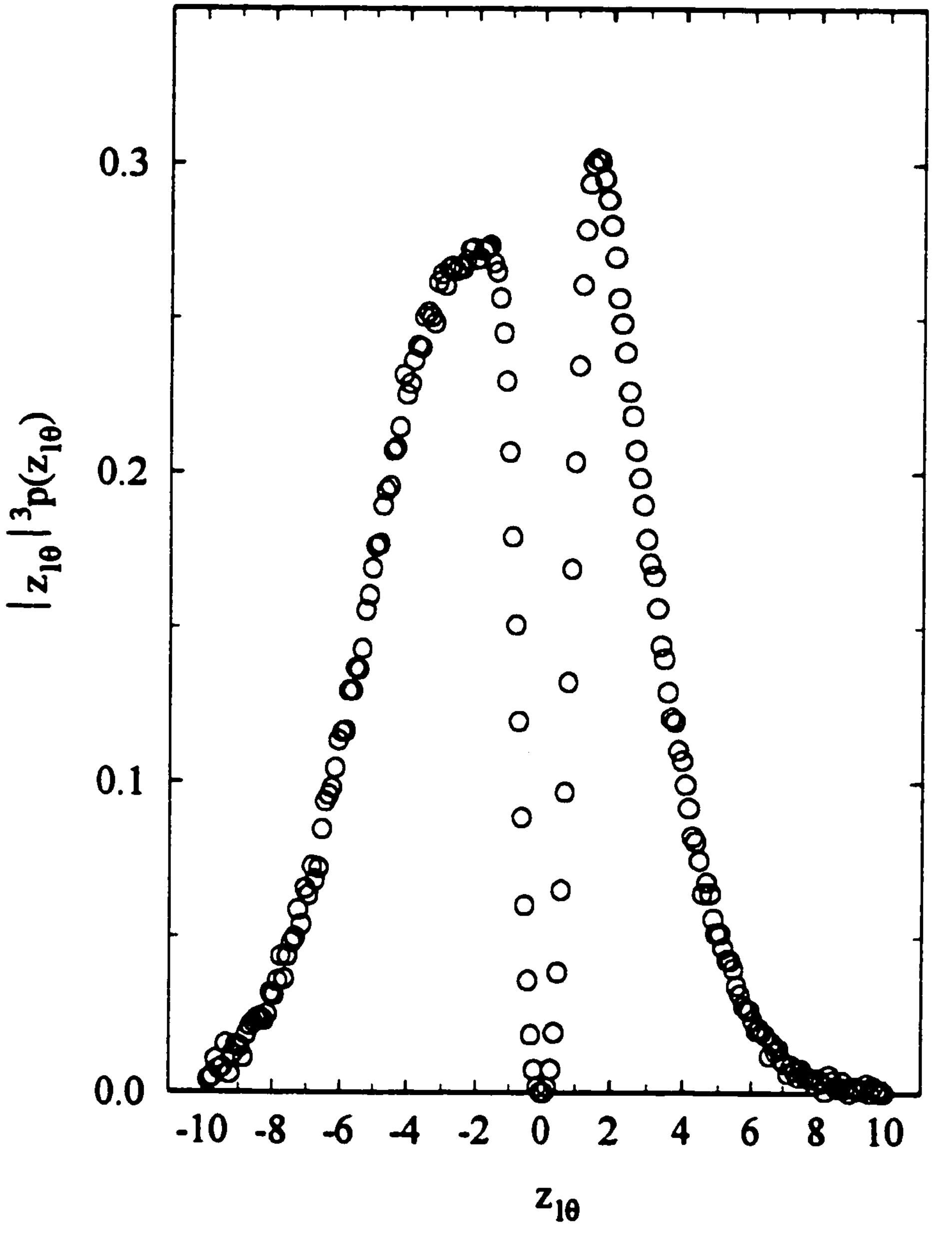

Fig. 8.29: Third moment of the pdf of the streamwise scalar derivative at $Re_\lambda = 200$.

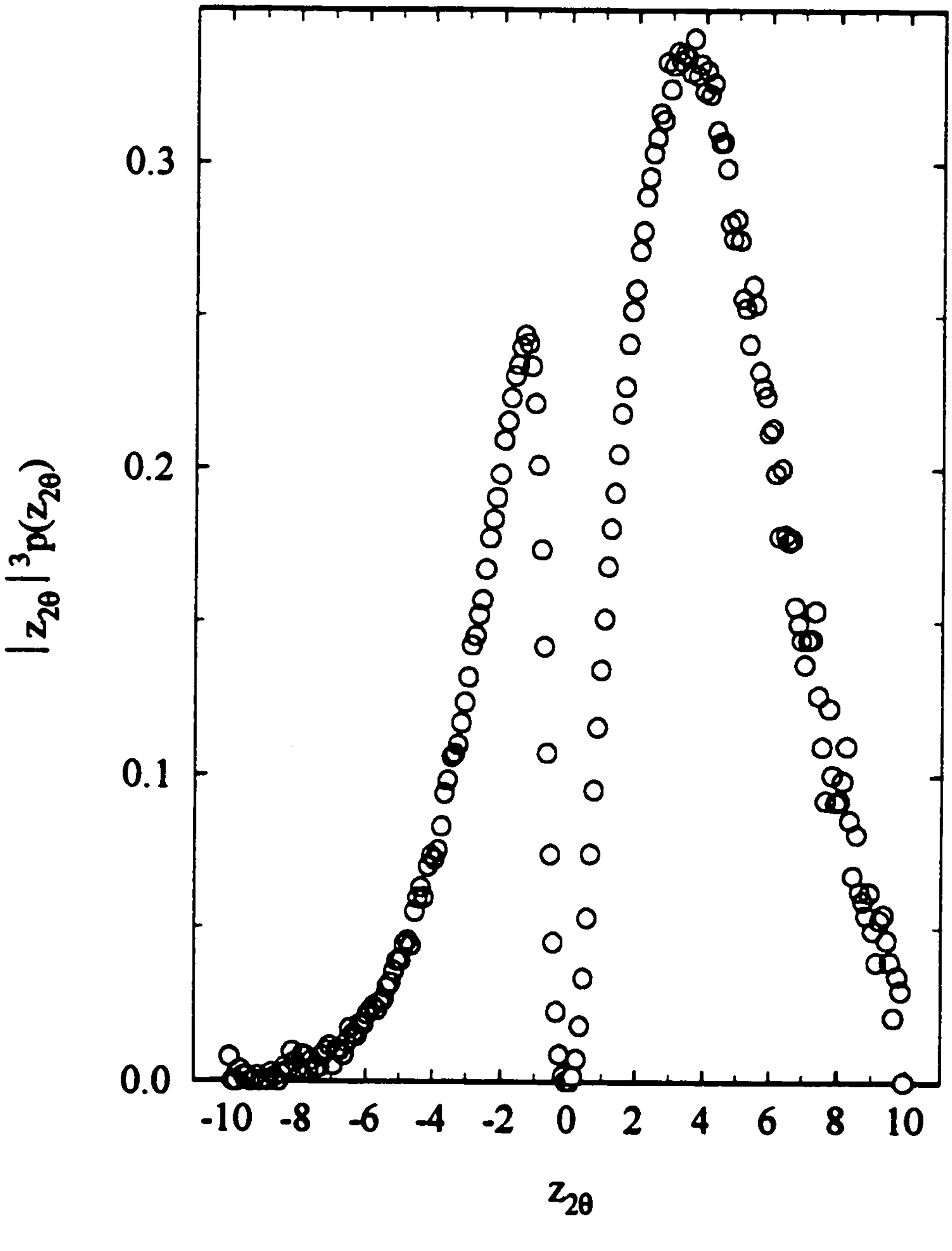

Fig. 8.30: Third moment of the pdf of the transverse scalar derivative at $Re_\lambda = 200$.

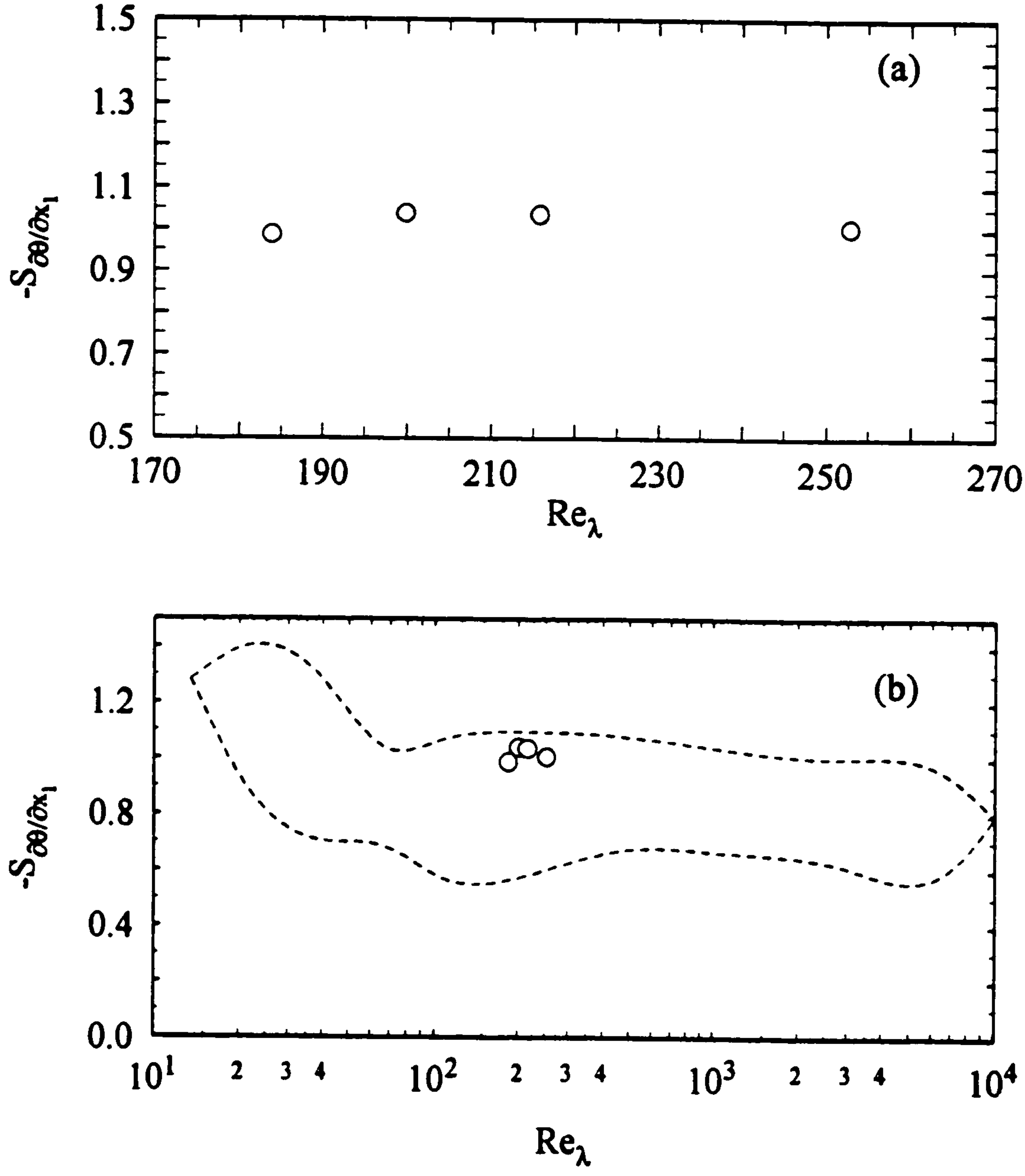

Fig. 8.31: (a) Variations of the skewness of the streamwise scalar derivative with Re_λ;

(b) replotted with fig. 7 of Sreenivasan and Antonia (1997).

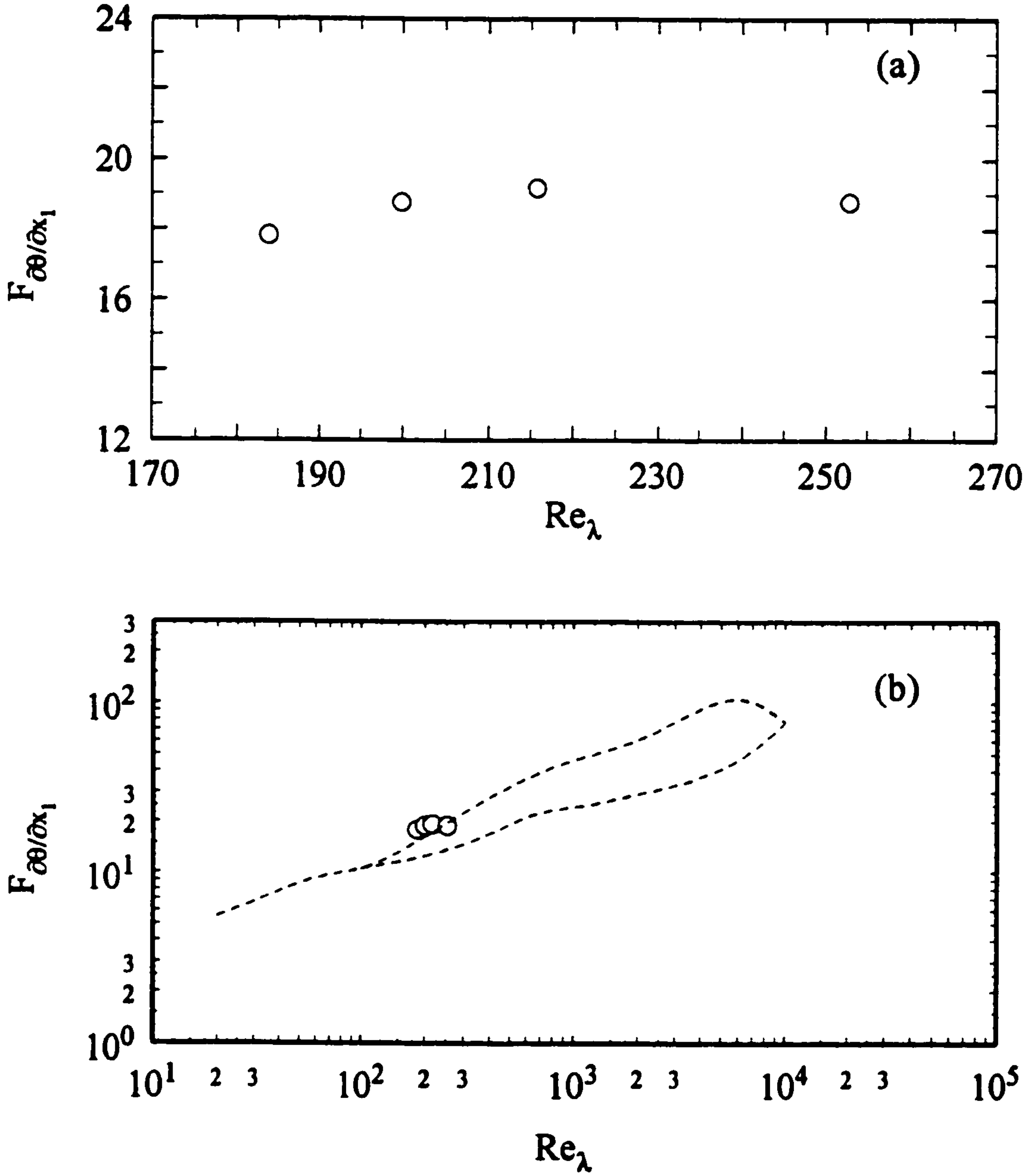

Fig. 8.32: (a) Variations of the flatness of the streamwise scalar derivative with Re_λ; (b) replotted with fig. 8 Sreenivasan and Antonia (1997).

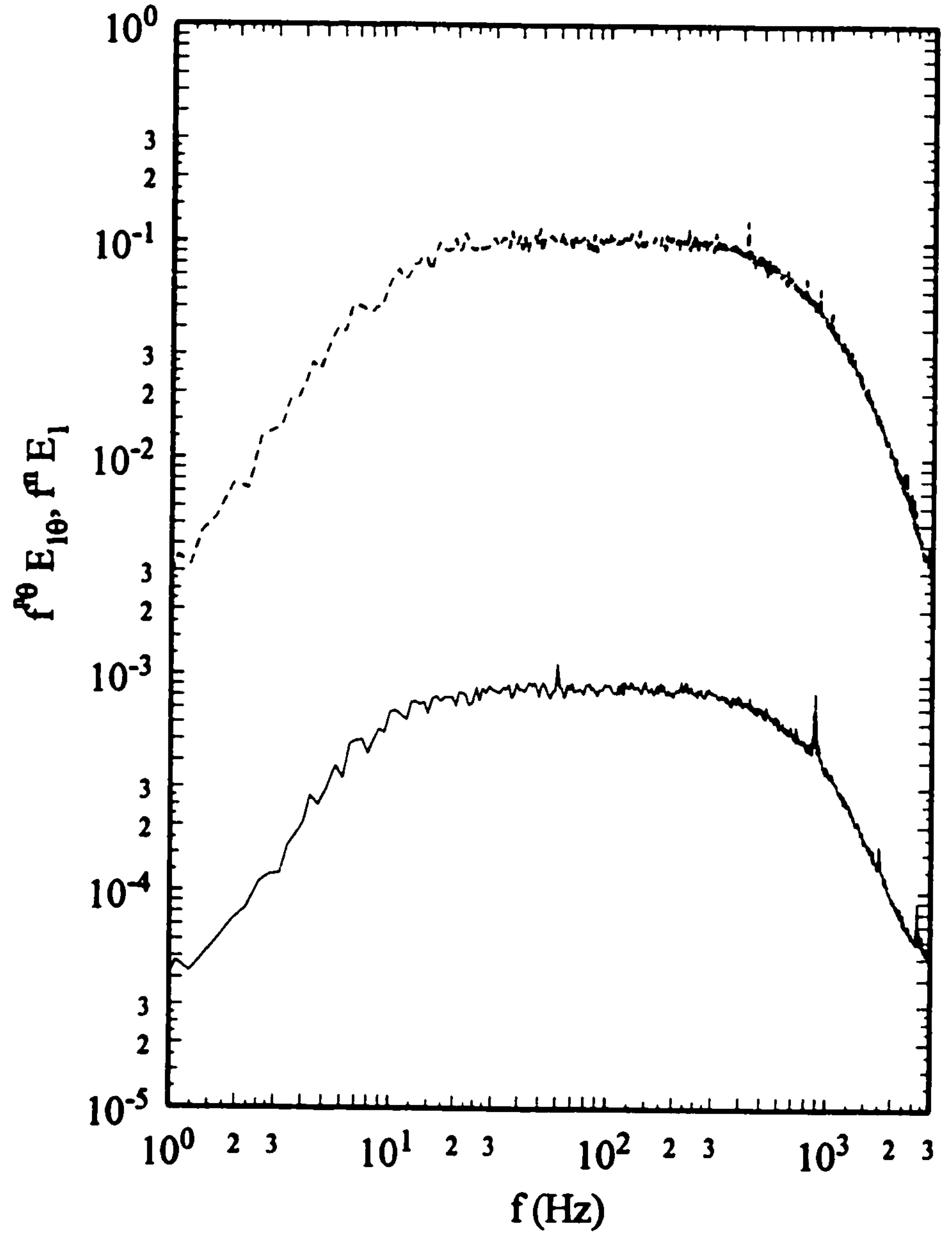

Fig. 8.33: Compensated one dimensional spectra at $Re_\lambda = 253$.

—Temperature fluctuation ($n_\theta = 1.24$); --- Streamwise velocity fluctuations ($n = 1.50$).

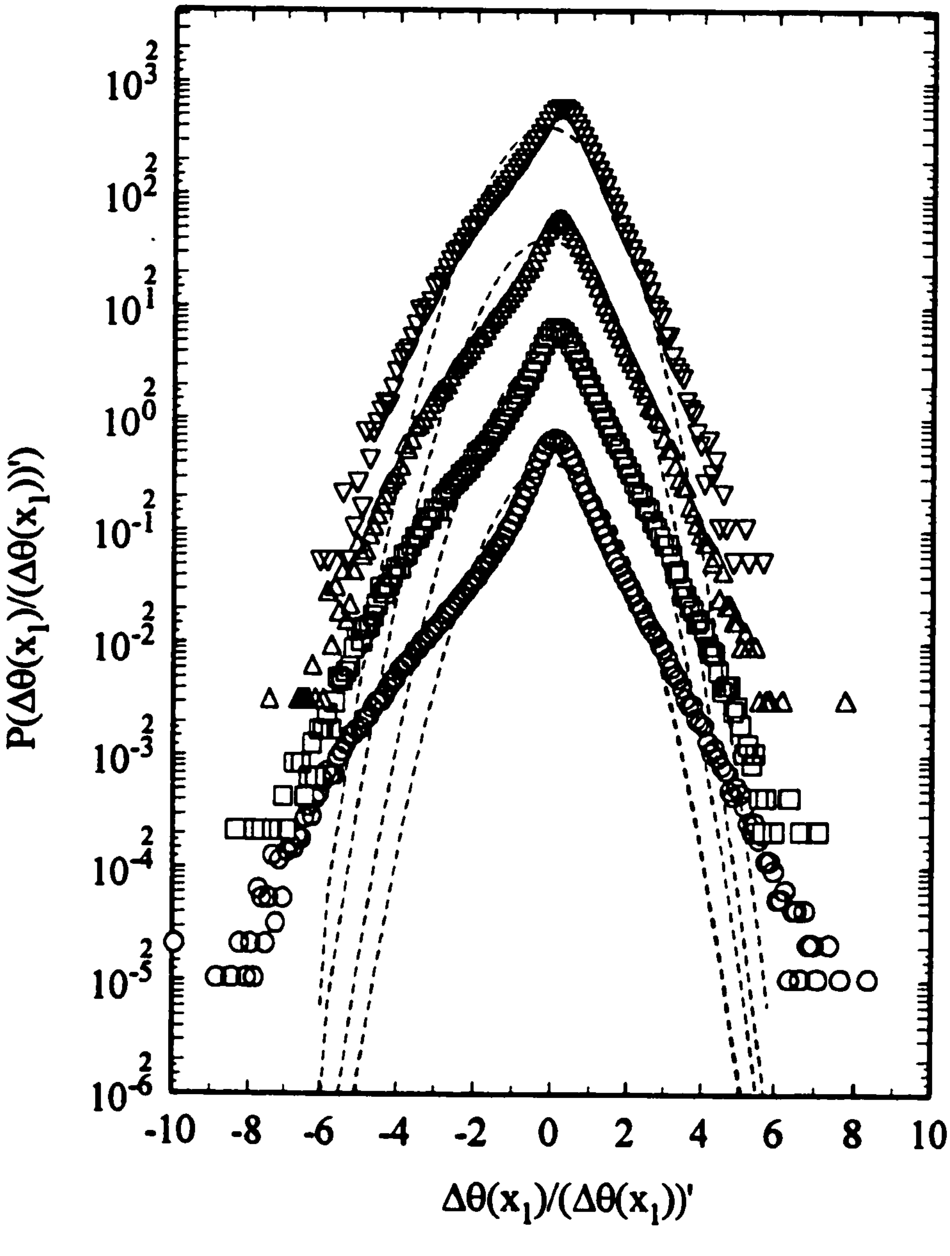

Fig. 8.34: Pdf of the streamwise scalar difference at $Re_\lambda = 253$.

○ $r/\eta = 20$; □ $r/\eta = 40$; △ $r/\eta = 60$; ▽ $r/\eta = 100$.

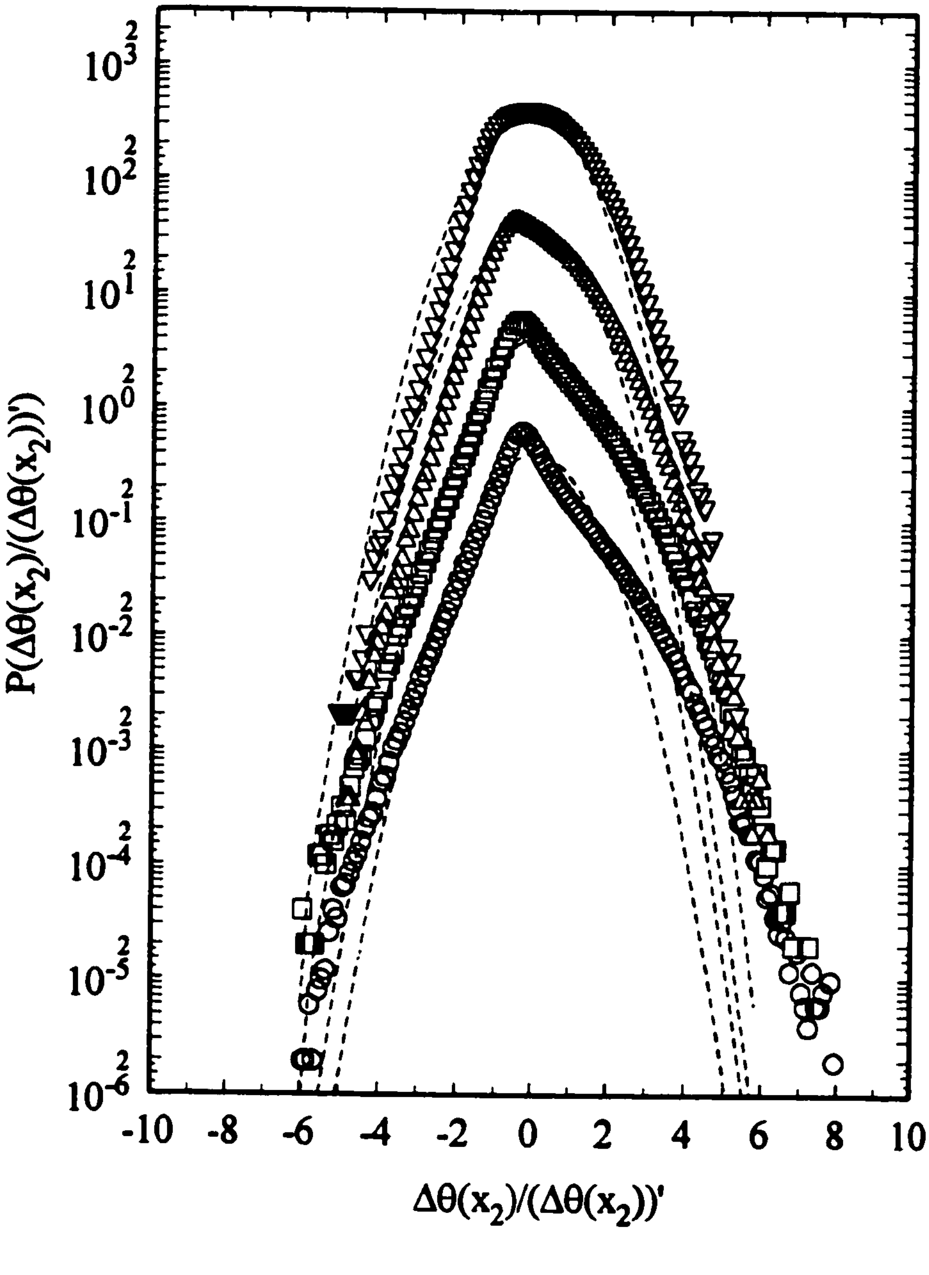

Fig. 8.35: Pdf of the transverse scalar difference at $Re_\lambda = 200$.

○ $r/\eta = 26$; □ $r/\eta = 37$; △ $r/\eta = 79$; ▽ $r/\eta = 156$.

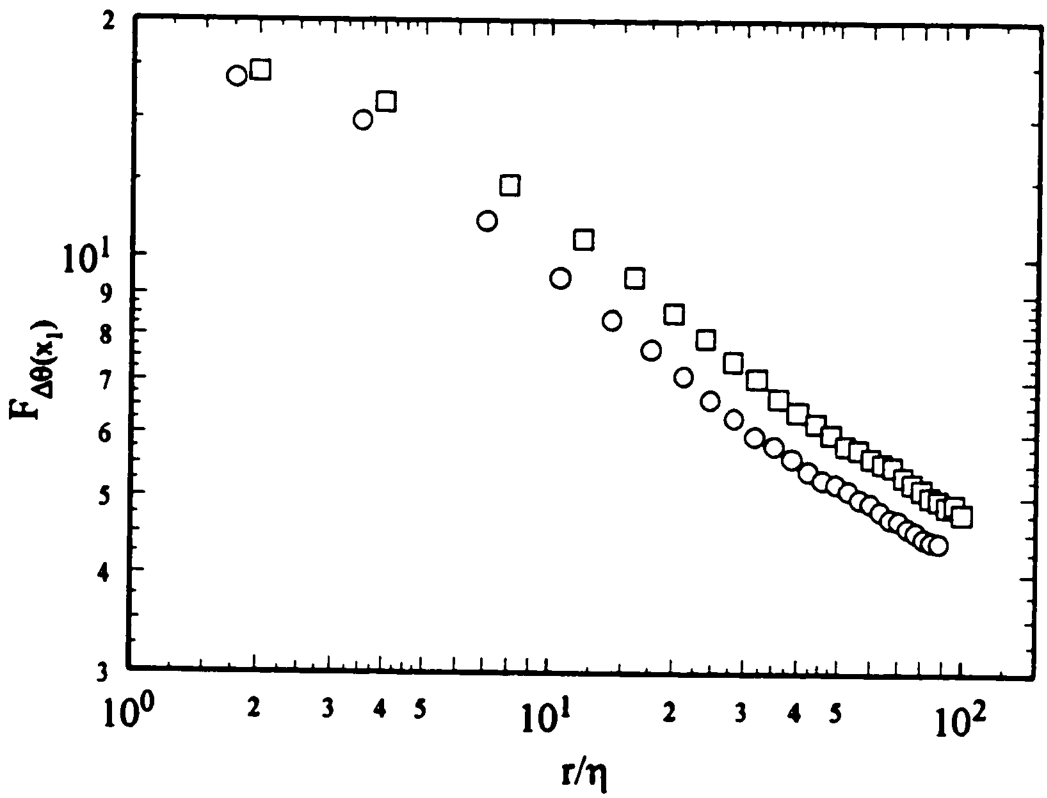

Fig. 8.36: Flatness of the streamwise scalar difference.

○ $Re_\lambda = 200$; □ $Re_\lambda = 253$.

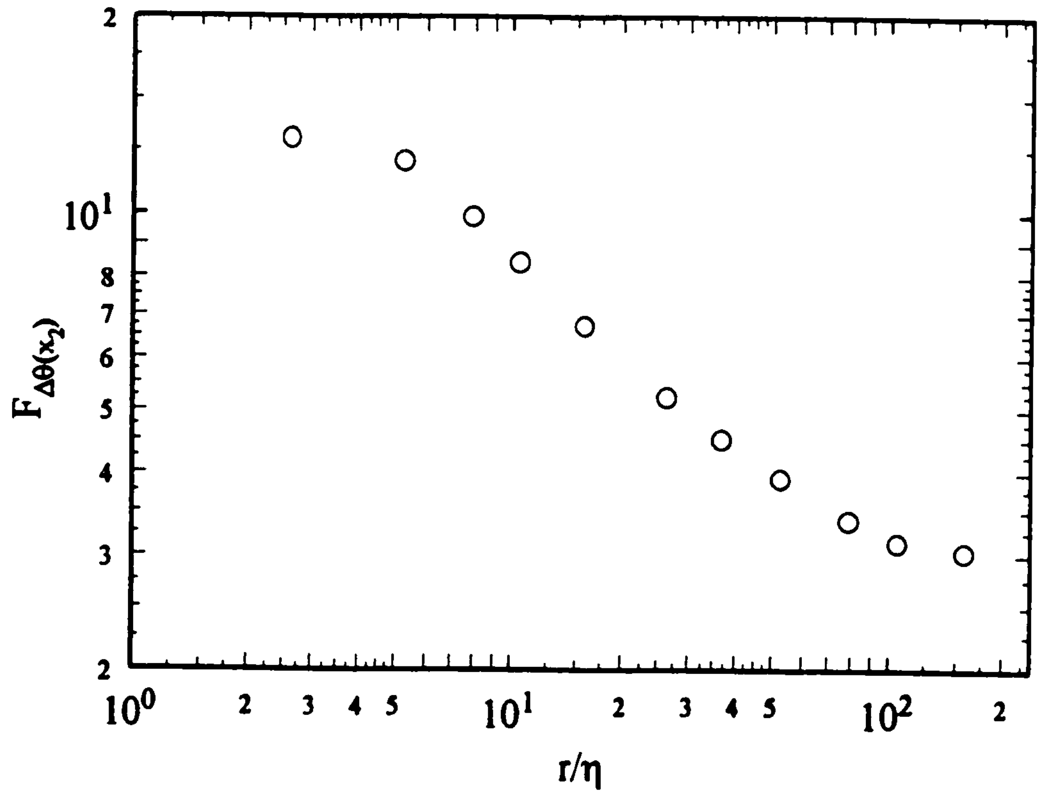

Fig. 8.37: Flatness of the transverse scalar difference at $Re_\lambda = 200$.

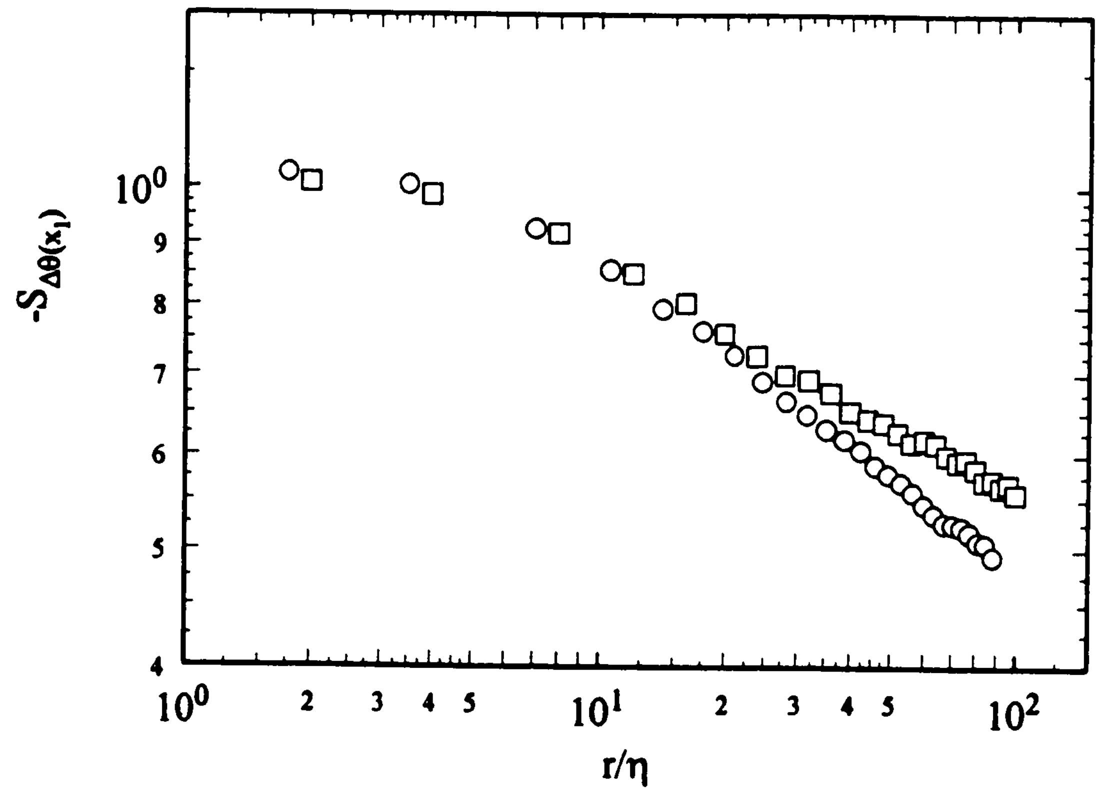

Fig. 8.38: Skewness of the streamwise scalar difference.

○ $Re_\lambda = 200$; □ $Re_\lambda = 253$.

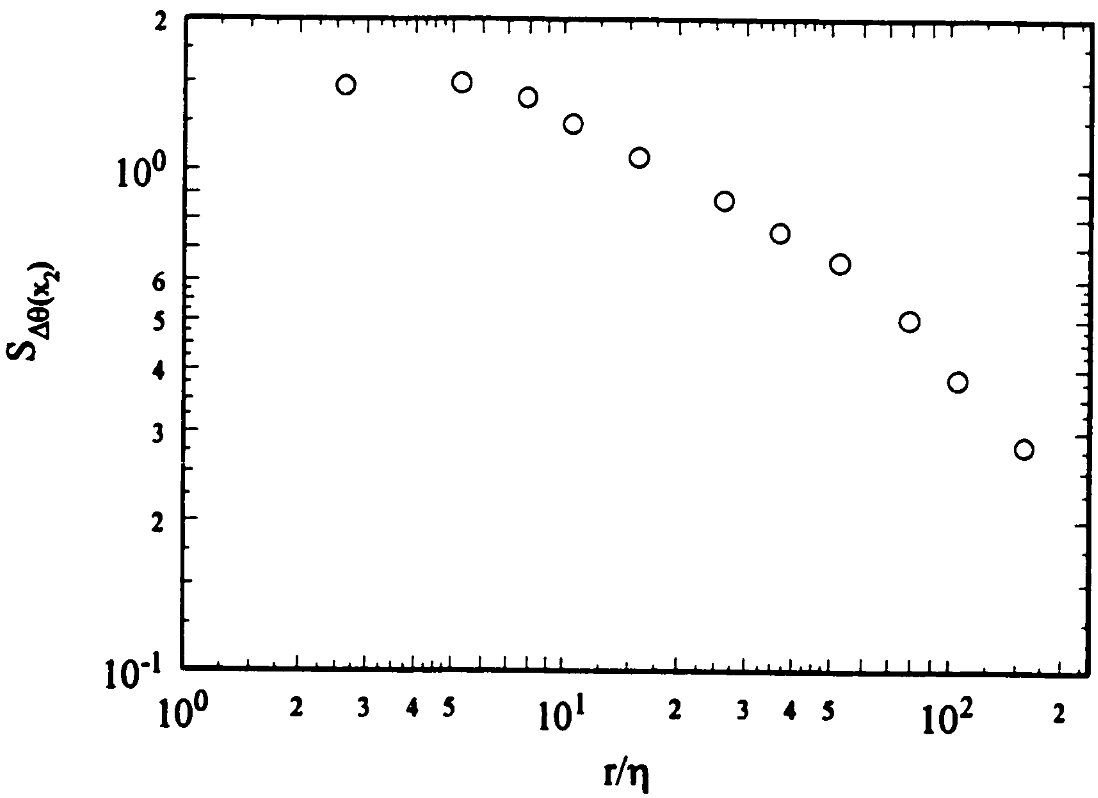

Fig. 8.39: Skewness of the transverse scalar difference at $Re_\lambda = 200$.

APPENDIX A

Mathematical Derivations

This appendix includes the derivations of equation 4.24 starting from equation 4.23 of Chapter 4.

I. The first term on the right hand side of equation 4.23 can be written as

$$<\overline{U}_j\frac{\partial\theta}{\partial x_j}\frac{\partial}{\partial\psi}\delta(\theta-\psi)> \;=\; \overline{U}_j<-\frac{\partial\theta}{\partial x_j}\frac{\partial}{\partial\theta}\delta(\theta-\psi)>$$
$$-\overline{U}_j<\frac{\partial}{\partial x_j}\delta(\theta-\psi)>=-\overline{U}_j\frac{\partial}{\partial x_j}<\delta(\theta-\psi)>$$

therefore

$$<\overline{U}_j\frac{\partial\theta}{\partial x_j}\frac{\partial}{\partial\psi}\delta(\theta-\psi)> \;=\; -\overline{U}_j\frac{\partial p}{\partial x_j}$$

II. $\partial\overline{T}/\partial x_j$ in the second term on the right hand side of equation 4.23 can be taken out of the average as

$$<u_j\frac{\partial\overline{T}}{\partial x_j}\frac{\partial}{\partial\psi}\delta(\theta-\psi)>=\frac{\partial\overline{T}}{\partial x_j}<u_j\frac{\partial}{\partial\psi}\delta(\theta-\psi)>$$

Using the procedure developed in equation 3.40, $<u_j\partial/\partial\psi\ \delta(\theta-\psi)>$ can be expressed as

$$\begin{aligned}<u_j\frac{\partial}{\partial\psi}\delta(\theta-\psi)> &= \int_{-\infty}^{\infty}p(\psi')<u_j\frac{\partial}{\partial\psi}\delta(\theta-\psi)|\theta=\psi'>d\psi'\\
&= -\int_{-\infty}^{\infty}p(\psi')<u_j\frac{\partial}{\partial\theta}\delta(\theta-\psi)|\theta=\psi'>d\psi'\\
&= -\int_{-\infty}^{\infty}p(\psi')<u_j\frac{\partial}{\partial\psi'}\delta(\psi'-\psi)|\theta=\psi'>d\psi'\\
&= -\int_{-\infty}^{\infty}p(\psi')\frac{\partial}{\partial\psi'}\delta(\psi'-\psi)<u_j|\theta=\psi'>d\psi'\end{aligned}$$

the last equation can be expanded as

$$-\int_{-\infty}^{\infty}\frac{\partial}{\partial\psi'}[p(\psi')\delta(\psi'-\psi)<u_j|\theta=\psi'>]d\psi' + \int_{-\infty}^{\infty}\delta(\psi'-\psi)\frac{\partial}{\partial\psi'}[p(\psi')<u_j|\theta=\psi']d\psi'$$
$$= -\ p(\psi'\delta(\psi'-\psi)<u_j|\theta=\psi'>]d\psi'|_{-\infty}^{\infty} + \frac{\partial}{\partial\psi}[p(\psi)<u_j|\theta=\psi>]$$

the first term in the above equation is zero, therefore,

$$<u_j\frac{\partial\overline{T}}{\partial x_j}\frac{\partial}{\partial\psi}\delta(\theta-\psi)> = \frac{\partial\overline{T}}{\partial x_j}\frac{\partial}{\partial\psi}[<u_j|\theta=\psi>p]$$

where $<u_j|\theta=\psi>$ is the conditional expectation of the velocity fluctuations conditional upon the scalar θ.

III. The third term on the right hand side of equation 4.23 can be expanded as

$$\begin{aligned}
<\frac{\partial\theta u_j}{\partial x_j}\frac{\partial}{\partial\psi}\delta(\theta-\psi)> &= <(u_j\frac{\partial\theta}{\partial x_j}+\theta\frac{\partial u_j}{\partial x_j})\frac{\partial}{\partial\psi}\delta(\theta-\psi)> \\
&= <u_j\frac{\partial\theta}{\partial x_j}\frac{\partial}{\partial\psi}\delta(\theta-\psi)> \\
&= -<u_j\frac{\partial}{\partial x_j}\delta(\theta-\psi)> \\
&= -\frac{\partial}{\partial x_j}<u_j\delta(\theta-\psi)> + <\frac{\partial u_j}{\partial x_j}\delta(\theta-\psi)> \\
&= -\frac{\partial}{\partial x_j}<u_j\delta(\theta-\psi)>
\end{aligned}$$

the second and last steps followed from continuity, $\partial u_j/\partial x_j = 0$. Again, employing the procedure of equation 3.40, $<u_j\,\delta(\theta-\psi)>$ can be expressed as

$$\begin{aligned}
<u_j\delta(\theta-\psi)> &= \int_{-\infty}^{\infty}p(\psi')<u_j\delta(\theta-\psi)|\theta=\psi'>d\psi' \\
&= \int_{-\infty}^{\infty}p(\psi')<u_j|\theta=\psi'>\delta(\psi'-\psi)d\psi' \\
&= p(\psi)<u_j|\theta=\psi>
\end{aligned}$$

therefore

$$<\frac{\partial\theta u_j}{\partial x_j}\frac{\partial}{\partial\psi}\delta(\theta-\psi) = -\frac{\partial}{\partial x_j}[<u_j|\theta=\psi>p]$$

IV. The forth term, in a straightforward manner, gives

$$-<\frac{\partial\theta\overline{u_j}}{\partial x_j}\frac{\partial}{\partial\psi}\delta(\theta-\psi)> = -\frac{\partial\theta\overline{u_j}}{\partial x_j}\frac{\partial}{\partial\psi}<\delta(\theta-\psi)>$$
$$= -\frac{\partial\theta\overline{u_j}}{\partial x_j}\frac{\partial p}{\partial\psi}$$

V. The last term on the right hand side of equation 4.23 is expanded as

$$\begin{aligned}
- <\gamma\frac{\partial^2\theta}{\partial x_j\partial x_j}\frac{\partial}{\partial\psi}\delta(\theta-\psi)> &= - <\gamma[\frac{\partial}{\partial x_j}(\frac{\partial\theta}{\partial x_j}\frac{\partial}{\partial\psi}\delta(\theta-\psi)) - \frac{\partial\theta}{\partial x_j}\frac{\partial}{\partial x_j}\frac{\partial}{\partial\psi}\delta(\theta-\psi)]> \\
&= - <\gamma\frac{\partial}{\partial x_j}[-\frac{\partial\psi}{\partial x_j}\frac{\partial}{\partial\psi}\delta(\theta-\psi)]> + <\gamma\frac{\partial\theta}{\partial x_j}\frac{\partial}{\partial x_j}\frac{\partial}{\partial\psi}\delta(\theta-\psi)> \\
&= <\gamma\frac{\partial^2}{\partial x_j\partial x_j}\delta(\theta-\psi)> + <\gamma\frac{\partial\theta}{\partial x_j}\frac{\partial}{\partial x_j}\frac{\partial}{\partial\psi}\delta(\theta-\psi)> \\
&= \gamma\frac{\partial^2 p}{\partial x_j\partial x_j} + \gamma<\frac{\partial\theta}{\partial x_j}(-\frac{\partial\theta}{\partial x_j}\frac{\partial}{\partial\psi})\frac{\partial}{\partial\psi}\delta(\theta-\psi)> \\
&= \gamma\frac{\partial^2 p}{\partial x_j\partial x_j} - <\gamma(\frac{\partial\theta}{\partial x_j})^2\frac{\partial^2}{\partial\psi^2}\delta(\theta-\psi)>
\end{aligned}$$

the second term of the above equation will be reduced as follows

$$<\gamma(\frac{\partial\theta}{\partial x_j})^2\frac{\partial^2}{\partial\psi^2}\delta(\theta-\psi)> = \frac{\partial^2}{\partial\psi^2}<\gamma(\frac{\partial\theta}{\partial x_j})^2\delta(\theta-\psi)>$$

the above step follows because θ and ψ are independent. Expressing $<\gamma(\partial\theta/\partial x_j)^2\,\delta(\theta\text{-}\psi)>$ in terms of a conditional expectation by employing the procedure of equation 3.40, one gets

$$
\begin{aligned}
<\gamma(\frac{\partial\theta}{\partial x_j})^2\delta(\theta-\psi)> &= \int_{-\infty}^{\infty} p(\psi')<\gamma(\frac{\partial\theta}{\partial x_j})^2\delta(\theta-\psi)|\theta=\psi'>d\psi' \\
&= \int_{-\infty}^{\infty} p(\psi')\delta(\psi'-\psi)<\gamma(\frac{\partial\theta}{\partial x_j})^2|\theta=\psi'>d\psi' \\
&= <\gamma(\frac{\partial\theta}{\partial x_j})^2|\theta=\psi>\, p
\end{aligned}
$$

the last term on the right hand side of equation 4.23 therefore, reduces to

$$
-<\gamma\frac{\partial^2\theta}{\partial x_j\partial x_j}\frac{\partial}{\partial\psi}\delta(\theta-\psi)> = \gamma\frac{\partial^2 p}{\partial x_j\partial x_j} - \frac{\partial^2}{\partial\psi^2}[<\gamma(\frac{\partial\theta}{\partial x_j})^2|\theta=\psi>p]
$$

Finally substituting for all the terms on the right hand side of equation 4.23 yields

$$
\begin{aligned}
\frac{\partial p}{\partial t} + \overline{U}_j\frac{\partial p}{\partial x_j} + \frac{\partial}{\partial x_j}[<u_j|\theta=\psi>p] + \frac{\partial\overline{\theta u_j}}{\partial x_j}\frac{\partial p}{\partial\psi} &= \gamma\frac{\partial^2 p}{\partial x_j\partial x_j} - \frac{\partial^2}{\partial\psi^2}[<\epsilon_\theta|\theta=\psi>p] \\
&+ \frac{\partial\overline{T}}{\partial x_j}\frac{\partial}{\partial\psi}[<u_j|\theta=\psi>p]
\end{aligned}
$$